

Novel imaging techniques for assessing disease affecting the right heart

Dr Daniel Knight

A dissertation submitted in partial fulfillment of
the requirements for the degree of **MD(Res)**

Division of Medicine
University College London
2015

I, Daniel Knight confirm that the work presented in this thesis is my own.

Where information has been derived from other sources, I confirm that this has been indicated in the thesis.

A handwritten signature in black ink, reading "D.S. Knight." The signature is written in a cursive style and is underlined with a single horizontal stroke.

Abstract

Right ventricular (RV) size and function are prognostic in congenital and acquired heart disease. Two-dimensional echocardiography (2DE) is the most readily available modality for RV assessment, but is limited by its complex shape. Furthermore, biventricular function is intimately related through a shared septum and pericardium. The simplest metric of left ventricular (LV) function is ejection fraction (LVEF). However, LVEF is often maintained in pulmonary hypertension (PH), for example. Therefore better indicators of LV function are required to identify patients at risk of deterioration. In this thesis, novel imaging techniques for assessing cardiac function in right heart disease are investigated.

The first experiment tested the hypothesis that single-beat three-dimensional echocardiography (3DE) accurately and reproducibly quantifies RV volumes. 3DE traditionally acquires sub-volumes over consecutive heartbeats, whereas novel 3DE transducers can acquire datasets in a single cardiac cycle. Single-beat 3DE was compared against CMRI in 100 subjects including patients with PH and carcinoid heart disease. Single-beat 3DE was feasible and accurate for RV volumetric quantification, but with limitations of test-retest reproducibility.

The second experiment tested the hypothesis that 2D knowledge-based reconstruction (2DKBR) accurately and reproducibly quantifies RV volumes. 2DKBR involves 2DE-acquired RV coordinates localized in 3D

space and connected by reference to a disease-specific RV catalogue. This was validated against CMRI in 28 PH patients, and test-retest reproducibility was assessed. 2DKBR was feasible and accurate for RV volumetric quantification in PH, and more reproducible than conventional 2DE.

The final experiment tested the hypothesis that multi-directional myocardial velocities could be assessed in PH by CMRI. A tissue phase mapping sequence was utilized in 40 PH patients and 20 healthy volunteers. Over a median follow-up period of 20 months, LV early diastolic wave velocities were the only independent predictors of functional capacity and clinical worsening in a model that includes conventional metrics of biventricular function.

Acknowledgements

I would like to thank Vivek Muthurangu for all of his help, support, and advice over the last five years. Vivek has been a constant source of help and enthusiasm since the outset of my clinical research, and, without his dedication and help, none of my research would have been possible. Furthermore, his support extends much further beyond this thesis, with his training and guidance being pivotal in shaping my future career.

In addition I would also like to thank the following people for their support and advice during my work: Jenny Steeden, whose patience, support and physics knowledge helped make my research possible; Joseph Davar, for all of his help and support as a supervisor; Gerry Coghlan, for all of his help, support and enthusiasm in anything PH-related; Andrew Taylor, for all of his help and support, and for introducing me to the UCL Centre for Cardiovascular Imaging; and to Agata Grasso (AEG), Michael Quail (MAQ), Johannes Schwaiger (JS) and James Willis for their contributions to reproducibility analyses and for their collaborative work. Furthermore, I would like to thank Wendy Norman and Rod Jones, the radiographers at ICH who have helped with scanning the participants for these studies.

I am extremely grateful to all of the patients and volunteers who have given up their time to take part in the studies described in this thesis, without whom none of the studies would be possible. I would also like to thank the British Heart Foundation (BHF) for funding my clinical research training fellowship.

Last, but by no means least, I would like to thank my wife Amy for all of her understanding, support and patience, for which I am truly grateful.

Contents

Declaration of Originality	2
Abstract	3
Acknowledgements	5
Contents	6
List of Figures	11
List of Tables	16
List of Equations	18
List of Acknowledgements	19
CHAPTER 1 Non-invasive Imaging of the Right Ventricle	21
1.1 Introduction	22
1.1.1 The right ventricle: a historical perspective	22
1.1.2 RV anatomy	24
1.1.3 RV function	26
1.1.4 Ventricular interdependence	27
1.2 Non-invasive imaging of the RV	28
1.2.1 2D Echocardiography	29
1.2.1.1 2DE linear dimensions	29
1.2.1.2 Fractional area change (FAC)	30
1.2.1.3 Doppler Tissue Imaging (DTI)-derived tricuspid lateral annular systolic velocity wave (S')	31
1.2.1.4 Tricuspid Annular Plane Systolic Excursion (TAPSE)	33
1.2.1.5 RV index of myocardial performance (RIMP) / Tei Index	34
1.2.1.6 Deformation imaging: strain and strain rate	36
1.2.2 Cardiac Magnetic Resonance Imaging (CMRI)	37
1.2.3 RV assessment by 2DE versus CMRI	41
1.3 The RV in pressure- and volume-overload states	44
1.3.1 Pressure-overload of the RV: Pulmonary Hypertension	44
1.3.2 Volume-overload of the RV: CHD	47
CHAPTER 2 Three-Dimensional Echocardiography of the Right Ventricle	49
2.1 Introduction	50
2.1.1 Aims	50
2.1.2 Personal Contribution	51

2.2 Literature Overview	51
2.2.1 Benefits of RV functional assessment using 3DE versus 2DE	52
2.2.2 The evolution of 3DE technology	53
2.2.2.1 ECG-gated multiple-beat 3DE of the RV	54
2.2.2.2 Real-time 3DE: single-beat full-volume 3DE of the RV	56
2.2.2.3 Commercially available 3DE RV post-processing algorithms.....	57
2.2.3 Comparison of 3DE versus MRI in PH for RV volumetric quantification	59
2.2.4 Test-retest reproducibility of 3DE for RV volumetric quantification.	60
2.2.5 Summary	62
2.3 Methods.....	63
2.3.1 Study Population	63
2.3.2 2DE	64
2.3.3 3DE	65
2.3.3.1 Image Acquisition	65
2.3.3.2 Post-Processing	66
2.3.4 Test-Retest Reproducibility of 3DE	68
2.3.5 CMRI	69
2.3.5.1 Image Acquisition	69
2.3.5.2 Post-Processing	70
2.3.6 Statistical Analysis	71
2.4 Results	72
2.4.1 Study Population Characteristics	72
2.4.2 3DE Technical Data	74
Volumetric Analysis by 3DE versus CMRI	75
2.4.3 RV Quantification by 3DE and 2DE versus CMRI	79
2.4.4 Test-Retest Intraobserver and Interobserver Reproducibility	79
2.5 Discussion	81
2.5.1 RV Remodelling in PH and CHD.....	81
2.5.2 Benefit of 3DE over 2DE for RV Assessment	82
2.5.3 Advantages of 3DE over CMRI for RV Assessment	83
2.5.4 Disadvantages of 3DE for RV Assessment.....	83
2.5.5 RV Volumetric Quantification by 3DE in Health and Disease	84
2.5.6 Operator experience and Reproducibility of 3DE RV Assessment .	85
2.6 Limitations	86
2.7 Conclusions	88

CHAPTER 3 Two-Dimensional Knowledge-Based Reconstruction of the Right Ventricle.	89
3.1 Introduction	90
3.1.1 Aims	91
3.1.2 Personal Contribution.....	91
3.2 Literature Overview.....	92
3.2.1 Heterogeneity of RV shape in response to disease	92
3.2.2 Development of the 2D KBR technique	93
3.2.2.1 Probe tracking	93
3.2.2.2 Piecewise smooth subdivision surface (PSSS) reconstruction method	95
3.2.2.3 Knowledge-based reconstruction (KBR)	97
3.2.3 Validation of volumetric assessment of RV function using KBR	
versus CMRI.....	99
3.2.4 Direct comparison of KBR versus 3DE RV post-processing	
algorithms	101
3.2.5 Summary.....	102
3.3 Methods.....	102
3.3.1 Study Population	103
3.3.2 Two-dimensional echocardiography and KBR	103
3.3.2.1 Image acquisition.....	103
3.3.2.2 Post-processing: RV FAC.....	105
3.3.2.3 Post-processing: KBR	105
3.3.2.4 FAC and 2DKBR test-retest reproducibility	109
3.3.3 Cardiac MRI	109
3.3.3.1 Image acquisition.....	109
3.3.3.2 Post-processing.....	109
3.3.4 Statistics.....	110
3.4 Results	111
3.4.1 Study Population Characteristics	111
3.4.2 2DKBR Technical Data	112
3.4.3 RV quantification by 2DKBR versus CMRI	112
3.4.4 Test-retest intraobserver and interobserver reproducibility	113
3.5 Discussion	115
3.5.1 Validation of the 2DKBR technique for RV Assessment.....	116
3.5.2 Test-retest reproducibility of 2DKBR RV Assessment	116
3.5.3 Utility of 2DE with KBR versus 3DE	117

3.6	Limitations	121
3.7	Conclusions	123
CHAPTER 4 Tissue Phase Mapping to assess Left Ventricular Myocardial Mechanics in Pulmonary Hypertension		124
4.1	Introduction	125
4.1.1	Aims	125
4.1.2	Personal Contribution.....	126
4.2	Literature Overview	127
4.2.1	Tissue Tagging.....	127
4.2.2	Displacement Encoding with Stimulated Echoes (DENSE)	129
4.2.3	Strain Encoded (SENC) Imaging	130
4.2.4	Tissue Phase Mapping (TPM).....	131
4.2.5	Summary.....	133
4.3	Methods.....	134
4.3.1	Study Population	134
4.3.2	Conventional CMRI Protocol and Image Post-Processing	135
4.3.3	Tissue Phase Mapping Protocol and Image Post-Processing	136
4.3.4	Statistics.....	137
4.4	Results	139
4.4.1	Study Population Characteristics	139
4.4.2	Myocardial Velocities in Normal Subjects and PH Patients	142
4.4.3	Regional Variations in Normal Subjects and PH Patients.....	145
4.4.4	Haemodynamic Correlates with Myocardial Velocities	147
4.4.5	Functional Correlates with Myocardial Velocities.....	147
4.4.6	Relationship between Myocardial Velocity and Clinical Worsening	150
4.5	Discussion	152
4.5.1	LV Myocardial Velocities in PH	152
4.5.2	Functional Correlates with Myocardial Velocities.....	154
4.5.3	Using TPM to assess RV function in PH.....	155
4.6	Limitations	156
4.7	Conclusions	157
CHAPTER 5 Conclusions and Future Work		158
5.1	Summary	159
5.2	Future Work	160
5.2.1	Three-Dimensional Echocardiography of the RV.....	160

5.2.1.1	3DE RV acquisition.....	160
5.2.1.2	3DE RV post-processing	162
5.2.2	Two-Dimensional Knowledge-Based Reconstruction of the RV ...	162
5.2.3	Tissue Phase Mapping for Myocardial Mechanics.....	164
5.3	Conclusion.....	166
References		167
Appendix 1		199
Appendix 2		212
Appendix 3		223
Appendix 4		235
Appendix 5		272
Appendix 6		280
Appendix 7		290

List of Figures

Figure 1-1: Drawings of the RV by Leonardo da Vinci.	23
Figure 1-2: A 3D multi-plane reconstruction of the RV from a balanced SSFP whole heart CMR sequence.	25
Figure 1-3: Normal human LV and RV pressure–volume loops.	26
Figure 1-4: The responses of the RV and LV to increases in afterload. .	27
Figure 1-5: RV major and minor axes end-diastolic dimensions measured in the 4-chamber view on transthoracic echocardiography.	29
Figure 1-6: RV fractional area change from the 4-chamber view in end-diastole (top) and end-systole (bottom) from a 2DE of a patient with PH.	30
Figure 1-7: RV S' using pulsed tissue Doppler imaging (TDI).	32
Figure 1-8: Offline analysis of RV colour-coded tissue Doppler.	32
Figure 1-9: RV TAPSE obtained from a zoomed M-mode image.	33
Figure 1-10: RV Tei index obtained by the separate acquisition of pulsed-wave Doppler of the tricuspid valve inflow (above) and RV outflow (below).	35
Figure 1-11: RV Tei index obtained by tissue Doppler imaging of the RV lateral tricuspid annulus.	35
Figure 1-12: Vector velocity imaging (VVI) speckle tracking echocardiography (STE) of the RV of a healthy volunteer.	36
Figure 1-13: A short-axis stack (in end-systole) of cines obtained from a healthy volunteer using a radial k-t SENSE CMRI sequence.	37
Figure 1-14: A transaxial stack (in end-diastole) of cines for RV volumetric analysis obtained from a healthy volunteer using a radial k-t SENSE CMRI sequence.	39
Figure 1-15: Severe carcinoid heart disease affecting the tricuspid (a-d) and pulmonary (e-f) valves.	48
Figure 2-1: Schematic of ECG-triggered multiple-beat 3DE data acquisition. Narrow pyramidal sub-volumes from four consecutive	

cardiac cycles are stitched together to form a single pyramidal volumetric data set.....	54
Figure 2-2: ECG-gated multiple beat 3DE of the RV. Figure (a) shows a volumetric RV data set with no stitching and good image quality on the short-axis slices (b) following acquisition. Figure (c) demonstrates stitching artefact (red dotted line) caused by breathing during scan acquisition, with stitching visible on reconstruction of the sub-volumes in the short-axis slices (d).....	55
Figure 2-3: The disk summation technique for 3DE RV reconstruction. .	57
Figure 2-4: The results of a semi-automated RV endocardial border detection algorithm, with the border tracking through the cardiac cycle in the sagittal (three levels), 4-chamber and coronal views displayed to the operator.	58
Figure 2-5: Surface-rendered cast of the RV following 3DE reconstruction with a time curve of global function during the cardiac cycle.....	59
Figure 2-6: A pyramidal dataset focusing upon a dilated RV in 4-chamber, sagittal and coronal views.....	65
Figure 2-7: Optimization of the RV cavity area in the three orthogonal views, and identification of landmarks.	66
Figure 2-8: The results of semi-automated border tracking.	68
Figure 2-9: Study protocol to investigate test-retest variability of 3DE assessment of the RV.....	69
Figure 2-10: A transaxial RV stack by CMRI with manual endocardial border tracing in end-diastole from a healthy volunteer using a radial k-t SENSE sequence.	70
Figure 2-11: Box and whisker plots of subjective image quality scores amongst three successive subgroups of patients (group 1 acquired in the earliest phase of the study, group 3 in the latest phase of the study). Image quality significantly improved with increasing experience with 3DE.....	74
Figure 2-12: Box and whisker plots of differences in stroke volume between modalities (expressed as a percentage of the CMRI reference value) for image scoring groups 1 to 4. There is a trend,	

albeit not statistically significant, for intermodality difference to increase with reductions in subjective image score. Median percentage intermodality differences in stroke volume (with 25 th to 75 th percentiles) by image score group were as follows: group 1 = 22% (-1 to 26), group 2 = 11% (-2 to 23), group 3 = 9% (3 to 16), group 4 = 2% (-6 to 19).....	75
Figure 2-13: Bland Altman analysis of bias (black solid line) and 95% limits of agreement (red dashed line) for 3DE versus CMRI quantification of RV EDV, ESV, SV and EF in patients with PH and carcinoid heart disease.....	78
Figure 2-14: Bland Altman analysis of bias (black solid line) and 95% limits of agreement (red dashed line) for 3DE versus CMRI quantification of RV EDV, ESV, SV and EF for subjects in the control populations.....	78
Figure 2-15: Receiver operating curves for 3DE, fractional area change (FAC), RV free wall peak systolic strain by speckle tracking echocardiography, and tricuspid annular plane systolic excursion (TAPSE) to identify RV dysfunction (defined as RVEF <50% by CMRI).....	79
Figure 2-16: Right ventricular outflow tract (RVOT) dropout by 3DE: (a) sternum or lung tissue commonly shadows the anterior RVOT; (b) due to the anterior retrosternal position and morphology of the RVOT, the anterior RVOT still might not be included in the 3DE pyramidal volume despite moving rib spaces in an attempt to avoid this shadowing. Adapted from Ostenfeld et al.[128].	84
Figure 3-1: Schematic of the 2DKBR set-up.....	94
Figure 3-2: Stage 1 of PSSS: Abstract control meshes for both RV (left) and LV (right) used by the PSSS reconstruction technique. These meshes incorporate knowledge about the location and shape of certain ventricular structures.....	96
Figure 3-3: Stage 2 of PSSS: The smooth surfaces of the LV (mesh) and RV (surface) having undergone the second stage of PSSS, entailing subdivision of the previously applied control mesh.....	97

Figure 3-4: Forest plots of results from previous studies of RV quantification by 2D KBR versus CMRI.	100
Figure 3-5: 2DKBR apparatus.....	104
Figure 3-6: Post-processed 2DKBR data from a participant with PH. ..	107
Figure 3-7: Bland Altman analysis of bias (black solid line) and 95% limits of agreement (red dashed line) for 2DKBR versus CMRI quantification of RV EDV, ESV, SV and EF. n = 27 (1 patient excluded due to movement artifact during 2DKBR study).	113
Figure 3-8: Bland Altman analysis of bias (black solid line) and 95% limits of agreement (red dashed line) for interobserver 2DKBR test-retest reproducibility of RV EDV, ESV, SV and EF. n = 25 (3 patients excluded due to movement artifact during 2DKBR study).	114
Figure 3-9: Demonstration of the interaction between the reconstructed 2DKBR polygon with a 4-chamber view 2DE scan plane.	119
Figure 4-1: Tissue tagging in a healthy volunteer from preparation pulse (left pane) through systole (middle pane) and into diastole (right pane), by which point the tag lines are fading.	128
Figure 4-2: In vivo systolic displacement measured by DENSE. (a) A displacement map showing through-plane motion. (b) A displacement map showing in-plane motion. (c) Magnitude reconstruction of the DENSE raw data.	129
Figure 4-3: Longitudinal strain measured by SENC.....	130
Figure 4-4: A TPM data set from a healthy volunteer. Clockwise from top left: magnitude data, and phase data in Z (through-plane), X and Y directions.....	132
Figure 4-5: LV velocity vector plots from a healthy volunteer and a PH patient at four time points in the cardiac cycle (indicated by the ECG trace).....	142
Figure 4-6: Line graphs of global radial, longitudinal and tangential LV velocities in a healthy volunteer (solid line) and a PH patient (dotted line).	144
Figure 4-7: Graphs demonstrating segmental variation in health (dotted line) and PH (--- line) in (a) E_{rad} time to peak, (b) E_{long} magnitude.	145

Figure 4-8: Velocity colour maps for (a) radial, (b) longitudinal, and (c) tangential LV motion from a control (top) and a PH patient (bottom).	146
Figure 5-1: A 3DE RV data set from a patient with severe carcinoid heart disease following administration of intravenous agitated colloid. ...	161
Figure 5-2: A 4D TPM breath hold data set from a healthy volunteer...	166

List of Tables

Table 1-1: Reproducibility studies of CMR metrics of RV size and function	40
Table 1-2: 2DE-derived metrics of RV function correlated against CMRI-derived RVEF.....	42
Table 1-3: Value of 2DE-derived metrics of RV function to identify RV dysfunction defined by CMRI.....	43
Table 1-4: Classification of pulmonary hypertension based upon aetiology. Reproduced from 5 th World Symposium on pulmonary hypertension (WSPH), Nice 2013.....	46
Table 1-5: Classes of drugs used to treat pulmonary hypertension.....	47
Table 2-1: Studies of test-retest reproducibility of 3DE RV assessment.	61
Table 2-2: Clinical characteristics of study populations	73
Table 2-3: Bias, limits of agreement and correlation between single-beat 3DE and CMRI for RV volumes and EFs.....	76
Table 2-4: RV volumes and EFs by single-beat 3DE versus CMRI.....	77
Table 2-5: Interobserver and intraobserver reproducibility for RV volumes and EF by 3DE and CMRI	80
Table 2-6: Interobserver and intraobserver test-retest reproducibility for RV metrics by 3DE.....	81
Table 3-1: Studies of RV quantification by 2D KBR versus CMRI	99
Table 3-2: Landmarks plotted in each 2DE RV plane to enable 2DKBR reconstruction.	108
Table 3-3: Patient characteristics.....	111
Table 3-4: RV volumes and ejection fractions by 2DKBR versus CMRI	112
Table 3-5: Test-retest reproducibility results for 2DKBR and 2DE RV metrics.	114
Table 3-6: Interobserver and intraobserver test-retest reproducibility of RV volumes and EF by 2DKBR, and RV areas and FAC by 2DE .	115
Table 4-1: Patient characteristics.....	140
Table 4-2: CMRI characteristics of control subjects versus PH patients	141

Table 4-3: Peak global myocardial velocities in controls versus patients with PH.....	143
Table 4-4: Correlations between abnormal global LV myocardial velocities in PH and haemodynamics.....	147
Table 4-5: Correlates of conventional and novel CMRI metrics with 6-MWD in pulmonary hypertension.....	149
Table 4-6: Univariate Cox regression analysis of conventional and novel CMRI metrics to predict disease progression in PH.	152

List of Equations

Equation 1-1: Fractional area change	31
Equation 1-2: Tei index	34
Equation 2-1: Stroke volume.....	70
Equation 2-2: Ejection fraction	70

List of Abbreviations

2D	Two-dimensional
2DE	Two-dimensional echocardiography
3D	Three-dimensional
3DE	Three-dimensional echocardiography
6-MWD	6-minute walking distance
BPM	Beats per minute
BSA	Body surface area
CHD	Carcinoid heart disease
CI	Confidence interval
CMRI	Cardiac magnetic resonance imaging
CO	Cardiac output
COV	Coefficient of variation
CTD	Connective tissue disease
CTEPH	Chronic thromboembolic pulmonary hypertension
DENSE	Displacement encoding with stimulated echoes
E_{long}	Peak longitudinal E wave
E_{rad}	Peak radial E wave
$E_{1\text{tang}}$	Peak first tangential E wave
$E_{2\text{tang}}$	Peak second tangential E wave
EDV	End-diastolic volume
EF	Ejection fraction
ESV	End-systolic volume
FAC	Fractional area change
FOV	Field of view
HR	Heart rate
ICC	Intraclass correlation coefficient
IQR	Interquartile range
KBR	Knowledge-based reconstruction
k-t	k-space and time
LOA	Limits of agreement
LV	Left ventricular
mPAP	Mean pulmonary artery pressure
PAH	Pulmonary arterial hypertension

PCMR	Phase-contrast magnetic resonance
PCWP	Pulmonary capillary wedge pressure
PH	Pulmonary hypertension
PSSS	Piecewise smooth subdivision surface
PVR	Pulmonary vascular resistance
RD	Relative difference
RHC	Right heart catheterization
ROC	Receiver operating characteristic
ROI	Region of interest
RV	Right ventricular
RVOT	Right ventricular outflow tract
S_{long}	Peak longitudinal S wave
S_{rad}	Peak radial S wave
$S1_{\text{tang}}$	Peak first tangential S wave
$S2_{\text{tang}}$	Peak second tangential S wave
SC	Septal curvature
SD	Standard deviation
SENC	Strain encoded
SENSE	Sensitivity encoded
SNR	Signal-to-noise ratio
STE	Speckle tracking echocardiography
SV	Stroke volume
T	Tesla
TAPSE	Tricuspid annular plane systolic excursion
TDI	Tissue Doppler imaging
TE	Echo time
TPM	Tissue phase mapping
TR	Repetition time
VENC	Velocity-encoded
VPS	Volumes per second
VVI	Vector velocity imaging
WHO	World Health Organization

CHAPTER 1 Non-invasive Imaging of the Right Ventricle

1.1 Introduction

Quantification of right ventricular (RV) size and function is prognostic in congenital and acquired heart disease[1-4]. However, this has proven challenging throughout history, and remains so in modern day cardiology.

1.1.1 The right ventricle: a historical perspective

The Greek philosopher Aristotle (384 – 322 B.C.) was the first to characterize the anatomy of the heart and circulation[5]. He described the right and left ventricles as part of a three-chambered model, with the right atrium separately identified as a morphological venous lake. Galen (129 – c. 200/c. 217 A.D.), a Greek physician, surgeon and philosopher, instead suggested that the right ventricle (RV) directly pulled in blood that had been created in the liver[6]. This theory of cardiac structure persisted throughout medieval Europe until the Renaissance revival of anatomy. Leonardo Da Vinci (1452 – 1519 A.D.) was the first person to accurately recognize the heart as a four-chambered structure. He was also credited for identifying the moderator band of the RV, albeit suggesting its function was to moderate the size of the RV by preventing its over-distension (Figure 1-1)[6-8]. Sir William Harvey in 1616 was the first person to correctly describe the function of the RV, stating that, “the right ventricle may be said to be made for the sake of transmitting blood through the lungs, not for nourishing them”[9, 10].

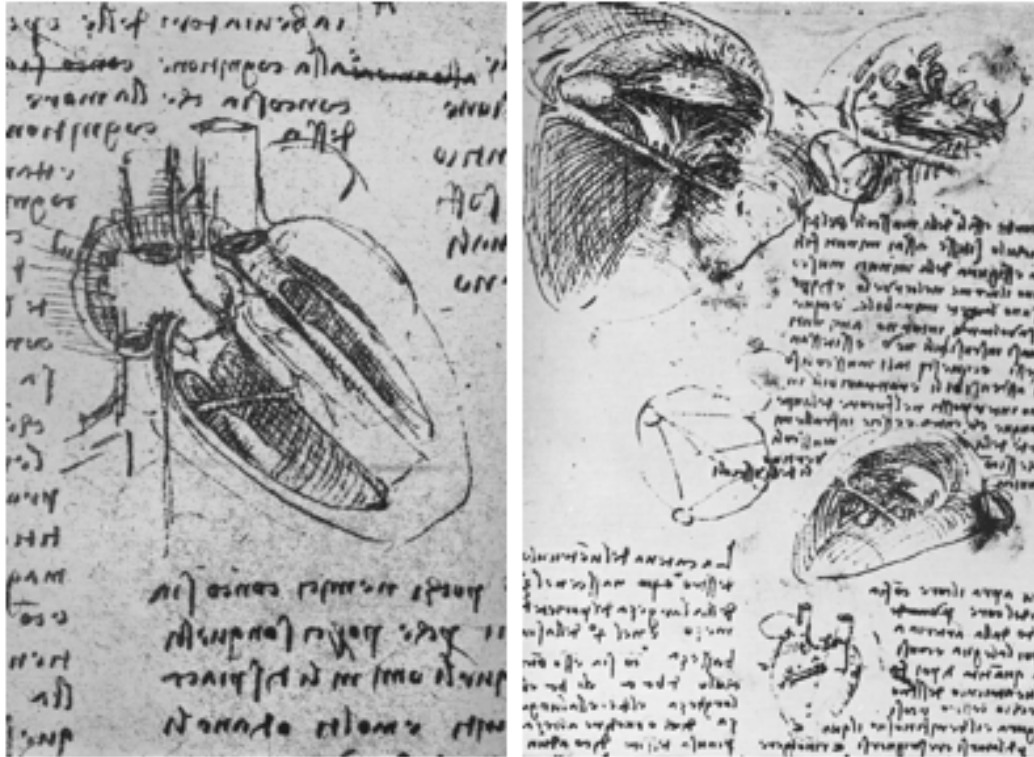


Figure 1-1: Drawings of the RV by Leonardo da Vinci.

From Quaderni d'Anatomia II (left) and IV (right). Reproduced from Leonardo da Vinci on movement of the heart and blood, K. D. Keele, 1952.

Importantly, Da Vinci's anatomical notes consistently refer to the intimate relationship between form and function in nature. This is exemplified by the anatomy and physiology of the RV: a thin-walled highly compliant cardiac chamber, accepting and ejecting blood as part of a low-pressure circulation. Da Vinci's anatomical drawings and notes were not fully published though until the early twentieth century, and hence did not significantly impact upon the fields of anatomy or physiology for several centuries[11]. Similarly, the RV is often described as a "forgotten" or "neglected" cardiac chamber, with a lack of awareness of the crucial role it plays in cardiac and pulmonary vascular diseases[12, 13]. In the first half of the twentieth century, animal studies focused upon the hypothesis that circulatory haemodynamics would not be compromised in the absence of RV contractile function. Experimental ablation of the RV was shown to neither reduce cardiac output nor increase systemic venous pressure in open-pericardium canine models[14, 15]. The importance of ventricular interdependence was neglected in this model, however, and

was only appreciated approximately thirty years later in a closed-chest canine model of RV infarction[16, 17]. Furthermore, surgical bypass of the RV by the Fontan procedure as a treatment for tricuspid atresia initially suggested that this cardiac chamber was functionally close to irrelevant[18]. Finally, the absence of any medical treatment for RV dysfunction contributed to prevent any serious consideration of investing time and money in this area.

The physiological importance of the RV, however, has increasingly been recognized in recent decades across a spectrum of congenital and acquired heart disease. In patients with left ventricular (LV) dysfunction for example, the presence of associated RV dysfunction is an independent predictor of worse prognosis[1, 2, 4]. In patients with pulmonary hypertension (PH) due to untreated severe mitral stenosis, RV failure may be the cause of death in as many as 60% to 70% of patients[19]. Heart failure due to RV dysfunction in congenital heart disease is both common and closely related to prognosis[20]. In PH, both symptom burden and survival are principally determined by the ability of the RV to function against raised afterload, rather than the degree of elevation of pulmonary arterial pressure itself[21]. The weight of clinical evidence concerning the importance of RV dysfunction in cardiac disease led the National Heart, Lung, and Blood Institute to recently identify RV pathophysiology as a crucial area for research[22]. However, the complex anatomy and physiology of the RV make it difficult to functionally assess by non-invasive cardiac imaging techniques.

1.1.2 RV anatomy

The RV is the most anteriorly positioned cardiac chamber, located immediately behind the sternum. It is thin-walled, normally 3-5mm in health, with prominent trabeculations and a complex geometry. Under normal loading conditions, the RV has a triangular shape when viewed from the side and a crescentic shape in the sagittal plane, wrapping around the conical left ventricle (Figure 1-2). The RV outflow tract is

located antero-cephalad to that of the LV, resulting in a crossover arrangement of the RV and LV outflow tracts. The RV cavity is divided into three components, namely the inlet, apical and outlet portions (Figure 1-2)[23]. The inlet portion extends from the tricuspid valve annulus, delineating the atrioventricular junction, to the insertions of the papillary muscles into the RV wall. The apical portion contains muscular trabeculations that are coarser than those of the LV. The outlet portion extends to the pulmonary valve, the most superiorly located of the cardiac valves, and is supported by the muscular subpulmonary infundibulum. Unlike the mitral and aortic valves that are in fibrous continuity in the LV, the pulmonary valve is separated from the tricuspid valve by the ventriculo-infundibular fold. The septomarginal trabeculation on the RV side of the interventricular septum is Y-shaped, giving rise to anterior and posterior arms that cradle the ventriculo-infundibular fold. The moderator band originates from the body of the Y-shaped septomarginal trabeculation, and is a structure that identifies the morphological RV. This carries a fascicle of the right bundle branch to the parietal wall of the RV.

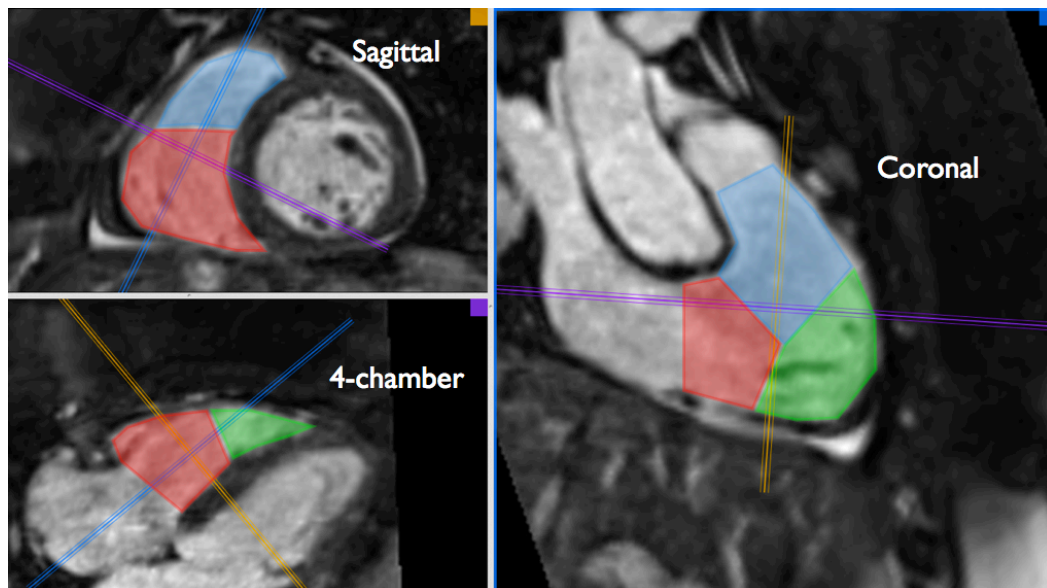


Figure 1-2: A 3D multi-plane reconstruction of the RV from a balanced SSFP whole heart CMR sequence.

The tripartite model of the RV is demonstrated, with inflow (red), outflow (blue), and apical (green) regions.

1.1.3 RV function

The orientation of RV myofibres and their arrangement into layers is responsible for the distinct contraction pattern of this chamber[23]. The superficial or subepicardial layer is composed of circumferentially oriented myofibres, parallel to the direction of the atrioventricular groove. The deep or subendocardial myofibres that line the RV cavity are aligned longitudinally from base to apex. These layers of differently aligned cardiomyocytes are responsible for the peristaltic RV contraction pattern starting at the inflow portion and progressing towards the infundibulum and outflow tract[24]. The longitudinal motion drawing the base towards the apex is accompanied by a bellows effect of inward motion of the free wall towards the interventricular septum, which bulges into the RV cavity[25].

Pressure-volume loops explain the relationship between RV contractility, preload and afterload. Under normal loading conditions the RV displays a trapezoidal-shaped pressure-volume loop (Figure 1-3)[26, 27].

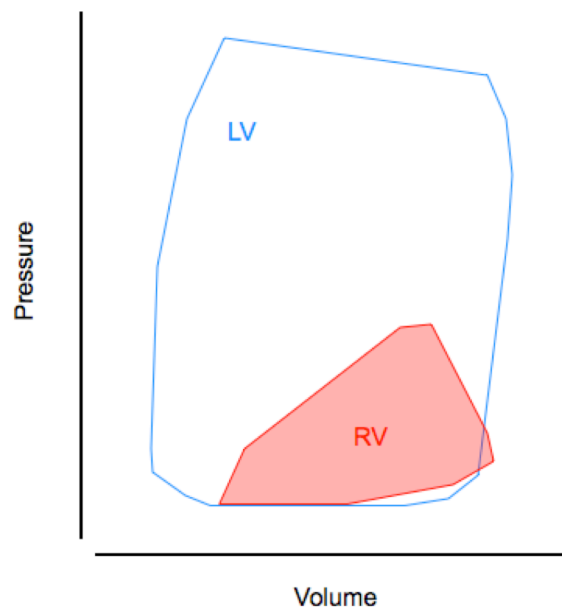


Figure 1-3: Normal human LV and RV pressure–volume loops.
The LV loop is rectangular, whereas the RV is more trapezoidal, with poorly defined isovolumic periods.

This is in contrast to the rectangular pressure-volume loop of the LV, which has well-defined isovolumic phases. Increased RV afterload results in a more square-shaped pressure-volume loop, but the RV has a much more limited capacity to adjust to these conditions than the LV (Figure 1-4)[28, 29]. The different embryological origin of RV myocytes from those of the LV might account, at least in part, for their differential responses when exposed to abnormal loading conditions[30-32]. Furthermore, both gene expression implicated in adaptive remodeling and the molecular changes in the myocardium in response to raised afterload differ between the LV and the RV[33-35].

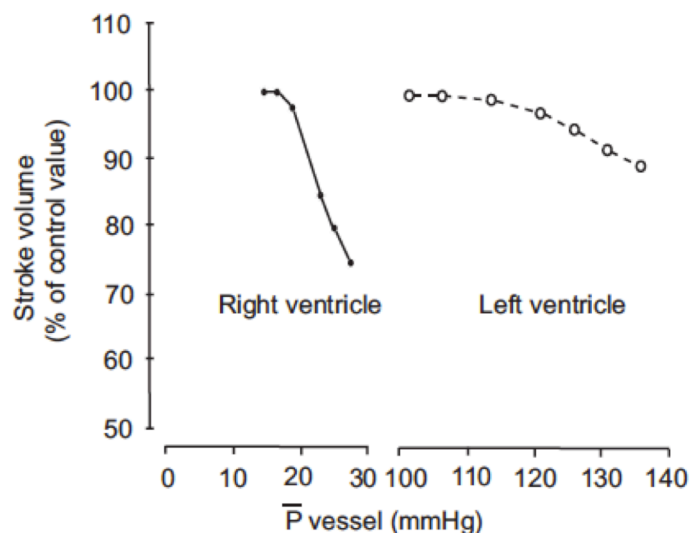


Figure 1-4: The responses of the RV and LV to increases in afterload.
Reproduced with permission from Haddad et al.[14]

1.1.4 Ventricular interdependence

Impaired LV performance in primary RV failure is not simply due to reduced RV stroke volume delivering lower LV preload via the pulmonary circulation. The direct effects of the size, shape and compliance of one ventricle on the same parameters of the other ventricle make a crucial contribution to the pathophysiology of RV dysfunction[36, 37]. Ventricular interdependence is mediated through three principal mechanisms: the interventricular septum, shared myocardial fibres, and a common pericardial sac.

The contribution of a shared septum to ventricular interdependence was first described in the early twentieth century. In patients with LV hypertrophy, encroachment of the interventricular septum on the RV cavity was noted to negatively affect RV filling, referred to as the Bernheim effect[38-40]. The “reverse Bernheim effect” has likewise been attributed to the deleterious impact on LV filling of abnormal interventricular septal dynamics in RV pressure or volume overload[41-44]. However, RV dilatation also reduces LV preload through raised LV diastolic pressure and increased intrapericardial pressure, manifest as pericardial constraint[16]. On the contrary, these haemodynamic abnormalities are not observed in open-pericardium animal models of RV distension.

Epicardial myofibres run in continuity across both ventricles, through which LV contraction in normal hearts can consequently give rise to traction of the RV free wall[14]. Chronic abnormalities of RV size, shape and contractility can thus result in LV microarchitectural abnormalities. Atrophic remodeling of the LV has been demonstrated in RV failure due to end-stage idiopathic PH[45], chronic thromboembolic PH[46], rheumatic mitral stenosis[47] and end-stage emphysema[48]. Furthermore, restoration of LV cavity size, stroke volume and mass has been shown to occur following pulmonary thromboendarterectomy, mitral valvuloplasty or orthotopic lung transplantation for these latter three conditions respectively.

1.2 Non-invasive imaging of the RV

Progressive developments in echocardiography and CMRI have brought these imaging modalities to the forefront of non-invasive RV assessment, without the need for ionizing radiation exposure.

1.2.1 2D Echocardiography

Despite the challenges of RV assessment using cardiac ultrasound, echocardiography remains the most widely utilized clinical imaging modality for this purpose. The American Society of Echocardiography recommends that RV size and systolic function should be measured by echocardiography in all clinical studies using at least one or a combination of the following parameters[49, 50].

1.2.1.1 2DE linear dimensions

The complex geometry and shape of the RV coupled with the relative paucity of anatomical landmarks confers difficulty for linear 2DE quantification of chamber size. Several linear 2DE measures have been suggested for assessing RV size[51]. The most reproducible metric is the RV basal diameter from an apical 4-chamber window, taken within one-third of the distance below the tricuspid valve annulus toward the RV apex (Figure 1-5)[52]. A basal diameter of >41mm from a RV-focused view is taken to indicate RV dilatation, although future work should be aimed at indexing these measures to body surface area. Furthermore, 2DE-derived linear dimensions do not correlate well with 3D-derived RV volumes[12, 53].

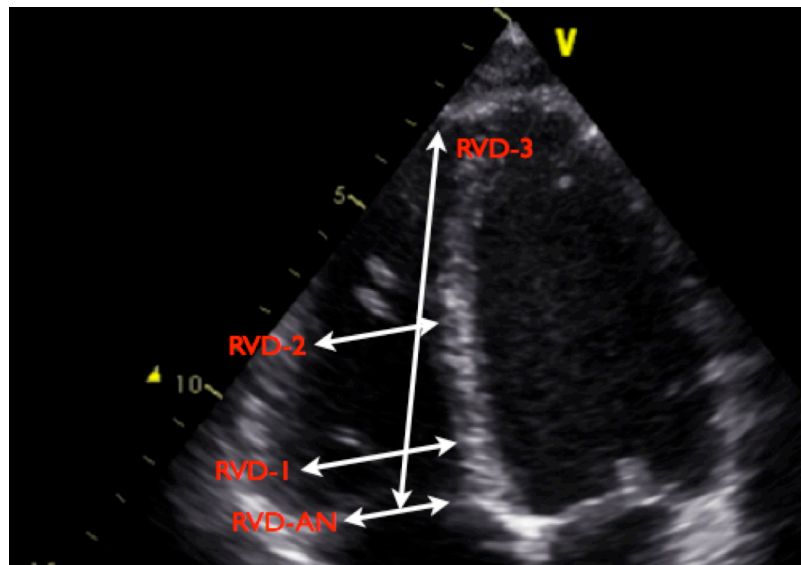


Figure 1-5: RV major and minor axes end-diastolic dimensions measured in the 4-chamber view on transthoracic echocardiography.

RVD-1 is the most reproducible 2DE RV dimension.

1.2.1.2 Fractional area change (FAC)

This is obtained by manually tracing the RV endocardial border in the 4-chamber view at end-diastole and at end-systole from the lateral tricuspid annulus along the free wall to the apex and back to medial tricuspid annulus, along the interventricular septum (Figure 1-6). The operator must include trabeculations, papillary muscles and the moderator band in the cavity area. Care must be taken to avoid foreshortening of the RV cavity.

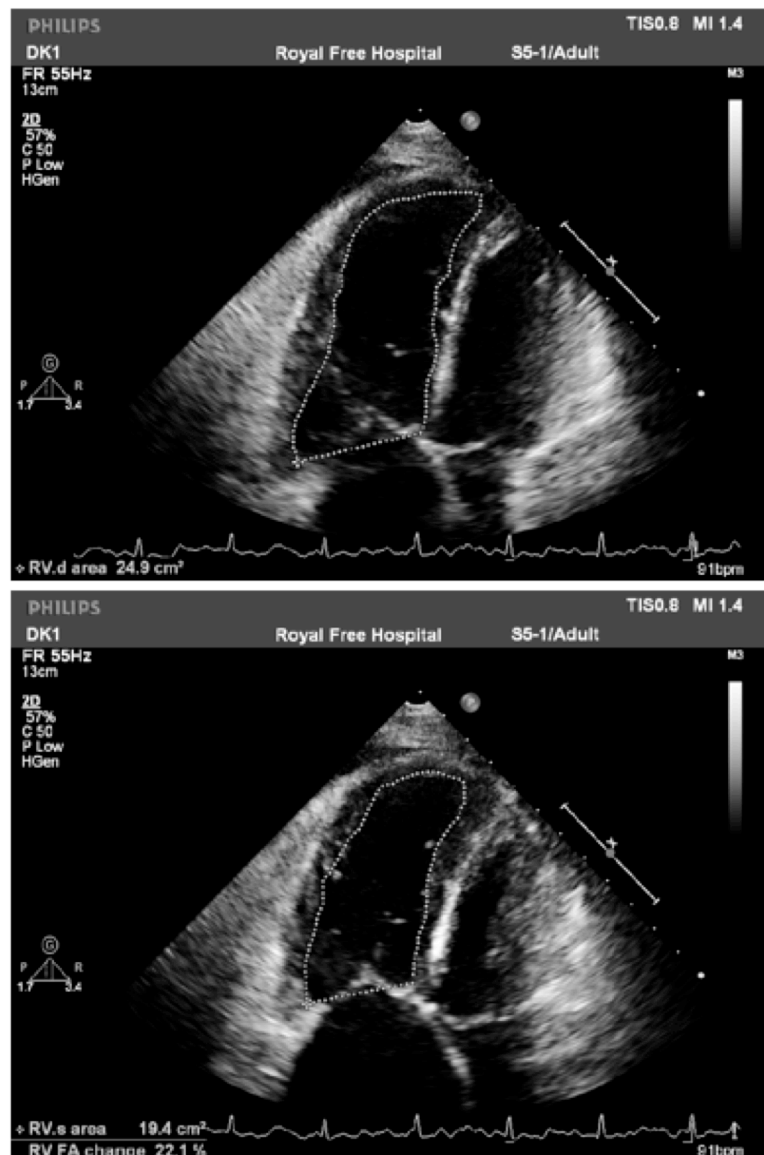


Figure 1-6: RV fractional area change from the 4-chamber view in end-diastole (top) and end-systole (bottom) from a 2DE of a patient with PH.

FAC is calculated as:

$$\frac{(\text{end diastolic area} - \text{end systolic area}) \times 100}{\text{end diastolic area}}$$

Equation 1-1: Fractional area change

RV FAC <35% is indicative of systolic dysfunction. This is a relatively easy measurement to acquire and reflects both longitudinal and radial components of RV contractility, which is particularly important in raised RV afterload[54]. However, this parameter completely neglects the contribution of the outflow portion of the RV to ejection, and hence may not accurately reflect global RV function. Furthermore, due to LV circumferential torsion and the crescentic shape of the RV, the end-diastolic and end-systolic RV images may be in different tomographic planes.

1.2.1.3 Doppler Tissue Imaging (DTI)-derived tricuspid lateral annular systolic velocity wave (S')

The motion of the lateral tricuspid annulus and the basal free wall segment can be reproducibly imaged from the apical 4-chamber window. Either pulsed tissue Doppler or colour-coded tissue Doppler can be used to measure the peak longitudinal velocity of excursion of the lateral tricuspid annulus and basal RV free wall, termed S'. An apical 4-chamber window optimized to visualize the RV is imaged, with S' obtained by one of two methods:

- (i) A tissue Doppler mode region of interest is placed over the RV free wall. The pulsed Doppler sample volume is placed over the tricuspid annulus and the basal segment of the RV free wall (Figure 1-7). The peak S' velocity is taken as the highest systolic velocity, with a value <9.5 cm/s indicating RV systolic dysfunction.
- (ii) The alternative approach is to acquire colour-coded tissue Doppler at high frame rates to be analyzed offline (Figure 1-8). This methodology provides lower velocities, because the encoded data represent mean rather than peak velocities.

Whilst easy to acquire, S' only provides a longitudinal measure of function, is angle-dependent, and is measured relative to the transducer. This parameter may therefore be influenced by overall heart motion. Furthermore, S' assumes that the function of a single RV region is representative of the function of the entire chamber.

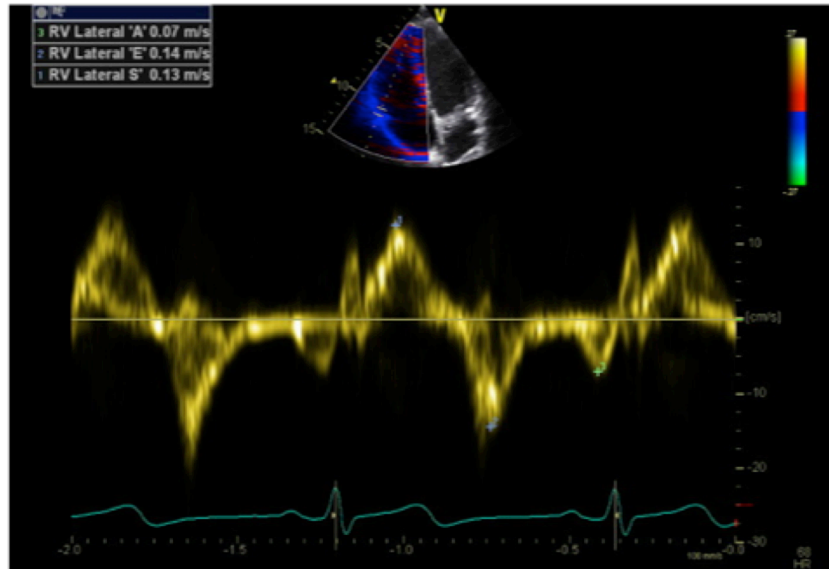


Figure 1-7: RV S' using pulsed tissue Doppler imaging (TDI).

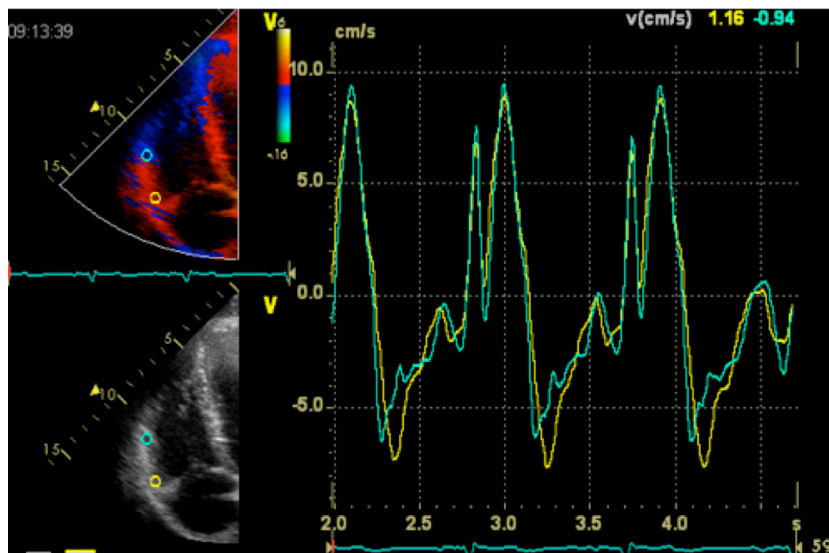


Figure 1-8: Offline analysis of RV colour-coded tissue Doppler.

1.2.1.4 Tricuspid Annular Plane Systolic Excursion (TAPSE)

The longitudinal systolic excursion of the lateral tricuspid annulus is visually readily apparent by 2DE. It can be measured by M-mode echocardiography with the cursor aligned along the direction of motion of the annulus in the apical four-chamber window (Figure 1-9). A cut-off value of <17mm indicates RV dysfunction. However, TAPSE is subject to translational motion of the RV rather than being reflective of myocardial shortening[55]. It is also angle-dependent and only represents the longitudinal motion of an isolated RV segment.

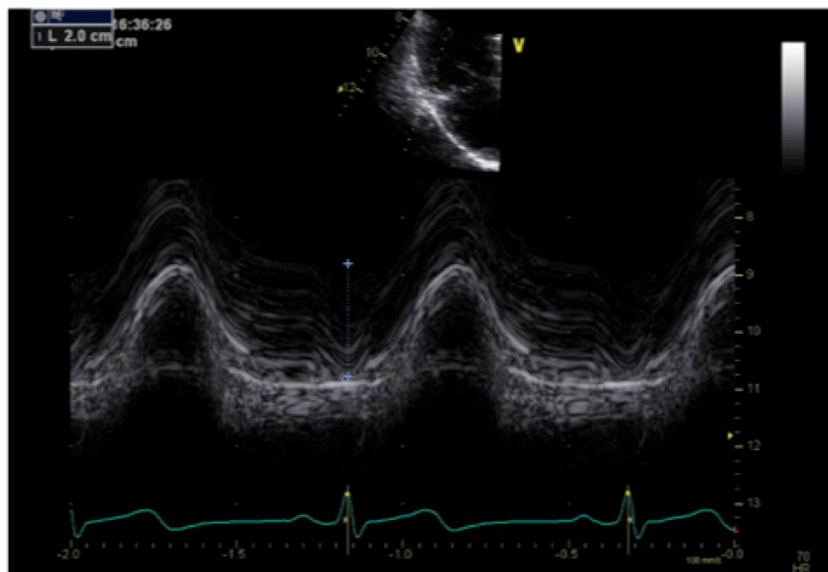


Figure 1-9: RV TAPSE obtained from a zoomed M-mode image.

1.2.1.5 RV index of myocardial performance (RIMP) / Tei Index

RIMP, also known as the Tei index or myocardial performance index (MPI), is described as both a global and physiological measure of RV function, since it combines information obtained in both systole and diastole. The MPI is defined as the proportion of the cardiac cycle effectively wasted in isovolumic time relative to the overall ejection time:

$$\frac{(\text{Isovolumic relaxation time} + \text{Isovolumic contraction time})}{\text{Ejection time}}$$

Equation 1-2: Tei index

The MPI can be obtained by two methods:

- (i) In the pulsed Doppler method, ejection time is measured by pulsed wave Doppler of RV outflow (time from the onset to the cessation of flow). The time period from tricuspid valve closure to opening is measured by pulsed wave Doppler of the tricuspid inflow (from the end of the trans-tricuspid A wave to the beginning of the trans-tricuspid E wave, Figure 1-10). These intervals are measured from different cardiac cycles in different echocardiography windows. Therefore beats with similar R-R intervals must be used, negating the application of this method in patients with arrhythmia. RIMP >0.43 by the pulsed wave Doppler method is defined as abnormal.
- (ii) Alternatively, all time intervals can be measured from a single cardiac cycle by using pulsed tissue Doppler of the tricuspid annulus (Figure 1-11). RIMP >0.54 by the DTI method suggests RV dysfunction.

Caution should be applied with RIMP in situations of raised right atrial pressure, as the value obtained can be pseudonormalized due to a reduced isovolumic relaxation time.

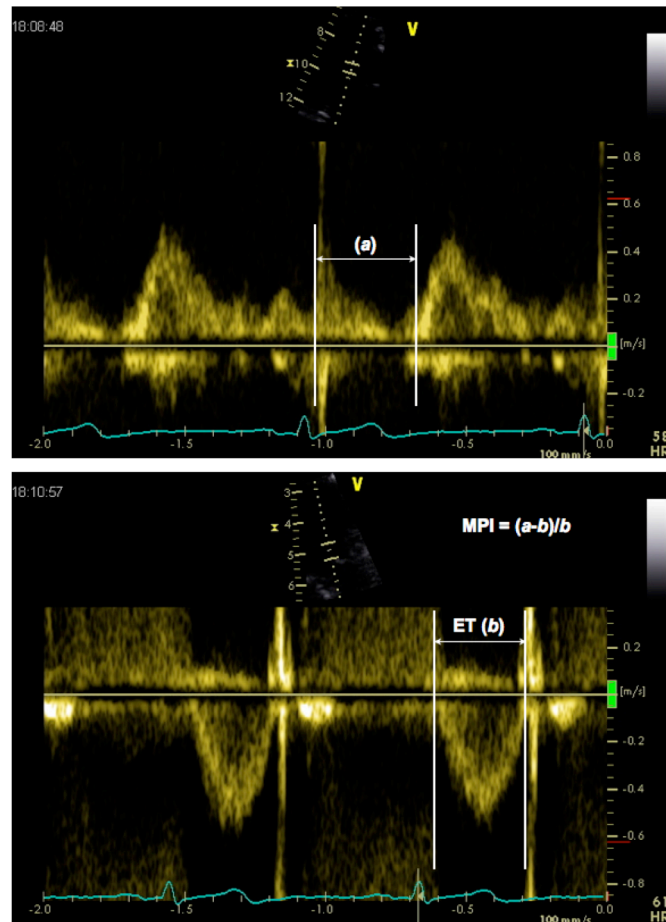


Figure 1-10: RV Tei index obtained by the separate acquisition of pulsed-wave Doppler of the tricuspid valve inflow (above) and RV outflow (below).

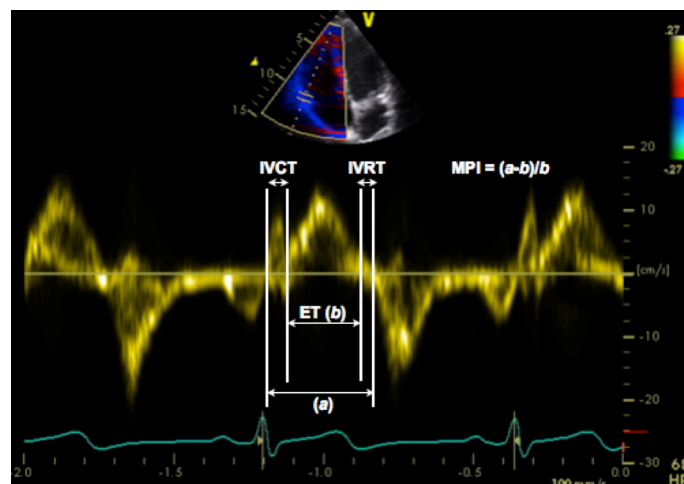


Figure 1-11: RV Tei index obtained by tissue Doppler imaging of the RV lateral tricuspid annulus.

1.2.1.6 Deformation imaging: strain and strain rate

Strain and strain rate are deformation parameters reflecting RV contractility. Strain is the percentage of systolic myocardial shortening, with this change over time measured by strain rate. RV longitudinal strain is determined by the percentage of systolic shortening of the free wall from base to apex in a RV-focused 4-chamber window (Figure 1-12). RV global longitudinal strain may either refer to the average of the RV free wall and the septal segments or the RV free wall segments alone, and must be considered when comparing studies.

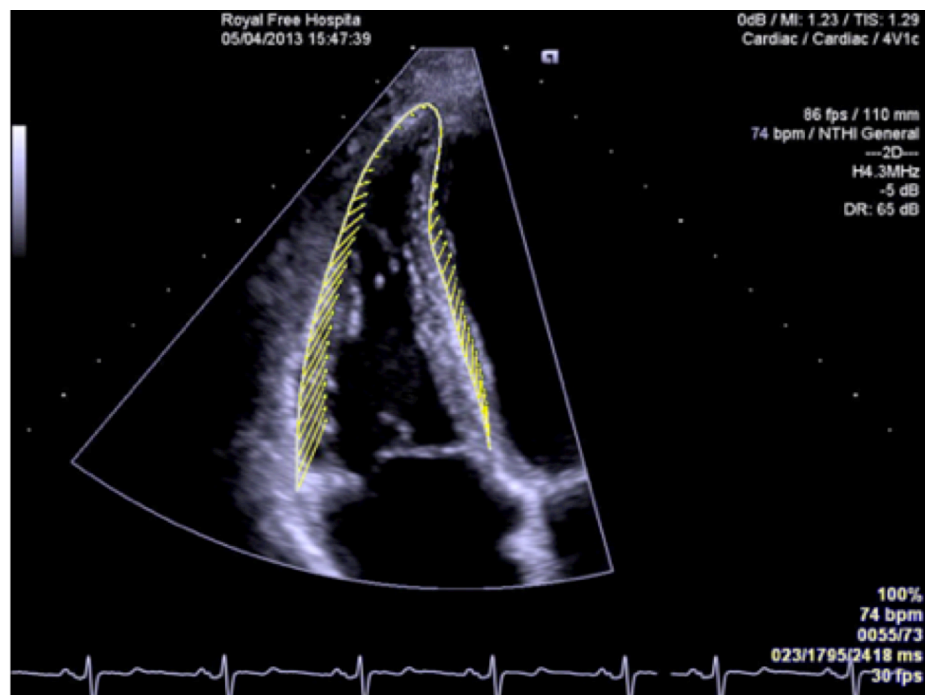


Figure 1-12: Vector velocity imaging (VVI) speckle tracking echocardiography (STE) of the RV of a healthy volunteer.

The direction and magnitude of the vectors represent myocardial deformation.

Deformation parameters can be measured using DTI, accepting the inherent limitations of angle dependency and lower signal from the mid-wall and apical segments. Alternatively, speckle-tracking echocardiography (STE) can be used. STE software performs frame-by-frame tracking of intrinsic myocardial speckles on sequential images using an algorithm involving correlation criteria and sums of absolute differences. Furthermore, vendor-specific post-processing smoothing

algorithms are applied, and in many cases this has been designed for application to the LV and later adapted for the RV.

STE requires high temporal resolution for accuracy, and care must be taken to avoid algorithmic smoothing compensating for poor quality 2DE datasets. Normative reference data are currently heavily weighted towards one vendor, and cannot be applied across all vendor platforms. However, global longitudinal RV free wall strain $> -20\%$ is generally regarded as abnormal.

1.2.2 Cardiac Magnetic Resonance Imaging (CMRI)

CMRI is the 'gold standard' imaging modality for assessing cardiac volumes[56, 57]. Image acquisition is not limited by windows afforded by intercostal rib spaces, body habitus or hyperinflated lungs, as can be the case with echocardiography. A contiguous stack of cines is acquired from the base to the apex of both ventricles (Figure 1-13). This cross-sectional approach also overcomes the complex shape and geometry of the RV that hinders 2D imaging approaches, allowing quantification of RV cavity volume measurements, stroke volume, ejection fraction and mass.

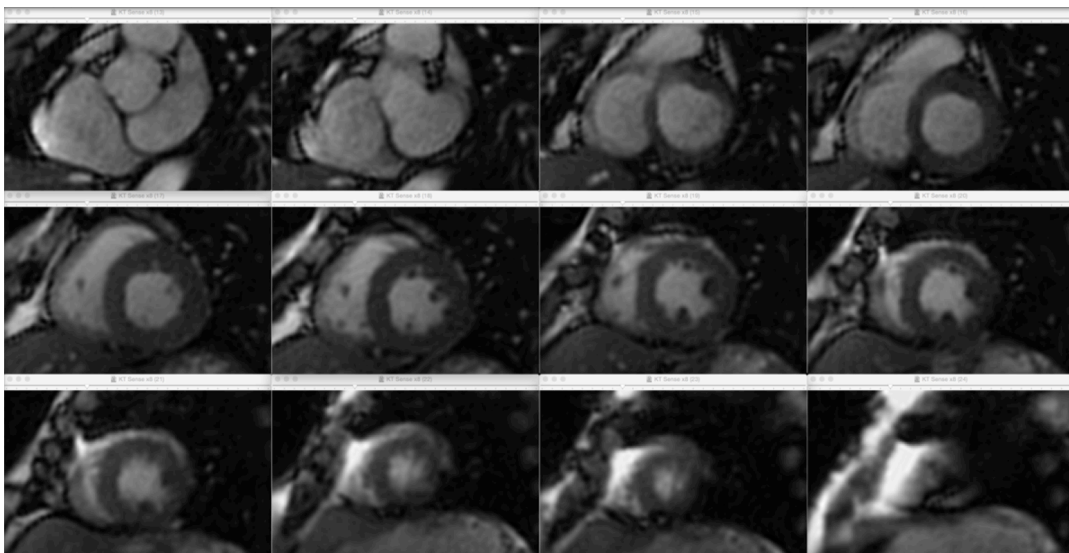


Figure 1-13: A short-axis stack (in end-systole) of cines obtained from a healthy volunteer using a radial k-t SENSE CMRI sequence.

Post-processing entails manual contouring for volumetric analysis. The endocardium is manually traced at end-diastole and end-systole for all slices in the stack of cines. Mass can also be derived by drawing epicardial regions of interest. End-diastolic and end-systolic volumes, ejection fraction and mass are then calculated by summation of the respective traced regions of interest, termed the disc summation method. The main difficulty in RV segmentation is distinguishing the endocardial border from the prominent trabeculations. Including RV trabeculations in the cavity blood pool volume is more reproducible and requires less post-processing time[58, 59]. It is clear that whichever methodology of RV segmentation is chosen, consensus training of professionals and standardization of post-processing protocols within clinical institutions is pivotal to optimizing RV quantification reproducibility by CMRI[60].

Whilst ideally suited for assessment of the RV, CMRI has well documented disadvantages. CMRI is significantly more expensive and less readily available than echocardiography[61]. The majority of permanent pacemakers and implantable cardiac defibrillators are considered a contraindication to MRI by the United States Food and Drug Administration (FDA) and by device manufacturers. However, the number of patients with an implanted pacing device that are estimated to require investigation with MRI has directed the European Society of Cardiology (ESC) to issue safety precautions for MRI in these patients[62]. Patients who are claustrophobic may also not be able to undergo investigation by this modality. Some widely quoted disadvantages of MRI, however, can be readily overcome. The conventional approach of acquiring each slice with breath-hold cine imaging results in long acquisition times and potential problems with multiple breath holds. However, these limitations can be overcome with high spatio-temporal resolution real-time MRI[63]. Finally, the acquisition of cines by MRI for volumetric analysis does not require contrast agents.

As with any imaging technique, the reliability of CMRI depends upon standardization of image acquisition and post-processing. Overall, several studies have reported good and clinically acceptable intraobserver, interobserver and interstudy reproducibility metrics for RV assessment by CMRI (Table 1-1) [64-66]. Conventional short-axis stacks of cines that are more suited to LV volumetric analysis were acquired in these studies. Further improvements in reproducibility have been reported instead using a transaxial stack of cines specifically for RV analysis[67, 68] (Figure 1-14). This is likely due to a number of reasons: easier identification of the tricuspid and pulmonary valves; avoidance of difficulty identifying the basal slice in the short-axis stack; and eliminating inaccuracies in post-processing caused by through-plane longitudinal motion of the RV when acquired in the short-axis. Consequently, the acquisition of a transaxial stack of cines is recommended for dedicated RV volumetric analysis[69].

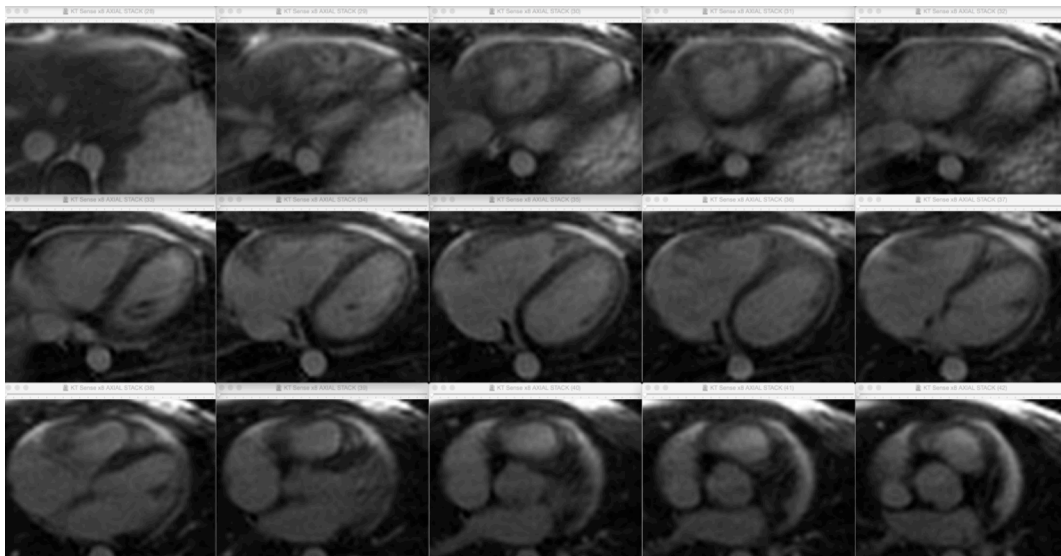


Figure 1-14: A transaxial stack (in end-diastole) of cines for RV volumetric analysis obtained from a healthy volunteer using a radial k-t SENSE CMRI sequence.

Investigator (year)	N	Study population	CMR sequence	Reproducibility study	CMRI-derived RV parameter: coefficient of variation (%)			
					EDV	ESV	EF	Mass
Grothues et al. (2004)	60	Normal subjects and patients with congestive heart failure or LVH	FLASH	Interstudy	6.2	14.1	8.3	8.7
Hudsmith et al. (2005)	12	Normal subjects	SSFP	(i) Intraobserver (ii) Interobserver (iii) Interstudy	(i) 9.0 (ii) 9.6 (iii) 7.4	-	(i) 5.3 (ii) 10.7 (iii) 11.4	-
Moolij et al. (2008)	60	Normal subjects or patients with ASD or TOF	SSFP	Interobserver	6.4	13.0	8.0	11.3

LVH = left ventricular hypertrophy, ASD = atrial septal defect, TOF = tetralogy of Fallot, FLASH = fast low-angle shot, SSFP = steady-state free precession

Table 1-1: Reproducibility studies of CMR metrics of RV size and function

1.2.3 RV assessment by 2DE versus CMRI

CMRI has been used as the reference standard for other modalities to quantitatively assess the RV for almost two decades[70]. Given the more limited availability and greater expense of this modality, some groups have instead attempted to define 2DE thresholds for stratifying those patients who may not require further RV assessment by CMRI [71]. However, 2DE measures of RV function, including 2D, M-mode, tissue Doppler and strain parameters, correlate poorly overall against CMRI-derived RV ejection fraction (EF) in both congenital and acquired RV disease populations[53, 72-79] (Table 1-2). Furthermore, different 2DE parameters have a diverse capacity for identifying RV dysfunction[73, 75, 77-79] (Table 1-3). The overall impression from this literature is that FAC, S' and RV systolic deformation parameters have the most superior profile for identifying CMRI-defined thresholds of RV dysfunction. FAC is consistently superior to TAPSE, likely due to the integration of radial and longitudinal components of motion, and also because the reference measure of RV EF by CMRI is similarly a global geometric parameter.

For these reasons, imaging modalities for the quantitative assessment of RV size and function should ideally use three-dimensional metrics[26].

Investigator (year)	N	Study population	Statistically significant r values against MRI-derived RVEF								
			FAC (%)	FLC (%)	S' (cm/s)	TAPSE (mm)	PGSS (%)	PLSS (%)	PSSR (s ⁻¹)	MPI	IVA (m/s ²)
Lytrivi et al. (2005)	35	Unselected children or adult congenital heart disease patients	-	-	0.29 (NS)	-	-	-	-0.33 (NS)	0.37	
Anavekar et al. (2007)	36	Unselected patients undergoing clinically indicated CMR	0.80	-	-	0.17 (NS)	-	-	-	-	
Wang et al. (2007)	53	Control subjects (n=43) and ARVC (n=10)	0.50	-	0.52	0.36*	-	0.41	0.35	0.14 (N/S)	
Lai et al. (2008)	87	Children or adults with: (i) Normal RV (n=31), (ii) Repaired TOF (n=33), (iii) ASD/PAPVC (n=23)	(i) 0.39 (NS) (ii) 0.54 (iii) 0.70	-	-	-	-	-	-	-	
Pavlicek et al. (2011)	233	Unselected congenital and acquired heart disease	0.47	0.38	0.48	0.34	-	0.36	-	0.43	
Van der Zwaan et al. (2011)	120	Congenital heart disease (RV: n=62; LV: n=27), healthy controls (n=31)	0.37	-	-	0.40	-	-	-	-	
Sato et al. (2012)	37	Consecutive patients with PH	0.40	-	0.63	0.86	-	-	-	-0.59	
Shiran et al. (2014)	45	Group I and group IV PH	0.87	-	-	0.80	-	-	-	-	
Focardi et al. (2015)	63	Unselected patients undergoing clinical CMR	0.77	-	0.52	0.45	-0.71	-0.86	-	-	

*Integral of tissue velocity utilized to measure tissue displacement.

FLC = Fractional long-axis change, PGSS = Peak global systolic strain (including septum), PLSS = Peak lateral systolic strain, PSSR = peak systolic strain rate, TOF=tetralogy of Fallot, ASD/PAPVC=atrial septal defect/partial anomalous pulmonary venous connection

Table 1-2: 2DE-derived metrics of RV function correlated against CMRI-derived RVEF.

Investigator (year)	N	Study population	CMRI definition of RV dysfunction	AUC								
				FAC (%)	FLC (%)	S' (cm/s)	TAPSE (mm)	PGSS (%)	PLSS (%)	PSSR (s ⁻¹)	MPI	IVA (m/s ²)
Wang et al. (2007)*	53	Control subjects (n=43) and ARVC (n=10)	RVEF <45%	0.83	-	0.87	0.82**	-	0.80	0.69	-	-
Pavlicek et al. (2011)	233	Unselected congenital and acquired heart disease	RVEF <50%	0.73	0.67	0.78	0.72	-	-	-	0.68	0.70
Van der Zwaan et al. (2011)	120	Congenital heart disease (I) EDVi >129mL/m ² (RV: n=62; LV: n=27), (ii) ESVi >58 mL/m ² , and/or (iii) RVEF <48%		0.76	-	-	0.72	-	-	-	-	-
Shiran et al. (2014)	45	Group I and group IV PH	RV FAC <35%	0.97	-	-	0.87	-	-	-	-	-
Focardi et al. (2015)	63	Unselected patients undergoing clinical CMR	RVEF <45%	0.78	-	-	0.66	0.78	0.92	-	-	-

*Stepwise multivariate analysis of all 2DE variables was performed to choose the best predictors of RVEF to undergo ROC analysis. Only FAC and S' independently predicted RVEF

**Integral of tissue velocity utilized to measure tissue displacement.

FLC = Fractional long-axis change, PGSS = Peak global systolic strain (including septum), PLSS = Peak lateral systolic strain, PSSR = peak systolic strain rate

Table 1-3: Value of 2DE-derived metrics of RV function to identify RV dysfunction defined by CMRI.

1.3 The RV in pressure- and volume-overload states

The comparison of two distinct imaging modalities is, at least in part, a reflection of the homogeneity of the subject cohorts that are studied. Acquired primary RV pressure- and volume-overload in vivo is best represented by the disease states of pulmonary hypertension (PH) and carcinoid heart disease (CHD) respectively.

1.3.1 Pressure-overload of the RV: Pulmonary Hypertension

The pathologic abnormalities in pulmonary arterial hypertension (PAH) constitute vasoconstriction, remodeling and endothelial proliferation of the pulmonary arterial tree. This culminates in raised pulmonary vascular resistance. The condition carries a high mortality rate of 20% to 40% at three years post-diagnosis[17]. However, the degree of raised pulmonary pressure is only of modest prognostic significance. It is, rather, the ability of the RV to function against this raised afterload that is the key determinant of symptoms and mortality[21]. Thus CMRI is ideally placed to provide highly prognostic data through RV functional quantification in PH[80, 81]. Moreover, interventricular septal dynamics assessed by both echocardiography and CMRI are highly revealing of the afterload conditions facing the RV[82-85].

PH can be due to a variety of causes, all of which require a tailored therapeutic approach (Table 1-4)[86]. Patients with PAH in whom the RV is more adapted to working against higher afterload, such as Eisenmenger's syndrome, have a better survival despite higher pulmonary pressures than those with a previously normal RV, such as idiopathic PAH[87]. Moreover, patients with idiopathic PAH have a better survival than those with systemic sclerosis-associated PAH despite similar pulmonary pressures[88]. Overall, patients with systemic-sclerosis associated PAH have the worst prognosis of all of the underlying disease aetiologies[89, 90]. The prognostic heterogeneity related to the cause of PAH is most likely due to the nature of RV involvement in the disease process. It is suggested that patients with Eisenmenger's syndrome retain

a foetal RV phenotype, whereby RV wall thickness equals that of the LV, from infancy to adolescence and adulthood[91]. The ability for the RV to offload via a right-to-left shunt may also contribute to the improved survival of the Eisenmenger's syndrome group, akin to the rationale of atrial septostomy as an interventional approach for decompensated PAH[92]. Patients with systemic sclerosis-associated PAH likely fare worst as a result of intrinsic RV systolic dysfunction possibly due to replacement fibrosis, further impairing the response to pulmonary arteriopathy[88].

Prior to the advent of medical therapies targeted at the reduction of pulmonary pressures, the field of PAH was morbidly referred to as "the kingdom of the near-dead"[93]. Pathobiological pathways targeted by PAH pharmacotherapy include endothelin, nitric oxide, platelet-derived growth factor and prostacyclin pathways (Table 1-5). These are introduced as monotherapy or combination therapy in an algorithmic approach[94]. Whilst there are no specific medical therapies available for the treatment of RV dysfunction, not all pulmonary vasodilator therapies are equal in terms of their impact on RV function. For example, sildenafil increases RV contractility through direct effects on the RV myocardium independent of its pulmonary vasodilator activity in a monocrotaline rodent model of PH[95].

-
- 1 Pulmonary arterial hypertension (PAH)**
 - 1.1 Idiopathic PAH
 - 1.2 Heritable PAH
 - 1.3 Drug and toxin induced
 - 1.4 Associated with:
 - 1.41 Connective tissue disease
 - 1.42 Human immunodeficiency virus (HIV) infection
 - 1.4.3 Portal hypertension
 - 1.4.4 Congenital heart diseases
 - 1.4.5 Schistosomiasis
 - 1' Pulmonary veno-occlusive disease and/or pulmonary capillary haemangiomatosis
 - 1'' Persistent pulmonary hypertension of the newborn (PPHN)
 - 2 Pulmonary hypertension due to left heart disease**
 - 2.1 Left ventricular systolic dysfunction
 - 2.2 Left ventricular diastolic dysfunction
 - 2.3 Valvular disease
 - 2.4 Congenital/acquired left heart inflow/outflow tract obstruction and congenital cardiomyopathies
 - 3 Pulmonary hypertension due to lung diseases and/or hypoxia**
 - 3.1 Chronic obstructive pulmonary disease
 - 3.2 Interstitial lung disease
 - 3.3 Other pulmonary diseases with mixed restrictive and obstructive pattern
 - 3.4 Sleep-disordered breathing
 - 3.5 Alveolar hypoventilation disorders
 - 3.6 Chronic exposure to high altitude
 - 3.7 Developmental lung diseases
 - 4 Chronic thromboembolic pulmonary hypertension (CTEPH)**
 - 5 Pulmonary hypertension with unclear multifactorial mechanisms**
 - 5.1 Haematologic disorders: chronic haemolytic anemia, myeloproliferative disorders, splenectomy
 - 5.2 Systemic disorders: sarcoidosis, pulmonary histiocytosis, lymphangioleiomyomatosis
 - 5.3 Metabolic disorders: glycogen storage disease, Gaucher disease, thyroid disorders
 - 5.4 Others: tumoural obstruction, fibrosing mediastinitis, chronic renal failure, segmental PH
-

Table 1-4: Classification of pulmonary hypertension based upon aetiology. Reproduced from 5th World Symposium on pulmonary hypertension (WSPH), Nice 2013.

Pathobiologic pathway targeted	Drugs
Endothelin	
Endothelin receptor antagonists	Ambrisentan, Bosentan, Macitentan
Nitric Oxide	
Soluble Guanylate Cyclase Stimulators	Riociguat
Phosphodiesterase Type-5 Inhibitors	Sildenafil, Tadalafil, Vardenafil
Platelet-Derived Growth Factor	
Tyrosine kinase inhibitor	Imatinib
Prostacyclin	
Prostanoids	Beraprost, Epoprostenol, Iloprost, Treprostinil
Prostacyclin IP-receptor Agonists	Selexipag

Table 1-5: Classes of drugs used to treat pulmonary hypertension.

1.3.2 Volume-overload of the RV: CHD

Carcinoid is a slow-developing cancer of the neuroendocrine system, occurring in approximately 1-2.5 per 100,000 of the population[96]. Carcinoid syndrome occurs when the tumour metastasizes to the liver, and vasoactive amines and peptides secreted by carcinoid tumour cells including 5-hydroxytryptamine (5HT) are able to reach the systemic circulation. CHD is present in up to 20% of patients with carcinoid syndrome at diagnosis, and is an independent predictor of worse prognosis[97]. CHD results from circulating 5HT reaching the right heart, causing the endocardial deposition of fibrous plaques on the tricuspid and pulmonary valves. Valve leaflets/cusps become thickened, retracted and have reduced mobility, eventually becoming fixed[98] (Figure 1-15). Functionally a combination of valvular regurgitation and stenosis occurs. Many patients are initially asymptomatic despite severe disease, but symptoms ultimately result from ensuing right heart volume-overload and systolic dysfunction[99]. Without valve replacement surgery, patients with RV dilatation have a worse outcome[100]. Valve replacement offers symptomatic relief and probable survival advantage, but predicting the optimal time to operate remains imprecise[101]. This decision will involve

an assessment of the impact of the valvulopathy on RV function, the monitoring of which by CMRI has been suggested[102].

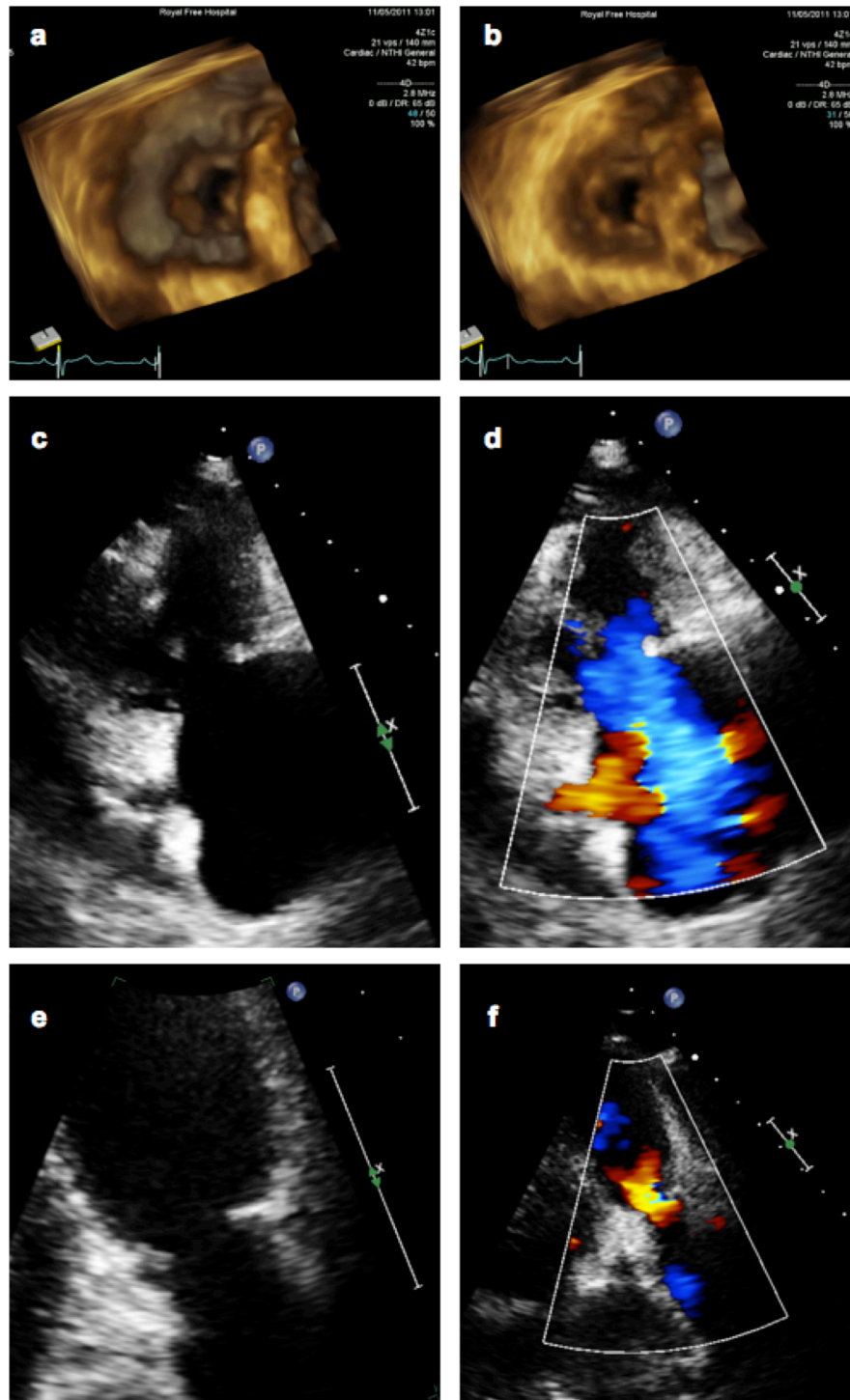


Figure 1-15: Severe carcinoid heart disease affecting the tricuspid (a-d) and pulmonary (e-f) valves.

Valve leaflets are fixed and retracted, with the valve orifice open throughout the cardiac cycle. This gives rise to free-flowing laminar TR (c-d) and PR (e-f). The tricuspid valve is visualized fixed open en face by 3DE in (a) end-diastole and (b) end-systole.

CHAPTER 2 Three-Dimensional Echocardiography of the Right Ventricle

2.1 Introduction

The most convenient imaging modality for assessing the right ventricle (RV) is two-dimensional echocardiography (2DE), but this is limited by the crescentic chamber shape and complex geometry, with inflow and outflow portions in different planes[12, 23]. Thus cardiac magnetic resonance imaging (CMRI) has become the “gold standard” imaging modality for RV quantification[103]. The comparative expense and limited availability of CMRI as the current reference standard favours the pursuit of novel approaches to RV quantification by cardiac ultrasound.

One possibility to overcome the limitations of 2DE is three-dimensional echocardiography (3DE). This technique has been previously compared against CMRI in a range of congenital and acquired diseases for RV volumetric quantification[104]. 3DE traditionally utilizes the disk summation method to reconstruct the RV following sequential slice acquisition over consecutive ECG-gated heartbeats[105]. This 3DE method, however, is limited by breath holding throughout successive cardiac cycles, stitching artifact during acquisition, and difficulties identifying inlet and outflow regions in the basal slices during post-processing[106]. More recently though, ultrasound transducer technology has been developed to enable the real-time acquisition of a 90° by 90° full volume dataset in a single cardiac cycle[107].

2.1.1 Aims

The aims of this study were to:

- Compare RV volumetric quantification by single-beat full-volume 3DE against CMRI in homogenous patient populations of acquired RV pressure- and volume-overload, namely, PH and CHD, respectively.
- Compare single-beat full-volume 3DE and 2DE functional indices in the identification of CMRI-defined RV dysfunction in PH.

- Evaluate the test-retest reproducibility of single-beat full-volume 3DE for both the acquisition and post-processing components of the technique.

2.1.2 Personal Contribution

To fulfill the above aims I have:

- Obtained ethical approval from the local institutional research ethics committee (North West London REC 2) and research and development (R&D) approval from the R&D departments at The Royal Free Hospital and Great Ormond Street Hospital NHS Trusts.
- Enrolled 100 participants in sinus rhythm with no contraindications to magnetic resonance imaging.
- Performed and post-processed comprehensive 2DE and single-beat full-volume 3DE studies of the RV for all participants.
- Repeated the 3DE studies of the RV for a subset of 20 randomly selected participants.
- Post-processed the CMRI studies for all participants to quantify the reference standard metrics of RV function.

The results from this work have been published by D. Knight, A. Grasso, M. Quail, V. Muthurangu, A. Taylor, C. Toumpanakis, M. Caplin, J. Coghlan and J. Davar, in the Journal of the American Society of Echocardiography, 2015, **28**(3), entitled; “Accuracy and reproducibility of right ventricular quantification in patients with pressure and volume overload using single-beat three-dimensional echocardiography” [108] (see Appendix 1).

2.2 Literature Overview

In this section, literature on the following areas will be discussed:

- Benefits of RV functional assessment using 3DE versus 2DE
- The evolution of 3DE technology

- Comparison of MRI versus 3DE in PH for RV volumetric quantification
- Test-retest reproducibility of 3DE for RV volumetric quantification

This overview highlights relevant papers that were found using the *PubMed* search engine. The search terms used included (a combination of):

- Three-dimensional echocardiography
- Right ventricle
- Magnetic resonance imaging
- Test-retest reproducibility
- Pulmonary hypertension

When a relevant paper was found, selected referenced papers were followed up and any subsequent papers that have cited this paper were also followed up.

2.2.1 Benefits of RV functional assessment using 3DE versus 2DE

The direct comparison of both 2DE and 3DE versus MRI for RV functional quantification has only been performed in one study of 120 patients with congenital heart disease, 62 (52%) of whom had disease primarily affecting the RV[78]. RV dysfunction was defined as any one of an indexed EDV $>129\text{mL/m}^2$, indexed ESV $>58\text{mL/m}^2$, and/or RVEF $<48\%$ by CMRI. The area under the ROC curve was then defined for both traditional 2DE RV functional metrics (FAC, AUC 0.76; TAPSE, AUC 0.72) and 3DE-derived RVEF (AUC 0.86). RVEF by 3DE was statistically significantly superior to TAPSE for identifying RV dysfunction. 2DE-derived RV FAC and 3DE-derived RV EF were most likely superior to TAPSE given that they constitute geometric measures of RV function similar to CMRI-derived RVEF.

The importance of 3DE providing global information on systolic function over 2DE measures focusing on RV longitudinal function has also been demonstrated in the post-cardiac surgery setting[109]. Post-surgical

reductions in TAPSE and peak RV systolic velocity are well documented, yet global systolic function by 3DE-derived RVEF was shown to be unchanged in 40 patients following mitral valve repair. The authors concluded that these discordant findings represent a geometric alteration in the RV post-operatively rather than true dysfunction, and hence surrogate 2DE measures of RV function should be interpreted with caution in this context.

2.2.2 The evolution of 3DE technology

There are two distinct 3DE methods in contemporary practice for the acquisition of 3D RV datasets: (i) electrocardiogram (ECG)-gated multiple-beat 3DE, and (ii) real-time or live 3DE[105].

There are also two different commercially available post-processing algorithms for 3DE RV datasets: (i) the disk summation method (or 'method of disks'), and, more recently (ii) the volumetric semi-automated border detection approach[105].

2.2.2.1 ECG-gated multiple-beat 3DE of the RV

The majority of contemporary *in vivo* clinical studies utilizing 3DE for the evaluation of RV volumes have been performed using multiple-beat gated 3DE. This technology involves the acquisition of serial sub-volume slices of the RV gated to consecutive heartbeats. The sub-volumes are then stitched together to form a 3D reconstruction (Figure 2-1).

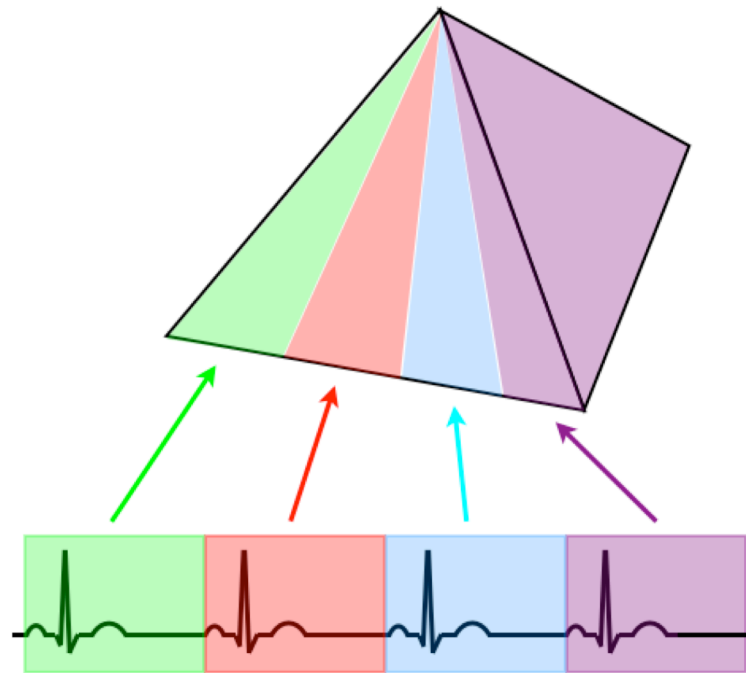


Figure 2-1: Schematic of ECG-triggered multiple-beat 3DE data acquisition. Narrow pyramidal sub-volumes from four consecutive cardiac cycles are stitched together to form a single pyramidal volumetric data set.

The limitations of this technique are inherent to the acquisition of sub-volumes over several cardiac cycles, usually of the order of 2 to 7 heartbeats. Patients with arrhythmia or who have difficulty with breath-holding are prone to stitching artifact, whereby the sub-volumes are consequently sub-optimally reconstructed into a volumetric dataset that ranges from inaccurate to unusable (Figure 2-2). This can occur with arrhythmia due to cavity volumes varying with changes in consecutive R-R intervals. Stitching artifact with respiratory motion results from changes in cardiac position in the thorax with breathing. A further limitation is that the volume being acquired can only be inspected after it is obtained, as images are not displayed in real-time.

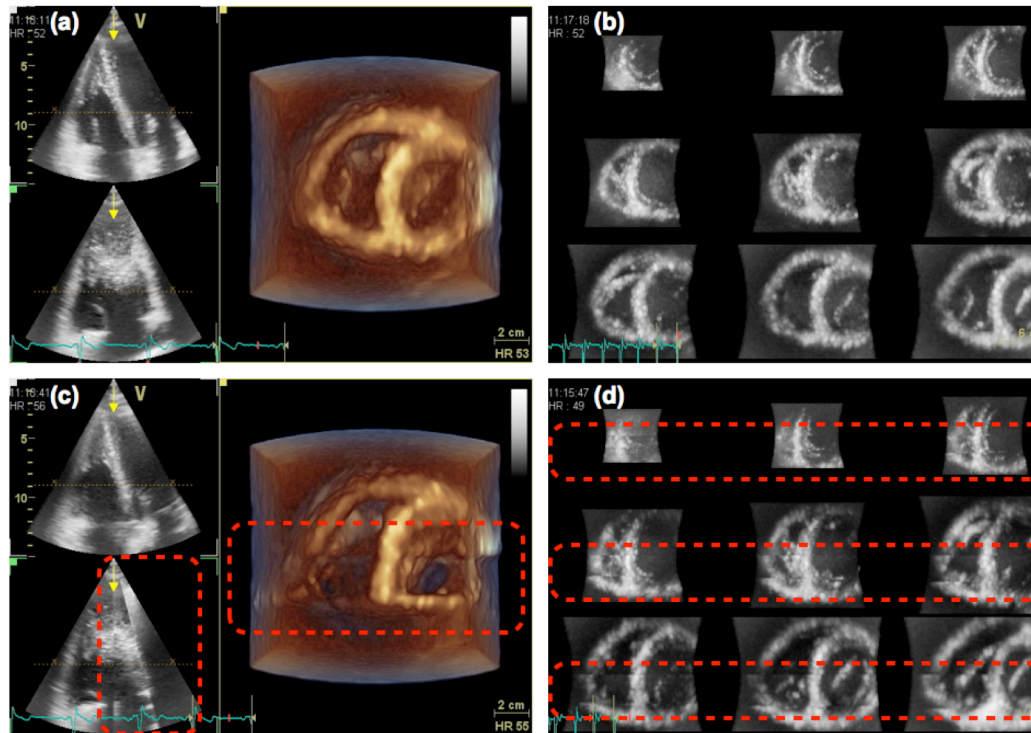


Figure 2-2: ECG-gated multiple beat 3DE of the RV. Figure (a) shows a volumetric RV data set with no stitching and good image quality on the short-axis slices (b) following acquisition. Figure (c) demonstrates stitching artefact (red dotted line) caused by breathing during scan acquisition, with stitching visible on reconstruction of the sub-volumes in the short-axis slices (d).

Studies using the multiple-gated 3DE technique tended to report an underestimation of RV volumes and EF by 3DE when compared against CMRI. A meta-analysis was performed of 23 studies including a total of 807 patients comparing RV volumetric assessment by 3DE versus CMRI through May 2010 [104]. All studies that were included were performed using multiple-beat gated 3DE acquisition. There was significant bias for underestimation of both RV volumes (RVEDV -13.9 mL $[-17.7, -10.1]$, $P < 0.00001$; RVESV -5.5 mL $[-7.6, -3.4]$, $P < 0.00001$) and EF (-0.9% $[-1.8, -0.1]$, $P = 0.03$) by 3DE. The factors accounting for a tendency for underestimation of RV volumes and EF by 3DE included younger participant age (mean age < 18 years, $P < 0.05$) and larger RV cavity size ($\text{EDV} > 200\text{ mL}$, $P < 0.05$).

A common reason that is cited for underestimation of RV volumes by 3DE is the observer tracing further inside the ventricular cavity due to blurred endocardial borders resulting from the lower spatial resolution compared to 2DE[13]. In an attempt to circumvent this post-processing limitation, it has previously been proposed that tracing on the 'white side' of the endocardial border limits volumetric underestimation by 3DE[110]. Whilst noting the findings of the meta-analysis, a small study of 33 patients of mixed left heart disease aetiologies comparing 3DE with CMRI has since conversely reported more volumetric underestimation for non-dilated RVs[111]. This was attributed to easier operator identification of trabeculae in dilated RV cavities.

2.2.2.2 Real-time 3DE: single-beat full-volume 3DE of the RV

More recently, advances in transducer technology have moved away from the acquisition of serial sub-volumes. The generation of simultaneous multiple ultrasound beams can now allow the acquisition of a full-volume dataset in a single heartbeat. This negates the need for ECG-gated acquisition, thus avoiding stitching artifact by enabling the acquisition of 3D full-volume datasets with irregular R-R intervals. The more rapid acquisition times also result in shorter breath-holds. The real-time nature of obtaining a full-volume dataset also permits the real-time display of orthogonal 2D imaging planes prior to and at the time of acquisition. This allows the operator to acquire a dataset when satisfied that it contains all of the structure(s) being studied.

Two studies have specifically investigated single-beat full-volume 3DE of the RV compared with CMRI. The first study investigated the effect of long-distance running on RV size and function using both 3DE and CMRI in 22 individuals before and after a 30 kilometre run[112]. Whilst 3DE was feasible in all subjects, it demonstrated a significant bias for underestimation of RV volumes. However, the authors reported a tendency to exclude trabeculae from the blood pool volume on 3DE, but to include RV trabeculae in the cavity volume on CMRI post-processing.

Therefore the post-processing techniques of the two modalities were fundamentally different, which could account for this bias. The second study of 61 patients of various cardiac disease aetiologies attending for same-day CMRI and single-beat 3DE found minimal bias for cavity volume quantification between modalities[113]. Notably, this study included trabeculae in the RV cavity volume during the post-processing stages of both modalities.

2.2.2.3 Commercially available 3DE RV post-processing algorithms

The disk summation method was the original technique for post-processing 3DE RV datasets. After allocating the end-diastolic and end-systolic frames, the operator manually traces the endocardial border in the axial plane for serial short-axis slices of a fixed height, usually 7 to 10mm thick (Figure 2-3). The axial planes can be cross-referenced to long-axis images to enable identification of the tricuspid annulus. The RV cavity is reconstructed by adding the known areas of the serial axial traces, termed disk summation.

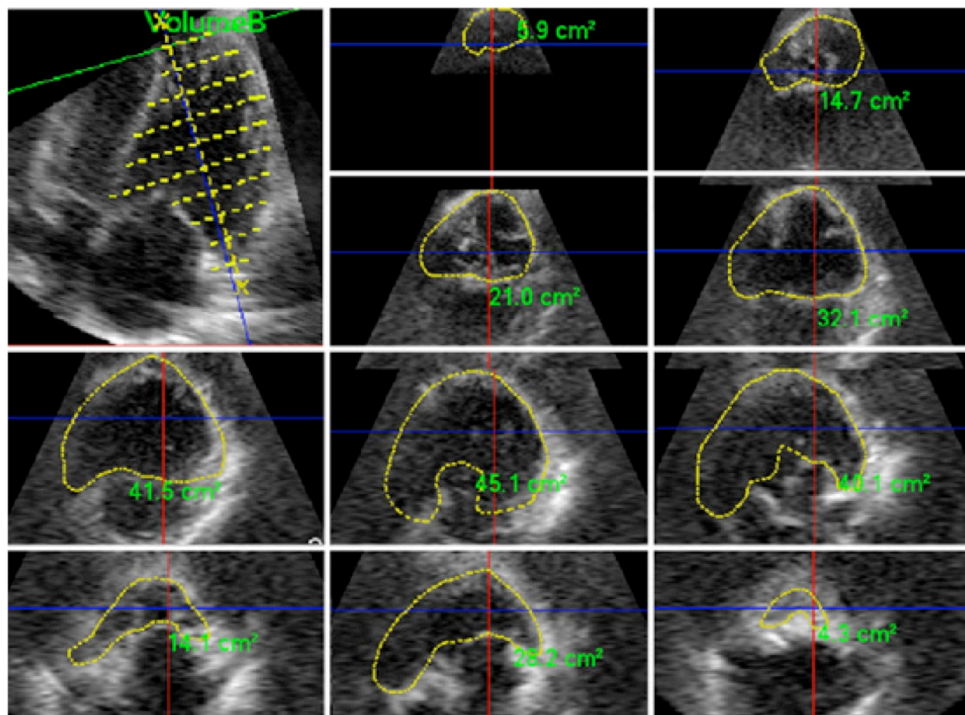


Figure 2-3: The disk summation technique for 3DE RV reconstruction.

A series of contiguous RV short-axis slices are displayed, corresponding to the disks on the 4-chamber view. The endocardial borders are traced manually. Reproduced with permission from Morikawa et al.[114]

More recently, semi-automated border detection methods have been utilized for volumetric analysis. Different semi-automated algorithms have been previously described[115, 116]. Commonly, a 3DE-acquired RV dataset is imported into the software and manipulated by rotating, angulating, and slicing in any of the three displayed orthogonal planes. The operator manually traces the endocardial contour for end-diastolic and end-systolic frames in sagittal, four-chamber and coronal planes. These cross-sectional planes allow visualization of the tricuspid annulus, the ventriculo-infundibular fold, RV outflow tract, and RV apex. A semi-automated border detection algorithm based on in vivo normal subjects and pathologic RV modeling is subsequently run (Figure 2-4), with the option of manual correction of the traced contours in the event of sub-optimal border tracking[116, 117].

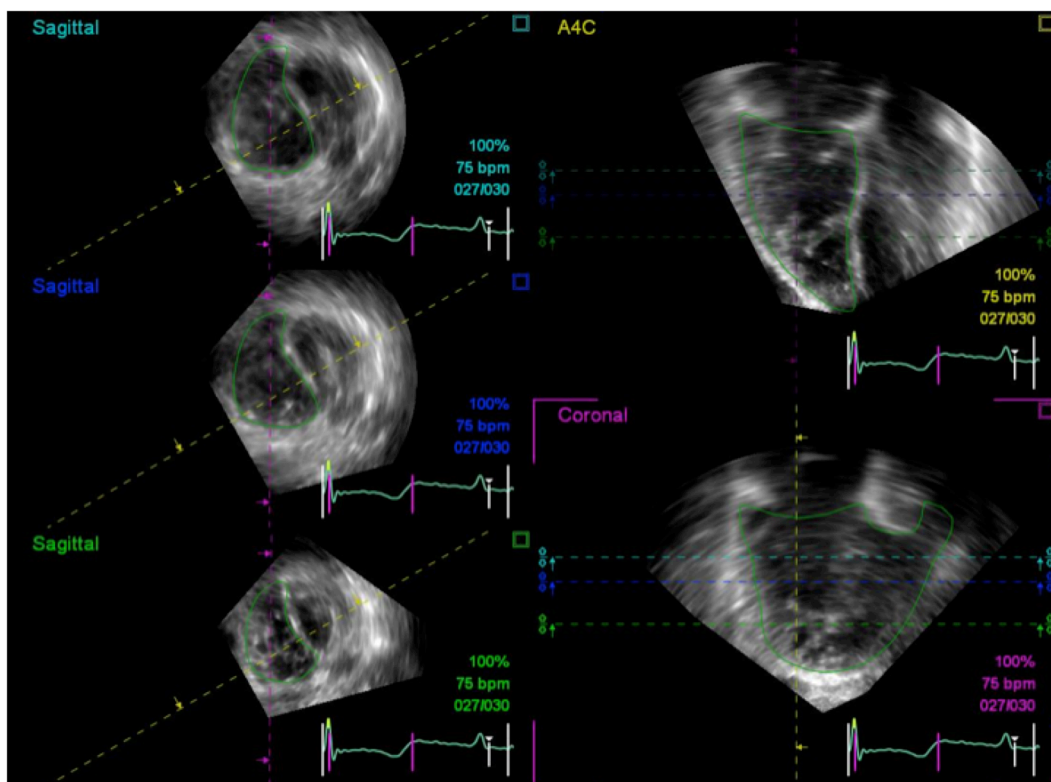


Figure 2-4: The results of a semi-automated RV endocardial border detection algorithm, with the border tracking through the cardiac cycle in the sagittal (three levels), 4-chamber and coronal views displayed to the operator.

A surface-rendered cast of the RV is then created, with accompanying RV EDV, ESV and EF automatically displayed (Figure 2-5)[105]. Segmental analysis of the inlet, apex and outlet portions of the RV can be performed with some software versions, and time curves of global and regional function during the cardiac cycle can also be generated.

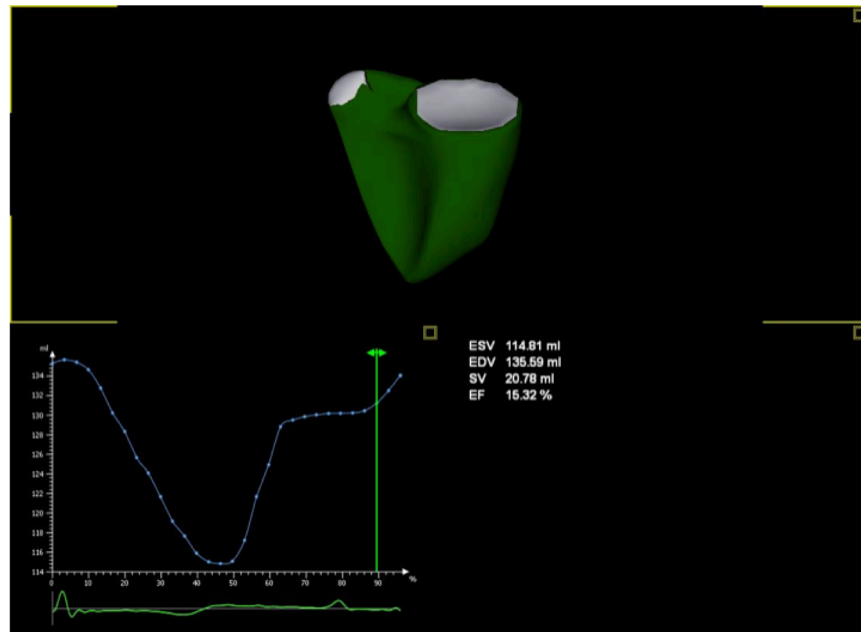


Figure 2-5: Surface-rendered cast of the RV following 3DE reconstruction with a time curve of global function during the cardiac cycle.

The volumetric semi-automated border detection approach is significantly more accurate than disk summation, in part due to less geometric assumptions and the superior ability to visually delineate the boundaries of the RV inlet and outlet portions[106]. As such it is the recommended 3DE post-processing technique for quantification of RV function[49].

2.2.3 Comparison of 3DE versus MRI in PH for RV volumetric quantification

All three studies specifically designed to investigate 3DE against CMRI for assessing RV volumes in PH utilized multiple-beat gated 3DE, with variable results reported. Grapsa et al. found minimal mean differences for 3D RV metrics using 3DE in 60 consecutive patients with newly diagnosed PH and 20 healthy controls[118]. However, there were wide limits of agreement for these parameters between modalities, particularly

in the PH patient population (RVEDV -3.7mL [-61.1, 53.7], $P < 0.001$; RVESV 0.0mL [± 48.8], $P < 0.001$; EF -1.3% [-15.5, 12.9], $P = 0.005$). Contrastingly, Morikawa et al. reported small underestimations of indexed RV volumes by 3DE in 30 patients with PH and 15 healthy volunteers, but with narrower limits of agreement (RVEDV -9.0mL/m² [-33, 15], $P < 0.001$; RVESV -3.5mL/m² [-13.1, 6.1], $P < 0.001$; EF -3.1% [-8.5, 2.3], $P < 0.001$)[114]. Finally, Li et al. also found a bias for underestimation of RV cavity volume measurements in a population of 23 patients with PH, but with clinically acceptable limits of agreement (RVEDV -9.7mL [-6.0, 25.5], $P < 0.001$; RVESV 3.4mL [-13.3, 20.1], $P < 0.001$; EF 2.4% [-6.6, 11.3], $P < 0.001$)[119]. This most recent study also stated in the methodology that two different 3DE transducers were used for ECG-gated recordings over 4 to 7 cardiac cycles, although one of the two transducers specified is actually capable of single-beat full-volume acquisition (4Z1C matrix-array transducer, Siemens Acuson SC2000).

2.2.4 Test-retest reproducibility of 3DE for RV volumetric quantification

The test-retest reproducibility of RV assessment by 3DE has been reported in five studies, all of which utilized multiple-beat gated 3DE (Table 2-1).

Investigator (year)	Number of subjects	Study population	3DE view	Test-retest study	Results
Gopal et al. (2007)	20	Healthy volunteers	Modified apical window	Interobserver	Percentage variability: EDV: 3.3%, ESV: 8.7%, SV: 10%, EF: 10.3%
Jenkins et al. (2007)	50	Post acute myocardial infarction	Modified apical window	Intraobserver	Highest correlations for RV metrics obtained using 3DE (versus 2DE)
Grapsa et al. (2010)	60	Newly diagnosed PAH	Modified apical window	Intraobserver	High ICCs and good limits of agreement
van der Zwaan et al. (2011)	28	21 congenital heart disease patients, 7 healthy controls	Modified apical window	Interobserver and intraobserver	Significant difference detected for interobserver EDV only
Renella et al. (2014)	13	Unselected patients from day 1 of life to 20 years old attending for clinically indicated echocardiogram	10 from subxiphoid window, 10 from apical window (7 studies not suitable for analysis)	"Interstudy": one observer analyzed two datasets acquired by separate sonographers	No significant differences for RV metrics obtained using 3DE

Table 2-1: Studies of test-retest reproducibility of 3DE RV assessment.

However, the methodology and statistical reporting of these studies varies widely. Despite acquiring repeated measures of RV size and function, the study of van der Zwaan et al. uses multiple paired t-tests to compare differences between serial acquisitions, which may underestimate potential differences between studies. Nevertheless, current American Society of Echocardiography (ASE) guidelines for RV assessment favour 3DE, partly due to its superior reproducibility than 2DE metrics when properly performed in echocardiography laboratories with appropriate training and experience[49, 50, 110, 120].

2.2.5 Summary

From the literature overview it is evident that 3DE is a feasible technique for RV functional quantification, with emerging recognition over traditional 2DE methods. However;

- Multiple-beat gated 3DE with disk summation reconstruction is limited by breath-holding throughout successive cardiac cycles, stitching artifacts during acquisition, and difficulties identifying inlet and outflow regions in the basal slices during post-processing.
- There is an abundance of data demonstrating a tendency for underestimation of RV volumes using multiple-beat gated 3DE, particularly in dilated RV cavities.
- There is a relative paucity of data comparing single-beat full-volume 3DE against CMRI for RV volumetric quantification, with no studies of this iteration of 3DE technology in homogeneous populations of acquired RV disease.
- There are no studies of test-retest reproducibility utilizing single-beat full volume 3DE technology. Furthermore, the statistical methodology for evaluating the test-retest reproducibility of 3DE-derived metrics could be optimized.

I aim to demonstrate the feasibility of contemporary ultrasound transducer technology that allows single-beat full-volume acquisition of a 90° X 90° 3D RV dataset. This will be applied to homogeneous patient populations

of pressure- and volume-overload, namely PH and CHD respectively. By comparing single-beat 3DE against CMRI for RV quantification, I aim to perform the largest study of the accuracy of this novel 3DE technique and the first study of its test-retest reproducibility. I will also provide data to investigate the incremental benefit of single-beat 3DE over 2DE-derived metrics for the identification of RV dysfunction.

2.3 Methods

A prospective cross-sectional study was performed that enrolled 100 participants in sinus rhythm with no contraindications to magnetic resonance imaging, all of whom underwent comprehensive 2DE, single-beat 3DE of the RV, and CMRI within 2 hours of one another.

2.3.1 Study Population

The participants were divided into four subgroups:

- A group of 49 consecutive patients with PH (diagnosed by right heart catheterization as a mean pulmonary artery pressure >25 mmHg and a pulmonary capillary wedge pressure <15 mmHg [121]) who presented for diagnosis and/or follow-up of PH by clinical evaluation and/or right heart catheterization as a disease model of RV pressure-overload. The aetiologies of PH included idiopathic ($n = 9$), connective tissue disease-associated ($n = 32$), and chronic thromboembolic disease ($n = 8$). Exclusion criteria comprised clinically significant restrictive or obstructive lung disease identified by pulmonary function tests, arrhythmia, and known independent left-sided cardiac disease unrelated to PH.
- A group of 20 consecutive patients undergoing 2DE for diagnosis and/or follow-up of CHD [122] were studied as a disease model of RV volume-overload.
- A control group of 20 healthy volunteers affiliated with our institution who were age and sex matched to the PH group.

- A control group of 11 age- and sex-matched patients with metastatic neuroendocrine tumour who were screened as negative by echocardiography for carcinoid valvular heart disease.

All control participants were eligible for study inclusion if they had no cardiac symptomatology, no medical histories of cardiac disease including hypertension, and were not taking any cardiac medications. Normal 2D transthoracic echocardiographic findings were also required to exclude any occult structural cardiac disease before study inclusion.

The study complied with the Declaration of Helsinki. The local institutional research ethics committee (North West London REC 2) approved the study and informed written consent was obtained from all participants.

2.3.2 2DE

All patients underwent comprehensive 2D and Doppler transthoracic echocardiography in the left lateral decubitus position using the Acuson Siemens SC2000 cardiac ultrasound system (Siemens Healthcare, Erlangen, Germany), with a 4V1c transducer (frequency bandwidth, 1.25-4.5 MHz). A standard study protocol was followed in conjunction with ASE guidelines for chamber quantification [50, 123] and the British Society of Echocardiography guidelines for PH assessment [124] as appropriate. RV function was assessed using TAPSE, RV FAC, and mean RV free wall peak systolic strain using syngo Vector Velocity Imaging (Siemens Medical Solutions USA, Inc., Mountain View, CA). A three-beat 2DE digital clip of an apical 4-chamber view optimized for RV visualization was acquired and exported to Velocity Vector Imaging, and 10 to 15 endocardial points were plotted in end-systole from the lateral to the medial tricuspid annulus [125]. The adequacy of speckle-tracking was visually checked and manually adjusted as required.

2.3.3 3DE

2.3.3.1 Image Acquisition

Single-beat full-volume 3D echocardiographic RV data sets were acquired using the 4Z1c matrix-array transducer (frequency bandwidth, 1.5–3.5 MHz; maximum depth, 30 cm; maximum field of view, $90^\circ \times 90^\circ$). Probe position started from the apical 4-chamber view with the patient in the left lateral decubitus position. Both the patient and transducer positions were subsequently modified for optimal simultaneous visualization of the tricuspid valve, cardiac apex, infundibulum, and RV outflow tract (RVOT) as assessed by the real-time 2D 4-chamber, basal sagittal, and coronal views, and by inclusion of the RV chamber in the pyramidal data set (Figure 2-6).

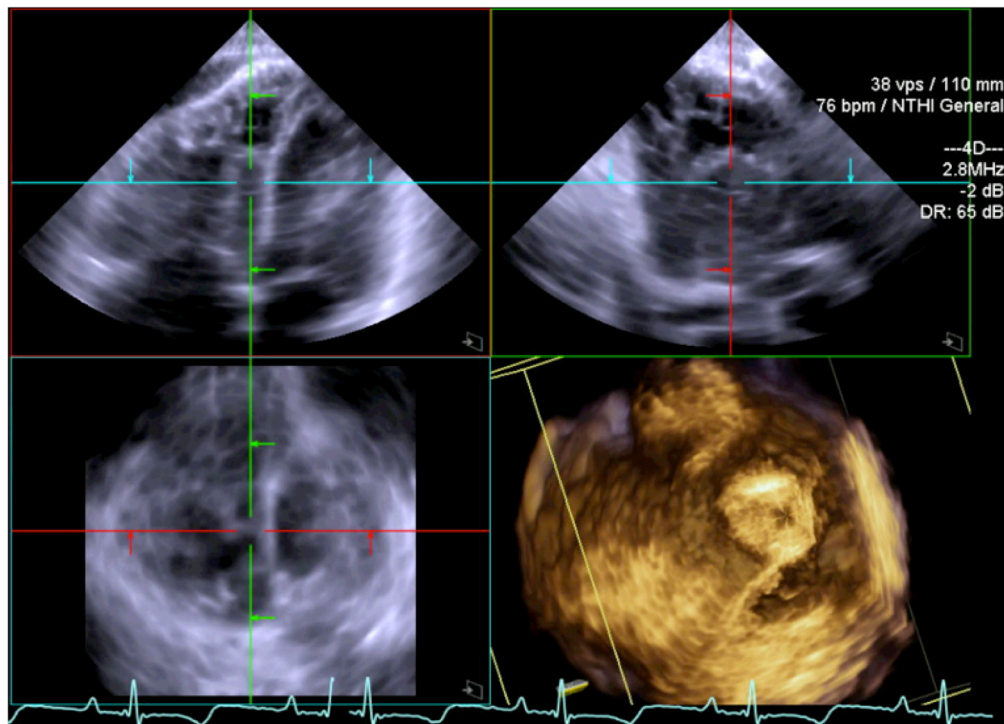


Figure 2-6: A pyramidal dataset focusing upon a dilated RV in 4-chamber, sagittal and coronal views.

Part of the LV is excluded from the volume pyramid (bottom right). Note the high volume rate (38 volumes per second).

In both my experience and that of previous 3DE RV studies, a more lateral apical window with posterior tilt of the probe tail was beneficial to visualize the infundibulum and RVOT in the coronal window[126]. Image depth and sector width were adjusted for maximal visualization of the RV

at the highest volume rate. At least three 3DE RV data sets were acquired during a breath-hold to ensure optimal image quality, which was subjectively graded on a five-point scale ranging from zero (very poor) to four (perfect) [127]. A score of two or less was attributed if ultrasound dropout was evident in greater than half of the RVOT border.

2.3.3.2 Post-Processing

Full-volume 3DE RV data sets were imported into the on-cart RV Analysis application. Manual adjustment of the RV data set was initially required to: (i) ensure the correct orientation of 4-chamber, sagittal, and coronal slices; (ii) maximize the RV cavity area and identify the most apical RV view on visual assessment of the 4-chamber window; and, (iii) allow the identification of cardiac landmarks. This process was performed in a stepwise approach by rotation and angulation of the 4-chamber window, with manipulation of this plane causing the simultaneous adjustment of the other two (sagittal and coronal) orthogonal planes (Figure 2-7).

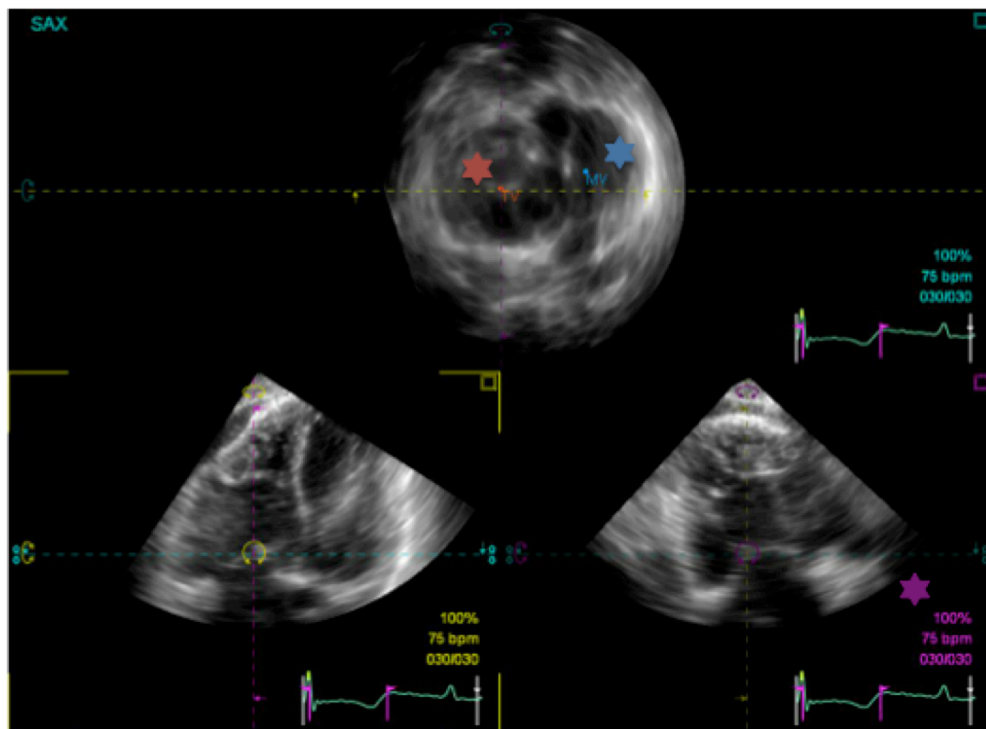


Figure 2-7: Optimization of the RV cavity area in the three orthogonal views, and identification of landmarks.

(MV=mitral valve indicated by the blue asterisk, TV=tricuspid valve indicated by the red asterisk). Note the RVOT seen in the coronal view (indicated by the purple asterisk).

Both atrioventricular valves followed by the left ventricular apex were identified as anatomic landmarks. When the apex of a dilated RV overrode that of the left ventricle, the most apical cardiac point was identified with the left ventricular apex marker. End-diastolic and end-systolic frames were assigned by visual identification of the largest and smallest RV 4-chamber areas, respectively.

Endocardial RV borders were traced at end-diastole and end-systole in 4-chamber, sagittal (basal level), and coronal views. The software algorithm obliges the operator to intersect the endocardial border tracing in sequential views with crosshair reference markers that are positioned in response to endocardial border traces from a preceding view. Therefore, correction of a previous slice tracing was undertaken when a crosshair position suggested a prior tracing error. Trabeculae were included in the blood pool volume. To assist with RVOT delineation in the basal sagittal view, the insertion point of the RV myocardium at the interventricular septum was routinely included in the endocardial tracing.

At the final stage, the algorithm presents the results of semi-automated contour tracking for the 4-chamber, coronal and basal, middle and apical short-axis views. Misalignment of endocardial contours prompted identification of the region of suboptimal tracking followed by manual correction of the original tracing. Automated volumetric reconstruction was accepted only once the semi-automated endocardial border tracking was visually satisfactory and represented meaningful RV shapes in all views (Figure 2-8), as optimization of this final reconstruction stage significantly affects the results generated [128].

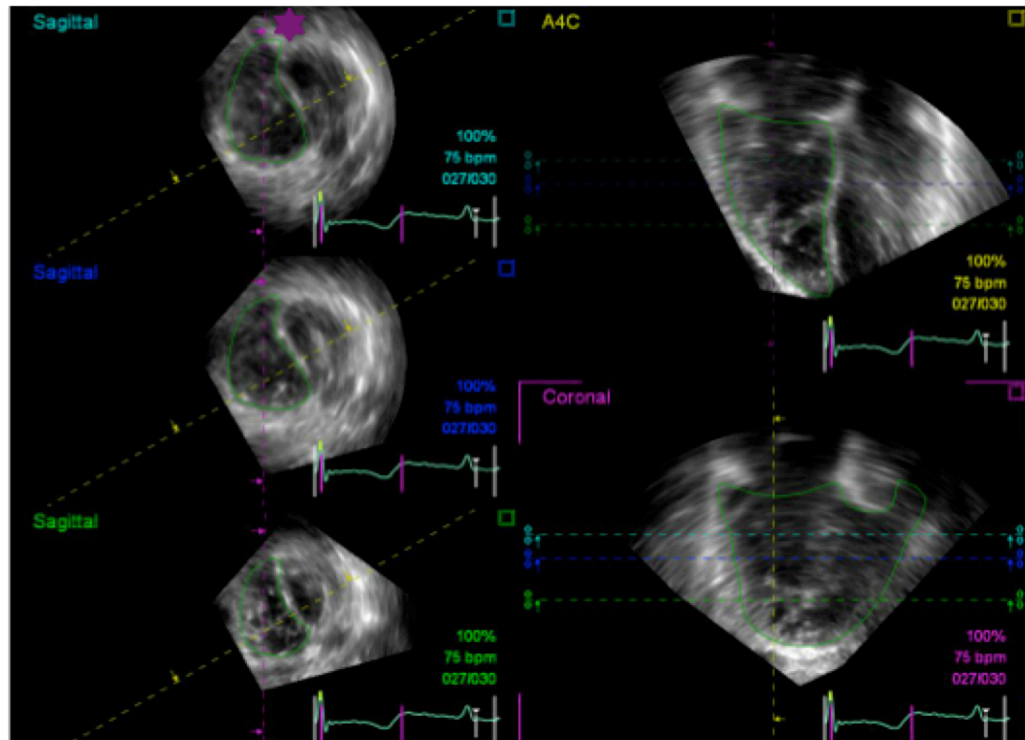


Figure 2-8: The results of semi-automated border tracking.

Note how the purple guideline (indicated by the purple asterix) bisects the tricuspid valve and RVOT in the short-axis views. This corresponds to the coronal RV reconstruction (highlighted), with clearly delineated RV inflow and outflow portions.

2.3.4 Test-Retest Reproducibility of 3DE

Reproducibility was studied in 20 randomly selected subjects (14 with PH, one with CHD, and five healthy volunteers) for both the 3DE acquisition and post-processing stages by two independent sonographers (D.S.K. and A.E.G.), as previously described (Figure 2-9) [129]. The two sonographers had equal experience with 2DE but differing levels of experience with 3DE RV full-volume acquisition (10 and 3 months, respectively). Data sets for intraobserver test-retest reproducibility were post-processed separately at time intervals of over 2 weeks.

Sonographer 1 (D.S.K.) obtained a 3DE RV data set, after which sonographer 2 (A.E.G.) independently obtained a 3DE RV data set. Then, sonographer 1 acquired a second separate 3DE RV data set. The sonographers, who were blinded to each other's results, performed post-processing of their own 3DE RV data sets.

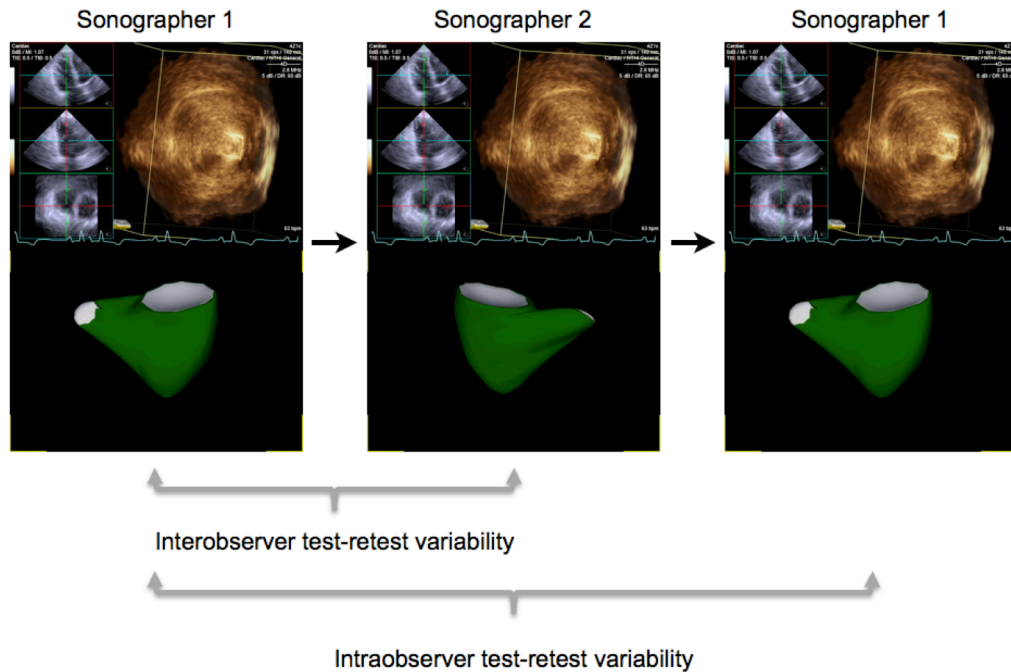


Figure 2-9: Study protocol to investigate test-retest variability of 3DE assessment of the RV.

Adapted from van der Zwaan et al.[129]

2.3.5 CMRI

2.3.5.1 Image Acquisition

All cardiac magnetic resonance images were acquired using a 1.5-T magnetic resonance scanner (Avanto; Siemens Healthcare) using a 12-element phased-array coil for signal reception and the body coil for signal transmission. A vector electrocardiographic system was used for cardiac gating. Ventricular volumes and great vessel flow were measured in all patients. Volumetric RV data were obtained using either retrospectively gated balanced steady-state free precession ($n = 19$) cine imaging of contiguous short-axis slices [130] or real-time radial k-t sensitivity encoding imaging ($n = 81$) of contiguous transaxial slices [63] depending on the pathology under investigation and the patient's ability to hold his or her breath. Real-time radial k-t sensitivity imaging allows the collection of high spatiotemporal resolution real-time images during free-breathing, and is part of the standard clinical CMRI work flow in paediatric PH populations [80]. Blood flow data were acquired in the ascending aorta, in the right and left branch pulmonary arteries, and at the level of the

atrioventricular valves using a velocity-encoded prospectively triggered spiral phase-contrast magnetic resonance flow sequence [131]. This provided an internal check for the RV volumetric data.

2.3.5.2 Post-Processing

All image post-processing was performed using “in-house” plug-ins for the open-source OsiriX Digital Imaging and Communications in Medicine (DICOM) software [63, 132, 133]. Endocardial RV borders were traced manually at end-diastole and end-systole, the time points of which were identified by the largest and smallest RV cavity areas, respectively (Figure 2-10). The inclusion of RV trabeculae was the same as that performed by 3DE post-processing.

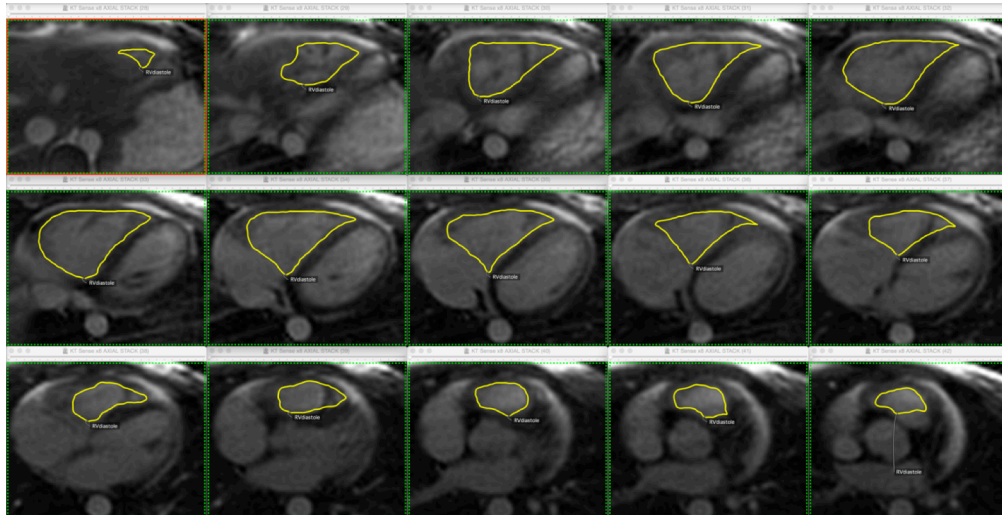


Figure 2-10: A transaxial RV stack by CMRI with manual endocardial border tracing in end-diastole from a healthy volunteer using a radial k-t SENSE sequence.

Ventricular stroke volume (SV) was calculated as:

$$\text{End diastolic volume} - \text{End systolic volume}$$

Equation 2-1: Stroke volume

Ejection fraction (EF) was calculated as:

$$\left(\frac{\text{Stroke volume}}{\text{End diastolic volume}} \right) \times 100$$

Equation 2-2: Ejection fraction

Phase-contrast magnetic resonance flow data were segmented using a semiautomatic vessel edge detection algorithm with manual operator correction[132]. The CMRI data sets for the patients who underwent 3DE test-retest reproducibility scans were also tested for interobserver (D.S.K. and M.A.Q.) and intraobserver post-processing reproducibility.

2.3.6 Statistical Analysis

Statistical analysis was performed using SPSS version 21.0 (IBM Corporation, Armonk, NY) and Prism 6.0b for Mac (GraphPad Software, Inc., La Jolla, CA). Normally distributed continuous data were expressed as mean \pm SD. Systematic differences between measurements were evaluated with Student paired t-tests (two-tailed), with Pearson correlation coefficients used to assess the relationship between 3DE- and CMRI-derived RV volumes and EF. Differences between the four participant subgroups were analyzed using one-way analysis of variance, with the Tukey post hoc tests identifying which specific means differed. P values <0.05 were considered statistically significant. Image scoring data were non-parametrically distributed, represented by medians with 25th and 75th percentiles. Rank sum tests were used for comparisons of image scoring data, with the Mann-Whitney U test and the Kruskal-Wallis test used for comparisons of two and three independent groups, respectively.

Intermodality, interobserver, and intraobserver agreement was studied using the Bland-Altman method [134], whereby the mean difference was presented as the bias and 95% limits of agreement around the bias expressed as the mean difference \pm 1.96 SDs. Differences between test-retest measurements were analyzed by one-way repeated measures analysis of variance, with the Bonferroni post hoc test identifying which specific means differed. The Greenhouse-Geisser correction was used if the assumption of sphericity had been violated. Test-retest variability was expressed using ICCs, relative differences, and COVs. The ICC was

quantified by the two-way random-effects model with absolute agreement. An ICC >0.85 was considered excellent. Relative differences were calculated by taking the absolute difference between two observations divided by the mean of the repeated observations and expressed as a percentage. COVs were calculated as the standard deviation of the difference between two acquisitions divided by their mean value and expressed as a percentage [135]. A COV $<10\%$ was considered excellent.

ROC curves were derived for 2D and 3D echocardiographic parameters to identify CMRI-derived RV EFs of $<50\%$ in patients with PH and healthy volunteers [75]. Patients with carcinoid disease were excluded from this analysis to avoid the confounding effects of the primary pathology of valvular regurgitation on ventricular function. The area under the ROC curve for an echocardiographic parameter is presented together with the optimal cut-off threshold for detecting CMRI-derived RV EF $<50\%$, defined as the value of the parameter that corresponded to the highest sum of sensitivity and specificity. The DeLong method was used to compare the areas under the curve between ROC curves [136] (Analyse-it Software, Ltd, Leeds, United Kingdom).

2.4 Results

2.4.1 Study Population Characteristics

Of 100 individuals who were recruited, four had unobtainable RV echocardiographic windows. The clinical characteristics of the final cohort of 96 subjects are presented in Table 2-2. Patients with PH had significantly larger and impaired RVs than controls, whereas the RVs of patients with CHD were also significantly dilated but with preserved EFs.

Variable (% of total)	PH	CHD	Healthy controls	Carcinoid (no valvulopathy)	<i>P</i> *
N	46 (48)	19 (20)	20 (21)	11 (11)	
Age (years)	56 ± 13	63 ± 8	50 ± 12	59 ± 10	
Female	35 (76)	7 (37)	15 (75)	7 (64)	
Height (cm)	164 ± 9	171 ± 10	169 ± 8	168 ± 10	0.035
Weight (kg)	69 ± 17	72 ± 18	72 ± 12	77 ± 20	0.54
BSA (m ²)	1.8 ± 0.2	1.8 ± 0.3	1.8 ± 0.2	1.9 ± 0.3	0.37
Heart rate (bpm)	74 ± 14	67 ± 13	68 ± 9	69 ± 12	0.19
RVEDV (mL/m ²)	87 ± 26	100 ± 35	64 ± 14	52 ± 8	<0.0001
RVESV (mL/m ²)	52 ± 25	33 ± 15	22 ± 7	16 ± 5	<0.0001
RVEF (%)	43 ± 14	68 ± 7	65 ± 7	71 ± 7	<0.0001
3DE temporal resolution (volumes per second)	34 ± 5	32 ± 7	40 ± 5	45 ± 6	<0.0001
PH patients (% of total)					
Mean PASP at RHC (mmHg)	44 ± 16				
Pulmonary vasodilators					
Endothelin antagonist	21 (46)				
PDE5 antagonist	31 (67)				
Prostanoid infusion	2 (4)				
Oral prostanoid	1 (2)				
Prostaglandin receptor agonist	1 (2)				
CHD patients					
Affected valves	TV = 19 (100), PV = 13 (68), MV =3 (16), AV = 3 (16)				
Data are expressed as mean ± SD.					
*One-way ANOVA between groups					

Table 2-2: Clinical characteristics of study populations

2.4.2 3DE Technical Data

Patient 3DE datasets had a significantly lower mean volume rate compared with controls because of the greater 3D sector angles (Table 2-2). However, the median image quality score was significantly higher among patients (3.00; interquartile range, 2.00–3.00) than controls (2.00 interquartile range, 1.00–3.00) ($P < 0.001$). The image quality among three successive, equally populated subgroups of patients significantly improved with increasing experience with 3DE (Figure 2-11; $P = 0.031$). There was a trend, albeit not statistically significant, for greater differences in SV between modalities with worse subjective image scores (Figure 2-12; $P < 0.13$ for percentage intermodality difference in SV for image score groups 1 and 2 combined versus groups 3 and 4 combined).

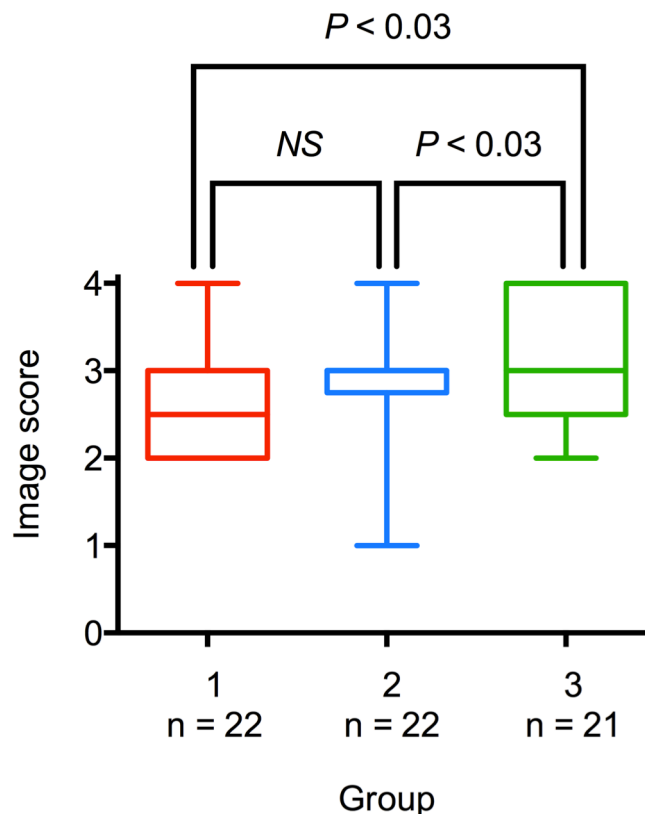


Figure 2-11: Box and whisker plots of subjective image quality scores amongst three successive subgroups of patients (group 1 acquired in the earliest phase of the study, group 3 in the latest phase of the study). Image quality significantly improved with increasing experience with 3DE.

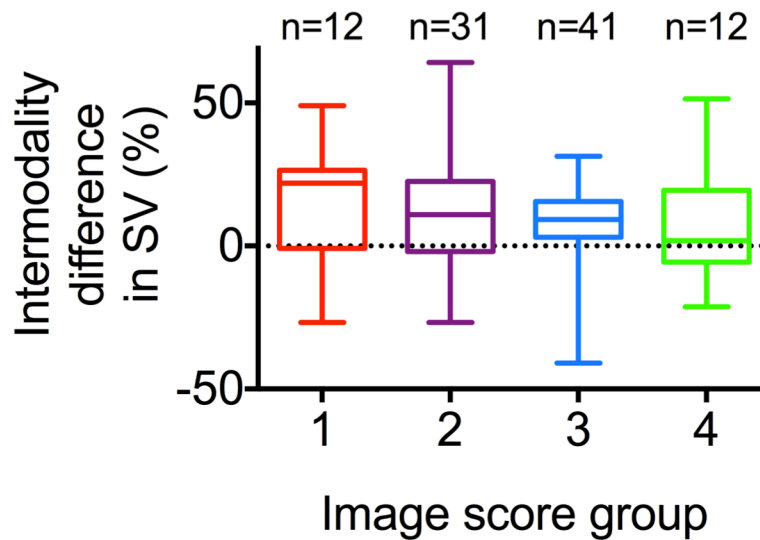


Figure 2-12: Box and whisker plots of differences in stroke volume between modalities (expressed as a percentage of the CMRI reference value) for image scoring groups 1 to 4. There is a trend, albeit not statistically significant, for intermodality difference to increase with reductions in subjective image score. Median percentage intermodality differences in stroke volume (with 25th to 75th percentiles) by image score group were as follows: group 1 = 22% (-1 to 26), group 2 = 11% (-2 to 23), group 3 = 9% (3 to 16), group 4 = 2% (-6 to 19).

Volumetric Analysis by 3DE versus CMRI

Correlation coefficients showed good to excellent correlations between modalities for RV metrics in patient groups, and moderate to good correlations for control subjects (Table 2-3). RV volumes and EF by 3DE showed differences with CMRI in both patient groups (Table 2-4), with a bias for underestimating stroke volume and EF but with overall acceptable limits of agreement (Figure 2-13). By contrast, 3DE underestimated EDV for control subjects, with a consequent negative bias for quantifying SV in this group (Figure 2-14).

Group	Measurements	Bias \pm SD	LOA	r	P*
All subjects	EDV (mL)	-2.3 \pm 13.7	-29.1:24.5	0.97	<0.0001
	ESV (mL)	5.2 \pm 9.5	-13.4:23.9	0.98	<0.0001
	SV (mL)	-7.5 \pm 11.8	-30.6:15.7	0.94	<0.0001
	EF (%)	-4.6 \pm 6.9	-18.2:9.0	0.91	<0.0001
PH	EDV (mL)	4.0 \pm 13.1	-21.6:29.7	0.97	<0.0001
	ESV (mL)	8.4 \pm 10.6	-12.3:29.1	0.98	<0.0001
	SV (mL)	-4.3 \pm 10.8	-25.5:17.0	0.82	<0.0001
	EF (%)	-4.8 \pm 8.3	-21.1:11.5	0.81	<0.0001
CHD	EDV (mL)	-3.1 \pm 10.1	-22.9:16.8	0.99	<0.0001
	ESV (mL)	5.4 \pm 8.2	-10.6:21.4	0.96	<0.0001
	SV (mL)	-8.6 \pm 13.9	-35.9:18.6	0.95	<0.0001
	EF (%)	-3.8 \pm 4.1	-11.9:4.2	0.82	<0.0001
Healthy controls	EDV (mL)	-11.9 \pm 9.0	-29.5:5.8	0.94	<0.0001
	ESV (mL)	-0.4 \pm 6.7	-13.6:12.9	0.88	<0.0001
	SV (mL)	-11.2 \pm 10.1	-31.0:8.7	0.84	<0.0001
	EF (%)	-3.9 \pm 6.5	-16.6:8.8	0.51	0.021
Carcinoid (no valvulopathy)	EDV (mL)	-10.1 \pm 15.0	-39.6:19.4	0.84	0.001
	ESV (mL)	2.1 \pm 5.5	-8.7:12.9	0.92	<0.0001
	SV (mL)	-12.2 \pm 12.3	-36.3:11.9	0.53	0.096
	EF (%)	-6.2 \pm 5.6	-17.1:4.7	0.69	0.019

*Pearson's correlation coefficient

Table 2-3: Bias, limits of agreement and correlation between single-beat 3DE and CMRI for RV volumes and EFs

Group	RV metrics	3DE	CMRI	<i>P</i> *
PH	EDV (mL)	158 ± 53	154 ± 52	0.043
	ESV (mL)	100 ± 44	92 ± 47	<0.0001
	SV (mL)	58 ± 18	63 ± 17	0.011
	EF (%)	39 ± 11	43 ± 14	0.00029
CHD	EDV (mL)	182 ± 69	185 ± 71	0.21
	ESV (mL)	67 ± 28	62 ± 3	0.01
	SV (mL)	115 ± 42	124 ± 45	0.014
	EF (%)	64 ± 5	68 ± 7	0.001
Healthy controls	EDV (mL)	105 ± 26	117 ± 27	<0.0001
	ESV (mL)	41 ± 12	41 ± 14	0.80
	SV (mL)	65 ± 16	76 ± 18	<0.0001
	EF (%)	61 ± 5	65 ± 7	0.014
Carcinoid (no valvulopathy)	EDV (mL)	88 ± 21	98 ± 27	0.05
	ESV (mL)	32 ± 13	30 ± 14	0.24
	SV (mL)	56 ± 10	68 ± 14	0.009
	EF (%)	64 ± 7	71 ± 7	0.004

Data are expressed as mean ± SD.

*Paired Student's *t*-test

Table 2-4: RV volumes and EFs by single-beat 3DE versus CMRI

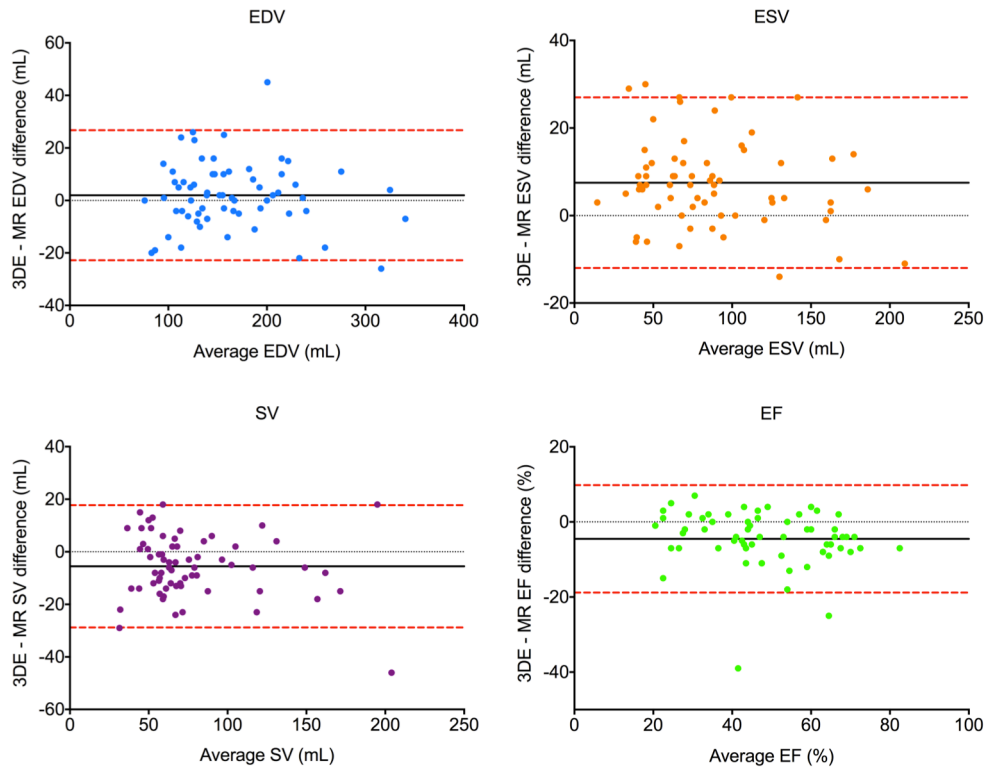


Figure 2-13: Bland Altman analysis of bias (black solid line) and 95% limits of agreement (red dashed line) for 3DE versus CMRI quantification of RV EDV, ESV, SV and EF in patients with PH and carcinoid heart disease.

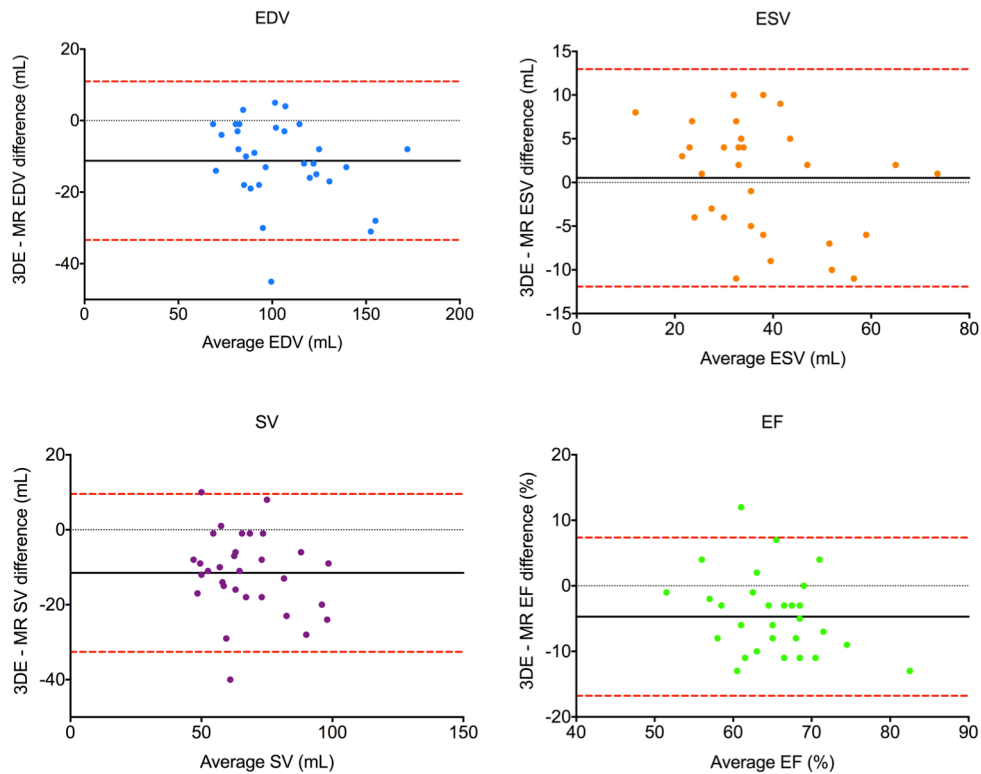


Figure 2-14: Bland Altman analysis of bias (black solid line) and 95% limits of agreement (red dashed line) for 3DE versus CMRI quantification of RV EDV, ESV, SV and EF for subjects in the control populations.

2.4.3 RV Quantification by 3DE and 2DE versus CMRI

3DE-derived RV EF was the most superior echocardiographic parameter for identifying CMRI-derived RV EF <50% (Figure 2-15; $P = 0.031$), with a sensitivity of 94%. A FAC of 39% (sensitivity, 85%) was the best conventional 2D echocardiographic measure, superior to both peak systolic strain and TAPSE ($P = 0.0443$). TAPSE was the weakest marker to predict CMRI-derived RV EF <50%, with a sensitivity of 56% at a cut-off threshold of 19 mm.

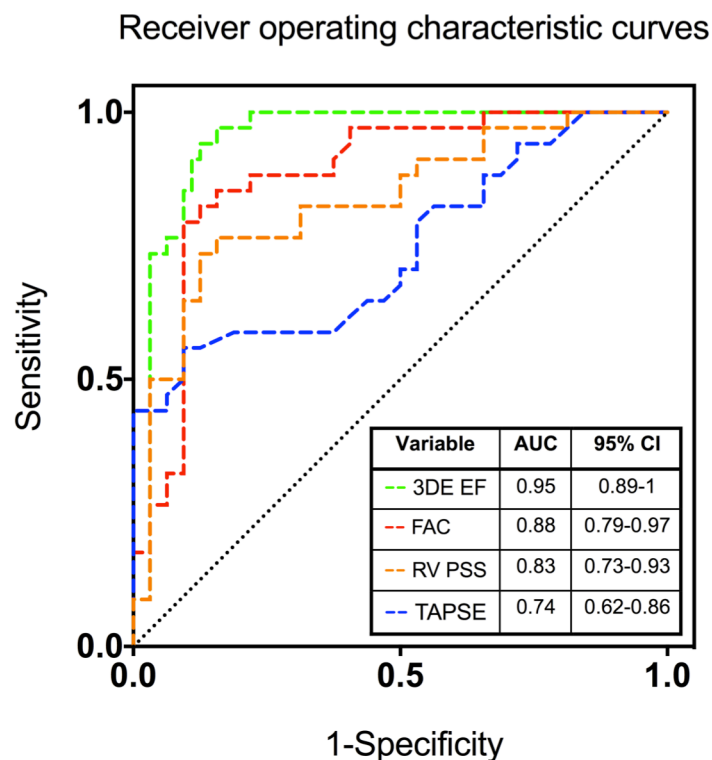


Figure 2-15: Receiver operating curves for 3DE, fractional area change (FAC), RV free wall peak systolic strain by speckle tracking echocardiography, and tricuspid annular plane systolic excursion (TAPSE) to identify RV dysfunction (defined as RVEF <50% by CMRI).

2.4.4 Test-Retest Intraobserver and Interobserver Reproducibility

Limits of agreement were acceptable for intra- and interobserver 3DE studies, with good to excellent ICCs (Table 2-5). However, there was a significant interobserver bias for underestimating RV EDV ($P = 0.001$; Table 2-6) that resulted in underestimation of SV ($P = 0.002$) and EF ($P = 0.033$), with accompanying large interobserver COVs and relative

differences. Moreover, despite no significant differences between intraobserver EDV and ESV, the differences translated into statistically significant test-retest differences for SV ($P = 0.032$) and EF ($P = 0.005$). The interobserver and intraobserver reproducibility for RV volumes and EF by CMRI showed no significant bias and superior limits of agreement compared with 3DE.

3DE Intraobserver				
RV metric	EDV (mL)	ESV (mL)	SV (mL)	EF (%)
ICC	0.992	0.974	0.96	0.906
CoV (%)	3.0	6.6	8.0	6.9
RD (%)	4.3	9.4	11.3	9.8
Bias	-0.2	4.6	-4.7	-3.6
LOA	-16.2:15.8	-12.8:22.0	-19.0:9.7	-12.2:5.0
SD	8.2	8.9	7.3	4.4
CMRI Intraobserver				
RV metric	EDV (mL)	ESV (mL)	SV (mL)	EF (%)
Bias	-2.6	-2.4	-0.1	0.7
LOA	-15.4:10.2	-11.3:6.5	-11.8:11.6	-5.9:7.2
SD	6.5	4.6	6.0	3.4
3DE Interobserver				
RV metric	EDV (mL)	ESV (mL)	SV (mL)	EF (%)
ICC	0.955	0.965	0.867	0.827
CoV (%)	7.7	8.0	16.6	9.4
RD (%)	10.3	11.4	23.5	13.3
Bias	-12.5	-2.0	-10.6	-4.0
LOA	-40.0:15.1	-24.0:20.1	-33.2:12.1	-16.2:8.3
SD	14.1	11.3	11.6	6.3
CMRI Interobserver				
RV metric	EDV (mL)	ESV (mL)	SV (mL)	EF (%)
Bias	-1.9	-2.80	1.1	0.9
LOA	-18.2:14.4	-13.1:7.5	-9.3:11.5	-4.1:5.8
SD	8.3	5.2	5.3	2.5

Table 2-5: Interobserver and intraobserver reproducibility for RV volumes and EF by 3DE and CMRI

RV metrics	Sonographer 1			Sonographer 2		
	1 st (S1.1)	2 nd (S1.2)	<i>P</i> * 1 st vs. 2 nd	Acquisition	<i>P</i> * vs. S1.1	<i>P</i> * vs. S1.2
EDV (mL)	145 ± 63	145 ± 62	NS	133 ± 59	0.003	0.003
ESV (mL)	78 ± 44	83 ± 42	NS	76 ± 39	NS	NS
SV (mL)	67 ± 31	63 ± 29	0.032	57 ± 27	0.002	0.046
EF (%)	48 ± 13	44 ± 12	0.005	44 ± 11	0.033	NS

Data are expressed as mean ± SD.

*One-way repeated measures ANOVA with Bonferroni post-hoc test.

Table 2-6: Interobserver and intraobserver test-retest reproducibility for RV metrics by 3DE

2.5 Discussion

This study demonstrates the feasibility of single-beat full volume 3DE for RV quantification in, to my knowledge, the largest homogenous acquired RV pressure- and volume-overloaded patient populations. The main findings of this study were:

- (i) Single-beat 3DE is an agreeable technique compared with CMRI for RV volumetric quantification.
- (ii) There is a demonstrable learning curve for RV assessment using 3DE.
- (iii) There is a significant underestimation of RV cavity volumes by 3DE in subjects with non-dilated RVs.
- (iv) Volumetric 3DE-derived parameters are of incremental benefit for identifying RV dysfunction compared with traditional 2DE measures.
- (v) There is significant intraobserver and interobserver test-retest variability in RV volumetric quantification using 3DE.

2.5.1 RV Remodelling in PH and CHD

Accurate quantitation of RV size and function is important in many congenital and acquired cardiac diseases, and is of particular relevance in the patient populations in this study. RV size and function are of greater prognostic significance in PH than the afterload to which the right

heart is exposed[21, 81], with RVEF being the key determinant of outcome regardless of changes in PVR afforded by pulmonary vasodilator therapy[137]. Similarly, right heart dilatation is independently associated with poor outcome in patients with advanced CHD[100]. However, the RV responds differently to pressure- and volume-overload conditions, with dilatation occurring in both but with relative preservation of function in elevated preload rather than afterload. What remains unclear is to what extent this preserved EF represents normality of function in the presence of severe tricuspid regurgitation, a valvular lesion common to all patients in this CHD cohort.

2.5.2 Benefit of 3DE over 2DE for RV Assessment

The incremental benefit of 3DE over 2DE has previously been shown in congenital heart disease[78], and single-beat 3DE showed similar added value over 2DE metrics in acquired RV pressure-overload. Whilst this is in part due to equivalent parameters being assessed by 3DE and CMRI, it is importantly also a reflection of the limitations of conventional 2DE measures. TAPSE had the poorest sensitivity for detecting impaired RV EF in PH, with a cut-off of 19mm having the highest combined sensitivity and specificity. This is higher than the recommended threshold of 16mm for detecting RV dysfunction[50], suggesting that TAPSE would have performed worse by current guidelines in this cohort. The rocking motion of the RV in pressure-overload can give rise to apparently normal TAPSE values[109], and TAPSE also does not account for the radial component of RV function that contributes significantly to RVEF[54]. By contrast FAC was the most superior 2DE marker for identifying RV dysfunction in PH, most likely a reflection of being the only 2DE marker that integrates both radial and longitudinal components of function. These findings are consistent with a previous study comparing 2DE markers of RV function in PH[77], and suggest that 3DE may have an important additive role in assessing RV function in this disease.

2.5.3 Advantages of 3DE over CMRI for RV Assessment

RV quantification by echocardiography is advantageous through being more readily available and less expensive than CMRI. Since the first use of 3DE for RV volumetric quantification[127], improvements in matrix array transducer technology permit the simultaneous visualization of orthogonal 2D RV planes at the time of acquisition. The technique used in this study allows a pyramidal dataset of up to 90° by 90° to be acquired at higher temporal resolutions than previously reported for 3DE[118]. Acquisition of a full-volume in a single heartbeat avoids stitching artifact associated with acquiring slices over serial heartbeats, and also confers the advantage of shorter breath-hold durations. These reasons might explain the narrower limits of agreement for RV volumetric parameters between single-beat 3DE and CMRI compared with previous data from adult PH groups using the disk summation method[114, 118].

2.5.4 Disadvantages of 3DE for RV Assessment

The disadvantages of echocardiography include constraints that afford inadequate transthoracic windows, including body habitus, hyperinflated lungs and chest deformities. Acquisition and post-processing was feasible in 96% of subjects, consistent with previous 3DE studies[113, 117]. However, patients with significant lung disease were excluded to ensure that PH was the predominant disease process in the RV pressure-overload group, and this may in turn have biased the echogenicity of the study population.

Whilst all post-processed 3DE datasets had a reconstructed RV polygon that tracked throughout the cardiac cycle, 45% of studies were judged by subjective image scoring to have some endocardial dropout of the outflow portion of the RV. This was reflected by a trend for increasing mean differences in stroke volumes between modalities with decreasing image quality, with mean differences of at least 11% when the RVOT was incompletely visualized. This is a consistent problem with 3DE that has been well documented previously due to the anterior position of the RV in

the thorax (Figure 2-16). Post-processing software extrapolates the endocardial borders during semi-automated border tracking[138], and hence whilst it is possible to analyze datasets with incomplete RVOT visualization, the accuracy of reconstructions will most likely deteriorate with progressive dropout in the outflow tract.

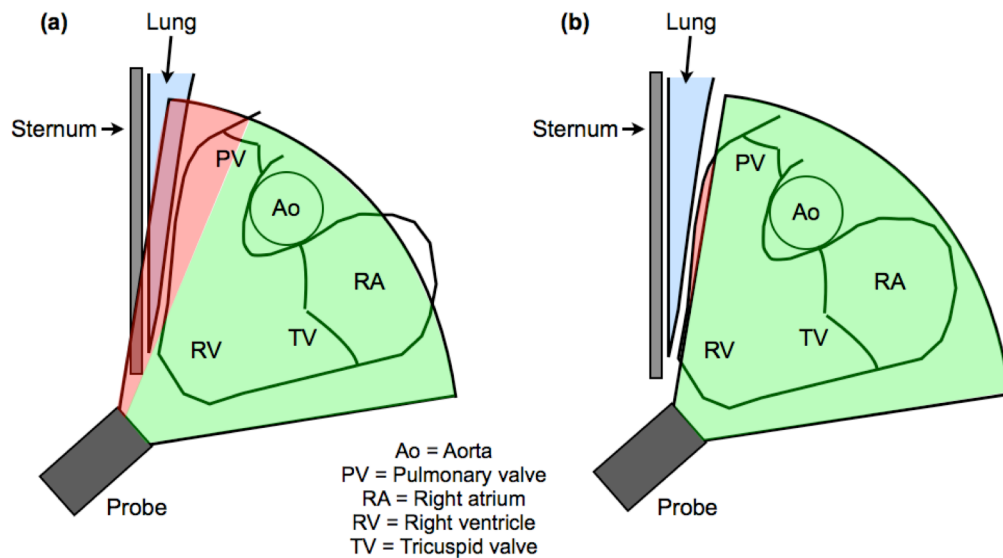


Figure 2-16: Right ventricular outflow tract (RVOT) dropout by 3DE: (a) sternum or lung tissue commonly shadows the anterior RVOT; (b) due to the anterior retrosternal position and morphology of the RVOT, the anterior RVOT still might not be included in the 3DE pyramidal volume despite moving rib spaces in an attempt to avoid this shadowing. Adapted from Ostenfeld et al.[128].

2.5.5 RV Volumetric Quantification by 3DE in Health and Disease

When comparing studies of RV quantification by 3DE, the homogeneity of the study population must be taken into account. The populations of acquired RV disease were favourable for the 3DE post-processing software algorithm, since it is set up for an adult-shaped RV rather than a subject with congenital heart disease[112]. This may be a reason why the limits of agreement were narrower than reported in patients with congenital heart disease[138]. No substantial bias was observed in either the PH or CHD groups, but subgroup analysis showed that end-diastolic volumes, and consequently stroke volumes, were underestimated in controls. This is despite the higher temporal resolution of images in this group, and is likely a result of low spatial resolution with single-beat 3DE.

Lower spatial resolution confers less ability to resolve myocardium and trabeculae, thus directing the operator to trace the endocardium further inside the RV cavity and hence underestimate volumes. This is supported by previous data showing greater variability and negative bias for 3DE to quantify RV volumes in non-dilated right hearts[111]. Conversely, RV endocardial delineation is known to be easier in the setting of RV hypertrophy or dilatation for both MRI and 3DE[111, 118], and is reflected by the higher image quality scores observed with the disease cohorts.

2.5.6 Operator experience and Reproducibility of 3DE RV Assessment

The progressive rise in 3DE image quality over the study duration reflects a significant learning curve with the technique also described in previous studies[78]. This is important clinically, as follow-up studies will vary depending upon operator experience for both acquisition and post-processing. This finding also reaffirms the recommendation of the ASE that, whilst 3DE RV assessment is preferred on the grounds of accuracy and reproducibility, it should be properly performed in echocardiography laboratories that have satisfactory training and experience with the technique[49, 50, 105].

Few studies so far have addressed 3DE test-retest reproducibility for both the acquisition and post-processing stages[118, 129]. The interobserver test-retest study demonstrated a second operator bias for EDV underestimation, conferring lower SV and EF measurements. This was a systematic error likely reflecting relative operator inexperience with the technique. The susceptibility of 3DE to underestimate RV volumes has been well documented[104], and the data from this study suggest that operator experience is related to this underestimation.

Furthermore, non-significant differences in intraobserver EDV and ESV nevertheless resulted in significant differences in SV and EF when the errors in the raw volumes are combined. Given that small changes in

endocardial border delineation are known to confer significant changes in 3DE-derived volumetric parameters in the LV[139], this is also likely to be a problem with 3DE reconstruction of the RV too. This is clinically important since a change of as little as 10mL in stroke volume by CMRI is clinically significant in PH [140], but a change of this magnitude may be masked by 3DE reproducibility error and/or the degradation of accuracy found with poorer quality 3DE datasets. For example, the interobserver measurement of RV stroke volume by 3DE showed a significant bias with a standard deviation over double that of CMRI. The CMRI reproducibility data shows narrow limits of agreement with no major bias between observers, consistent with previous reproducibility studies of RV quantification by transaxial slices[67, 141] and sensitive enough for detecting small changes in RV indices on serial studies.

2.6 Limitations

This study is a single-centre study based upon acquisitions made by one sonographer with experience using single-beat 3DE for RV volumetric quantification. As demonstrated by the test-retest reproducibility data, results cannot be applied across operators with variable experience of 3DE RV analysis.

Patients with arrhythmia were excluded due to the extra variability introduced by irregular cardiac cycles when comparing modalities. Single-beat acquisition is advantageous over traditional disk summation techniques that are limited by stitching artifact due to irregular R-R intervals, and this patient group requires further investigation with the technique.

There was a bias to underestimate cavity size particularly in control subjects, but the study was not designed to compare the accuracy of the technique in patients with large versus small cavity sizes. This question should be addressed in a separate prospectively designed analysis of large versus small RVs.

The sensitivity and specificity values for 3DE and 2DE to identify MRI-derived RVEF <50% were calculated by applying the ROC cut-off values to the same patients used to derive them as described previously[78], hence representing a "best case" scenario. A more appropriate method would be to identify cut-off values using ROC analysis in a derivation group, then prospectively evaluating the cut-off values in a separate test group in whom outcomes could be verified independently. Thus the diagnostic performances of the cut-off values found in this study need to be confirmed independently.

Finally, the study was not designed to provide CMRI test-retest reproducibility similar to the 3DE study design for acquisition and post-processing. However, CMRI does not have the same acquisition window restrictions inherent to transthoracic echocardiography, as contiguous transaxial RV slices of fixed thickness are acquired from the base of the right heart to the main pulmonary artery with the patient in the supine position. Nevertheless, this difference in technique methodology is a potential source of discrepancy, with the reference standard of CMRI building volumes from multiple slices compared with the full-volume datasets of 3DE[106]. Previous data overall suggest similar or slightly improved coefficients of variation for interstudy reproducibility of CMRI metrics of RV size and function to the 3DE-derived data in this study[64-66]. These studies analyzed short-axis stacks of cines, unlike this study protocol of acquiring transaxial stacks that is reported to confer improved reproducibility for RV assessment[67, 68]. Furthermore, similar statistical scrutiny in a test-retest format on the same patients who underwent 3DE test-retest reproducibility assessment would be required for direct comparison of CMRI reproducibility.

2.7 Conclusions

Single-beat full volume 3DE is a feasible technique for quantifying RV size and function in acquired right heart pressure- and volume-overload. The limits of agreement of 3DE are acceptable compared with CMRI, but may not be sensitive enough to detect small yet clinically significant responses to treatment demonstrated by this modality[140]. The test-retest reproducibility of 3DE suggests a significant learning curve that needs to be considered, and thus results cannot necessarily be extrapolated to less experienced operators. Nevertheless, 3DE showed incremental benefit over conventional 2DE measures, suggesting an important role in assessing acquired RV pathology. Future work should focus upon improving spatial resolution to optimize RV endocardial delineation, and in particular for adequate visualization of the RVOT in non-dilated RVs.

CHAPTER 3 Two-Dimensional Knowledge-Based Reconstruction of the Right Ventricle.

3.1 Introduction

Non-invasive imaging to quantify RV size and function should ideally yield three-dimensional data[26]. Despite advances in 3DE technology allowing acquisition of a full-volume RV data set in a single heartbeat, several disadvantages of RV volumetric quantification by 3DE persist:

- The adequate visualization of all RV regions, in particular the RV outflow tract (RVOT), can be technically difficult by 3DE[138, 142]
- There is an inherent operator learning curve associated with 3DE for RV assessment. Therefore, whilst the American Society of Echocardiography (ASE) favour the use of 3DE over 2DE for RV assessment, they stipulate that this applies to echocardiography laboratories with appropriate training and experience[49].
- Both spatial and temporal resolutions are more limited with 3DE compared with 2DE. The more limited spatial resolution of 3DE may partly account for underestimation of RV cavity volumes by this technique[104].
- The current commercially available 3DE RV post-processing algorithms do not account for the variability encountered of RV geometry in different disease states[112].

Some of the limitations of 3DE are not encountered with 2DE. Individual 2DE planes can interrogate specific RV regions, such as the inlet, apex and outlet portions. 2DE is also a more routine clinical imaging modality than 3DE, with spatial and temporal resolutions that are higher than those of 3D ultrasound. However, 2DE alone is insufficient to fully characterize a complex geometric 3D shape such as that of the RV. The transthoracic windows used for 2DE RV acquisition will also vary with respect to probe position, partly accounting for the inferior reproducibility of 2DE-acquired metrics compared with 3DE.

A hybrid approach affording the technical advantages of 2DE combined with the ability to reconstruct a 3D RV polygon would be most advantageous. Two-dimensional knowledge-based reconstruction (2D

KBR) is a novel technique that utilizes 2DE acquisition combined with additional technology for both the image acquisition and post-processing stages for volumetric RV quantitation. The KBR component utilizes a reference library of RV shapes from specific RV diseases to contribute to the final reconstruction of a 3D RV polygon.

3.1.1 Aims

The aims of this study were to:

- Provide further validation data for 2D KBR RV quantification in PH through comparison against CMRI.
- Evaluate the test-retest reproducibility for both the acquisition and post-processing components of this novel technique for volumetric quantification of RV function.
- Investigate the comparable test-retest reproducibility of a conventional 2DE metric, namely RV FAC, from the same four-chamber data sets utilized in the KBR reconstructions.

3.1.2 Personal Contribution

To fulfill the above aims I have:

- Obtained ethical approval from the local institutional research ethics committee (North West London REC 2) and research and development (R&D) approval from the R&D departments at The Royal Free Hospital and Great Ormond Street Hospital NHS Trusts.
- Enrolled 28 participants in sinus rhythm with no contraindications to magnetic resonance imaging.
- Performed and post-processed comprehensive 2DE and KBR studies of the right ventricle for all participants.
- Repeated the acquisition and post-processing stages for both FAC and KBR of RV functional parameters for all 28 participants.
- Post-processed the CMRI studies for all participants to quantify the reference standard metrics of RV function.

The results from this work have been published by D. Knight, J. Schwaiger, S. Krupickova, J. Davar, V. Muthurangu and J. Coghlan, in the Journal of the American Society of Echocardiography, 2015, **28**(8), entitled; “Accuracy and Test-Retest Reproducibility of Two-Dimensional Knowledge-Based Volumetric Reconstruction of the Right Ventricle in Pulmonary Hypertension” [143] (see Appendix 2).

3.2 Literature Overview

In this section, literature on the following areas will be discussed:

- Heterogeneity of RV shape in response to disease
- Development of the 2D KBR technique
- Volumetric assessment of RV function using KBR
- KBR versus 3DE post-processing algorithms

This overview highlights relevant papers that were found using the *PubMed* search engine. The search terms used included (a combination of):

- Knowledge-based reconstruction (KBR)
- Right ventricle
- Echocardiography
- Piecewise smooth subdivision surface (PSSS) reconstruction
- Cardiac MRI

When a relevant paper was found, the referenced papers were followed up and any subsequent papers that have cited this paper were also followed up.

3.2.1 Heterogeneity of RV shape in response to disease

There is significant regional heterogeneity in both global and regional RV shapes in congenital and acquired right heart disease. The anatomy of the RVOT is particularly variable in different congenital heart disease groups[144]. The contribution from the RV outflow tract is known to be an important determinant of the overall accuracy of RV volumetric

assessment[145]. Moreover, the contribution of the RVOT to overall ejection has prognostic implications in tetralogy of Fallot[146]. This has in turn prompted investigation of modified 2DE parameters in order to account for this regional variation of RV function[147].

In acquired RV disease, several studies have shown different patterns of RV segmental dysfunction. McConnell's sign describes regional wall motion abnormalities sparing the right ventricular apex being particularly suggestive of acute pulmonary embolism[148]. The pattern of regional wall motion abnormalities encountered in RV myocardial infarction will be dependent upon the culprit coronary artery[14]. Approximately four out of five of patients with arrhythmogenic right ventricular dysplasia have reduced RV function accounted for by regional wall motion abnormalities that vary in location[149]. Even within the disease spectrum of PH, there are known differences in RV shape that are encountered amongst different aetiological subtypes, such as idiopathic PH versus connective tissue disease-associated PH[150].

Therefore there is evidence to suggest that, whilst 3D assessment of the RV should be the preferred form of chamber quantitation, this should also take into account the spectrum of RV shapes and geometries encountered across different diseases.

3.2.2 Development of the 2D KBR technique

The 2D KBR technique investigated in this study utilizes novel technology for both the raw 2DE data acquisition and the post-processing RV polygon reconstruction stages.

3.2.2.1 Probe tracking

Data acquisition for 2D KBR relies upon using magnetic fields to track the spatial location and orientation of the 2DE probe, and consequently localization of the 2DE image planes in 3D space[151-154]. A magnetic localizer is attached to the probe, in this study mounted on a plastic

sheath moulded to the shape of the 2DE probe. This localizer detects orthogonal magnetic fields generated by a magnetic field transmitter, located either underneath or hung above the examination couch (Figure 3-1). The spatial location and orientation of the 2DE probe to which the receiver is attached, and thus the 2DE image plane itself, can be detected and located within the volume of orthogonal magnetic fields generated by the transmitter.

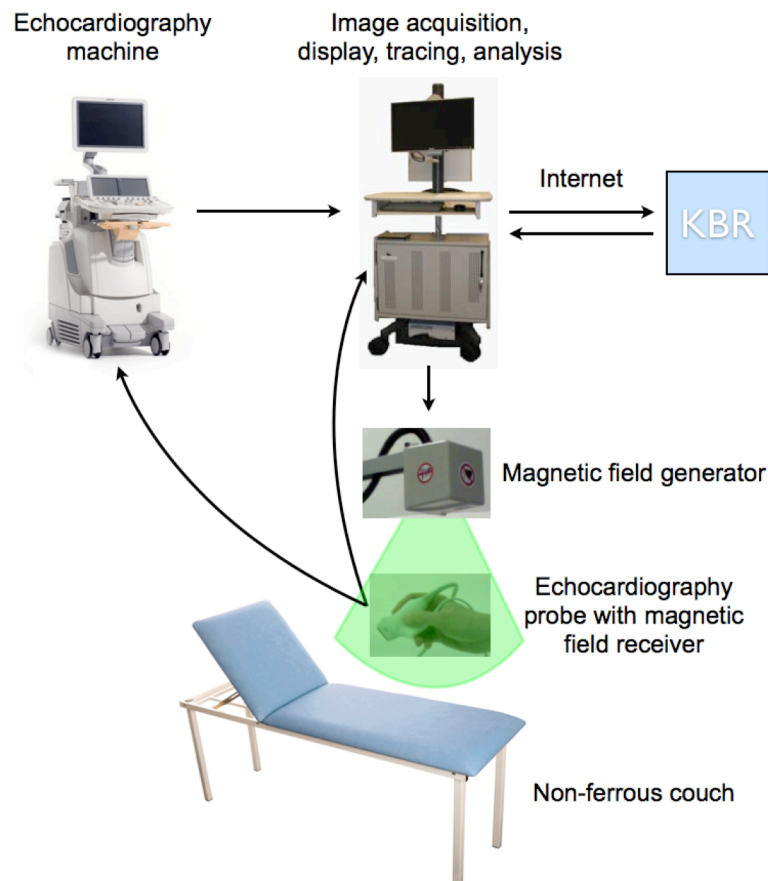


Figure 3-1: Schematic of the 2DKBR set-up.

The performance of the magnetic tracking system is optimized through calibration of the device on the specific 2DE ultrasound machine to which it is connected[153]. Whilst the localizer can operate in a range of up to 91 centimetres from the magnetic field transmitter, the optimal range for precision is within 25 to 60 centimetres[155]. The distance from the probe localizer to the magnetic field transmitter is indicated to the operator on the screen whilst acquisition takes place, and indicates to the user when the probe localizer is outside the optimal distance range. The localization

device has an accuracy of 0.74mm for locating a point target in vitro, and a resolution for measuring distances between point targets of $-0.12 \pm 0.76\text{mm}$ [156]. Objects that would interfere with the magnetic field must be kept away from the field transmitter and receiver by a pre-determined distance. In a previous iteration of the system, a non-ferromagnetic bed was required to prevent interference with the field transmitter that was placed below the bed[157]. The iteration of the system utilized in this study comprised the magnetic field generator hung over the patient using a mechanical arm. A cushioned wedge was placed on the echocardiography couch to ensure that the metallic couch apparatus did not interfere with the magnetic field.

Acquiring data by tracking the 2DE probe allows the sonographer to obtain images from any available 2DE window that permits visualization of any part of the RV. This is a specific advantage compared with 3DE, allowing unrestricted probe positioning and movement. This is especially important with respect to the potential for RVOT visualization by 2DE versus 3DE echocardiography windows (Figure 2-16).

3.2.2.2 Piecewise smooth subdivision surface (PSSS) reconstruction method

The PSSS reconstruction method[158] fits, subdivides and smoothens a volumetric mesh to the 2D RV endocardial borders that were identified and defined by the operator. These endocardial borders are delineated prior to the PSSS reconstruction either traditionally by manual tracing or, more simply, by using points plotted by the operator combined with knowledge-based reconstruction (KBR, see section 1.2.2.3). The PSSS method accepts raw data input from any combination of 2DE image planes. Therefore the visualization and localization of RV structures can be defined from the 2DE windows that most optimally display them, independently of the echocardiography probe orientation or position. PSSS is the only reconstruction method that has been shown to

reproduce the 3D shapes of the LV and RV chambers with anatomical accuracy[156, 159-161].

Reconstruction of the 3D endocardial surface by the PSSS method consists of a two-step reconstruction algorithm[156, 159, 162-164]. The first step comprises translating, rotating and scaling a triangulated control mesh to fit it to the traced or plotted data representing the RV endocardium. The raw traced or plotted data includes anatomic landmarks labeled by the operator. This allows parts of the fitted control mesh to be marked as sharp edges and vertices, corresponding to, for example, valvular annuli or the angle between the RV septum and free wall. This also allows knowledge of regions of complex shape such as the outflow tract to be integrated into the fitting of the control mesh to the endocardial borders (Figure 3-2).

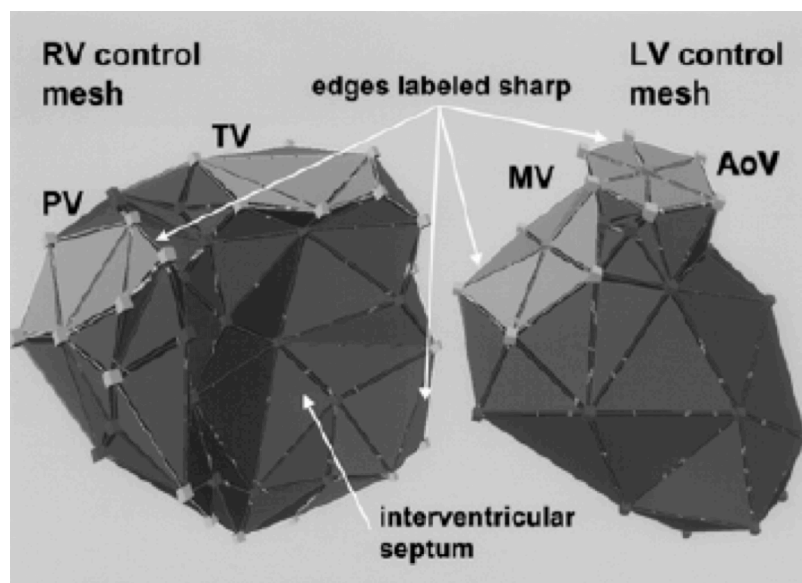


Figure 3-2: Stage 1 of PSSS: Abstract control meshes for both RV (left) and LV (right) used by the PSSS reconstruction technique. These meshes incorporate knowledge about the location and shape of certain ventricular structures.

Reproduced with permission from Hubka et al.[159].

The second step involves repeatedly refining the control mesh through subdividing the mesh twice. This entails automated repositioning of the mesh vertices to minimize the residual distances between the raw endocardial border data and the subdivided mesh, whilst also satisfying predetermined smoothness parameters for the 3D reconstruction (Figure 3-3).

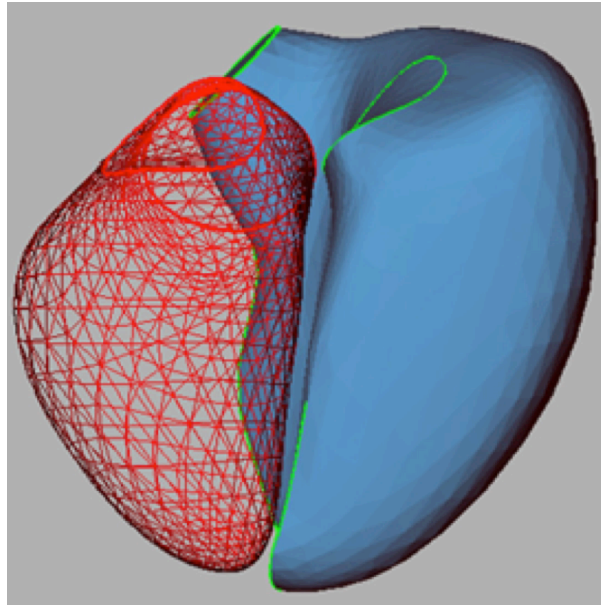


Figure 3-3: Stage 2 of PSSS: The smooth surfaces of the LV (mesh) and RV (surface) having undergone the second stage of PSSS, entailing subdivision of the previously applied control mesh.

Reproduced with permission from Sheehan et al.[164].

3.2.2.3 Knowledge-based reconstruction (KBR)

In KBR, knowledge of the expected shape of the RV and of the range of shapes that it can adopt in disease processes is utilized to streamline the post-processing workflow for volumetric analysis. Sparse user input consists of points plotted at anatomical landmarks by the operator, which are used to identify RV endocardium. This is instead of the more laborious approach of conventional manual endocardial border tracing. The KBR algorithm then integrates the knowledge of the RV shape to fill in the gaps between the points to create a border. The accuracy of PSSS using plotted endocardial landmarks combined with KBR has been validated against PSSS using conventional manual endocardial border tracing[164].

As already discussed, RV remodeling in response to haemodynamic overload results in a diverse range of cavity shapes. The KBR algorithm integrates a priori knowledge of the shape of the RV in specified disease processes in the reconstruction of 3D RV volumes. This knowledge consists of reference to databases or catalogues of fully traced MRI-derived RV volumes of specified disease aetiologies, with a wide spectrum of RV volumes and shapes. In this case of this study, the KBR database was accessed via a secure Internet connection (Figure 3-1). The databases include normal right ventricles, repaired tetralogy of Fallot, pulmonary hypertension and post-atrial switch transposition of the great arteries. Furthermore, RV KBR assessment in patients with adult congenital heart disease with RV-to-pulmonary artery (PA) conduits was more recently performed using a specific database of fully traced CMR-derived RV volumes of patients with RV-PA conduits[165]. The number of fully traced RV volumes that make up each KBR reference catalogue database is not specified by the system vendor (Ventripoint, Inc., Seattle, WA). However, the reconstructed RV volumes of 110 patients with tetralogy of Fallot comprised the KBR database in one validation study[164].

3.2.3 Validation of volumetric assessment of RV function using KBR versus CMRI

Six studies have compared 2D KBR for volumetric RV assessment against CMRI in a total of 158 subjects (Table 3-1)[157, 165-169].

Investigator (year)	N	Patient characteristics
Dragelescu et al. (2011)	30	Repaired tetralogy of Fallot
Dragelescu et al. (2012)	40	Repaired tetralogy of Fallot
Kutty et al. (2012)	15	Repaired d-transposition of great arteries
Bhave et al. (2013)	27	Pulmonary hypertension
Neukamm et al. (2014)	29	Repaired tetralogy of Fallot and PVR
Wheeler et al. (2015)	17	Congenital heart disease (tetralogy of Fallot, pulmonary atresia with ventricular septal defect, or truncus arteriosus) with RV to PA conduit

Table 3-1: Studies of RV quantification by 2D KBR versus CMRI

There is a small tendency for RV cavity volumetric underestimation, but less so than previously reported with 3DE and with clinically acceptable limits of agreement (Figure 3-4).

The reproducibility of 2D KBR RV echocardiography has not been studied in a test-retest format. Only interobserver and intraobserver post-processing reproducibility analyses of the same data sets acquired by a single observer have been described to date. Overall, good metrics of post-processing reproducibility were reported in all studies.

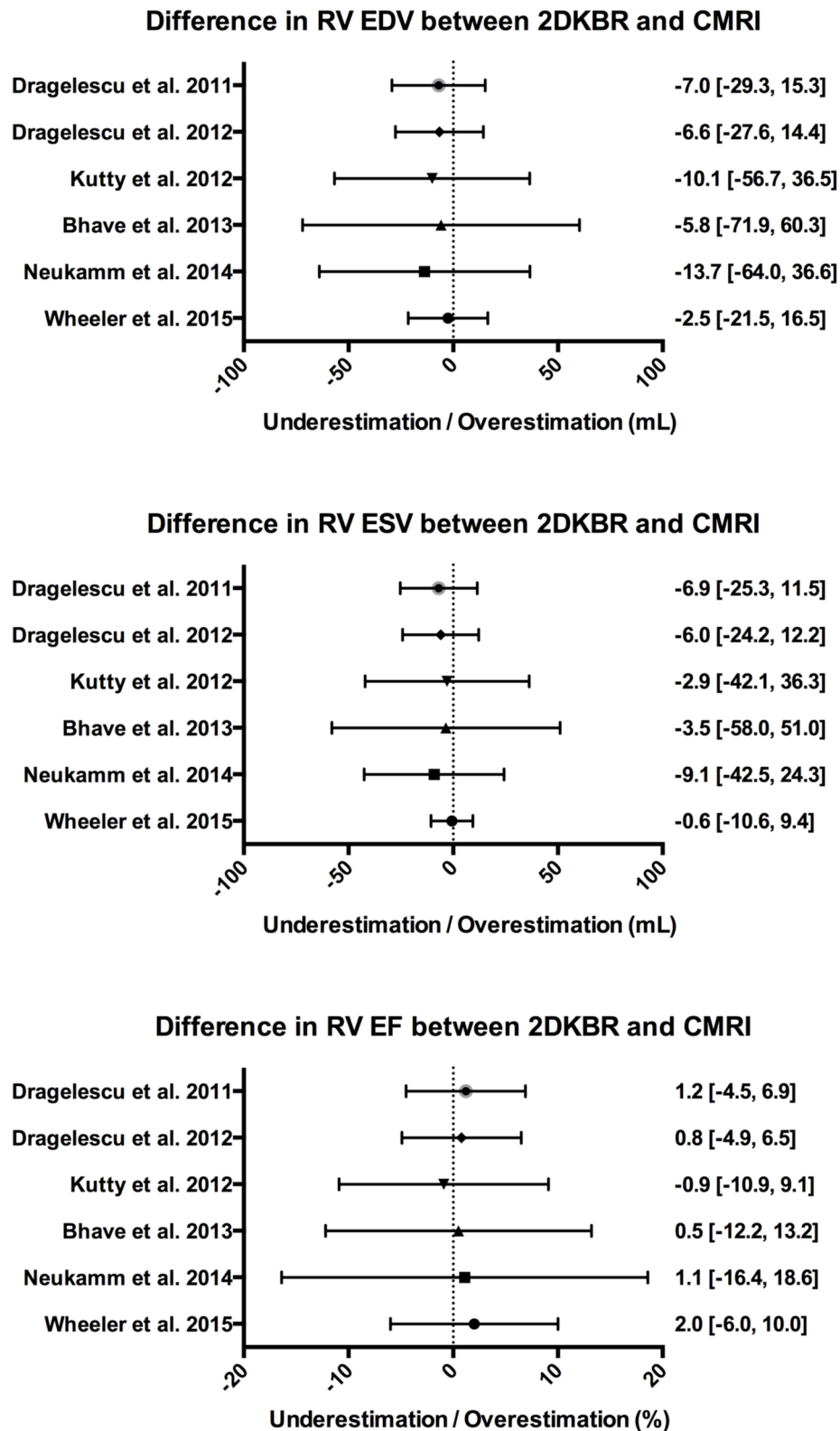


Figure 3-4: Forest plots of results from previous studies of RV quantification by 2D KBR versus CMRI.

3.2.4 Direct comparison of KBR versus 3DE RV post-processing algorithms

The differential response of RV shape and remodeling by disease state has been suggested as a limitation of the accuracy of conventional 3DE RV reconstruction post-processing algorithms, which are based upon normal RV cavity shapes[112]. Therefore KBR offers a novel volumetric reconstruction post-processing technique to compare with the current clinical standard of the volumetric semi-automated border detection approach[49]. Currently, there are limited data to provide such a comparison.

Laser et al. studied 3DE-acquired RV data sets post-processed with KBR against CMRI[170]. The authors note that this could provide a potential advantage for RV echocardiography in patients with arrhythmia and consequent R-R interval variability. However, the study itself was performed utilizing a multiple-beat gated 3DE system acquired over 4 sub-volumes in 60 subjects in sinus rhythm (40 patients with RV disease and 20 healthy volunteers), negating this theoretical advantage. Nevertheless, analysis of 3DE-acquired RV datasets using KBR post-processing was both feasible and accurate compared to CMRI.

A further criticism of the study is that the comparative accuracies of the KBR and conventional 3DE post-processing algorithms with the same 3DE datasets were not examined against CMRI. The only study comparing the accuracy and reproducibility of both 2D KBR and 3DE versus CMRI is by Dragelescu et al.[167]. The 2D KBR technique had higher feasibility than 3DE, was more accurate than the conventional Beutel method against CMRI, and had better post-processing reproducibility than 3DE.

3.2.5 Summary

From the literature overview, it is clear that a more disease-specific approach needs to be considered for 3D RV echocardiography assessment. 2D KBR is recognized as a feasible and accurate novel technique for RV functional quantification. Furthermore, 2D KBR takes into account the heterogeneity of geometric alterations encountered in congenital and acquired RV pathology. However;

- There are a limited number of studies comparing RV assessment by 2D KBR versus CMRI.
- There is only one small study comparing 2D KBR to CMRI in an adult acquired RV disease population (PH).
- There are no studies of reproducibility in a test-retest format for 2D KBR RV quantification for both the acquisition and post-processing components of the technique.

I aim to perform the first test-retest study of 2D KBR for RV volumetric quantification in an adult population of acquired RV pressure overload. This will be compared against the reproducibility of 2DE-acquired RV FAC using the same 2DE raw data from which the KBR volumetric reconstruction is performed. I will also provide further validation data for the technique against CMRI in PH.

3.3 Methods

A prospective cross-sectional study was performed that enrolled 28 patients in sinus rhythm with no contraindications to magnetic resonance imaging, all of whom underwent comprehensive 2D transthoracic echocardiography and CMRI on the same day (median scan interval, 116 min; interquartile range, 104–150 minutes).

3.3.1 Study Population

All participants had presented for diagnosis and/or follow-up of PH (diagnosed by right heart catheterization as a mean pulmonary artery pressure $>25\text{mmHg}$ and a pulmonary capillary wedge pressure $<15\text{mmHg}$ [121]). The aetiologies of PH were idiopathic ($n = 5$), connective tissue disease associated ($n = 14$), chronic thromboembolic disease ($n = 8$) and portopulmonary ($n = 1$). Exclusion criteria were arrhythmia and known independent left-sided cardiac disease unrelated to PH.

The study complied with the Declaration of Helsinki. The local institutional research ethics committee (North West London REC 2) approved the study and informed written consent was obtained from all participants

3.3.2 Two-dimensional echocardiography and KBR

3.3.2.1 Image acquisition

All patients underwent comprehensive 2D and Doppler transthoracic echocardiography in the left lateral decubitus position using the Philips iE33 echocardiographic system (Philips Medical Systems, Andover, MA) with the S5-1 transducer (frequency bandwidth, 1–5 MHz). A standard clinical protocol for all examinations was followed in conjunction with American Society of Echocardiography guidelines for chamber quantification [50, 123].

A magnetic localizer was attached to the S5-1 transducer by a moulded plastic sheath. The magnetic localizer was connected to a dedicated console, from which a mechanical arm with an attached magnetic field generator hung over the patient (Figure 3-5; VentriPoint Diagnostics Ltd., Seattle, WA). The localizer mounted on the ultrasound transducer were calibrated to detect orthogonal magnetic fields from the generator hanging over the patient. A cushioned wedge was placed on the echocardiography couch to ensure that the metallic couch apparatus did not interfere with the magnetic field, and patients were instructed to

remain entirely stationary in the left lateral decubitus position for the duration of a study acquisition. The ultrasound depth required to visualize all relevant structures was determined before commencing the study and remained fixed throughout.

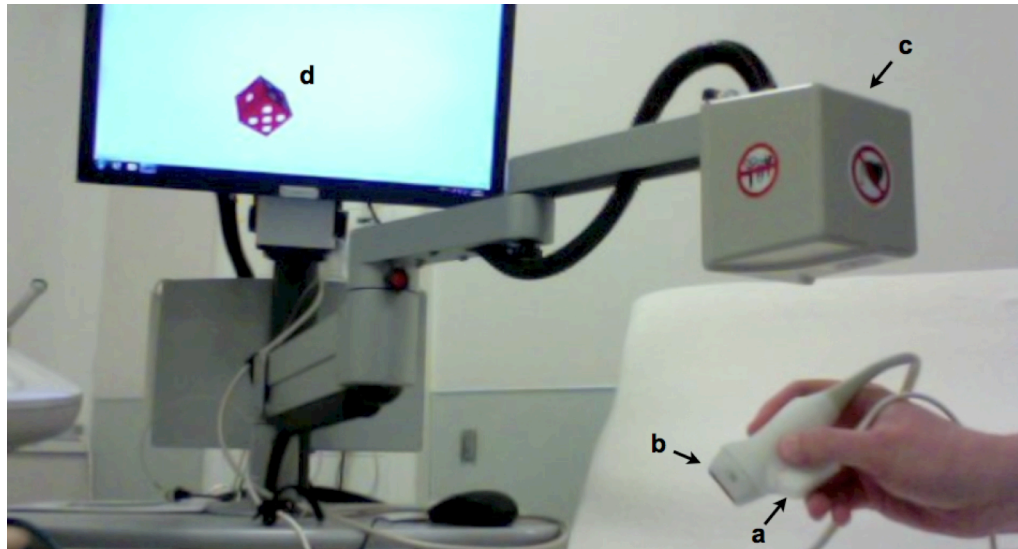


Figure 3-5: 2DKBR apparatus.

A localizing transducer (a) attached by a moulded plastic sheath to a conventional 2DE probe (b) detects orthogonal magnetic fields emitted by the generator (c) attached to the mechanical arm that hangs over the patient. Here in the 2DKBR calibration module the die on the screen (d) represents the 2DE probe, which moves synchronously with any movement of the 2DE probe. Note the cushioned wedge in the background that is placed on the echocardiography couch to ensure that the metallic apparatus underneath couch does not interfere with detection of the magnetic fields.

Seven 2D transthoracic echocardiographic views were obtained in all subjects: parasternal long axis, parasternal short axis at the papillary muscle and apical levels, parasternal RV inflow, parasternal RV outflow including pulmonary valve hinge points and infundibulum, apical four chamber, and an off-axis RV apical view. The 2D KBR acquisition from each view consists of a 2-second period (usually containing two or three heartbeats) acquired during end-expiratory breath-holds. The electrocardiograph was connected to the echocardiographic system via the dedicated 2D KBR console, and the console images were reproduced from the echocardiographic system's video output and digitized at 30 frames/second. Image quality was subjectively graded on a 5-point scale from 0 (very poor) to 4 (perfect) [127].

3.3.2.2 Post-processing: RV FAC

End-diastolic and end-systolic frames were assigned by visual identification of the largest and smallest RV four-chamber cavity areas, respectively, on the 2D KBR console. These frames were exported to the open-source OsiriX DICOM software for the measurement of RV FAC by tracing the RV endocardium in both frames as described in 1.2.1.2.

3.3.2.3 Post-processing: KBR

The largest and smallest RV cavity areas were visually identified as end-diastole and end-systole, respectively, on the 2D KBR console in the four-chamber view. The software subsequently assigned the same time interval between these frames to all other views. Due to the peristaltic contraction pattern of the RV and the abnormal interventricular septal dynamics in PH, identifying the smallest RV cavity area can be subject to variation when inspecting different 2D views[24]. The smallest RV cavity size determined from the four-chamber view, however, has been shown to be a convenient, consistent and accurate method to identify RV end-systole for determining RV volumes[171].

On the 2D KBR console, a series of anatomic RV landmarks were identified on the 2D echocardiography images (Figure 3-6, Table 3-2) in the end-diastolic frames and subsequently in the end-systolic frames. A minimum of 26 points was plotted for each of the end-diastolic and end-systolic data sets. RV endocardial points were placed at the junction between trabeculations and myocardium. The plotted anatomic landmarks with their respective 3D spatial coordinates were then submitted via the Internet to a secure remote server for remote processing by a proprietary 2D KBR algorithm. The algorithm interpolates between the plotted points by referencing against a catalogue of RV shapes generated by CMRI from patients with known diagnoses of PH.

End-diastolic and end-systolic 3D models of the right ventricle were reviewed in a systematic fashion. Intersections between the borders of

the 3D model and the original 2D scan plane were inspected to ensure concordance between 2D images and 3D reconstructions (Figure 3-6), and marked points were checked for alignment with the surface of the 3D model. Where significant deviations between the reconstructed model and either the plotted points and/or 2D echocardiographic endocardial borders existed, points were re-plotted and the algorithm was rerun. Where significant border versus 2D image misalignment suggested a shift in patient position or an inadequate breath-hold, all points from that 2D view were removed, and the erroneous 2D echocardiographic view was excluded from the 2D KBR reconstruction. A maximum of one view of the seven required in the data acquisition protocol could be excluded for any given study because of a change in patient position or an inadequate breath-hold. If this problem was encountered in more than one of the seven required views, the entire study was excluded from the final analysis.

The final check entailed inspection of the nested view of end-diastolic and end-systolic models to verify alignment of the tricuspid and pulmonary annular planes (Figure 3-6). The final 2D KBR polygon was assessed for precision by subjectively scoring on a 5-point scale depending on the proximity of intersections of the plotted landmarks with the reconstructed polygon: 4 (all points intersect), 3 (three or fewer points significantly deviate from polygon), 2 (five or fewer points significantly deviate from polygon), 1 (seven or fewer points significantly deviate from polygon), and 0 (poor agreement).

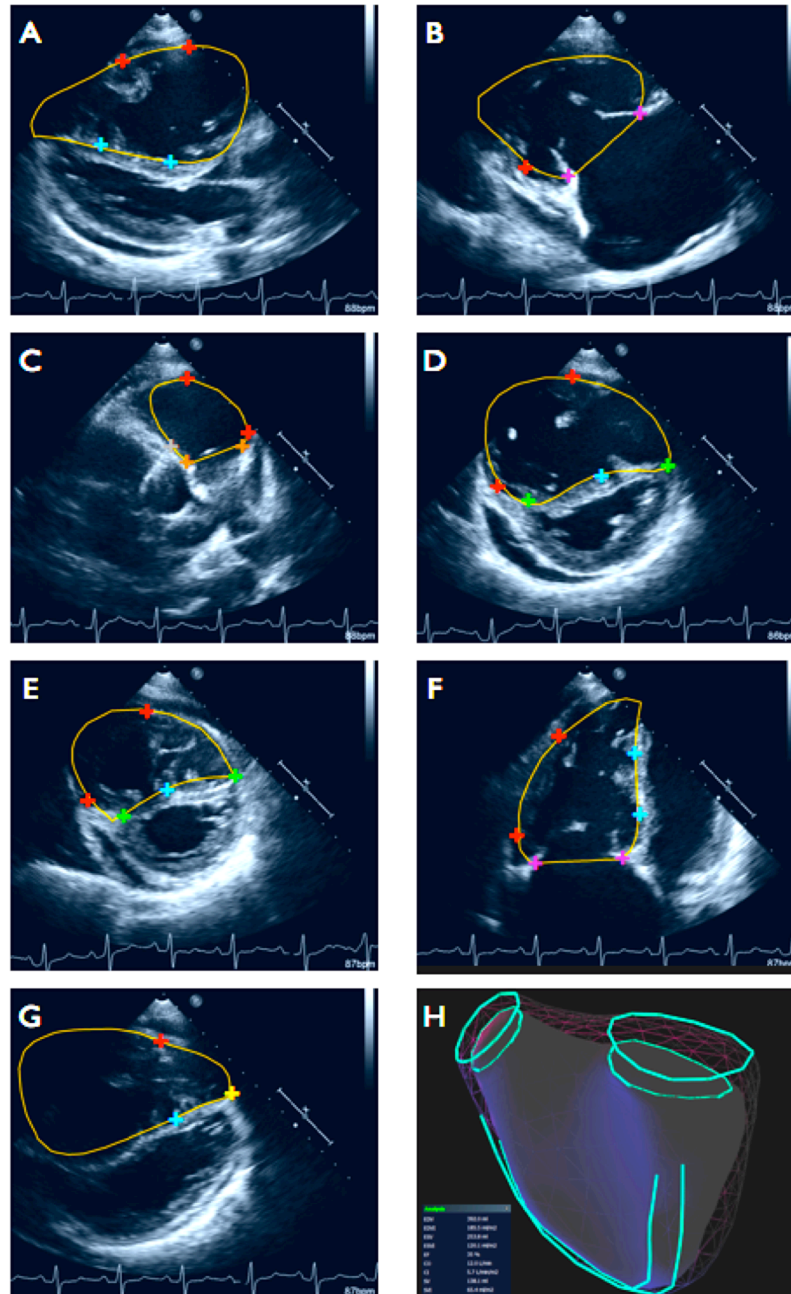


Figure 3-6: Post-processed 2DKBR data from a participant with PH.

All required 2DE scan planes are displayed: (a) parasternal long-axis (PLAX), (b) PLAX RV inflow, (c) PLAX RV outflow including infundibulum and pulmonary valve hinge points, (d) parasternal short-axis (PSAX) at mid-cavity (papillary muscle) level, (e) PSAX apical level, (f) 4-chamber RV, (g) off-axis RV apical view (note how the RV apex rides over the LV apex). The different coloured cross-hairs represent user-defined plots for different RV structures; for example, red crosses are plotted along the RV endocardium, turquoise crosses along the RV side of the interventricular septum, a yellow cross at the RV apex, orange crosses at the pulmonary valve annulus, and purple crosses at the tricuspid valve annulus. The yellow border tracings are superimposed projections of the 2DKBR RV reconstruction onto the original 2DE scan data, also showing how the polygon extends beyond the original 2DE image sector. Landmarks can be checked and repositioned by the user if required, and the 2DKBR algorithm is re-run. A final check is the nested view (h) of end-diastolic and end-systolic polygons to ensure alignment of tricuspid and pulmonary valve orifices.

2DE view	Landmarks plotted							
	Endocardium	IVS	IVS/RV angle	TV annulus	PV annulus	Infundibulum	Basal RV free wall	RV apex
PLAX	✓	✓						
PSAX-PM	✓	✓	✓					
PSAX-apical	✓	✓	✓					
PSAX-RVIT	✓			✓				
PSAX-RVOT	✓				✓	✓		
A4Ch	✓	✓		✓			✓	
Off-axis apical RV	✓	✓						✓

PLAX = parasternal long axis; PSAX = parasternal short axis; PM = papillary muscle level; RVIT = right ventricular inflow tract; RVOT = right ventricular outflow tract; A4Ch = apical four chamber.

Table 3-2: Landmarks plotted in each 2DE RV plane to enable 2DKBR reconstruction.

3.3.2.4 FAC and 2DKBR test-retest reproducibility

All subjects underwent serial 2DE acquisition and post-processing by two independent sonographers (D.S.K. and J.S.) as described previously (see section 2.3.4)[129]. The two sonographers had similar experience of 2D transthoracic echocardiography (over 4 years each), and received the same vendor training for the 2DKBR system. Sonographer 1 (D.S.K.) obtained a 2DKBR data set, following which sonographer 2 (J.S.) independently obtained a 2DKBR data set. Following this, sonographer 1 acquired a second 2DKBR dataset. The sonographers, who were blinded to each other's results and the results from cardiac MRI, performed post-processing of their own datasets for FAC and 2DKBR. Datasets analyzed for intraobserver test-retest reproducibility were post-processed separately at time intervals of more than two weeks.

3.3.3 Cardiac MRI

3.3.3.1 Image acquisition

All CMRI images were acquired using a 1.5 Tesla MR scanner (Avanto, Siemens, Erlangen, Germany) using a 12-element phased array coil for signal reception and the body coil for signal transmission. A vector electrocardiogram system was used for cardiac gating. In all patients, ventricular volumes and great vessel flow were measured as previously described[142]. Volumetric RV data was obtained using real-time radial k - t SENSE imaging of contiguous transaxial slices[63, 80].

3.3.3.2 Post-processing

All image post-processing was performed using 'in-house' plug-ins for the open source OsiriX DICOM software[63, 132, 133]. Endocardial RV borders were traced manually at end-diastole and end-systole, the time points of which were identified by the largest and smallest RV cavity areas respectively (Figure 2-10). The inclusion of RV trabeculations was the same as that performed by echocardiography post-processing. RV volumetric parameters were calculated as described in section 2.3.5.2.

3.3.4 Statistics

Statistical analysis was performed using SPSS 22.0 (IBM Corporation, Armonk, New York, USA) and Prism 6.0b for Mac (GraphPad Software, Inc., La Jolla, California, USA). All continuous data were normally distributed and expressed as mean \pm standard deviation (SD). Systematic differences between measurements were evaluated with Student's paired *t*-test (two-tailed). *P*-values < 0.05 were considered statistically significant. Intermodality agreement was studied using the Bland-Altman method, whereby the mean difference was presented as the bias and 95% limits of agreement around the bias expressed as the mean difference ± 1.96 SD[134].

Differences between test-retest measurements were analyzed by one-way repeated measures ANOVA, with the Bonferroni post-hoc test identifying which specific means differed. The Greenhouse-Geisser correction was used if the assumption of sphericity had been violated. Test-retest variability was expressed using intraclass correlation coefficients (ICC), relative differences (RD) and coefficients of variation (COV). The ICC was quantified by the two way random effects model with absolute agreement. An ICC > 0.85 was considered excellent. RDs were calculated by taking the absolute difference between two observations divided by the mean of the repeated observations and expressed as a percent. COVs were calculated as the standard deviation of the difference between two acquisitions divided by their mean value, and expressed as a percentage[135]. A COV $\leq 10\%$ was considered excellent.

3.4 Results

3.4.1 Study Population Characteristics

The clinical characteristics of the 28 participants are presented in Table 3-3, all of whom had adequate 2DE windows for the specified protocol.

Variable	Number (%)
Number of patients	28
Age (years)	54 ± 13
Female	20 (71)
Height (cm)	165 ± 11
Weight (kg)	71 ± 18
Body surface area (m ²)	1.8 ± 0.3
Heart rate (bpm)	79 ± 13
Mean PASP at RHC (mmHg)	47 ± 12
Pulmonary vasodilators (% of total)	
Endothelin antagonist	11 (39)
PDE5 antagonist	18 (64)
Oral prostanoid	1 (4)
Inhaled prostanoid	1 (4)
CMRI RV parameters	
RVEDV (mL/m ²)	98 ± 26
RVESV (mL/m ²)	59 ± 23
RVEF (%)	41 ± 11
Data are expressed as mean ± SD	

Table 3-3: Patient characteristics

3.4.2 2DKBR Technical Data

Participant heart rates recorded on the 2DE loop acquired first were similar to those recorded on the 2DE loop acquired last ($P = 0.90$). Image acquisition for one data set took of the order of approximately 5 minutes per patient, with 2DKBR post-processing and analysis taking no longer than about 15 minutes. Good mean subjective scores were observed for 2DE image acquisition (2.9 ± 0.9) and 2DKBR reconstruction (3.2 ± 0.7), with moderate correlation between the two scores ($r = 0.54$, $P = 0.003$).

3.4.3 RV quantification by 2DKBR versus CMRI

RV volumes and EF for all participants measured by 2DKBR showed no significant differences with CMRI (Table 3-4), with no significant bias and clinically acceptable limits of agreement (Figure 3-7).

Measurement	2DKBR	CMRI	P^*
RVEDV (mL)	179 ± 66	176 ± 61	0.16
RVESV (mL)	107 ± 47	106 ± 47	0.63
RVSV (mL)	73 ± 27	70 ± 26	0.26
RVEF (%)	42 ± 10	41 ± 11	0.66

Data are expressed as mean \pm SD

*Paired Student's t -test

n = 27 (1 patient excluded due to movement artifact during 2DKBR study)

Table 3-4: RV volumes and ejection fractions by 2DKBR versus CMRI

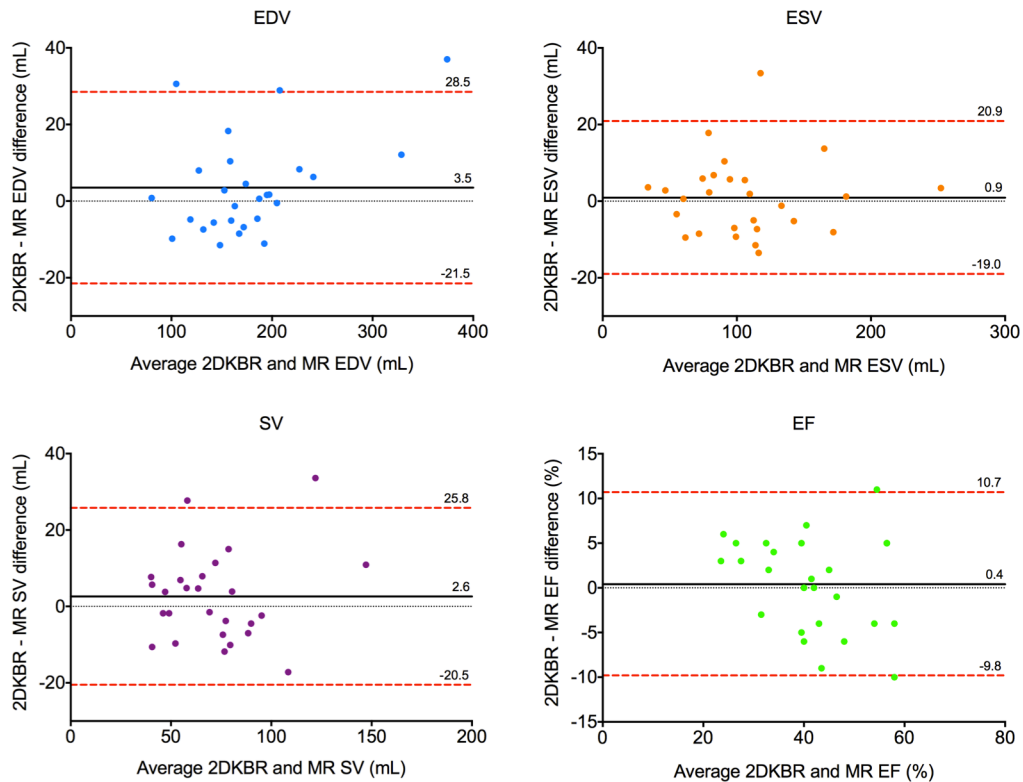


Figure 3-7: Bland Altman analysis of bias (black solid line) and 95% limits of agreement (red dashed line) for 2DKBR versus CMRI quantification of RV EDV, ESV, SV and EF. n = 27 (1 patient excluded due to movement artifact during 2DKBR study).

3.4.4 Test-retest intraobserver and interobserver reproducibility.

One patient moved in the first dataset acquisition, one patient moved in the third dataset acquisition, and two patients moved in both the second and third dataset acquisitions. The 2DKBR datasets for these four individuals were therefore excluded from the final test-retest reproducibility analysis due to significant movement artifact.

Good reproducibility metrics and acceptable limits of agreement were observed for the 24 intra- and interobserver 2DKBR test-retest studies (Table 3-5, Figure 3-8).

2DKBR variable	Intraobserver			Interobserver		
	ICC	COV (%)	RD (%)	ICC	COV (%)	RD (%)
RVEDV (mL)	0.985	3.0	4.2	0.986	3.9	5.5
RVESV (mL)	0.987	4.3	6.1	0.960	7.7	10.9
RVSV (mL)	0.953	8.3	11.7	0.856	11.7	16.5
RVEF (%)	0.919	6.4	9.0	0.758	10.5	14.8

2DE variable	ICC	COV (%)	RD (%)	ICC	COV (%)	RD (%)
RVEDA (cm ²)	0.885	9.0	12.7	0.394	25.0	35.4
RVESA (cm ²)	0.931	9.3	13.2	0.440	31.0	43.9
RV FAC (%)	0.784	18.1	25.6	0.619	20.8	29.4

Table 3-5: Test-retest reproducibility results for 2DKBR and 2DE RV metrics.

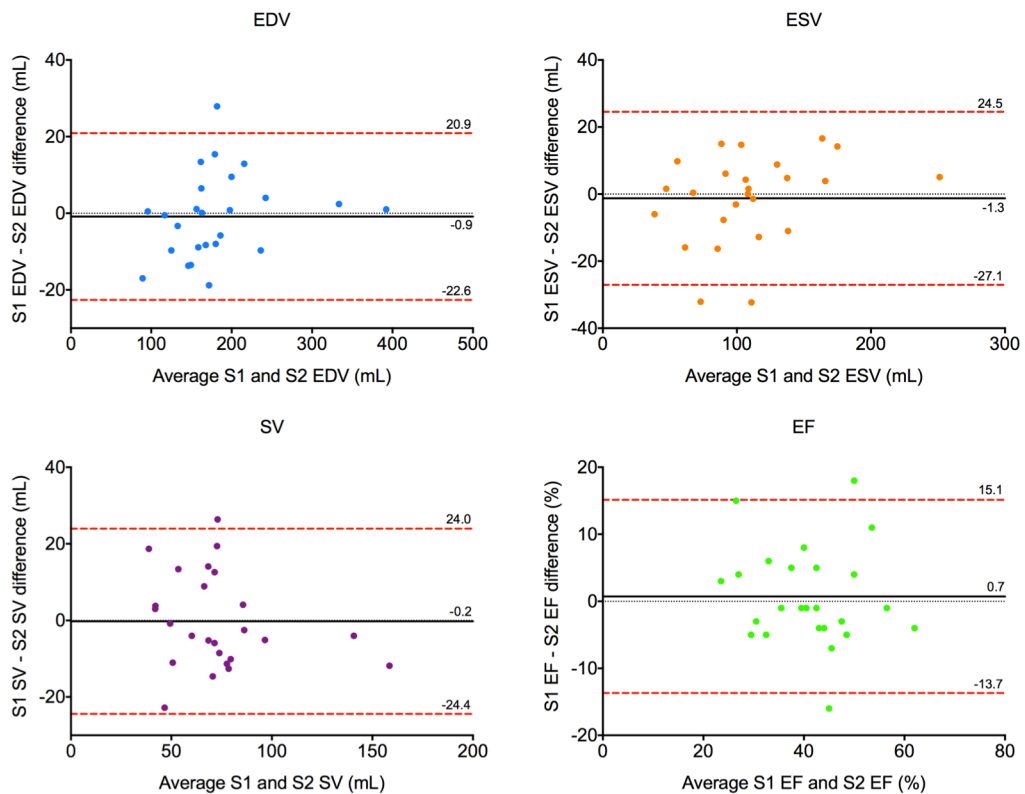


Figure 3-8: Bland Altman analysis of bias (black solid line) and 95% limits of agreement (red dashed line) for interobserver 2DKBR test-retest reproducibility of RV EDV, ESV, SV and EF. n = 25 (3 patients excluded due to movement artifact during 2DKBR study).

S1 = sonographer 1, S2 = sonographer 2.

There were no significant differences for RV volumes or EF between serial 2DKBR studies, but significant intra- and interobserver test-retest variability was demonstrated for serial RV areas and FAC (Table 3-6).

2DKBR variable**	S1.1	S2	S1.2	P*
RVEDV (mL)	184 ± 68	185 ± 65	180 ± 66	0.17
RVESV (mL)	110 ± 49	111 ± 45	111 ± 48	0.80
RVSV (mL)	74 ± 27	74 ± 30	69 ± 27	0.15
RVEF (%)	41 ± 10	41 ± 11	40 ± 10	0.39
2DE variable***	S1.1	S2	S1.2	P*
RVEDA (cm ²)	23 ± 6	32 ± 7	23 ± 7	<0.001
RVESA (cm ²)	15 ± 6	22 ± 6	16 ± 6	<0.001
RV FAC (%)	36 ± 15	31 ± 10	34 ± 14	0.05

S1 = Sonographer 1 (1.1 = first acquisition, 1.2 = repeat acquisition)

S2 = Sonographer 2

Data are expressed as mean ± SD

*One-way repeated measures ANOVA

**n = 24 (4 patients excluded due to movement artifact)

***n = 27 (1 patient had an unanalyzable 4 chamber image that precluded FAC but not 2DKBR)

Table 3-6: Interobserver and intraobserver test-retest reproducibility of RV volumes and EF by 2DKBR, and RV areas and FAC by 2DE

3.5 Discussion

The main findings of this study were:

- (i) 2DKBR is a feasible and accurate technique for RV quantification in PH.
- (ii) This study provides the first test-retest reproducibility data for 2DKBR volumetric RV assessment and 2DE RV assessment by FAC.
- (iii) The 2DKBR technique demonstrated good test-retest reproducibility, with no significant differences between serial interobserver and intraobserver test-retest studies.
- (iv) Conventional RV assessment by 2DE-derived FAC has significant intraobserver and interobserver test-retest variability.

3.5.1 Validation of the 2DKBR technique for RV Assessment

2DKBR is an emerging technique that has been validated in congenital heart disease populations[157, 167, 168] and more recently in a small population of PH patients[166]. The limits of agreement in this study are clinically acceptable compared with the gold standard of cardiac MRI, slightly more favourable than those obtained previously in idiopathic PH[166], and similar to previous work in children following surgical repair of tetralogy of Fallot[167].

A potential explanation for these differences might be due to the quantification of RV volumes by CMRI using a transaxial stack of RV slices rather than the short-axis stack approach. This has the advantage of avoiding partial voluming of the basal RV slices that is of particular relevance in PH due to the relative preservation of longitudinal over radial function[54]. A transaxial slice orientation facilitates the identification of the inflow and outflow components of the RV, and ultimately confers better reproducibility for RV volumetric quantification by CMRI[67, 68, 141]. The 2DKBR hardware used in this study also differs from that in previous studies in terms of the position of the magnetic field generator either above or underneath the patient bed. The equipment comprised a magnetic field generator suspended directly above the patient's chest. However, the magnetic field generator location above or below the echocardiography couch should not theoretically affect the spatial detection of the 2DE probe localizer.

3.5.2 Test-retest reproducibility of 2DKBR RV Assessment

To my knowledge, this is the first study designed to assess the test-retest reproducibility of 2DKBR. Importantly, the 2DKBR technique showed no significant differences for interobserver or intraobserver test-retest reproducibility, whereas FAC had significant test-retest variability. The only previous study of test-retest reproducibility of 2DE RV area metrics had a comparable intraobserver test-retest coefficient of variation for RV

FAC of 16.5%[52]. The reproducibility of FAC post-processing alone (not including variability in image acquisition) has also been shown to have significant interobserver bias and wide limits of agreement in children following surgical repair of tetralogy of Fallot compared with 2DKBR[167]. The test-retest reproducibility of 2DKBR RV volumetric quantification is also improved compared to that previously demonstrated by 3DE in either congenital heart disease[129] or acquired PH[142].

The superior reproducibility of 2DKBR compared with conventional 2DE and that previously reported for 3DE may be accounted for by several reasons. Firstly, FAC and 3DE require good endocardial delineation to trace the RV border, whereas 2DKBR requires the user to define single points along the endocardium rather than the border in its entirety. Secondly, in contrast to 2D FAC, the 3D spatial localization of the 2DE probe compensates for the acquisition variability in transthoracic windows between operators[156]. Finally, post-processing reproducibility is also likely to be enhanced by the KBR process. The software allows simultaneous display of the raw 2DE data intersecting with the reconstructed endocardial borders and 3D polygon. The user then has the option of readjusting or adding plotted points when the intersections between reconstructed borders and the borders visualized on the raw 2DE images are not in agreement. The current study protocol mandated a review of the reconstructed RV polygon endocardial borders relative to the original 2DE images, with editing, adjustment and/or addition of plotted points if required. Thus the KBR process itself confers an element of reproducibility to the technique.

3.5.3 Utility of 2DE with KBR versus 3DE

Compared to 3DE, the use of 2DE technology for data acquisition also has methodological advantages. Fundamentally, spatial and temporal resolutions of 2DE are higher than those of 3DE. Underestimation of RV volumes is a known limitation of 3DE due to the inferior spatial resolution conferring blurred endocardial borders and thus a visually smaller RV

cavity[104]. In particular, the contribution from the RVOT is known to be an important determinant of the overall accuracy of RV volumes[145]. However, accurate visualization of this region can be technically difficult by 3DE (Figure 2-16)[108, 126, 138]. The 2DKBR acquisition protocol includes dedicated imaging of the RVOT by 2DE, affording higher spatial resolution when imaging this region that may contribute to more accurate volumetric quantification (Figure 3-9).

There are further technical advantages of the requirement for image acquisition from multiple acoustic windows by 2DE. Each region of the RV can be visualized from acoustic windows with optimal border definition. Axial resolution is superior to lateral resolution with ultrasound imaging[155]. Therefore structures can be preferentially identified in views in which their appearance is affected more by the axial resolution of the ultrasound system. Image acquisition from multiple acoustic windows also allows perpendicular rather than oblique cuts through the RV wall, thereby reducing errors in identifying endocardial borders because of beam width[153].

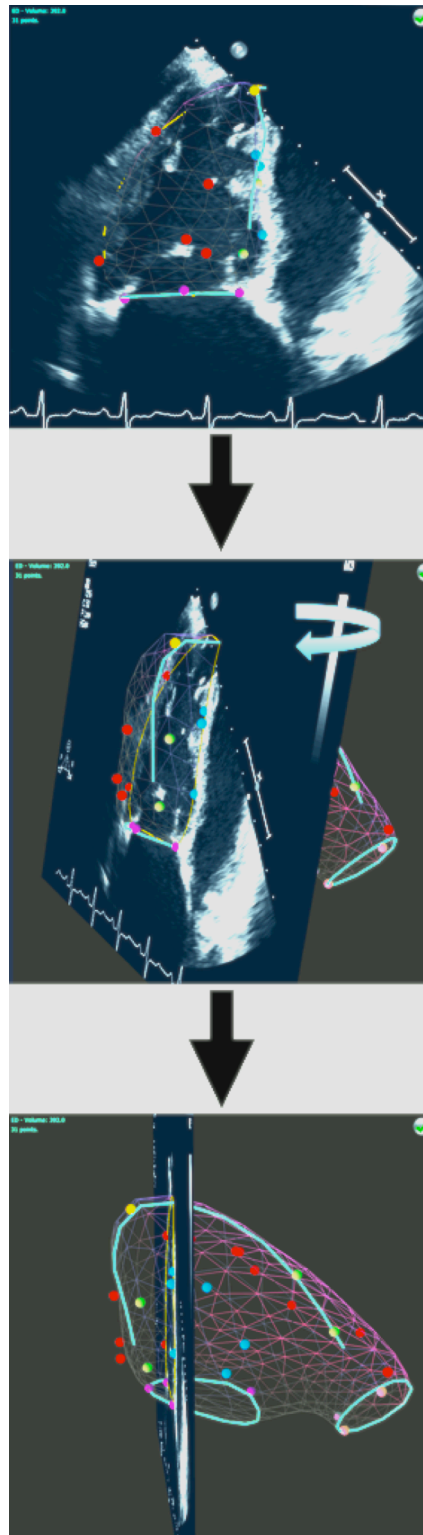


Figure 3-9: Demonstration of the interaction between the reconstructed 2DKBR polygon with a 4-chamber view 2DE scan plane.

The reconstructed polygon can be rotated in any direction (here through 90° from top to bottom, indicated by the curved arrow). Any original 2DE acquisition can be displayed (here, the 4-chamber view) and viewed in relation to the polygon by clicking on one of the dots. In this way the reconstructed polygon can be inspected to ensure accurate alignment with the original 2DE data. From this view it is also readily appreciable how much of the RV, predominantly the outflow portion, is neglected in a standard 4-chamber view used to derive FAC.

The utility of applying a knowledge-based approach to reconstruction of the RV polygon is reflected by the known differences in RV shapes that are encountered not only in congenital and acquired disease, but also between different subtypes of PH[150]. Algorithms for RV reconstruction by conventional 3DE are typically based upon generic healthy adult RV shapes rather than taking into account differences in congenital populations, or subtle changes in volume- and pressure-overload states[112]. Furthermore, the subjective image scoring suggests that the requirement for the identification of plotted landmarks only for PSSS with KBR rather than manually tracing the whole endocardial border still permits adequate reconstruction despite cases of poor quality transthoracic 2DE windows.

However, subtle changes in RV function may nevertheless be masked by the margins of error demonstrated in the study. CMRI data demonstrates that a change in RV stroke volume in PH of as little as 10mL can be regarded as clinically significant[140], and therefore 2DKBR may not be able to differentiate minor variations in RV volumes from the variance in reproducibility. CMRI does not have the same acquisition window restrictions and variability inherent to transthoracic echocardiography, with datasets consisting of contiguous fixed thickness RV slices acquired from the base of the right heart to the main pulmonary artery with the patient in the supine position. A further consideration with respect to the use of 2DKBR in the serial evaluation of patients is that a change in RV volume might confer a change in cavity shape, which could also have implications for the application of the KBR algorithm to follow-up studies.

The disadvantage of obtaining data from several 2DE planes is that they are acquired over separate cardiac cycles. Image acquisition over several cardiac cycles with potential beat-to-beat variability is also a limitation shared by traditional disk summation 3DE and by CMRI, but not with single-beat full-volume 3DE. However, no significant differences were found in heart rates between the start and end of the studies. Acquiring

several 2DE planes also requires reproducible breath-holding and a stable patient position throughout the study. Repeated breath-holding is also conventionally associated with CMRI, but we used a real-time high spatiotemporal resolution sequence as per our institution protocol for PH imaging that allows free breathing and the rapid acquisition of ventricular volumes[63]. Once image acquisition for a 2DKBR study has commenced, the operator is unable to manoeuvre the patient to optimize TTE windows. Therefore an optimal patient position for parasternal and apical views has to be decided upon prior to commencing 2DKBR data acquisition. These optimal breath-hold and positional constraints may confer difficulty when applied to acutely unwell individuals, and hence 2DKBR is more likely to be practically applicable in the stable outpatient setting. It should also be remembered that whilst global volumetric indices of RV function are highly prognostic, they do not account for the heterogeneity in RV regional function in different disease states as shown by 2DE and 3DE deformation imaging[172, 173]. Finally, 2DKBR includes the RV trabeculations together with the blood volume, which may in turn impact upon the accuracy of volumetric indices. However, this is also a limitation shared with 3DE techniques, and has been shown by CMRI to improve reproducibility metrics compared with excluding trabeculations from the RV cavity volume[59].

3.6 Limitations

This study represents a single-centre experience with a small participant sample size. However, we have supported the validation data for 2DKBR obtained by previous single-centre studies using similar sample sizes[157, 166, 167], and a total of 84 2DE studies were performed in this study for test-retest reproducibility purposes. The increase in excluded studies with successive repeated scans was more due to the serial 2DE scan acquisition protocol for test-retest reproducibility, rather than the 2DKBR technique itself. Only one out of twenty-eight patients moved in the first 2DE dataset image acquisition. Therefore this limitation is unlikely to be so prevalent for individual clinical scans, and the study analysis

times would allow for reacquisition of a second dataset within a scheduled clinical echocardiogram.

Patients with arrhythmia were specifically excluded from this study, but patients with atrial fibrillation (AF), for example, would require a different approach to 2DKBR post-processing. In AF, the end-diastolic frame for each view would have to be manually selected by visually determining the largest RV cavity size. This could theoretically affect the border alignment of the reconstructed polygon, as different cardiac cycles in separate views will inherently have different end-diastolic volumes due to the variability of irregular R-R intervals. Several reconstructions could be performed on the same dataset by selecting different cardiac cycles for each reconstruction, with the resulting 2DKBR RV metrics averaged over the number of cardiac cycles analyzed. However, the accuracy and reproducibility of this approach using 2DKBR in AF requires further investigation.

Finally, CMRI reproducibility data was not acquired in a test-retest format that allowed comparison of the acquisition and post-processing variability of this technique. However, as detailed above, the acquisition stage of CMRI consists of a set acquisition of cross-sectional, fixed thickness, contiguous cranio-caudal slices that include the entirety of the heart with the patient supine. Therefore CMRI fundamentally has less potential for acquisition variability compared with 2DE, which has imaging windows obtained from different rib spaces acquired in non-uniform patient positions.

3.7 Conclusions

Novel 2DKBR is a feasible and clinically reproducible technique for RV volumetric quantification in PH, with superior test-retest reproducibility compared with 2DE FAC for quantifying RV function. It offers the benefits of employing operator experience with conventional 2DE for image acquisition, and utilizes algorithmic reconstruction that takes into account the heterogeneity in shape of the RV cavity in different disease states. The applicability of 2DKBR to serial follow-up studies for assessing the response to treatment should be the focus for further work in advancing this novel echocardiography technique.

CHAPTER 4 Tissue Phase Mapping to assess Left Ventricular Myocardial Mechanics in Pulmonary Hypertension

4.1 Introduction

Pulmonary hypertension (PH) is characterized by increased pulmonary artery pressure and right ventricular (RV) failure. CMRI is the reference standard method of assessing RV function and is now routinely used in PH. Several studies have shown that CMRI-derived RV volumes and ejection fraction (EF) are prognostic in this condition[80, 81].

It has also been shown that left ventricular ejection fraction (LVEF) is reduced in late stage PH[45]. However, the majority of PH patients have normal LVEF, and LV function is not prognostic[81]. Nevertheless, it is likely that these patients do have abnormal LV mechanics due to ventricular interdependence[44, 174-177]. This could result in additional functional deficits, as is the case in patients with RV failure due to congenital heart disease[178]. Consequently, assessment of LV myocardial mechanics may be clinically useful in this patient population.

The most comprehensive way of evaluating LV mechanics is to assess the regional and geometric components of LV motion. There are several CMRI methods that can be used to assess these metrics. In this study, I used tissue phase mapping (TPM) to assess radial, longitudinal and tangential myocardial velocities in patients with PH[179-182]. As this type of evaluation has not been performed in this population before, it is of uncertain clinical value. Therefore, my general aim was to explore the utility of TPM measures of LV myocardial mechanics in patients with PH.

4.1.1 Aims

The specific aims of this feasibility study were:

- To assess global and regional LV myocardial mechanics in healthy volunteers and in patients with PH with preserved LVEF.
- To determine the relationship between LV myocardial velocities and exercise capacity.
- To test the ability of LV myocardial velocities to predict clinical worsening.

4.1.2 Personal Contribution

To fulfill the above aims for this study I have:

- Obtained ethical approval from the local institutional research ethics committee (North West London REC 2) and research and development (R&D) approval from the R&D departments at The Royal Free Hospital and Great Ormond Street Hospital NHS Trusts.
- Enrolled 60 participants (40 patients with PH and 20 age- and sex-matched healthy volunteers) in sinus rhythm with no contraindications to magnetic resonance imaging.
- Performed and post-processed comprehensive CMRI studies for all participants.

This has contributed to the writing of two papers:

- The results of the development and validation of the novel TPM sequence have been published by J. Steeden, D. Knight, S. Bali, D. Atkinson, A. Taylor and V. Muthurangu, in *Magnetic Resonance in Medicine*, 2014, **71**(1), entitled; “Self-navigated tissue phase mapping using a golden-angle spiral acquisition-proof of concept in patients with pulmonary hypertension” [108] (see Appendix 3).
- The results of the application of the novel TPM sequence have been submitted with revisions for consideration of publication by D. Knight, J. Steeden, S. Moledina, A. Jones, J.G. Coghlan and V. Muthurangu, entitled; “Left ventricular diastolic dysfunction in pulmonary hypertension predicts functional capacity and clinical worsening: a tissue phase mapping study” (see Appendix 4).

4.2 Literature Overview

In this section, the different CMRI techniques to assess regional and geometric components of myocardial motion will be summarized, specifically:

- Tissue tagging.
- Displacement encoding with stimulated echoes (DENSE).
- Strain encoding (SENC).
- Tissue phase mapping (TPM).

This overview highlights relevant papers that were found using *PubMed*. The search terms used included (a combination of):

- Magnetic resonance imaging.
- Tissue/phase velocity mapping.
- Myocardial mechanics.
- Pulmonary hypertension.

When a relevant paper was found, the referenced papers were followed up and any subsequent papers that have cited this paper were also followed up.

4.2.1 Tissue Tagging

Tissue tagging is the most clinically utilized CMRI technique for assessing regional myocardial motion, originally described in 1998[183]. Tissue tagging sequences consist of a preparation phase where lines or a grid of magnetic saturation, termed tags, are imposed on the myocardium at one time point. This time point is usually immediately after the R wave on the scanner vector cardiogram (VCG). This is followed by an imaging phase that shows the deformation of the tags through the cardiac cycle (Figure 4-1). Since magnetization is an intrinsic property of the underlying myocardium, the tagged lines, which form part of the tissue, follow myocardial motion. In this way tissue deformation is demonstrated visually from the time of application of the tagging pulses. This permits an immediate qualitative visual assessment of myocardial deformation without the need for post-processing.

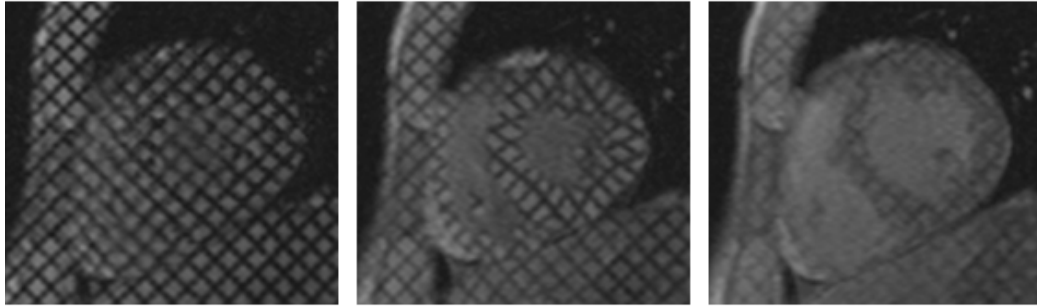


Figure 4-1: Tissue tagging in a healthy volunteer from preparation pulse (left pane) through systole (middle pane) and into diastole (right pane), by which point the tag lines are fading.

Tissue tagging can also be analyzed quantitatively with the deformation outputs of strain, strain rate and torsion. The most reproducible and accurate tagging-derived parameters are circumferential strain and strain rate[184]. The typical spatial and temporal resolutions of a Spatial Modulation of Magnetization (SPAMM) preparation tagging sequence are 1.6x1.6mm and 32ms respectively acquired during a breathhold over 14 cardiac cycles[185]. Accelerated imaging techniques have also been applied to reduce acquisition times to 5 cardiac cycles[186].

Tissue tagging has demonstrable clinical application for assessing regional myocardial function in many conditions, including coronary artery disease[187, 188], myocardial infarction[189-191], LV hypertrophy[192], ventricular dyssynchrony analysis[193, 194], and dilated[194-196] and hypertrophic heart muscle disease[197-199]. It has also been used in the multi-centre MESA trial to investigate risk factor analysis of left ventricular function[200].

There are several disadvantages of the tissue tagging technique. The tags fade over time, which generally limits their use to the first two-thirds of the cardiac cycle. Additionally, the tag takes time to apply, resulting in a gap in image acquisition (normally at the beginning of each R-wave). Deformation measurement by tagging utilizes a single 2D image plane, thus ignoring through-plane motion. For truly complete cardiac motion analysis by tagging, a fully 3D tagged dataset has been described but this requires multiple breathholds over an acquisition time of between 30 to

40 minutes[201]. The spatial resolution of tagging is limited by the tag spacing, thus precluding applicability to investigate myocardial motion of the thin RV wall. Finally, the quantitative analysis of tissue tagging is complex, involving time-consuming post-processing.

4.2.2 Displacement Encoding with Stimulated Echoes (DENSE)

DENSE encodes tissue displacement pixel by pixel, in-plane[202] or through-plane[203], directly into the phase of a magnetic resonance image (Figure 4-2).

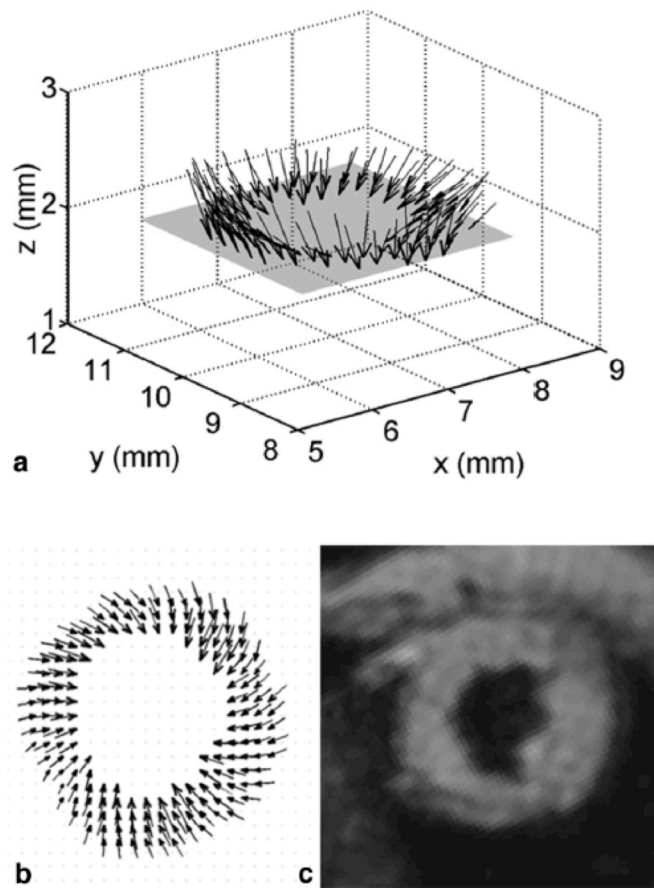


Figure 4-2: In vivo systolic displacement measured by DENSE. (a) A displacement map showing through-plane motion. (b) A displacement map showing in-plane motion. (c) Magnitude reconstruction of the DENSE raw data.

Reproduced with permission from Epstein et al.[203].

DENSE is neither widely available nor a standard clinical CMRI sequence, and has predominantly been applied in the research setting with limited clinical application to date. However, potential clinical utility has been demonstrated in patients with myocardial infarction[204], non-ischaemic cardiomyopathy[205], and constrictive pericarditis in the post-pericardectomy setting[206].

The post-processing of DENSE is relatively simple and quick. Strain curves can be created from both 2D[207, 208] and 3D[209, 210] tissue tracking post-processing techniques. However, the DENSE sequence itself has intrinsically low signal-to-noise ratio (SNR) and, like tagging, the encoding does not last for the entire cardiac cycle due to T1 recovery. The original description of DENSE implemented a cardiac and respiratory gated unsegmented acquisition, with a spatial resolution of 1x1.9mm acquired over 4.3 minutes[202]. Since this original implementation, echo combination techniques such as fast cine-DENSE[211] have been performed to reduce acquisition times and increase SNR with good levels of precision for measuring deformation[205].

4.2.3 Strain Encoded (SENC) Imaging

Of the techniques described here, SENC is the most recent CMRI sequence used to investigate myocardial motion[212] (Figure 4-3).

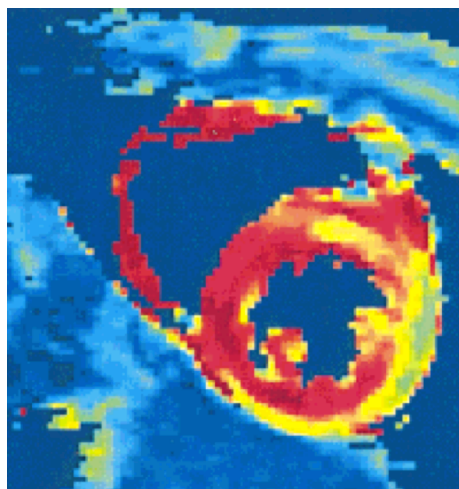


Figure 4-3: Longitudinal strain measured by SENC.
Reproduced with permission from Osman et al.[212]

As is the case with DENSE, SENC is also neither widely available nor a standard clinical CMRI sequence. SENC measures through-plane strain; longitudinal strain is hence measured from a short-axis image plane, and circumferential strain from a long-axis image plane. Radial strain cannot be measured by SENC. The strain is directly related to pixel intensity, and therefore post-processing is relatively simple using this technique. However, as with tagging and DENSE imaging, the whole cardiac cycle cannot be analyzed. Furthermore, like DENSE imaging, SENC has a relatively low SNR.

SENC has been applied to patients with myocardial infarction[213, 214], coronary artery disease[215-217] and heart failure[218]. It also has application for RV myocardial motion analysis in healthy volunteers[219] and in patients with PH[220].

4.2.4 Tissue Phase Mapping (TPM)

Phase velocity mapping in one direction is widely available as a standard clinical sequence on most clinical CMRI scanners. It is a commonly used, well established sequence that is considered the gold standard method for measuring blood flow velocity[221]. A bipolar gradient is used for velocity encoding directly into the phase of the signal pixel by pixel. The application of phase velocity mapping to measure myocardial velocities first occurred over 30 years ago[222]. In order to analyze three-dimensional myocardial motion, velocity can be sequentially encoded in three orthogonal directions in a pre-selected 2D short-axis slice position. This permits the simultaneous collection of x, y and z velocities (relative to the image plane), which can then be converted to radial, circumferential and longitudinal (through-plane) velocities respectively (Figure 4-4).

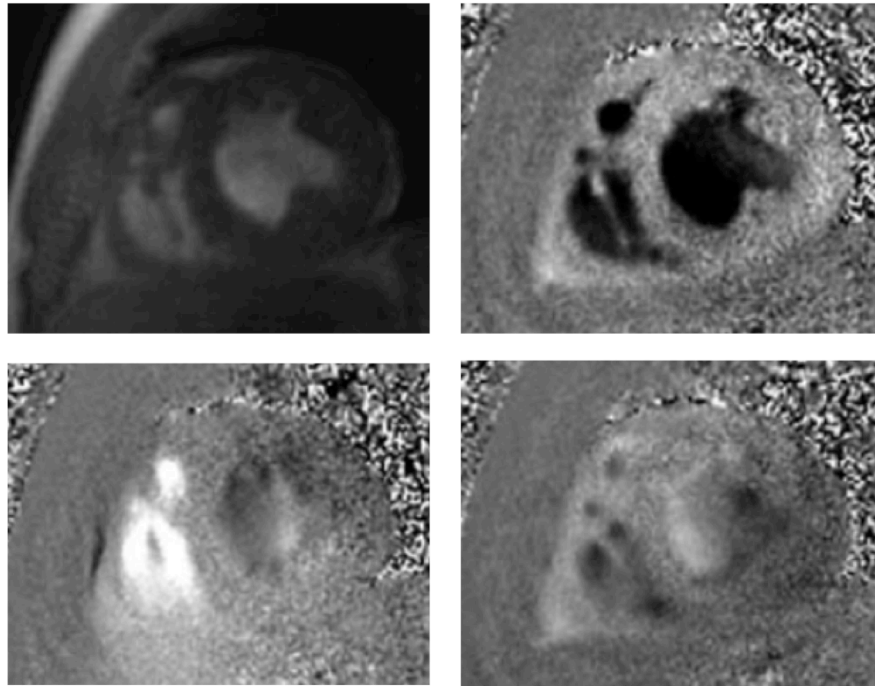


Figure 4-4: A TPM data set from a healthy volunteer. Clockwise from top left: magnitude data, and phase data in Z (through-plane), X and Y directions.

Unlike the three aforementioned CMRI techniques, allows the simultaneous measurement of multi-directional velocity-encoded data throughout the entire cardiac cycle with high spatiotemporal resolution [181, 182]. The main disadvantage of TPM is susceptibility to motion artifacts and phase distortion. This complicates the calculation of deformation parameters from the raw TPM data, as the errors can be propagated; strain can be determined by integrating velocities with respect to time[223], and strain rate by calculating the spatial derivatives of the velocities at each pixel[224]. Nevertheless, TPM has been widely used for the assessment of LV mechanics in health[180, 181, 225-227] and disease, including myocardial infarction[228, 229], coronary artery disease[230, 231], cardiac failure and ventricular dyssynchrony[232], and dilated[179] and hypertrophic[233] heart muscle disease.

Similar data could be acquired using either tissue Doppler imaging (TDI) or speckle tracking echocardiography (STE). Of particular interest is STE, which allows measurement of radial, longitudinal and circumferential myocardial deformation. This technique has also been shown to have

utility in PH for the investigation of LV myocardial mechanics[177]. However, unlike TPM, the simultaneous acquisition of through plane motion to obtain longitudinal velocities from a short-axis plane is not possible on echocardiography. Images from both a short-axis plane and also multiple apical planes would have to be acquired in order to provide radial, longitudinal and circumferential motion data from all LV walls. Furthermore, CMRI is the most accurate method for assessing biventricular function, and accordingly has become increasingly used in PH. Therefore it is desirable to also have a CMRI method for the comprehensive assessment of myocardial mechanics.

4.2.5 Summary

From the literature review it can be concluded that:

- TPM is technically advantageous over echocardiography or other CMRI methods for the assessment of myocardial motion. In particular, multi-directional velocity-encoded data can be simultaneously acquired throughout the entire cardiac cycle.
- There has been a limited application of CMRI to the investigation of myocardial mechanics in PH despite evidence of LV dysfunction in advanced disease.

I aim to apply a novel TPM sequence by CMRI to investigate LV myocardial mechanics in PH for the first time. In particular, I will investigate patients from a population with ostensibly normal LV function by conventional clinical markers, namely LVEF. I also aim to assess the relationship between TPM metrics of LV function and functional capacity, and the ability of these metrics to predict clinical worsening against conventional global measures of cardiac function.

4.3 Methods

A prospective cross-sectional study was performed that enrolled 60 participants in sinus rhythm with no contraindications to magnetic resonance imaging.

4.3.1 Study Population

The study population consisted of 40 consecutive patients with PH and 20 healthy volunteers.

Inclusion criteria for patients were:

- PH diagnosed by right heart catheterization (RHC): mean pulmonary artery pressure (mPAP) >25mmHg and pulmonary capillary wedge pressure (PCWP) <15mmHg[121], or
- Presentation for routine out-patient clinical evaluation with known PH, and/or RHC for diagnosis or follow-up of PH.

Exclusion criteria for patients were:

- Left-sided cardiac disease unrelated to PH (including ischaemic heart disease, LV dysfunction or hypertrophy, and left-sided valve disease).
- Clinically significant restrictive or obstructive lung disease identified by pulmonary function tests.
- Arrhythmia.
- Contraindications to CMRI.

Exclusion criteria for healthy volunteers were:

- Past medical history of cardiovascular disease (including hypertension).
- History of cardiac medications.
- Arrhythmia.
- Contraindications to CMRI.

All patients underwent the CMRI study between 3rd October 2012 and 24th November 2013. All participants were imaged using a 1.5T MR scanner (Magnetom Avanto, Siemens Healthcare, Erlangen, Germany). All patients underwent a 6-minute walk distance test (6-MWD). Twenty-nine patients (73%) underwent clinically-indicated right heart catheterization within 40 days of CMRI (median 8 days, IQR 12 days).

The study complied with the Declaration of Helsinki. The local institutional research ethics committee (North West London REC 2) approved the study and informed written consent was obtained from all participants.

4.3.2 Conventional CMRI Protocol and Image Post-Processing

Biventricular volumetric data were obtained as described previously, using a radial *k-t* SENSE real-time sequence[63], with contiguous transaxial and short-axis ventricular stacks acquired for RV and LV analyses respectively. Through-plane flow data were acquired in the ascending aorta, right and left branch pulmonary arteries, and for mitral valve inflow, using a velocity-encoded, prospectively-triggered spiral PCMR sequence[131].

All images were processed using in-house plug-ins for the open source OsiriX DICOM software platform (OsiriX Foundation, Geneva, Switzerland)[133]. Endocardial borders were traced manually at end-diastole and end-systole of both ventricles to assess biventricular function. This allowed evaluation of end diastolic volume (EDV) and end systolic volume (ESV), and calculation of stroke volume (SV) and ejection fraction (EF)[63]. Aortic and pulmonary artery flow were measured from the PCMR data, which were segmented using a semi-automatic vessel edge detection algorithm with manual operator correction[132]. Transmitral E and A wave peaks were measured from the mitral valve inflow PCMR data, allowing calculation of E/A ratio. Septal curvature was assessed using the mid-ventricular short axis cine images, as described previously[83].

4.3.3 Tissue Phase Mapping Protocol and Image Post-Processing

Myocardial velocities were acquired using a respiratory self-navigated, cardiac gated, velocity encoded golden-angle spiral sequence[182]. To summarize, a *two-sided* flow-encoding scheme (with positive and negative bipolar pulses applied for each velocity-encoding direction) was used to enable high temporal-resolution imaging (rather than conventional one-sided flow-encoding where four flow-encoded readouts are required). Data were continuously acquired, with each consecutive flow-encoding couplet rotated by the golden-angle. Consecutive spiral pairs (10 in each window) are combined to produce low temporal resolution (315ms) real-time images. These real-time data are used to create an image based respiratory navigator, used to select 30% of the expiratory spiral interleaves for the final retrospectively cardiac-gated reconstruction. Sequence parameters: TE/TR 3.85/14.9ms, FOV 450mm, Matrix: 384x384, uniformly distributed spiral interleaves required to fill k-space: 30 (for each of the three phase-encoded directions), slice thickness: 7mm, VENC: 30cm/s, Flip angle: 25°, pixel bandwidth: 930Hz/pixel. This achieved a temporal resolution of 27.14ms, with a spatial resolution 1.17x1.17mm, giving approximately 40 cardiac phases. The nominal scan time, assuming a heart rate of 60bpm and 100% respiratory efficiency, would be 1 minute 30 seconds, resulting in a scan time of approximately 4 to 5 minutes per subject depending upon heart rate. TPM data were acquired in mid-ventricular short-axis, which was chosen by reference to a 4-chamber cine at end-systole.

This sequence does not include any black blood pulses (as conventionally used in TPM) as this would have disrupted the continuous acquisition of data necessary for calculation of the respiratory navigator and retrospective cardiac gating. No off-resonance correction was performed as this would have increased the scan time or reduced the temporal resolution of the scan. Some minor image blurring was observed around fat tissue, but this did not severely affect the velocity measurements as the fat was generally spatially separated from the

myocardium. Background phase offsets were minimized in the TPM data by optimizing the flow gradients and correcting for Maxwell terms. This resulted in no observable background phase offsets in the data.

All images were processed using an in-house plug-in for OsiriX[133]. For each dataset, endocardial and epicardial ventricular borders were manually segmented on the magnitude images to create a ventricular region of interest (ROI). The ventricular ROI was further split into four segments: septal, anterior, lateral and inferior. Bulk motion correction was performed[234], before transformation of the in-plane velocities to an internal polar coordinate system positioned at the centre-of-mass of the LV. This allowed motion to be described in terms of radial (V_{rad}), tangential (V_{tang}) and longitudinal (V_{long}) velocities[227]. For each direction, global velocities were calculated by averaging the velocity in a given direction (radial, longitudinal and tangential) within the ventricular ROI in each frame. Regional velocities were calculated by averaging the velocities in each segment. Peak systolic (S wave) and early diastolic (E wave) values were quantified from the longitudinal, radial and tangential velocity-time curves. The tangential S (S1 and S2) and E (E1 and E2) wave peaks were biphasic. Vector field plots and colour-coded position-time maps were generated for each myocardial velocity component to allow easy visualization of the results.

4.3.4 Statistics

STATA 13 was used for statistical analyses. Data were examined for normality using the Shapiro-Wilk test. Descriptive statistics are expressed as mean \pm standard deviation (SD) when normally distributed and median (inter-quartile range, IQR) when non-normally distributed. Proportions are expressed as percentages. Independent samples t-tests with Welch's correction for unequal variances were used to compare parametric data in PH patients and controls (n=11). The Mann-Whitney-U test was used for non-parametric data (n=9). Fisher's exact test was used to compare proportions data (n=3). For subgroup analysis, PH patients were divided

into 3 groups: PH associated with connective tissue disease (CTD), PH not associated with CTD, and chronic thromboembolic PH (CTEPH). The Kruskal-Wallis test was used to test for equality of abnormal global myocardial velocities ($n=5$) between the different sub-groups of PH. The group of tests comparing controls to patients was considered a single family of statistical inferences and the familywise error rate was controlled using Bonferroni correction. Specifically, 28 statistical comparator tests were adjusted for resulting in a corrected critical p-value of <0.0018 .

Random-effects generalized least squares models were used to compare myocardial velocities in the four myocardial segments. Interaction terms for the myocardial segment and presence of disease were included in the models. This analysis was only performed if the global velocities were abnormal (E_{rad} , E_{long} , $S2_{\text{tang}}$, $E1_{\text{tang}}$, and $E2_{\text{tang}}$). In addition, this analysis was used to assess the timing of the E_{rad} peak, which on visual inspection appeared to vary between segments. Bonferroni correction was required to control the familywise error rate in this group of 6 generalized least squares models, and the adjusted critical p-value was 0.0083.

To assess the relationships between abnormal myocardial velocities and haemodynamic parameters a 2-stage procedure was employed. Firstly, simple univariate analysis was performed using Pearson's correlation coefficient. This allowed selection of the conventional CMRI biventricular parameters and afterload metrics with the strongest correlation to the abnormal myocardial velocities. To identify independent predictors of myocardial velocity these variables were entered into random-effects generalized least squares models. Variables in this model with a p-value of <0.05 were considered statistically significant.

A similar 2-stage analysis was performed to assess the relationship between 6-MWD and CMRI data. From the univariate analysis, the strongest correlating E and S wave peaks and conventional CMRI metrics were identified. These were then entered into a multiple linear regression

model to determine covariates that were independently associated with 6-MWD. Variables in this model with a p-value of <0.05 were considered statistically significant.

All patients were followed up until death, transplantation, progression to intravenous epoprostenol, or the end of the study (February 25th, 2015). The decision to list a patient for transplantation or commence intravenous vasodilator therapy was based upon clinical assessment of deterioration in functional class and/or RHC-derived haemodynamic data. CMRI data were not used in these management decisions and the physicians involved in the patients' care were blinded to the CMRI results. Univariate Cox proportional hazards analysis was used to assess the predictive ability of all CMRI variables in the 34 patients without proximal CTEPH and not treated with intravenous epoprostenol. The primary outcome was freedom from death, transplantation or progression to intravenous therapy. The E and S waves and conventional CMRI metrics with the greatest hazard ratios were entered into a multivariable Cox proportional hazards analysis to determine which covariates were independent predictors of clinical worsening. A p-value of <0.05 was taken as statistically significant.

4.4 Results

4.4.1 Study Population Characteristics

There was no difference in the age distributions of PH patients and controls (50 years (IQR 45-59) versus 47 years (IQR 42-54) respectively, $p=0.30$). Thirty-out-of-forty patients were female versus 16 out of 20 controls ($p=0.76$). Patient characteristics and underlying diagnoses are detailed in Table 4-1. The largest sub-group had PH associated with CTD (20/40), the next largest sub-group (12/40) had PH not associated with CTD (10/12 had idiopathic PAH), followed by patients with CTEPH (8/40). All patients were normotensive at the time of study (median systolic BP 110mmHg, IQR: 105-120mmHg; mean diastolic BP 72 ± 11 mmHg). Thirty-two patients were receiving PH therapy at the time of CMRI study.

	Number (%)
Aetiology[86]	
1. PAH	11 (28)
- 1.1 Idiopathic	10
- 1.2 Heritable	1
1.4 Associated with (APAH):	21 (53)
- 1.4.1 CTD	20
- Limited cutaneous systemic sclerosis	13
- Diffuse cutaneous systemic sclerosis	2
- Systemic lupus erythematosus	3
- Sjögren's syndrome	1
- Mixed CTD	1
- 1.4.3 Portal Hypertension	1
4 CTEPH	8 (20)
- Proximal (operable)	5
- Distal (inoperable)	3
Right Heart Catheterization (RHC) data (n=29)	
Time interval between CMRI and RHC	8 (IQR 12)
Mean pulmonary artery pressure (mPAP, mmHg)	46±13
Pulmonary vascular resistance (PVR, dyn·s/cm ⁵)	523 (IQR 286-450)
World Health Organization class (%)	
I	1 (2.5)
II	14 (35)
III	22 (55)
IV	3 (7.5)
6-minute walking distance (6-MWD, metres)	372 (IQR 286-450)
Vasodilator therapy	
Phosphodiesterase type 5 inhibitor	28 (70)
Endothelin receptor antagonist	22 (55)
Intravenous prostacyclin	1 (3)
Treatment regimens	
Treatment naive	8 (20)
Oral monotherapy	14 (35)
Dual combination oral therapy	16 (40)
Triple combination therapy	1 (3)
Additional PH therapies	
Oral prostacyclin	1 (3)
Inhaled prostacyclin	1 (3)
Tyrosine-kinase inhibitor	2 (5)

Table 4-1: Patient characteristics.

Conventional CMRI metrics from normal subjects and PH patients are shown in Table 4-2. In PH, the RV was dilated with reduced RVEF and the LV was compressed with reduced SV. In addition, septal curvature was lower (or reversed in 65% of patients). Nevertheless, LVEF and E/A ratio were not significantly different between patients and controls.

	Normal	PH patient	p-value
RVEDV	130 (104-156)	158 (128-204)	0.0056
RVESV	38 (31-63)	103 (70-133)	<0.00001*
RVSV	87 (74-99)	62 (48-75)	0.0006*
RVEF	65±8	40±12	<0.00001*
LVEDV	134 (108-139)	88 (74-109)	0.0001*
LVESV	42±16	32±13	0.012
LVSV	85±19	62±18	<0.00001*
LVEF	67±8	66±9	0.61
LV cardiac output	5.6 (4.8-6.4)	4.6 (3.8-5.5)	0.0094
Septal curvature	1.09±0.10	-0.20±0.58	<0.00001*
E/A ratio	1.56 (1.23-2.88)	1.33 (1.11-2.36)	0.31

Values are mean±SD, or median (interquartile range).

*indicates statistical significance ($p < 0.0018$ following Bonferroni correction).

Table 4-2: CMRI characteristics of control subjects versus PH patients

Median 6-MWD in PH patients was 372m (IQR: 286-450m). Twenty-nine PH patients underwent clinically-indicated right heart catheterization within 40 days of CMRI (median 8 days, IQR 12 days). Median pulmonary vascular resistance (PVR) was 523 dyn·s/cm⁵ (IQR 402-717 dyn·s/cm⁵) and average mPAP was 46±13mmHg. All patients had a PCWP<15mmHg.

4.4.2 Myocardial Velocities in Normal Subjects and PH Patients

Myocardial velocities were acquired successfully in all subjects. Figure 4-5 shows representative LV velocity vectors in a normal subject and a patient with PH.

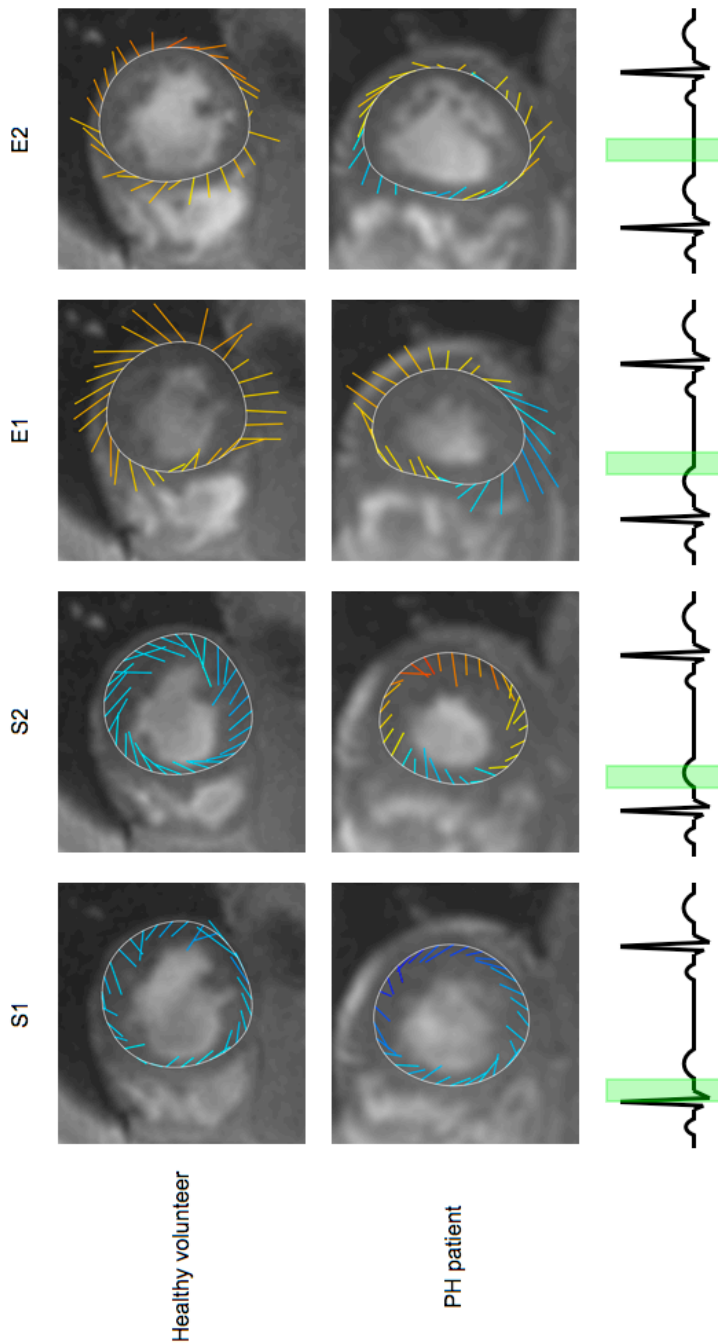


Figure 4-5: LV velocity vector plots from a healthy volunteer and a PH patient at four time points in the cardiac cycle (indicated by the ECG trace).

The line colours represent longitudinal velocities: yellow/red or blue represent myocardial motion towards or away from the apex respectively. The line orientation and length represents the vector sum of the radial and tangential velocities. Note the biphasic tangential systolic (S1 and S2) and early diastolic (E1 and E2) motions. In health, this follows an anti-clockwise then clockwise motion in systole and diastole. In PH, however, there is reversal of early diastolic tangential untwisting directions: clockwise untwisting occurs prior to anti-clockwise untwisting.

Global myocardial peak velocities in normal subjects and PH patients are summarized in Table 4-3.

Global LV velocity	Normal	PH patient	p-value
S _{rad}	2.4±0.4	2.3±0.5	0.14
E _{rad}	3.1±0.5	2.3±1.0	0.001*
S _{long}	3.3±1.0	3.3±1.1	0.98
E _{long}	4.2 (3.4,5.5)	2.6 (1.7,3.3)	<0.00001*
S1 _{tang}	-1.8±0.7	-1.4±0.8	0.064
S2 _{tang}	1.3±0.6	0.50±0.69	0.0001*
E1 _{tang}	-0.4±0.6	1.4±0.5	<0.00001*
E2 _{tang}	0.9 (0.7,1.3)	-0.8 (-1.1,-0.3)	<0.00001*

Values are mean±SD, or median (interquartile range).

*indicates statistical significance ($p < 0.0018$ following Bonferroni correction).

Table 4-3: Peak global myocardial velocities in controls versus patients with PH.

Patients with PH had reduced LV peak E_{rad}, E_{long} and S2_{tang} velocities, with reversal and significant change in both E_{tang} peaks. This can be appreciated in Figure 4-6, which shows representative global radial, longitudinal, and tangential velocity curves from a normal subject and a PH patient. Reversal of both E_{tang} waves was highly discriminatory for the presence of PH. All patients had a reversed E1_{tang} compared to 4/20 normal subjects ($p < 0.0001$), while 32/40 patients had a reversed E2_{tang} compared to 2/20 normal subjects ($p < 0.0001$). The magnitude of all abnormal global myocardial velocity peaks did not differ between aetiological groups ($p > 0.59$).

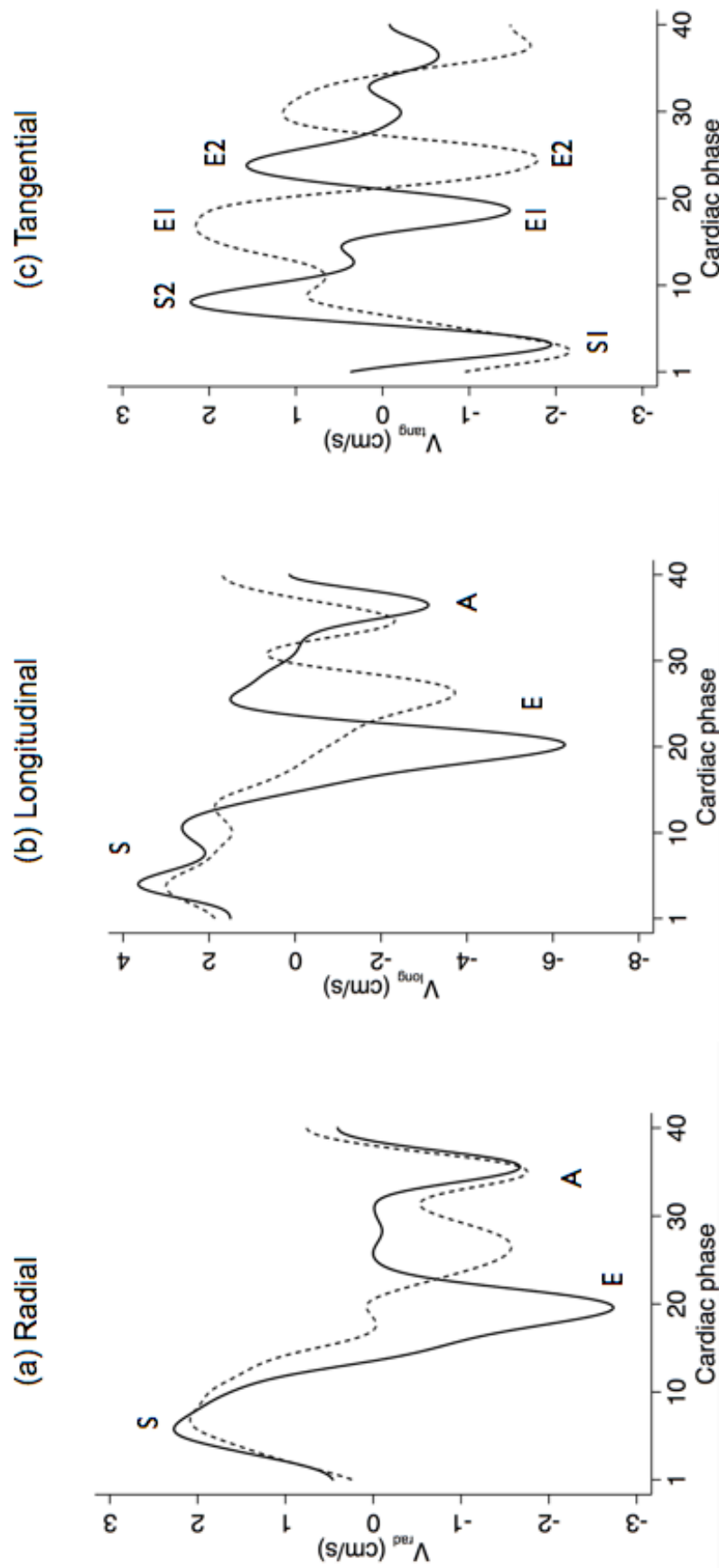


Figure 4-6: Line graphs of global radial, longitudinal and tangential LV velocities in a healthy volunteer (solid line) and a PH patient (dotted line). The RR intervals for both subjects have been scaled to the same value for illustrative purposes. S, E and A waves are evident radially and longitudinally. Biphasic systolic (S1 and S2) and early diastolic (E1 and E2) waves are observed tangentially. Cardiac cycles are normalized for heart rate for illustrative purposes. Global E_{rad} and E_{long} velocities are markedly reduced in PH. The tangential S2 wave is also reduced in PH. The reverse direction of untwisting of biphasic early diastolic tangential waves was evident in all PH patients.

4.4.3 Regional Variations in Normal Subjects and PH Patients

In patients, there was a trend towards E_{rad} velocity peaking in the anterior segment first (approximately 80ms, $p=0.026$) as seen in Figure 4-7. However, there was no significant regional difference in the magnitude of the E_{rad} peaks ($p>0.07$). Figure 4-8a shows radial LV myocardial velocities as a function of position and time in a normal subject and a patient with PH.

Longitudinal velocity maps are shown in Figure 4-8b. In normal subjects, E_{long} peak velocity was similar in the inferior wall and septum ($p=0.88$) but higher in the anterior ($p=0.008$) and lateral walls ($p<0.001$). However, in patients, this regional variation was less distinct (Figure 4-7) with only a trend towards higher E_{long} peak in the lateral segment ($p=0.012$).

Figure 4-8c shows tangential velocity maps in a normal subject and patient. There were no regional variations in tangential velocity peaks in controls or patients.

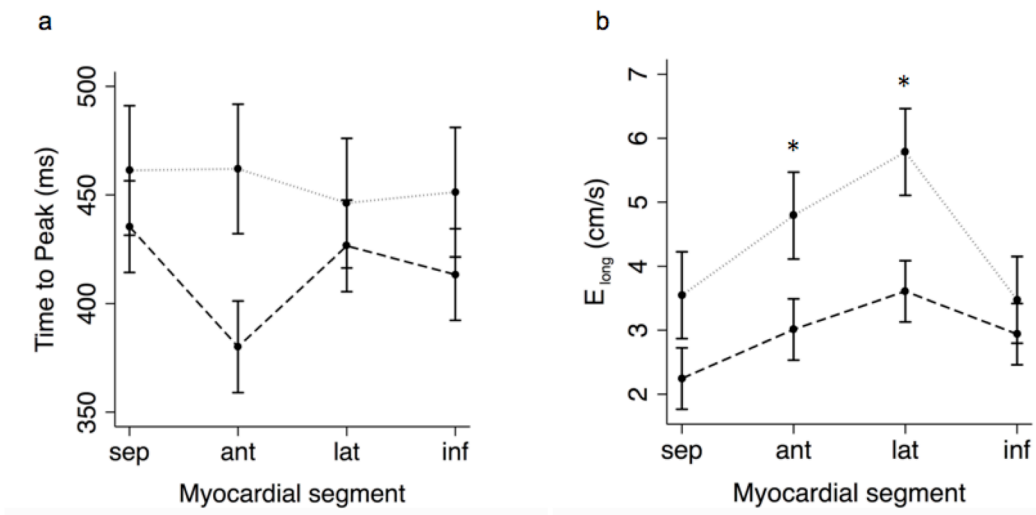


Figure 4-7: Graphs demonstrating segmental variation in health (dotted line) and PH (--- line) in (a) E_{rad} time to peak, (b) E_{long} magnitude.

(a) There is a trend for an earlier E_{rad} time to peak for the anterior segment in PH. There is no regional heterogeneity in E_{rad} time to peak in health.

(b) The anterior and lateral walls had higher E_{long} peak velocities than the inferior wall and septum in health. Regional variation in the magnitude of E_{long} velocities is less distinct in PH, with only the lateral segment having a tendency, albeit not statistically significant, for higher E_{long} velocities.

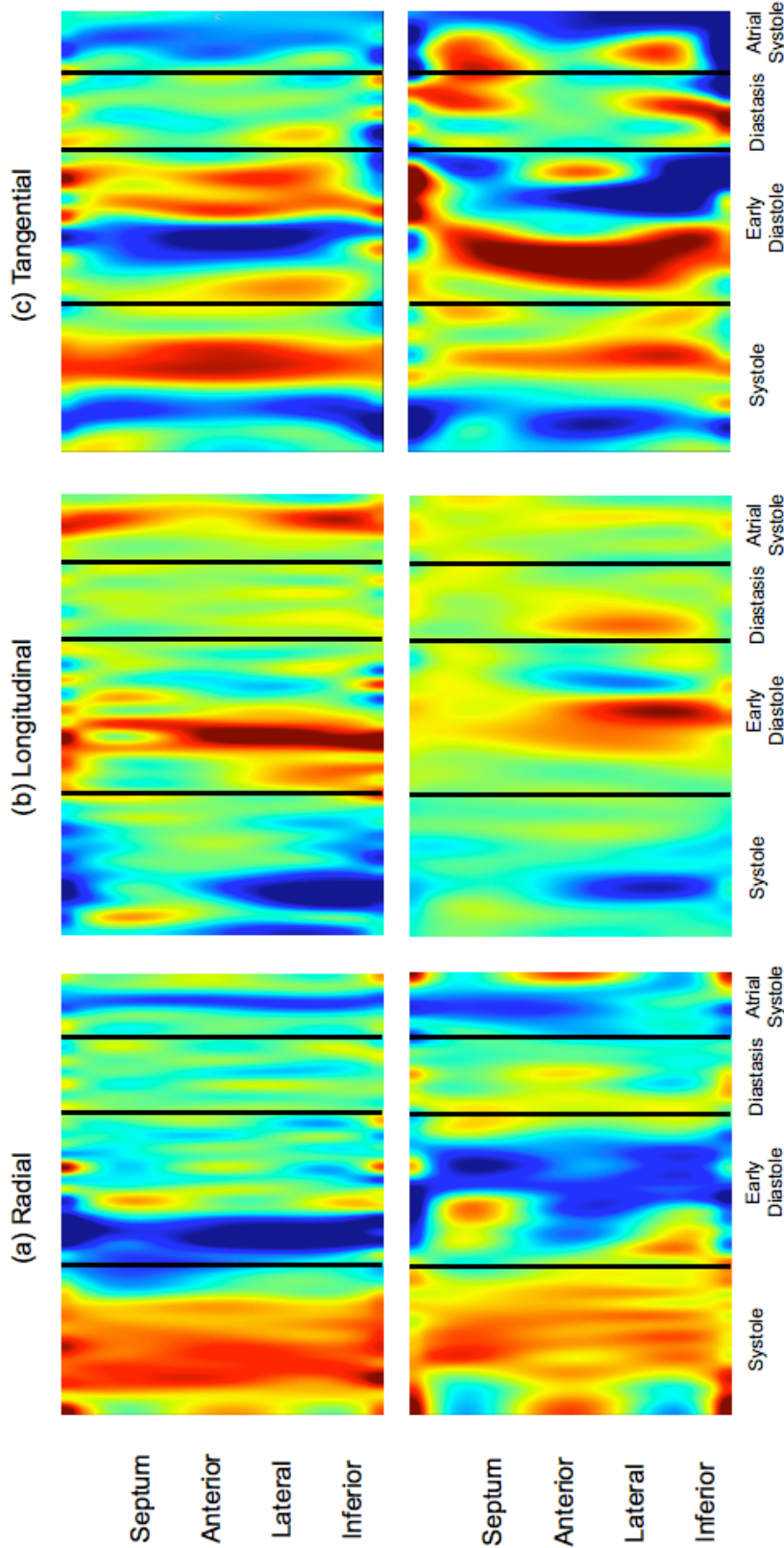


Figure 4-8: Velocity colour maps for (a) radial, (b) longitudinal, and (c) tangential LV motion from a control (top) and a PH patient (bottom). The maps represent motion of sequential LV segments (y-axis) throughout the cardiac cycle (x-axis). The wave colour (blue or red) indicates direction of motion, with colour intensity representing relative magnitude of the segmental velocity. There are segmental E wave abnormalities in all components of motion:
 (a) Radially: In health, E wave timing is uniform throughout LV segments. In early diastole in PH, the anterior segment tends to move outwards (E_{rad} wave) first whilst the septum continues to move inwards.
 (b) Longitudinally: In health, peak anterolateral segment E_{long} waves are of significantly greater magnitude, compared with only a trend for greater lateral segment E_{long} waves in PH.
 (c) Tangentially: Reversal of E1 and E2 waves was observed in all patients.

4.4.4 Haemodynamic Correlates with Myocardial Velocities

Univariate haemodynamic correlates with abnormal global myocardial velocities are shown in Table 4-4.

	E_{rad}		E_{long}		$S2_{tang}$		$E1_{tang}$		$E2_{tang}$	
	r	p	r	p	r	p	r	p	r	p
SC	0.40	0.01	0.33	0.041	-0.041	0.80	-0.24	0.13	0.13	0.43
mPAP	-0.60	0.0005	-0.41	0.027	0.17	0.38	0.17	0.38	-0.19	0.32
PVR	-0.47	0.011	-0.27	0.16	0.046	0.82	0.14	0.49	-0.16	0.43
RVEDV	-0.26	0.11	-0.41	0.0087	0.0024	0.99	0.24	0.14	0.071	0.66
RVESV	-0.45	0.004	-0.51	0.0007	0.030	0.86	0.35	0.023	0.062	0.71
RVSV	0.33	0.038	0.1006	0.54	-0.074	0.65	-0.17	0.29	0.040	0.81
LVEDV	0.34	0.035	0.13	0.43	0.083	0.61	-0.18	0.27	0.20	0.22
LVESV	0.061	0.71	-0.035	0.83	0.24	0.13	-0.093	0.57	0.29	0.067
LVSV	0.45	0.0032	0.22	0.18	-0.063	0.70	-0.20	0.23	0.077	0.64
E/A ratio	0.43	0.0077	0.38	0.019	-0.016	0.93	0.031	0.85	-0.0035	0.98

Table 4-4: Correlations between abnormal global LV myocardial velocities in PH and haemodynamics.

Univariate haemodynamic correlates with abnormal global myocardial velocities are shown in Table 4. Both peak E_{rad} and E_{long} strongly correlated with mPAP, RVESV and E/A ratio. In addition, peak E_{rad} also correlated with LVSV. The first global E_{tang} peak only correlated with RVESV ($r=0.35$, $p=0.023$). The second E_{tang} and S_{tang} peaks did not correlate with any of the tested metrics ($p>0.1$). In a generalized least squares model that included mPAP, RVESV, LVSV and E/A, only RVESV was independently predictive of either longitudinal or radial E wave velocities ($\beta=-0.43$, $p=0.001$).

4.4.5 Functional Correlates with Myocardial Velocities

All correlates with 6-MWD are shown in Table 4-5. The strongest E wave myocardial velocity correlate with 6-MWD was the global E_{rad} peak ($r=0.58$, $p=0.0001$). The strongest S wave myocardial velocity was the lateral S_{rad} peak ($r=0.48$, $p=0.0018$). The conventional RV metric with the strongest correlation to 6-MWD was RVEF ($r=0.54$, $p=0.0003$) and the

strongest conventional LV metric was LVSV ($r=0.39$, $p=0.013$). In addition, there was a significant correlation between 6-MWD and E/A ratio ($r=0.39$, $p=0.013$). When these metrics were inputted into a multiple linear regression analysis, only global E_{rad} ($\beta=0.41$, $p=0.017$) and lateral S_{rad} ($\beta=0.33$, $p=0.028$) were independent predictors of 6-MWD.

	6-MWD, r	p-value
RVEDV	-0.22	0.17
RVESV	-0.41	0.0079
RVSV	0.35	0.027
RVEF	0.54	0.0003*
LVEDV	0.22	0.16
LVESV	-0.075	0.65
LVSV	0.39	0.013*
LVEF	0.37	0.021
LVCO	0.17	0.29
SC	0.18	0.26
E/A ratio	0.4	0.013*
LV global S_{rad}	0.36	0.024
LV anterior S_{rad}	0.29	0.067
LV septal S_{rad}	0.28	0.078
LV inferior S_{rad}	0.072	0.66
LV lateral S_{rad}	0.48	0.0018*
LV global E_{rad}	0.58	0.0001*
LV anterior E_{rad}	-0.024	0.88
LV septal E_{rad}	0.55	0.0002
LV inferior E_{rad}	0.24	0.13
LV lateral E_{rad}	0.54	0.0003
LV global S_{long}	0.19	0.24
LV anterior S_{long}	0.2	0.22
LV septal S_{long}	0.18	0.27
LV inferior S_{long}	0.19	0.24
LV lateral S_{long}	0.012	0.94

<i>(continued)</i>	6-MWD, r	p-value
LV global E_{long}	0.53	0.0004
LV anterior E_{long}	0.39	0.014
LV septal E_{long}	0.5	0.0011
LV inferior E_{long}	0.49	0.0015
LV lateral E_{long}	0.35	0.028
LV global $S1_{\text{tang}}$	0.35	0.025
LV anterior $S1_{\text{tang}}$	0.3	0.057
LV septal $S1_{\text{tang}}$	0.46	0.0025
LV inferior $S1_{\text{tang}}$	0.39	0.014
LV lateral $S1_{\text{tang}}$	0.3	0.065
LV global $E1_{\text{tang}}$	-0.15	0.36
LV anterior $E1_{\text{tang}}$	-0.081	0.62
LV septal $E1_{\text{tang}}$	0.077	0.64
LV inferior $E1_{\text{tang}}$	-0.13	0.41
LV lateral $E1_{\text{tang}}$	-0.071	0.66
LV global $S2_{\text{tang}}$	0.14	0.39
LV anterior $S2_{\text{tang}}$	0.065	0.69
LV septal $S2_{\text{tang}}$	0.072	0.66
LV inferior $S2_{\text{tang}}$	0.11	0.49
LV lateral $S2_{\text{tang}}$	0.12	0.47
LV global $E2_{\text{tang}}$	-0.075	0.65
LV anterior $E2_{\text{tang}}$	0.056	0.73
LV septal $E2_{\text{tang}}$	-0.12	0.47
LV inferior $E2_{\text{tang}}$	-0.21	0.2
LV lateral $E2_{\text{tang}}$	-0.19	0.25

Table 4-5: Correlates of conventional and novel CMRI metrics with 6-MWD in pulmonary hypertension.

4.4.6 Relationship between Myocardial Velocity and Clinical Worsening

All five patients who had operable proximal CTEPH underwent subsequent thromboendarterectomy, and one PAH patient was already receiving intravenous vasodilator therapy at the time of CMRI study. Clinical worsening was studied in the remaining 34 patients. Over a median follow-up period of 20 months (IQR 7.9 months), 8 patients were started on intravenous therapy and 1 died.

Metrics that predicted clinical worsening on univariate cox regression analysis are shown in Table 4-6. The strongest predictive E wave myocardial velocity was global E_{long} peak (6.3x increase in hazard per SD reduction in the magnitude of the peak velocity). The strongest conventional RV metric was RVEF (2.4x increase in hazard per SD reduction in RVEF). In addition, septal curvature was also predictive of clinical worsening (3.6x increase in hazard per SD distortion of septum towards the LV). Conventional LV metrics and E/A ratio did not predict clinical worsening. When global E_{long} peak, RVEF and SC were inputted into a multivariable cox regression model, only global E_{long} was an independent predictor of clinical worsening ($p=0.009$).

	HR (95% CI)	p-value
Age	0.76 (0.41-1.42)	0.39
LVEF	0.78 (0.39-1.55)	0.47
LVEDV	0.82 (0.39-1.72)	0.6
LVESV	1.03 (0.55-1.95)	0.92
LVSV	0.69 (0.31-1.55)	0.37
LVCO	1.08 (0.58-2.01)	0.81
RVEF	0.42 (0.19-0.93)	0.032*
RVEDV	2.18 (1.05-4.51)	0.037
RVESV	2.16 (1.08-4.30)	0.029
RVSV	0.99 (0.48-2.04)	0.98
SC	0.28 (0.11-0.75)	0.011*

(continued)	HR (95% CI)	p-value
HR	1.72 (0.89-3.34)	0.11
E/A ratio	0.94 (0.46-1.94)	0.88
LV global S_{rad}	0.46 (0.19-1.12)	0.087
LV anterior S_{rad}	0.71 (0.33-1.53)	0.38
LV septal S_{rad}	0.72 (0.36-1.48)	0.37
LV inferior S_{rad}	0.74 (0.34-1.61)	0.45
LV lateral S_{rad}	0.68 (0.34-1.33)	0.26
LV global S_{long}	1.00 (0.54-1.85)	1
LV anterior S_{long}	1.36 (0.75-2.45)	0.32
LV septal S_{long}	1.60 (0.82-3.13)	0.17
LV inferior S_{long}	0.69 (0.33-1.47)	0.34
LV lateral S_{long}	0.57 (0.24-1.32)	0.19
LV global $S1_{tang}$	0.68 (0.34-1.36)	0.27
LV anterior $S1_{tang}$	0.79 (0.41-1.52)	0.48
LV septal $S1_{tang}$	0.63 (0.31-1.29)	0.21
LV inferior $S1_{tang}$	0.72 (0.37-1.44)	0.36
LV lateral $S1_{tang}$	0.57 (0.27-1.20)	0.14
LV global $S2_{tang}$	1.27 (0.72-2.25)	0.41
LV anterior $S2_{tang}$	1.17 (0.66-2.10)	0.59
LV septal $S2_{tang}$	1.52 (0.88-2.61)	0.13
LV inferior $S2_{tang}$	1.36 (0.73-2.54)	0.34
LV lateral $S2_{tang}$	1.12 (0.61-2.05)	0.72
LV global E_{rad}	0.29 (0.13-0.69)	0.005
LV anterior E_{rad}	0.95 (0.46-1.96)	0.88
LV septal E_{rad}	0.74 (0.32-1.72)	0.48
LV inferior E_{rad}	0.67 (0.33-1.35)	0.26
LV lateral E_{rad}	0.56 (0.29-1.09)	0.089
LV global E_{long}	0.16 (0.047-0.58)	0.005*
LV anterior E_{long}	0.50 (0.22-1.13)	0.098
LV septal E_{long}	0.33 (0.15-0.72)	0.005
LV inferior E_{long}	0.37 (0.12-1.20)	0.098
LV lateral E_{long}	0.23 (0.065-0.82)	0.023

(continued)	HR (95% CI)	p-value
LV global $E_{1\text{tang}}$	0.66 (0.34-1.28)	0.22
LV anterior $E_{1\text{tang}}$	0.93 (0.47-1.86)	0.85
LV septal $E_{1\text{tang}}$	0.99 (0.47-2.07)	0.97
LV inferior $E_{1\text{tang}}$	0.62 (0.30-1.28)	0.2
LV lateral $E_{1\text{tang}}$	0.50 (0.23-1.11)	0.087
LV global $E_{2\text{tang}}$	1.11 (0.58-2.13)	0.74
LV anterior $E_{2\text{tang}}$	1.53 (0.71-3.31)	0.28
LV septal $E_{2\text{tang}}$	1.02 (0.52-1.98)	0.96
LV inferior $E_{2\text{tang}}$	0.89 (0.46-1.70)	0.72
LV lateral $E_{2\text{tang}}$	1.27 (0.73-2.20)	0.4

Table 4-6: Univariate Cox regression analysis of conventional and novel CMRI metrics to predict disease progression in PH.

4.5 Discussion

This is the first study to use CMRI tissue phase mapping to assess LV myocardial velocities in patients with PH. The main findings of this study were:

- i) Patients with PH had reduced global E_{rad} and E_{long} velocities, and reversal of both E_{tang} waves.
- ii) Peak global E_{rad} velocity was an independent predictor of 6-MWD.
- iii) Peak global E_{long} peak velocity was an independent predictor of clinical worsening.

These results demonstrate that LV myocardial mechanics are negatively affected by RV pressure overload and may contribute to symptoms and clinical worsening.

4.5.1 LV Myocardial Velocities in PH

In keeping with previous studies, these results indicate that PH is primarily associated with early diastolic LV dysfunction[175, 177, 235]. Specifically, peak E wave velocities were lower in patients compared to

age and sex matched controls. Importantly, LVSV was not an independent predictor of E wave velocities. Thus, it is unlikely that reduced pulmonary venous return is the main reason for this finding. Interestingly, the only independent predictor of reduced E wave velocity was increased RVESV. This suggests a link between RV dilation and LV diastolic dysfunction, which I believe is mediated through external constraint of the LV. It is easily understood that LV filling can be reduced by abnormal septal dynamics[178]. However, it is also possible that the pericardium also plays an important part. As the RV dilates, the whole of the pericardium becomes stretched and less compliant[16, 236]. This could constrain the inferior and lateral LV walls and additionally reduce LV filling. This idea is backed up by animal studies of acute RV dilation, where removal of the pericardium normalizes LV filling[237, 238]. The fact that the anterior segment is not constrained by the pericardium or septum may explain the trend towards its earlier E_{rad} peak, further corroborating this hypothesis. The exact mechanism underlying the reversal of the E_{tang} peaks is not clear from the results. A possible explanation might be the significant geometric alterations seen in patients with PH, but this requires further study.

It should be noted that these diastolic abnormalities could be the result of LV remodeling and intrinsic myocardial stiffening. This is particularly pertinent in the study patient population due to the high prevalence of CTD, which is known to cause diastolic dysfunction[239]. However, E wave velocities were similar across aetiological subgroups, suggesting that the results were not due to CTD-specific LV remodeling. It is possible that PH itself could cause changes in LV structure such as myocardial fibrosis or fibre reorientation[240]. Techniques such as T1 Mapping and myocardial diffusion tensor imaging may be better placed to determine if these factors are also important[241].

4.5.2 Functional Correlates with Myocardial Velocities

This study has shown that lower radial and longitudinal E wave velocities are associated with reduced 6-MWD. This is in keeping with E wave velocities being a marker for diastolic dysfunction, which is known to limit augmentation of stroke volume during exercise. In keeping with the pivotal role of stroke volume, it is unsurprising that resting LVSV also correlated with 6-MWD. However, global E_{rad} was an independent predictor of 6-MWD in a model adjusted for resting LVSV. This suggests that resting E_{rad} may be a better predictor of exercise stroke volume augmentation than resting LVSV. In addition, the lateral S_{rad} peak was also predictive of 6-MWD. This is interesting because the population S_{rad} peaks were similar in patients and controls. Nevertheless, patients did have greater variance in S_{rad} , which may explain the exercise findings. The increased peak systolic velocity seen in some patients is probably an attempt to maintain cardiac output in the face of worsening disease. Conversely, the reduced peak velocity found in other patients is possibly due to intrinsic LV systolic dysfunction or abnormal septal interactions.

This study has also found that E wave velocities, in particular global E_{long} , predicted clinical worsening. This is probably because patients with impaired diastolic function have less cardiac reserve and are therefore more symptomatic. This increases the likelihood of up-titration of therapy or death. The reasons why longitudinal rather than radial E wave is a better predictor of progression are not obvious from the data. One possibility is that longitudinal velocities might integrate more measures of cardiac dysfunction than simply reduced LV filling. Importantly, E/A ratio was similar in patients and controls and did not independently predict 6-MWD or clinical worsening. This demonstrates the benefits of TPM over conventional measures of diastolic dysfunction.

In keeping with previous studies, RVEF did correlate with 6-MWD and predicted clinical worsening[80]. However, RVEF was not an independent predictor of exercise capacity in a model including global E_{rad} , nor was it

an independent predictor of clinical worsening in a model adjusted for global E_{long} . These results suggest that reduced LV diastolic function may be more important than RV function itself. This is consistent with studies in patients with other forms of RV pressure overload. For instance, in congenital heart disease it has been shown that improved exercise capacity after relief of RV outflow obstruction is primarily due to better LV filling[178].

4.5.3 Using TPM to assess RV function in PH

An important limitation of this study is that RV TPM metrics were not assessed. RV deformation parameters by STE are prognostic in PAH[242]. Therefore, given that RV dysfunction is a hallmark of PH, a comprehensive assessment of biventricular myocardial mechanics would be advantageous. CMRI would be particularly well placed to provide this information over echocardiography given that it is not limited by imaging planes afforded by intercostal rib spaces. By contrast, a specific limitation of STE is that it tends to only provide reproducible deformation assessment of the RV free wall from a single acoustic window, namely the apical 4-chamber view.

Although RV data are not reported in this study, it has been shown that it is possible to assess RV TPM metrics using this technique[182]. The sequence used in the current study was originally designed and validated in order to measure clinically relevant myocardial velocities in both the LV and the RV (Appendix 3)[182]. Specifically, an image-based respiratory navigator calculated from the TPM data itself was constructed. This enabled the long acquisition times required for the collection of velocity-encoded data in three directions during free breathing. In particular, this was of sufficiently high spatiotemporal resolution to enable TPM assessment of the thin RV free wall. Furthermore, the sequence proof of concept study demonstrated the feasibility of TPM data acquisition from 20 healthy volunteers and also 10 patients with PH.

However, a limitation of short axis TPM is that it is not possible to correct for longitudinal bulk motion. In the LV this is not a significant problem as longitudinal bulk motion is limited. However, in severe PH the RV displays a rocking motion that results in errors in longitudinal velocity assessment[55]. During the course of data acquisition in the current study it became clear that the rocking motion of the RV in PH presented a significant limitation to the application of this sequence in this setting. As a result, the meaningfulness of the RV TPM data became uncertain. In all likelihood these problems of TPM used to assess RV motion in PH were not previously encountered during the sequence validation study for two reasons; firstly due to the low number of patients with PH, and secondly because the healthy volunteers in that study were neither age- nor sex-matched with the patient cohort.

4.6 Limitations

This feasibility study represents a single centre experience of applying TPM to a small cohort of patients. Furthermore, the low mortality in this population required a more broadly defined composite outcome measure that included transplant and intravenous therapy. These 'softer' outcome measures are more susceptible to bias, although CMRI was not used to make clinical management decisions in this study.

Another important limitation of this study was the heterogeneity of the population and in particular the high number of patients with CTD, possibly limiting the applicability of the results to the majority of PH patients. Therefore, this can only be considered a feasibility study demonstrating that TPM data may be of clinical interest in this group of patients. Nevertheless, the positive findings do warrant further work in this area. Furthermore, no differences in haemodynamics were found between the sub-groups, suggesting that the data is valid across a 'real world' patient population.

Other limitations include the fact that catheter haemodynamic data was not available in all patients, but septal curvature nevertheless correlated strongly with the recent cardiac catheter data. In order to ensure a streamlined acquisition protocol, sequences for tissue characterization were not acquired. Myocardial involvement in connective tissue disease, for example, has been demonstrated by CMRI[241, 243]. However, the magnitude and waveform characteristics of myocardial motion were consistent irrespective of disease aetiology or treatment. The study exclusion criteria also required the absence of post-capillary PH and known left-sided heart disease. In future studies, it will be vital that these deficiencies are addressed.

4.7 Conclusions

Novel TPM by CMRI is feasible in PH, permitting accurate quantification of global and regional myocardial velocities. TPM metrics of LV diastolic dysfunction in PH reliably discriminate between health and disease, and are also strongly predictive of functional capacity. TPM may also be incrementally beneficial in identifying clinical worsening in PH compared with conventional CMRI metrics of RV function. These feasibility data support the application of the technique to a larger group of patients over a longer follow-up period. This would allow full determination of the prognostic capacity of LV TPM metrics in PH. Future work should also be directed at assessing the response of these novel biomarkers to vasodilator therapy.

CHAPTER 5

Conclusions and Future Work

5.1 Summary

The present work has focused on the application of novel echocardiography and CMRI techniques to provide a more comprehensive assessment of cardiac function in acquired disease of the right heart.

Chapter 2 presented a comparison of single-beat full-volume 3DE for RV volumetric quantification against CMRI in large homogeneous patient populations of RV pressure- and volume-overload. The technique was feasible, with clinically acceptable limits of agreement compared with the clinical reference standard. However, limitations of this contemporary 3DE method include the operator learning curve associated with using the technique, reduced accuracy when applied to non-dilated RV cavities, and its test-retest reproducibility.

Previous literature also suggests that commercially available 3DE post-processing algorithms may be too generic to apply to the clinical spectrum of RV diseases and their respective heterogeneous chamber shapes. In order to overcome this limitation and to take advantage of the clinical familiarity and higher spatiotemporal resolution of 2DE, chapter 3 presented a validation study of novel 2D KBR for RV volumetric quantification against CMRI in a patient population with PH. 2D KBR was feasible, accurate and had good test-retest reproducibility in patients with acquired RV pressure-overload. Moreover, the reproducibility metrics were significantly better than those for conventional RV FAC, which was obtained from the same 4-chamber loops that also constituted the 2D KBR datasets.

These two echocardiography techniques represented novel non-invasive methods to quantify RV size and global systolic function. Chapter 4 presented the application of a novel CMRI tissue phase mapping (TPM) sequence to provide a more comprehensive understanding of biventricular myocardial mechanics in PH. TPM metrics of LV diastolic

function were significantly abnormal in PH, with reversal of LV tangential E waves observed in all patients and being highly discriminative for the presence of PH. More importantly, abnormal LV E wave velocities were the only independent predictors of functional capacity and clinical worsening in a model that included conventional metrics of biventricular function. This is most likely to be a manifestation of ventricular interdependence due to RV distention in PH, and may be a pathophysiological step towards the previously reported finding of LV atrophic remodeling in advanced disease.

5.2 Future Work

Future developments related to these novel imaging techniques are described in turn.

5.2.1 Three-Dimensional Echocardiography of the RV

Further work aimed at improving 3DE RV assessment can be divided into acquisition and post-processing components.

5.2.1.1 3DE RV acquisition

Contrast-enhancement could have a role for 3DE RV assessment given the reported difficulties in differentiating trabeculations from endocardium, and there is significant scope for further work in this area. Contrast-enhancement has previously been reported to be beneficial for the accuracy and reproducibility of 3DE assessment of the LV, particularly in patients with suboptimal transthoracic echocardiography windows[244-246]. Agitated colloid is known to be an effective, safe and inexpensive agent for right heart chamber opacification[247]. My anecdotal experience using this method was of visually improved endocardial delineation (Figure 5-1), consistent with reports of improved RV endocardial visualization with contrast when using 2DE[248]. However, this was at the expense of the ability of the semi-automated border-tracking algorithm to identify and track the endocardium. Given that this compromised the

working of the vendor-specific post-processing software, this approach precluded any analysis of contrast-enhanced 3DE RV datasets and thus had to be abandoned.

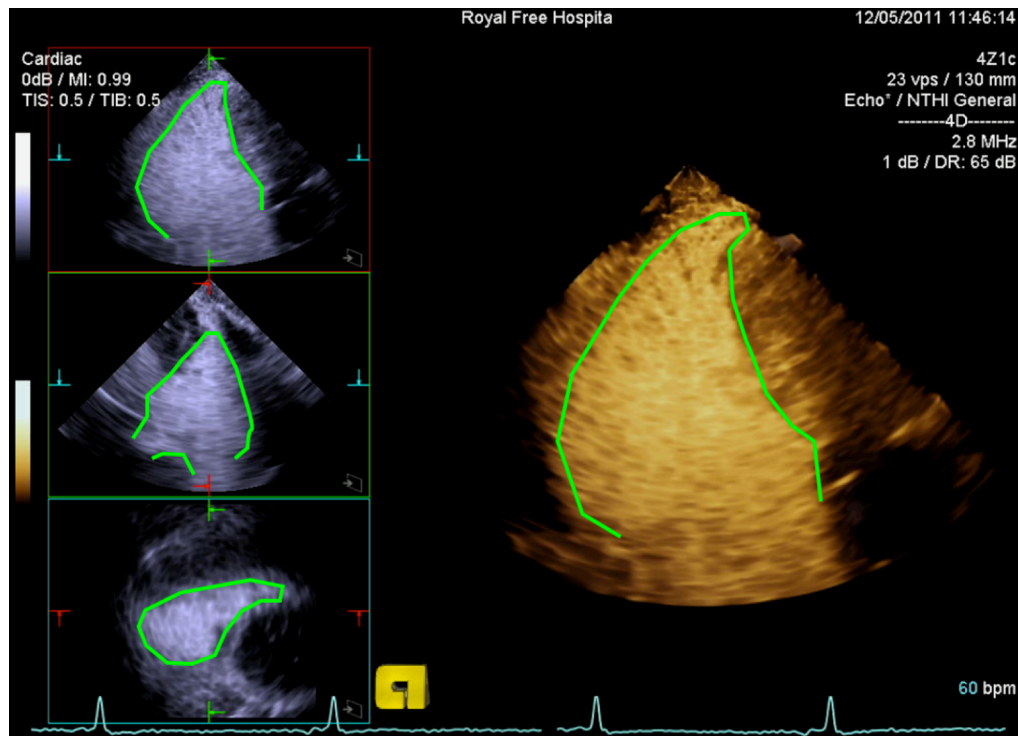


Figure 5-1: A 3DE RV data set from a patient with severe carcinoid heart disease following administration of intravenous agitated colloid.

Endocardial borders in the 4-chamber (top left), coronal (middle) and sagittal (bottom) windows have been delineated for illustrative purposes.

There are to date few studies of contrast-enhanced 3DE RV assessment. The feasibility of RV contrast-enhancement has been shown in vitro and in vivo in a small 3DE study using agitated saline contrast[249]. Datasets in this study were manually post-processed using the summation of disks, bypassing any potential interference with automated border-tracking post-processing algorithms. Van der Zwaan et al. also published their experience of contrast-enhanced 3DE of the RV in abstract form[250]. Intravenous echocardiography contrast was reported to visually improve RV endocardial contour definition, but generated smaller RV volumes. One possible reason for this result might be that dense contrast-enhancement of the cavity could interfere with the generally accepted advice to trace 'on the white side' of the RV endocardium when post-processing 3DE data sets.

5.2.1.2 3DE RV post-processing

A new iteration of the commercially available 3DE RV post-processing software has recently been reported[251]. This has been prompted by the known difficulty in obtaining RV coronal views and RVOT visualization of consistently satisfactory quality. This novel approach for 3DE RV volumetric analysis utilized a method without post-processing coronal views, instead using multiple short-axis views extracted from RV-focused 3DE datasets acquired as described in Chapter 2. The new post-processing technique was of clinically acceptable accuracy versus CMRI, and had reasonable reproducibility metrics. Importantly, the novel post-processing method showed improved accuracy for RV volumetric quantification compared with the standard post-processing algorithm in a subset of 30 patients with 3DE datasets of suboptimal quality.

Ongoing developments in the post-processing of RV 3DE datasets should also not be limited to global metrics. Given the evolving improvements in ultrasound transducer technology and the spatiotemporal resolution of single-beat full-volume 3DE, the quantitative analysis of RV shape and curvature parameters from transthoracic 3DE datasets can now be studied[252]. By quantitatively analyzing RV regional curvature from 3DE-derived dynamic endocardial surfaces, the curvature of the RV inflow portion was shown to be a more robust predictor of mortality in PH compared with conventional 3DE metrics including RV volumes and EF. The application of this methodology, both by this custom 3DE method and also by KBR, merits further development and application to the spectrum of congenital and acquired heart diseases affecting the right heart.

5.2.2 Two-Dimensional Knowledge-Based Reconstruction of the RV

Contrast-enhancement for improved RV endocardial visualization on 2DE would immediately lend itself to the 2D KBR as described in Chapter 3, as cavity opacification might assist the operator in plotting the endocardial points[247, 248]. This would also not interfere with the KBR post-

processing algorithm, as the KBR reconstruction process is independent of the raw 2DE image data when reconstructing a 3D RV volume.

A side-by side comparison of 3DE versus 2D KBR in a small sample size favoured 2D KBR for accuracy[167]. However, the relative contributions of 2DE (for acquisition) and KBR (for post-processing) to the accuracy of the technique remain undefined. The ability to acquire a full-volume 3DE RV dataset in a single cardiac cycle has been demonstrated in Chapter 2, and the feasibility of applying KBR to 3DE-derived RV datasets has also previously been demonstrated[170]. Using a 3DE dataset with KBR post-processing would make the technique theoretically quicker for image acquisition and less prone to error introduced by patient movement or breathing. Furthermore, the extra specialist equipment used to spatially localize the position of the 2DE ultrasound probe would not be required with a single-beat full-volume 3DE acquisition. However, the higher spatiotemporal resolution of 2DE and familiarity with this modality may instead be advantageous. Further study should be undertaken to define the optimal ultrasound mode to acquire RV datasets for KBR post-processing.

Given the accuracy of the technique, the clinical utility and sensitivity of 2D KBR to detect changes in RV size and function in response to treatment should be studied in large patient populations. Changes in RV volumes and function following treatment were detected at follow-up echocardiography study using 2D KBR in a small group of patients with PH, published by our group in abstract form[253]. Just over half of a group of 22 patients with PH had a demonstrable reduction in indexed RV EDV of more than 10% during a mean follow-up period of 6 months. Furthermore, all of those patients also showed reductions in NT-proBNP levels by at least two-thirds, or NT-proBNP levels were already normal or near normal at baseline. The ability to track changes in RV size and/or function in response to treatment by a 2DE technique would be of great clinical value in PH, certainly in terms of technique availability and cost

compared with CMRI. This is especially important in terms of global health resources given that the prevalence of pulmonary vascular disease is far higher in developing countries than in the developed world[254].

5.2.3 Tissue Phase Mapping for Myocardial Mechanics

TPM is a promising technique for the comprehensive assessment of myocardial mechanics. In the small cohort of PH patients that were studied, TPM metrics of LV diastolic function were highly discriminative between health and disease, and were the only independent predictors of functional capacity and clinical worsening in a model that included conventional metrics of biventricular function. The low mortality in this small population, however, required a more broadly defined composite outcome measure that included transplant and intravenous therapy. Therefore, this can only be considered a feasibility study demonstrating that TPM data may be of clinical interest in this group of patients. Nevertheless, the positive findings do warrant further work in this area and support the application of the technique to a larger group of patients over a longer follow-up period. This would allow full determination of the prognostic capacity of LV TPM metrics in PH. Future work in the PH setting should also be directed at assessing the response of these novel biomarkers to vasodilator therapy.

Increasing the speed of data acquisition would be helpful to apply the technique to larger study populations. Recently, it has been shown that it is possible to acquire TPM data in a breath hold using a spiral SENSE acquisition.[255] This opens up the possibility of the rapid acquisition of myocardial velocity data, which would make this technique more clinically feasible. The sequence used in this study has since been adapted in-house allowing the acquisition of high spatiotemporal resolution LV TPM data in a single breath hold. This is currently being validated and applied in ongoing work to assess LV function in, amongst other studies, paediatric patients with chronic kidney disease.

Further work should also be directed at addressing the limitations of applying the technique to RV assessment in patients with PH. As discussed, we have demonstrated the feasibility of the novel TPM sequence to assess RV function[182]. However, the inability to correct for longitudinal bulk motion is a particular limitation of short axis TPM when applied to the rocking motion of the RV in severe PH[55]. A simple approach would be to perform TPM in the 4-chamber view for simultaneous assessment of in-plane longitudinal and radial motion of the RV. This analysis could be extended to study RV deformation. Parameters that could be assessed include strain, by integrating velocities with respect to time[223]; and strain rate, by calculating the spatial derivatives of the velocities at each pixel[224].

A further step in the application of TPM could involve the use of 4D phase contrast techniques. Acquisitions of 4D TPM data sets have previously been carried out, allowing velocities to be extracted from any point in the myocardium without the need for prior slice positioning[256, 257]. However, this is at the expense of lengthy scan times of up to 30 to 40 minutes. A pilot breath hold 4D phase contrast sequence of approximately 20 seconds duration has been developed in-house within our group for future validation (Figure 5-2). However, the inferior spatiotemporal resolution of a 3D phase contrast technique would not be suitable for analysis of the thin RV myocardium, and would likely be restricted to LV functional analysis.

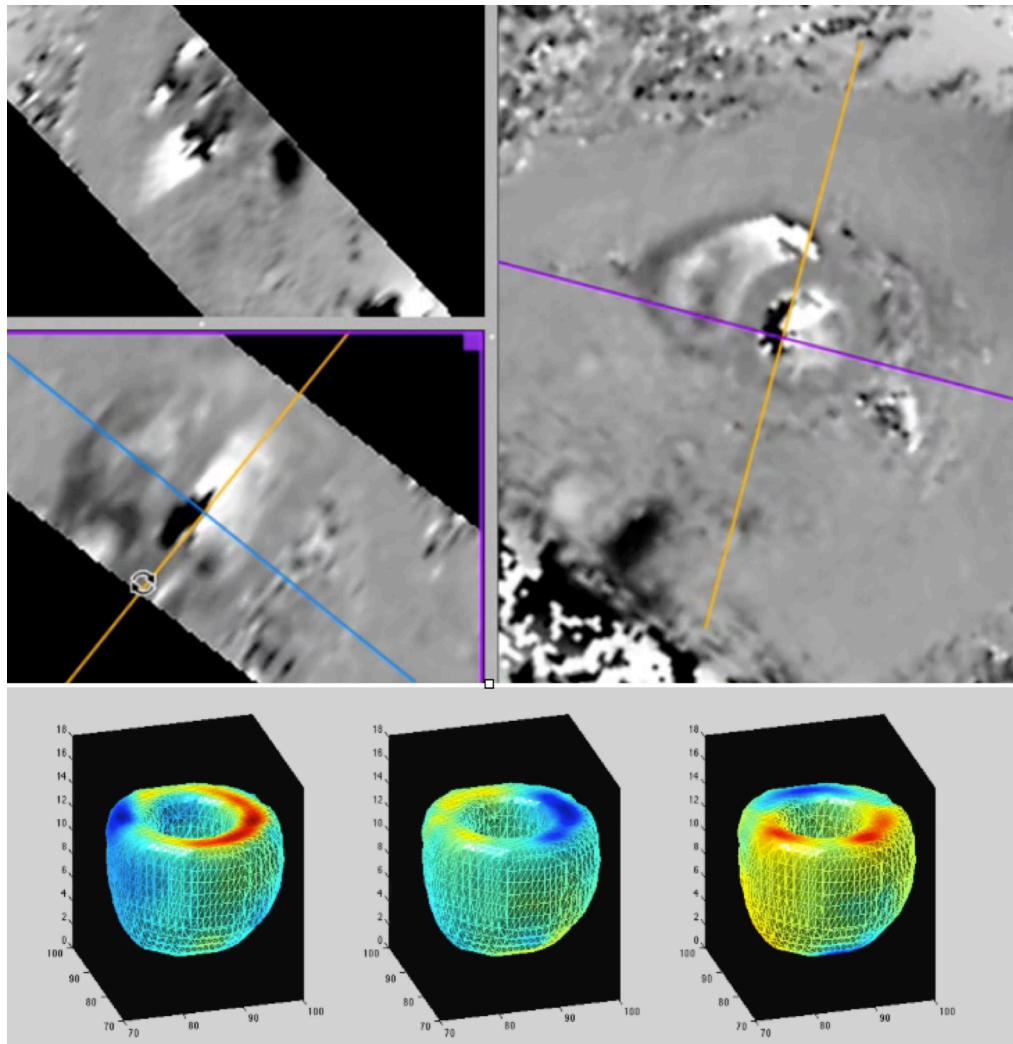


Figure 5-2: A 4D TPM breath hold data set from a healthy volunteer.

The raw phase contrast data shows a short-axis view (top right) and the corresponding 4-chamber view (middle right). The bottom images demonstrate reconstruction of the post-processed data for LV velocities in x, y and z.

Courtesy of Dr Vivek Muthurangu

5.3 Conclusion

This thesis has investigated the feasibility of novel echocardiography and CMRI techniques to investigate cardiac function in patients with acquired right heart disease. These techniques not only have demonstrable feasibility in a clinical setting, but they also provide incremental benefit over conventional clinical non-invasive metrics used to monitor patients with PH. I am optimistic that future work using these novel techniques and the continued application of advances in imaging technology to non-invasive diagnostic cardiology could be of benefit to the clinical management of these patients.

References

- [1] de Groote P, Millaire A, Foucher-Hossein C, Nogue O, Marchandise X, Ducloux G, Lablanche JM. Right ventricular ejection fraction is an independent predictor of survival in patients with moderate heart failure. *J Am Coll Cardiol.* 1998;32:948-54.
- [2] Ghio S, Gavazzi A, Campana C, Inserra C, Klersy C, Sebastiani R, Arbustini E, Recusani F, Tavazzi L. Independent and additive prognostic value of right ventricular systolic function and pulmonary artery pressure in patients with chronic heart failure. *J Am Coll Cardiol.* 2001;37:183-8.
- [3] Knauth AL, Gauvreau K, Powell AJ, Landzberg MJ, Walsh EP, Lock JE, del Nido PJ, Geva T. Ventricular size and function assessed by cardiac MRI predict major adverse clinical outcomes late after tetralogy of Fallot repair. *Heart.* 2008;94:211-6.
- [4] Sun JP, James KB, Yang XS, Solankhi N, Shah MS, Arheart KL, Thomas JD, Stewart WJ. Comparison of mortality rates and progression of left ventricular dysfunction in patients with idiopathic dilated cardiomyopathy and dilated versus nondilated right ventricular cavities. *Am J Cardiol.* 1997;80:1583-7.
- [5] Shoja MM, Tubbs RS, Loukas M, Ardalan MR. The Aristotelian account of "heart and veins". *Int J Cardiol.* 2008;125:304-10.
- [6] Shoja MM, Agutter PS, Loukas M, Benninger B, Shokouhi G, Namdar H, Ghabili K, Khalili M, Tubbs RS. Leonardo da Vinci's studies of the heart. *Int J Cardiol.* 2013;167:1126-33.
- [7] Keele KD. Leonardo da Vinci, and the movement of the heart. *Proc R Soc Med.* 1951;44:209-13.
- [8] Keele KD. Leonardo da Vinci on movement of the heart and blood. Philadelphia: Lippincott; 1952.
- [9] Goldstein J. The right ventricle: what's right and what's wrong. *Coron Artery Dis.* 2005;16:1-3.
- [10] Harvey W. *Exercitatio Anatomica de Motu Cordis et Sanguinis in Animalibus*; 1628.

- [11] da Vinci L. Quaderni d'anatomia, I–VI: Fogli della Royal Library di Windsor, pubblicati da CL Vangensten, A Fonahn, H Hopstock. Christiana: J. Dybwad; 1911–1916.
- [12] Mertens LL, Friedberg MK. Imaging the right ventricle--current state of the art. *Nat Rev Cardiol*. 2010;7:551-63.
- [13] Mor-Avi V, Sugeng L, Lindner JR. Imaging the forgotten chamber: is the devil in the boundary? *J Am Soc Echocardiogr*. 2010;23:141-3.
- [14] Haddad F, Hunt SA, Rosenthal DN, Murphy DJ. Right ventricular function in cardiovascular disease, part I: Anatomy, physiology, aging, and functional assessment of the right ventricle. *Circulation*. 2008;117:1436-48.
- [15] Kagan A. Dynamic responses of the right ventricle following extensive damage by cauterization. *Circulation*. 1952;5:816-23.
- [16] Goldstein JA, Vlahakes GJ, Verrier ED, Schiller NB, Tyberg JV, Ports TA, Parmley WW, Chatterjee K. The role of right ventricular systolic dysfunction and elevated intrapericardial pressure in the genesis of low output in experimental right ventricular infarction. *Circulation*. 1982;65:513-22.
- [17] Haddad F, Doyle R, Murphy DJ, Hunt SA. Right ventricular function in cardiovascular disease, part II: pathophysiology, clinical importance, and management of right ventricular failure. *Circulation*. 2008;117:1717-31.
- [18] Fontan F, Baudet E. Surgical repair of tricuspid atresia. *Thorax*. 1971;26:240-8.
- [19] Lewis BM, Gorlin R, Houssay HE, Haynes FW, Dexter L. Clinical and physiological correlations in patients with mitral stenosis. *V. Am Heart J*. 1952;43:Unknown.
- [20] Davlouros PA, Niwa K, Webb G, Gatzoulis MA. The right ventricle in congenital heart disease. *Heart*. 2006;92 Suppl 1:i27-38.
- [21] Chin KM, Kim NH, Rubin LJ. The right ventricle in pulmonary hypertension. *Coron Artery Dis*. 2005;16:13-8.
- [22] Voelkel NF, Quaife RA, Leinwand LA, Barst RJ, McGoon MD, Meldrum DR, Dupuis J, Long CS, Rubin LJ, Smart FW, Suzuki YJ,

- Gladwin M, Denholm EM, Gail DB. Right ventricular function and failure: report of a National Heart, Lung, and Blood Institute working group on cellular and molecular mechanisms of right heart failure. *Circulation*. 2006;114:1883-91.
- [23] Ho SY, Nihoyannopoulos P. Anatomy, echocardiography, and normal right ventricular dimensions. *Heart*. 2006;92 Suppl 1:i2-13.
- [24] Geva T, Powell AJ, Crawford EC, Chung T, Colan SD. Evaluation of regional differences in right ventricular systolic function by acoustic quantification echocardiography and cine magnetic resonance imaging. *Circulation*. 1998;98:339-45.
- [25] Haber I, Metaxas DN, Geva T, Axel L. Three-dimensional systolic kinematics of the right ventricle. *Am J Physiol Heart Circ Physiol*. 2005;289:H1826-33.
- [26] Redington AN. Right ventricular function. *Cardiol Clin*. 2002;20:341-9, v.
- [27] Sheehan F, Redington A. The right ventricle: anatomy, physiology and clinical imaging. *Heart*. 2008;94:1510-5.
- [28] Dell'Italia LJ, Walsh RA. Application of a time varying elastance model to right ventricular performance in man. *Cardiovasc Res*. 1988;22:864-74.
- [29] MacNee W. Pathophysiology of cor pulmonale in chronic obstructive pulmonary disease. Part One. *Am J Respir Crit Care Med*. 1994;150:833-52.
- [30] Bogaard HJ, Abe K, Vonk Noordegraaf A, Voelkel NF. The right ventricle under pressure: cellular and molecular mechanisms of right-heart failure in pulmonary hypertension. *Chest*. 2009;135:794-804.
- [31] Rochais F, Mesbah K, Kelly RG. Signaling pathways controlling second heart field development. *Circ Res*. 2009;104:933-42.
- [32] Zaffran S, Kelly RG, Meilhac SM, Buckingham ME, Brown NA. Right ventricular myocardium derives from the anterior heart field. *Circ Res*. 2004;95:261-8.

- [33] Kaufman BD, Desai M, Reddy S, Osorio JC, Chen JM, Mosca RS, Ferrante AW, Mital S. Genomic profiling of left and right ventricular hypertrophy in congenital heart disease. *J Card Fail.* 2008;14:760-7.
- [34] Mital S. Right ventricle in congenital heart disease: is it just a "weaker" left ventricle? *Arch Mal Coeur Vaiss.* 2006;99:1244-51.
- [35] Urashima T, Zhao M, Wagner R, Fajardo G, Farahani S, Quertermous T, Bernstein D. Molecular and physiological characterization of RV remodeling in a murine model of pulmonary stenosis. *Am J Physiol Heart Circ Physiol.* 2008;295:H1351-H68.
- [36] Dell'Italia LJ. The right ventricle: anatomy, physiology, and clinical importance. *Curr Probl Cardiol.* 1991;16:653-720.
- [37] Santamore WP, Dell'Italia LJ. Ventricular interdependence: significant left ventricular contributions to right ventricular systolic function. *Prog Cardiovasc Dis.* 1998;40:289-308.
- [38] Bernheim. De l'asystolie veineuse dans l'hypertrophie du coeur gauche par stenose concomitante du ventricule droit. *Rev Med.* 1910;30:785-801.
- [39] Huang MT, Goodman MA, Delaney TB. Pre-infarction angina secondary to calcific aortic stenosis with Bernheim's effect. *Clin Cardiol.* 1978;1:107-11.
- [40] Lee FA. Hemodynamics of the right ventricle in normal and disease states. *Cardiol Clin.* 1992;10:59-67.
- [41] Alpert JS. The effect of right ventricular dysfunction on left ventricular form and function. *Chest.* 2001;119:1632-3.
- [42] Hsia HH, Haddad F. Pulmonary hypertension: a stage for ventricular interdependence? *J Am Coll Cardiol.* 2012;59:2203-5.
- [43] Lazar JM, Flores AR, Grandis DJ, Orie JE, Schulman DS. Effects of chronic right ventricular pressure overload on left ventricular diastolic function. *Am J Cardiol.* 1993;72:1179-82.
- [44] Marcus JT, Vonk Noordegraaf A, Roeleveld RJ, Postmus PE, Heethaar RM, Van Rossum AC, Boonstra A. Impaired left ventricular filling due to right ventricular pressure overload in primary pulmonary

hypertension: noninvasive monitoring using MRI. *Chest*. 2001;119:1761-5.

[45] Manders E, Bogaard HJ, Handoko ML, van de Veerdonk MC, Keogh A, Westerhof N, Stienen GJ, Dos Remedios CG, Humbert M, Dorfmueller P, Fadel E, Guignabert C, van der Velden J, Vonk-Noordegraaf A, de Man FS, Ottenheijm CA. Contractile dysfunction of left ventricular cardiomyocytes in patients with pulmonary arterial hypertension. *J Am Coll Cardiol*. 2014;64:28-37.

[46] Hardziyenka M, Campian ME, Reesink HJ, Surie S, Bouma BJ, Groenink M, Klemens CA, Beekman L, Remme CA, Bresser P, Tan HL. Right ventricular failure following chronic pressure overload is associated with reduction in left ventricular mass: evidence for atrophic remodeling. *J Am Coll Cardiol*. 2011;57:921-8.

[47] Tischler MD, Sutton MS, Bittl JA, Parker JD. Effects of percutaneous mitral valvuloplasty on left ventricular mass and volume. *Am J Cardiol*. 1991;68:940-4.

[48] Rensing BJ, McDougall JC, Breen JF, Vigneswaran WT, McGregor CG, Rumberger JA. Right and left ventricular remodeling after orthotopic single lung transplantation for end-stage emphysema. *J Heart Lung Transplant*. 1997;16:926-33.

[49] Lang RM, Badano LP, Mor-Avi V, Afilalo J, Armstrong A, Ernande L, Flachskampf FA, Foster E, Goldstein SA, Kuznetsova T, Lancellotti P, Muraru D, Picard MH, Rietzschel ER, Rudski L, Spencer KT, Tsang W, Voigt JU. Recommendations for cardiac chamber quantification by echocardiography in adults: an update from the American Society of Echocardiography and the European Association of Cardiovascular Imaging. *J Am Soc Echocardiogr*. 2015;28:1-39 e14.

[50] Rudski LG, Lai WW, Afilalo J, Hua L, Handschumacher MD, Chandrasekaran K, Solomon SD, Louie EK, Schiller NB. Guidelines for the echocardiographic assessment of the right heart in adults: a report from the American Society of Echocardiography endorsed by the European Association of Echocardiography, a registered branch of the

European Society of Cardiology, and the Canadian Society of Echocardiography. *J Am Soc Echocardiogr*. 2010;23:685-713; quiz 86-8.

[51] Foale R, Nihoyannopoulos P, McKenna W, Kleinebenne A, Nadazdin A, Rowland E, Smith G. Echocardiographic measurement of the normal adult right ventricle. *Br Heart J*. 1986;56:33-44.

[52] Willis J, Augustine D, Shah R, Stevens C, Easaw J. Right ventricular normal measurements: time to index? *J Am Soc Echocardiogr*. 2012;25:1259-67.

[53] Lai WW, Gauvreau K, Rivera ES, Saleeb S, Powell AJ, Geva T. Accuracy of guideline recommendations for two-dimensional quantification of the right ventricle by echocardiography. *Int J Cardiovasc Imaging*. 2008;24:691-8.

[54] Kind T, Mauritz GJ, Marcus JT, van de Veerdonk M, Westerhof N, Vonk-Noordegraaf A. Right ventricular ejection fraction is better reflected by transverse rather than longitudinal wall motion in pulmonary hypertension. *J Cardiovasc Magn Reson*. 2010;12:35.

[55] Giusca S, Dambrauskaite V, Scheurwegs C, D'Hooge J, Claus P, Herbots L, Magro M, Rademakers F, Meyns B, Delcroix M, Voigt JU. Deformation imaging describes right ventricular function better than longitudinal displacement of the tricuspid ring. *Heart*. 2010;96:281-8.

[56] Geva T. Is MRI the preferred method for evaluating right ventricular size and function in patients with congenital heart disease?: MRI is the preferred method for evaluating right ventricular size and function in patients with congenital heart disease. *Circ Cardiovasc Imaging*. 2014;7:190-7.

[57] Grothues F, Smith GC, Moon JC, Bellenger NG, Collins P, Klein HU, Pennell DJ. Comparison of interstudy reproducibility of cardiovascular magnetic resonance with two-dimensional echocardiography in normal subjects and in patients with heart failure or left ventricular hypertrophy. *Am J Cardiol*. 2002;90:29-34.

[58] Schulz-Menger J, Bluemke DA, Bremerich J, Flamm SD, Fogel MA, Friedrich MG, Kim RJ, von Knobelsdorff-Brenkenhoff F, Kramer CM, Pennell DJ, Plein S, Nagel E. Standardized image interpretation and post

- processing in cardiovascular magnetic resonance: Society for Cardiovascular Magnetic Resonance (SCMR) board of trustees task force on standardized post processing. *J Cardiovasc Magn Reson*. 2013;15:35.
- [59] Winter MM, Bernink FJ, Groenink M, Bouma BJ, van Dijk AP, Helbing WA, Tijssen JG, Mulder BJ. Evaluating the systemic right ventricle by CMR: the importance of consistent and reproducible delineation of the cavity. *J Cardiovasc Magn Reson*. 2008;10:40.
- [60] Beerbaum P, Barth P, Kropf S, Sarikouch S, Kelter-Kloepping A, Franke D, Gutberlet M, Kuehne T. Cardiac function by MRI in congenital heart disease: impact of consensus training on interinstitutional variance. *J Magn Reson Imaging*. 2009;30:956-66.
- [61] Prakash A, Powell AJ, Geva T. Multimodality noninvasive imaging for assessment of congenital heart disease. *Circ Cardiovasc Imaging*. 2010;3:112-25.
- [62] Brignole M, Auricchio A, Baron-Esquivias G, Bordachar P, Boriani G, Breithardt OA, Cleland J, Deharo JC, Delgado V, Elliott PM, Gorenek B, Israel CW, Leclercq C, Linde C, Mont L, Padeletti L, Sutton R, Vardas PE, Zamorano JL, Achenbach S, Baumgartner H, Bax JJ, Bueno H, Dean V, Deaton C, Erol C, Fagard R, Ferrari R, Hasdai D, Hoes AW, Kirchhof P, Knuuti J, Kolh P, Lancellotti P, Linhart A, Nihoyannopoulos P, Piepoli MF, Ponikowski P, Sirnes PA, Tamargo JL, Tendera M, Torbicki A, Wijns W, Windecker S, Kirchhof P, Blomstrom-Lundqvist C, Badano LP, Aliyev F, Bansch D, Baumgartner H, Bsata W, Buser P, Charron P, Daubert JC, Dobreanu D, Faerestrand S, Hasdai D, Hoes AW, Le Heuzey JY, Mavrakis H, McDonagh T, Merino JL, Nawar MM, Nielsen JC, Pieske B, Poposka L, Ruschitzka F, Tendera M, Van Gelder IC, Wilson CM. 2013 ESC Guidelines on cardiac pacing and cardiac resynchronization therapy: the Task Force on cardiac pacing and resynchronization therapy of the European Society of Cardiology (ESC). Developed in collaboration with the European Heart Rhythm Association (EHRA). *Eur Heart J*. 2013;34:2281-329.
- [63] Muthurangu V, Lurz P, Critchely JD, Deanfield JE, Taylor AM, Hansen MS. Real-time assessment of right and left ventricular volumes

- and function in patients with congenital heart disease by using high spatiotemporal resolution radial k-t SENSE. *Radiology*. 2008;248:782-91.
- [64] Grothues F, Moon JC, Bellenger NG, Smith GS, Klein HU, Pennell DJ. Interstudy reproducibility of right ventricular volumes, function, and mass with cardiovascular magnetic resonance. *Am Heart J*. 2004;147:218-23.
- [65] Hudsmith LE, Petersen SE, Francis JM, Robson MD, Neubauer S. Normal human left and right ventricular and left atrial dimensions using steady state free precession magnetic resonance imaging. *J Cardiovasc Magn Reson*. 2005;7:775-82.
- [66] Mooij CF, de Wit CJ, Graham DA, Powell AJ, Geva T. Reproducibility of MRI measurements of right ventricular size and function in patients with normal and dilated ventricles. *J Magn Reson Imaging*. 2008;28:67-73.
- [67] Alfakih K, Plein S, Bloomer T, Jones T, Ridgway J, Sivananthan M. Comparison of right ventricular volume measurements between axial and short axis orientation using steady-state free precession magnetic resonance imaging. *J Magn Reson Imaging*. 2003;18:25-32.
- [68] Atalay MK, Chang KJ, Grand DJ, Haji-Momenian S, Machan JT, Sheehan FH. The Transaxial Orientation Is Superior to Both the Short Axis and Horizontal Long Axis Orientations for Determining Right Ventricular Volume and Ejection Fraction Using Simpson's Method with Cardiac Magnetic Resonance. *ISRN Cardiol*. 2013;2013:268697.
- [69] Kramer CM, Barkhausen J, Flamm SD, Kim RJ, Nagel E. Standardized cardiovascular magnetic resonance (CMR) protocols 2013 update. *J Cardiovasc Magn Reson*. 2013;15:91.
- [70] Aebischer N, Meuli R, Jeanrenaud X, Koerfer J, Kappenberger L. An echocardiographic and magnetic resonance imaging comparative study of right ventricular volume determination. *Int J Card Imaging*. 1998;14:271-8.
- [71] Alghamdi MH, Grosse-Wortmann L, Ahmad N, Mertens L, Friedberg MK. Can simple echocardiographic measures reduce the number of cardiac magnetic resonance imaging studies to diagnose right ventricular

enlargement in congenital heart disease? J Am Soc Echocardiogr. 2012;25:518-23.

[72] Anavekar NS, Gerson D, Skali H, Kwong RY, Yucel EK, Solomon SD. Two-dimensional assessment of right ventricular function: an echocardiographic-MRI correlative study. Echocardiography. 2007;24:452-6.

[73] Focardi M, Cameli M, Carbone SF, Massoni A, De Vito R, Lisi M, Mondillo S. Traditional and innovative echocardiographic parameters for the analysis of right ventricular performance in comparison with cardiac magnetic resonance. Eur Heart J Cardiovasc Imaging. 2015;16:47-52.

[74] Lytrivi ID, Lai WW, Ko HH, Nielsen JC, Parness IA, Srivastava S. Color Doppler tissue imaging for evaluation of right ventricular systolic function in patients with congenital heart disease. J Am Soc Echocardiogr. 2005;18:1099-104.

[75] Pavlicek M, Wahl A, Rutz T, de Marchi SF, Hille R, Wustmann K, Steck H, Eigenmann C, Schwerzmann M, Seiler C. Right ventricular systolic function assessment: rank of echocardiographic methods vs. cardiac magnetic resonance imaging. Eur J Echocardiogr. 2011;12:871-80.

[76] Sato T, Tsujino I, Ohira H, Oyama-Manabe N, Yamada A, Ito YM, Goto C, Watanabe T, Sakaue S, Nishimura M. Validation study on the accuracy of echocardiographic measurements of right ventricular systolic function in pulmonary hypertension. J Am Soc Echocardiogr. 2012;25:280-6.

[77] Shiran H, Zamanian RT, McConnell MV, Liang DH, Dash R, Heidary S, Sudini NL, Wu JC, Haddad F, Yang PC. Relationship between echocardiographic and magnetic resonance derived measures of right ventricular size and function in patients with pulmonary hypertension. J Am Soc Echocardiogr. 2014;27:405-12.

[78] van der Zwaan HB, Geleijnse ML, McGhie JS, Boersma E, Helbing WA, Meijboom FJ, Roos-Hesselink JW. Right ventricular quantification in clinical practice: two-dimensional vs. three-dimensional echocardiography

compared with cardiac magnetic resonance imaging. *Eur J Echocardiogr.* 2011;12:656-64.

[79] Wang J, Prakasa K, Bomma C, Tandri H, Dalal D, James C, Tichnell C, Corretti M, Bluemke D, Calkins H, Abraham TP. Comparison of novel echocardiographic parameters of right ventricular function with ejection fraction by cardiac magnetic resonance. *J Am Soc Echocardiogr.* 2007;20:1058-64.

[80] Moledina S, Pandya B, Bartsota M, Mortensen KH, McMillan M, Quyam S, Taylor AM, Haworth SG, Schulze-Neick I, Muthurangu V. Prognostic significance of cardiac magnetic resonance imaging in children with pulmonary hypertension. *Circ Cardiovasc Imaging.* 2013;6:407-14.

[81] van Wolferen SA, Marcus JT, Boonstra A, Marques KM, Bronzwaer JG, Spreeuwenberg MD, Postmus PE, Vonk-Noordegraaf A. Prognostic value of right ventricular mass, volume, and function in idiopathic pulmonary arterial hypertension. *Eur Heart J.* 2007;28:1250-7.

[82] Galie N, Hinderliter AL, Torbicki A, Fourme T, Simonneau G, Pulido T, Espinola-Zavaleta N, Rocchi G, Manes A, Frantz R, Kurzyna M, Nagueh SF, Barst R, Channick R, Dujardin K, Kronenberg A, Leconte I, Rainisio M, Rubin L. Effects of the oral endothelin-receptor antagonist bosentan on echocardiographic and doppler measures in patients with pulmonary arterial hypertension. *J Am Coll Cardiol.* 2003;41:1380-6.

[83] Pandya B, Quail MA, Steeden JA, McKee A, Odille F, Taylor AM, Schulze-Neick I, Derrick G, Moledina S, Muthurangu V. Real-time magnetic resonance assessment of septal curvature accurately tracks acute hemodynamic changes in pediatric pulmonary hypertension. *Circ Cardiovasc Imaging.* 2014;7:706-13.

[84] Raymond RJ, Hinderliter AL, Willis PW, Ralph D, Caldwell EJ, Williams W, Ettinger NA, Hill NS, Summer WR, de Boisblanc B, Schwartz T, Koch G, Clayton LM, Jobsis MM, Crow JW, Long W. Echocardiographic predictors of adverse outcomes in primary pulmonary hypertension. *J Am Coll Cardiol.* 2002;39:1214-9.

- [85] Ryan T, Petrovic O, Dillon JC, Feigenbaum H, Conley MJ, Armstrong WF. An echocardiographic index for separation of right ventricular volume and pressure overload. *J Am Coll Cardiol*. 1985;5:918-27.
- [86] Simonneau G, Gatzoulis MA, Adatia I, Celermajer D, Denton C, Ghofrani A, Gomez Sanchez MA, Krishna Kumar R, Landzberg M, Machado RF, Olschewski H, Robbins IM, Souza R. Updated clinical classification of pulmonary hypertension. *J Am Coll Cardiol*. 2013;62:D34-41.
- [87] Hopkins WE, Ochoa LL, Richardson GW, Trulock EP. Comparison of the hemodynamics and survival of adults with severe primary pulmonary hypertension or Eisenmenger syndrome. *J Heart Lung Transplant*. 1996;15:100-5.
- [88] Tedford RJ, Mudd JO, Girgis RE, Mathai SC, Zaiman AL, Houston-Harris T, Boyce D, Kelemen BW, Bacher AC, Shah AA, Hummers LK, Wigley FM, Russell SD, Saggarr R, Saggarr R, Maughan WL, Hassoun PM, Kass DA. Right ventricular dysfunction in systemic sclerosis-associated pulmonary arterial hypertension. *Circ Heart Fail*. 2013;6:953-63.
- [89] Benza RL, Miller DP, Gomberg-Maitland M, Frantz RP, Foreman AJ, Coffey CS, Frost A, Barst RJ, Badesch DB, Elliott CG, Liou TG, McGoon MD. Predicting survival in pulmonary arterial hypertension: insights from the Registry to Evaluate Early and Long-Term Pulmonary Arterial Hypertension Disease Management (REVEAL). *Circulation*. 2010;122:164-72.
- [90] Hesselstrand R, Wildt M, Ekmehag B, Wuttge DM, Scheja A. Survival in patients with pulmonary arterial hypertension associated with systemic sclerosis from a Swedish single centre: prognosis still poor and prediction difficult. *Scand J Rheumatol*. 2011;40:127-32.
- [91] Hopkins WE, Waggoner AD. Severe pulmonary hypertension without right ventricular failure: the unique hearts of patients with Eisenmenger syndrome. *Am J Cardiol*. 2002;89:34-8.
- [92] Rothman A, Sklansky MS, Lucas VW, Kashani IA, Shaughnessy RD, Channick RN, Auger WR, Fedullo PF, Smith CM, Kriett JM, Jamieson

- SW. Atrial septostomy as a bridge to lung transplantation in patients with severe pulmonary hypertension. *Am J Cardiol.* 1999;84:682-6.
- [93] Robin ED. The kingdom of the near-dead. The shortened unnatural life history of primary pulmonary hypertension. *Chest.* 1987;92:330-4.
- [94] Galie N, Corris PA, Frost A, Girgis RE, Granton J, Jing ZC, Klepetko W, McGoon MD, McLaughlin VV, Preston IR, Rubin LJ, Sandoval J, Seeger W, Keogh A. Updated treatment algorithm of pulmonary arterial hypertension. *J Am Coll Cardiol.* 2013;62:D60-72.
- [95] Nagendran J, Archer SL, Soliman D, Gurtu V, Moudgil R, Haromy A, St Aubin C, Webster L, Rebeyka IM, Ross DB, Light PE, Dyck JR, Michelakis ED. Phosphodiesterase type 5 is highly expressed in the hypertrophied human right ventricle, and acute inhibition of phosphodiesterase type 5 improves contractility. *Circulation.* 2007;116:238-48.
- [96] Bhattacharyya S, Davar J, Dreyfus G, Caplin ME. Carcinoid heart disease. *Circulation.* 2007;116:2860-5.
- [97] Pellikka PA, Tajik AJ, Khandheria BK, Seward JB, Callahan JA, Pitot HC, Kvolz LK. Carcinoid heart disease. Clinical and echocardiographic spectrum in 74 patients. *Circulation.* 1993;87:1188-96.
- [98] Bhattacharyya S, Toumpanakis C, Caplin ME, Davar J. Usefulness of N-terminal pro-brain natriuretic peptide as a biomarker of the presence of carcinoid heart disease. *Am J Cardiol.* 2008;102:938-42.
- [99] Bhattacharyya S, Toumpanakis C, Caplin ME, Davar J. Analysis of 150 patients with carcinoid syndrome seen in a single year at one institution in the first decade of the twenty-first century. *Am J Cardiol.* 2008;101:378-81.
- [100] Moller JE, Pellikka PA, Bernheim AM, Schaff HV, Rubin J, Connolly HM. Prognosis of carcinoid heart disease: analysis of 200 cases over two decades. *Circulation.* 2005;112:3320-7.
- [101] Bhattacharyya S, Raja SG, Toumpanakis C, Caplin ME, Dreyfus GD, Davar J. Outcomes, risks and complications of cardiac surgery for carcinoid heart disease. *Eur J Cardiothorac Surg.* 2011;40:168-72.

- [102] Bhattacharyya S, Toumpanakis C, Burke M, Taylor AM, Caplin ME, Davar J. Features of carcinoid heart disease identified by 2- and 3-dimensional echocardiography and cardiac MRI. *Circ Cardiovasc Imaging*. 2010;3:103-11.
- [103] Vonk-Noordegraaf A, Souza R. Cardiac magnetic resonance imaging: what can it add to our knowledge of the right ventricle in pulmonary arterial hypertension? *Am J Cardiol*. 2012;110:25S-31S.
- [104] Shimada YJ, Shiota M, Siegel RJ, Shiota T. Accuracy of right ventricular volumes and function determined by three-dimensional echocardiography in comparison with magnetic resonance imaging: a meta-analysis study. *J Am Soc Echocardiogr*. 2010;23:943-53.
- [105] Lang RM, Badano LP, Tsang W, Adams DH, Agricola E, Buck T, Faletra FF, Franke A, Hung J, de Isla LP, Kamp O, Kasprzak JD, Lancellotti P, Marwick TH, McCulloch ML, Monaghan MJ, Nihoyannopoulos P, Pandian NG, Pellikka PA, Pepi M, Roberson DA, Shernan SK, Shirali GS, Sugeng L, Ten Cate FJ, Vannan MA, Zamorano JL, Zoghbi WA. EAE/ASE recommendations for image acquisition and display using three-dimensional echocardiography. *J Am Soc Echocardiogr*. 2012;25:3-46.
- [106] Sugeng L, Mor-Avi V, Weinert L, Niel J, Ebner C, Steringer-Mascherbauer R, Bartolles R, Baumann R, Schummers G, Lang RM, Nesser HJ. Multimodality comparison of quantitative volumetric analysis of the right ventricle. *JACC Cardiovasc Imaging*. 2010;3:10-8.
- [107] Bhan A, Kapetanakis S, Monaghan MJ. Three-dimensional echocardiography. *Heart*. 2010;96:153-63.
- [108] Knight DS, Grasso AE, Quail MA, Muthurangu V, Taylor AM, Toumpanakis C, Caplin ME, Coghlan JG, Davar J. Accuracy and reproducibility of right ventricular quantification in patients with pressure and volume overload using single-beat three-dimensional echocardiography. *J Am Soc Echocardiogr*. 2015;28:363-74.
- [109] Tamborini G, Muratori M, Brusoni D, Celeste F, Maffessanti F, Caiani EG, Alamanni F, Pepi M. Is right ventricular systolic function

reduced after cardiac surgery? A two- and three-dimensional echocardiographic study. *Eur J Echocardiogr.* 2009;10:630-4.

[110] Gopal AS, Chukwu EO, Iwuchukwu CJ, Katz AS, Toole RS, Schapiro W, Reichek N. Normal values of right ventricular size and function by real-time 3-dimensional echocardiography: comparison with cardiac magnetic resonance imaging. *J Am Soc Echocardiogr.* 2007;20:445-55.

[111] Fang F, Chan A, Lee AP, Sanderson JE, Kwong JS, Luo XX, Li S, Yu CM. Variation in right ventricular volumes assessment by real-time three-dimensional echocardiography between dilated and normal right ventricle: comparison with cardiac magnetic resonance imaging. *Int J Cardiol.* 2013;168:4391-3.

[112] Schattke S, Wagner M, Hattasch R, Schroeckh S, Durmus T, Schimke I, Sanad W, Spethmann S, Scharhag J, Huppertz A, Baumann G, Borges AC, Knebel F. Single beat 3D echocardiography for the assessment of right ventricular dimension and function after endurance exercise: Intraindividual comparison with magnetic resonance imaging. *Cardiovasc Ultrasound.* 2012;10:6.

[113] Zhang QB, Sun JP, Gao RF, Lee AP, Feng YL, Liu XR, Sheng W, Liu F, Yang XS, Fang F, Yu CM. Feasibility of single-beat full-volume capture real-time three-dimensional echocardiography for quantification of right ventricular volume: validation by cardiac magnetic resonance imaging. *Int J Cardiol.* 2013;168:3991-5.

[114] Morikawa T, Murata M, Okuda S, Tsuruta H, Iwanaga S, Murata M, Satoh T, Ogawa S, Fukuda K. Quantitative analysis of right ventricular function in patients with pulmonary hypertension using three-dimensional echocardiography and a two-dimensional summation method compared to magnetic resonance imaging. *Am J Cardiol.* 2011;107:484-9.

[115] Iriart X, Montaudon M, Lafitte S, Chabaneix J, Reant P, Balbach T, Houle H, Laurent F, Thambo JB. Right ventricle three-dimensional echography in corrected tetralogy of fallot: accuracy and variability. *Eur J Echocardiogr.* 2009;10:784-92.

- [116] Niemann PS, Pinho L, Balbach T, Galuschky C, Blankenhagen M, Silberbach M, Broberg C, Jerosch-Herold M, Sahn DJ. Anatomically oriented right ventricular volume measurements with dynamic three-dimensional echocardiography validated by 3-Tesla magnetic resonance imaging. *J Am Coll Cardiol*. 2007;50:1668-76.
- [117] Tamborini G, Brusoni D, Torres Molina JE, Galli CA, Maltagliati A, Muratori M, Susini F, Colombo C, Maffessanti F, Pepi M. Feasibility of a new generation three-dimensional echocardiography for right ventricular volumetric and functional measurements. *Am J Cardiol*. 2008;102:499-505.
- [118] Grapsa J, O'Regan DP, Pavlopoulos H, Durighel G, Dawson D, Nihoyannopoulos P. Right ventricular remodelling in pulmonary arterial hypertension with three-dimensional echocardiography: comparison with cardiac magnetic resonance imaging. *Eur J Echocardiogr*. 2010;11:64-73.
- [119] Li Y, Wang Y, Zhai Z, Guo X, Yang Y, Lu X. Real-Time Three-Dimensional Echocardiography to Assess Right Ventricle Function in Patients with Pulmonary Hypertension. *PLoS One*. 2015;10:e0129557.
- [120] Jenkins C, Chan J, Bricknell K, Strudwick M, Marwick TH. Reproducibility of right ventricular volumes and ejection fraction using real-time three-dimensional echocardiography: comparison with cardiac MRI. *Chest*. 2007;131:1844-51.
- [121] Galie N, Hoeper MM, Humbert M, Torbicki A, Vachiery JL, Barbera JA, Beghetti M, Corris P, Gaine S, Gibbs JS, Gomez-Sanchez MA, Jondeau G, Klepetko W, Opitz C, Peacock A, Rubin L, Zellweger M, Simonneau G. Guidelines for the diagnosis and treatment of pulmonary hypertension: the Task Force for the Diagnosis and Treatment of Pulmonary Hypertension of the European Society of Cardiology (ESC) and the European Respiratory Society (ERS), endorsed by the International Society of Heart and Lung Transplantation (ISHLT). *Eur Heart J*. 2009;30:2493-537.
- [122] Plockinger U, Gustafsson B, Ivan D, Szpak W, Davar J. ENETS Consensus Guidelines for the Standards of Care in Neuroendocrine Tumors: echocardiography. *Neuroendocrinology*. 2009;90:190-3.

- [123] Lang RM, Bierig M, Devereux RB, Flachskampf FA, Foster E, Pellikka PA, Picard MH, Roman MJ, Seward J, Shanewise JS, Solomon SD, Spencer KT, Sutton MS, Stewart WJ. Recommendations for chamber quantification: a report from the American Society of Echocardiography's Guidelines and Standards Committee and the Chamber Quantification Writing Group, developed in conjunction with the European Association of Echocardiography, a branch of the European Society of Cardiology. *J Am Soc Echocardiogr*. 2005;18:1440-63.
- [124] Howard LS, Grapsa J, Dawson D, Bellamy M, Chambers JB, Masani ND, Nihoyannopoulos P, Simon RGJ. Echocardiographic assessment of pulmonary hypertension: standard operating procedure. *Eur Respir Rev*. 2012;21:239-48.
- [125] Hardegree EL, Sachdev A, Villarraga HR, Frantz RP, McGoon MD, Kushwaha SS, Hsiao JF, McCully RB, Oh JK, Pellikka PA, Kane GC. Role of serial quantitative assessment of right ventricular function by strain in pulmonary arterial hypertension. *Am J Cardiol*. 2013;111:143-8.
- [126] Leibundgut G, Rohner A, Grize L, Bernheim A, Kessel-Schaefer A, Bremerich J, Zellweger M, Buser P, Handke M. Dynamic assessment of right ventricular volumes and function by real-time three-dimensional echocardiography: a comparison study with magnetic resonance imaging in 100 adult patients. *J Am Soc Echocardiogr*. 2010;23:116-26.
- [127] Kjaergaard J, Petersen CL, Kjaer A, Schaadt BK, Oh JK, Hassager C. Evaluation of right ventricular volume and function by 2D and 3D echocardiography compared to MRI. *Eur J Echocardiogr*. 2006;7:430-8.
- [128] Ostenfeld E, Carlsson M, Shahgaldi K, Roijer A, Holm J. Manual correction of semi-automatic three-dimensional echocardiography is needed for right ventricular assessment in adults; validation with cardiac magnetic resonance. *Cardiovasc Ultrasound*. 2012;10:1.
- [129] van der Zwaan HB, Geleijnse ML, Soliman OI, McGhie JS, Wiegers-Groeneweg EJ, Helbing WA, Roos-Hesselink JW, Meijboom FJ. Test-retest variability of volumetric right ventricular measurements using real-time three-dimensional echocardiography. *J Am Soc Echocardiogr*. 2011;24:671-9.

- [130] Puranik R, Tsang VT, Broadley A, Nordmeyer J, Lurz P, Muthialu N, Derrick G, Walker F, Cullen S, de Leval M, Bonhoeffer P, Taylor AM, Muthurangu V. Functional outcomes after the Ross (pulmonary autograft) procedure assessed with magnetic resonance imaging and cardiopulmonary exercise testing. *Heart*. 2010;96:304-8.
- [131] Steeden JA, Atkinson D, Hansen MS, Taylor AM, Muthurangu V. Rapid flow assessment of congenital heart disease with high-spatiotemporal-resolution gated spiral phase-contrast MR imaging. *Radiology*. 2011;260:79-87.
- [132] Odille F, Steeden JA, Muthurangu V, Atkinson D. Automatic segmentation propagation of the aorta in real-time phase contrast MRI using nonrigid registration. *J Magn Reson Imaging*. 2011;33:232-8.
- [133] Rosset A, Spadola L, Ratib O. OsiriX: an open-source software for navigating in multidimensional DICOM images. *J Digit Imaging*. 2004;17:205-16.
- [134] Bland JM, Altman DG. Statistical methods for assessing agreement between two methods of clinical measurement. *Lancet*. 1986;1:307-10.
- [135] Tamborini G, Marsan NA, Gripari P, Maffessanti F, Brusoni D, Muratori M, Caiani EG, Fiorentini C, Pepi M. Reference values for right ventricular volumes and ejection fraction with real-time three-dimensional echocardiography: evaluation in a large series of normal subjects. *J Am Soc Echocardiogr*. 2010;23:109-15.
- [136] DeLong ER, DeLong DM, Clarke-Pearson DL. Comparing the areas under two or more correlated receiver operating characteristic curves: a nonparametric approach. *Biometrics*. 1988;44:837-45.
- [137] van de Veerdonk MC, Kind T, Marcus JT, Mauritz GJ, Heymans MW, Bogaard HJ, Boonstra A, Marques KM, Westerhof N, Vonk-Noordegraaf A. Progressive right ventricular dysfunction in patients with pulmonary arterial hypertension responding to therapy. *J Am Coll Cardiol*. 2011;58:2511-9.
- [138] van der Zwaan HB, Helbing WA, McGhie JS, Geleijnse ML, Luijnenburg SE, Roos-Hesselink JW, Meijboom FJ. Clinical value of real-time three-dimensional echocardiography for right ventricular

quantification in congenital heart disease: validation with cardiac magnetic resonance imaging. *J Am Soc Echocardiogr*. 2010;23:134-40.

[139] Mor-Avi V, Jenkins C, Kuhl HP, Nesser HJ, Marwick T, Franke A, Ebner C, Freed BH, Steringer-Mascherbauer R, Pollard H, Weinert L, Niel J, Sugeng L, Lang RM. Real-time 3-dimensional echocardiographic quantification of left ventricular volumes: multicenter study for validation with magnetic resonance imaging and investigation of sources of error. *JACC Cardiovasc Imaging*. 2008;1:413-23.

[140] van Wolferen SA, van de Veerdonk MC, Mauritz GJ, Jacobs W, Marcus JT, Marques KM, Bronzwaer JG, Heymans MW, Boonstra A, Postmus PE, Westerhof N, Vonk Noordegraaf A. Clinically significant change in stroke volume in pulmonary hypertension. *Chest*. 2011;139:1003-9.

[141] Fratz S, Schuhbaeck A, Buchner C, Busch R, Meierhofer C, Martinoff S, Hess J, Stern H. Comparison of accuracy of axial slices versus short-axis slices for measuring ventricular volumes by cardiac magnetic resonance in patients with corrected tetralogy of fallot. *Am J Cardiol*. 2009;103:1764-9.

[142] Knight DS, Grasso AE, Quail MA, Muthurangu V, Taylor AM, Toumpanakis C, Caplin ME, Coghlan JG, Davar J. Accuracy and Reproducibility of Right Ventricular Quantification in Patients with Pressure and Volume Overload Using Single-Beat Three-Dimensional Echocardiography. *J Am Soc Echocardiogr*. 2014.

[143] Knight DS, Schwaiger JP, Krupickova S, Davar J, Muthurangu V, Coghlan JG. Accuracy and Test-Retest Reproducibility of Two-Dimensional Knowledge-Based Volumetric Reconstruction of the Right Ventricle in Pulmonary Hypertension. *J Am Soc Echocardiogr*. 2015;28:989-98.

[144] Saremi F, Ho SY, Sanchez-Quintana D. Morphological assessment of RVOT: CT and CMR imaging. *JACC Cardiovasc Imaging*. 2013;6:631-5.

- [145] Horton KD, Meece RW, Hill JC. Assessment of the right ventricle by echocardiography: a primer for cardiac sonographers. *J Am Soc Echocardiogr.* 2009;22:776-92; quiz 861-2.
- [146] Davlouros PA, Kilner PJ, Hornung TS, Li W, Francis JM, Moon JC, Smith GC, Tat T, Pennell DJ, Gatzoulis MA. Right ventricular function in adults with repaired tetralogy of Fallot assessed with cardiovascular magnetic resonance imaging: detrimental role of right ventricular outflow aneurysms or akinesia and adverse right-to-left ventricular interaction. *J Am Coll Cardiol.* 2002;40:2044-52.
- [147] Hui W, Abd El Rahman MY, Dsebissowa F, Gutberlet M, Alexi-Meskishvili V, Hetzer R, Lange PE, Abdul-Khaliq H. Comparison of modified short axis view and apical four chamber view in evaluating right ventricular function after repair of tetralogy of Fallot. *Int J Cardiol.* 2005;105:256-61.
- [148] McConnell MV, Solomon SD, Rayan ME, Come PC, Goldhaber SZ, Lee RT. Regional right ventricular dysfunction detected by echocardiography in acute pulmonary embolism. *Am J Cardiol.* 1996;78:469-73.
- [149] Yoerger DM, Marcus F, Sherrill D, Calkins H, Towbin JA, Zareba W, Picard MH. Echocardiographic findings in patients meeting task force criteria for arrhythmogenic right ventricular dysplasia: new insights from the multidisciplinary study of right ventricular dysplasia. *J Am Coll Cardiol.* 2005;45:860-5.
- [150] Leary PJ, Kurtz CE, Hough CL, Waiss MP, Ralph DD, Sheehan FH. Three-dimensional analysis of right ventricular shape and function in pulmonary hypertension. *Pulm Circ.* 2012;2:34-40.
- [151] Dorosz JL, Bolson EL, Waiss MS, Sheehan FH. Three-dimensional visual guidance improves the accuracy of calculating right ventricular volume with two-dimensional echocardiography. *J Am Soc Echocardiogr.* 2003;16:675-81.
- [152] Jiang L, Vazquez de Prada JA, Handschumacher MD, Guererro JL, Vlahakes GJ, King ME, Weyman AE, Levine RA. Three-dimensional

echocardiography: in vivo validation for right ventricular free wall mass as an index of hypertrophy. *J Am Coll Cardiol*. 1994;23:1715-22.

[153] Leotta DF, Munt B, Bolson EL, Kraft C, Martin RW, Otto CM, Sheehan FH. Quantitative three-dimensional echocardiography by rapid imaging from multiple transthoracic windows: in vitro validation and initial in vivo studies. *J Am Soc Echocardiogr*. 1997;10:830-9.

[154] Linker DT, Moritz WE, Pearlman AS. A new three-dimensional echocardiographic method of right ventricular volume measurement: in vitro validation. *J Am Coll Cardiol*. 1986;8:101-6.

[155] Leotta DF, Detmer PR, Martin RW. Performance of a miniature magnetic position sensor for three-dimensional ultrasound imaging. *Ultrasound Med Biol*. 1997;23:597-609.

[156] Legget ME, Leotta DF, Bolson EL, McDonald JA, Martin RW, Li XN, Otto CM, Sheehan FH. System for quantitative three-dimensional echocardiography of the left ventricle based on a magnetic-field position and orientation sensing system. *IEEE Trans Biomed Eng*. 1998;45:494-504.

[157] Dragulescu A, Grosse-Wortmann L, Fackoury C, Riffle S, Waiss M, Jaeggi E, Yoo SJ, Friedberg MK, Mertens L. Echocardiographic assessment of right ventricular volumes after surgical repair of tetralogy of Fallot: clinical validation of a new echocardiographic method. *J Am Soc Echocardiogr*. 2011;24:1191-8.

[158] Hoppe H, DeRose T, Duchamp T, Halstead M, Jin H, McDonald J, Schweitzer J, Stuetzle W. Piecewise smooth surface reconstruction. *Computer Graphics (SIGGRAPH '94 Proceedings)*. 1994:295-302.

[159] Hubka M, Bolson EL, McDonald JA, Martin RW, Munt B, Sheehan FH. Three-dimensional echocardiographic measurement of left and right ventricular mass and volume: in vitro validation. *Int J Cardiovasc Imaging*. 2002;18:111-8.

[160] Munt BI, Leotta DF, Bolson EL, Coady K, Martin RW, Otto CM, Sheehan FH. Left ventricular shape analysis from three-dimensional echocardiograms. *J Am Soc Echocardiogr*. 1998;11:761-9.

- [161] Wong SP, Johnson RK, Sheehan FH. Rapid and accurate left ventricular surface generation from three-dimensional echocardiography by a catalog based method. Rapid LV surface generation by three-dimensional echo. *Int J Cardiovasc Imaging*. 2003;19:9-17.
- [162] Clark TJ, Sheehan FH, Bolson EL. Characterizing the normal heart using quantitative three-dimensional echocardiography. *Physiol Meas*. 2006;27:467-508.
- [163] Hubka M, Mantei K, Bolson E, Coady K, Sheehan F. Measurement of right ventricular mass and volume by three-dimensional echocardiography by freehand scanning. *Comput Cardiol*. 2000;27:703-6.
- [164] Sheehan FH, Kilner PJ, Sahn DJ, Vick GW, 3rd, Stout KK, Ge S, Helbing WA, Lewin M, Shurman AJ, Buechel EV, Litt HI, Waiss MP. Accuracy of knowledge-based reconstruction for measurement of right ventricular volume and function in patients with tetralogy of Fallot. *Am J Cardiol*. 2010;105:993-9.
- [165] Wheeler M, Leipsic J, Trinh P, Raju R, Alaamri S, Thompson CR, Moss R, Munt B, Kiess M, Grewal J. Right Ventricular Assessment in Adult Congenital Heart Disease Patients with Right Ventricle-to-Pulmonary Artery Conduits. *J Am Soc Echocardiogr*. 2015;28:522-32.
- [166] Bhawe NM, Patel AR, Weinert L, Yamat M, Freed BH, Mor-Avi V, Gomberg-Maitland M, Lang RM. Three-dimensional modeling of the right ventricle from two-dimensional transthoracic echocardiographic images: utility of knowledge-based reconstruction in pulmonary arterial hypertension. *J Am Soc Echocardiogr*. 2013;26:860-7.
- [167] Dragulescu A, Grosse-Wortmann L, Fackoury C, Mertens L. Echocardiographic assessment of right ventricular volumes: a comparison of different techniques in children after surgical repair of tetralogy of Fallot. *Eur Heart J Cardiovasc Imaging*. 2012;13:596-604.
- [168] Kutty S, Li L, Polak A, Gribben P, Danford DA. Echocardiographic knowledge-based reconstruction for quantification of the systemic right ventricle in young adults with repaired D-transposition of great arteries. *Am J Cardiol*. 2012;109:881-8.

- [169] Neukamm C, Try K, Norgard G, Brun H. Right ventricular volumes assessed by echocardiographic three-dimensional knowledge-based reconstruction compared with magnetic resonance imaging in a clinical setting. *Congenit Heart Dis*. 2014;9:333-42.
- [170] Laser KT, Horst JP, Barth P, Kelter-Klopping A, Haas NA, Burchert W, Kececioglu D, Korperich H. Knowledge-based reconstruction of right ventricular volumes using real-time three-dimensional echocardiographic as well as cardiac magnetic resonance images: comparison with a cardiac magnetic resonance standard. *J Am Soc Echocardiogr*. 2014;27:1087-97.
- [171] Edwards R, Shurman A, Sahn DJ, Jerosch-Herold M, Kilner PJ, Sheehan FH. Determination of right ventricular end systole by cardiovascular magnetic resonance imaging: a standard method of selection. *Int J Cardiovasc Imaging*. 2009;25:791-6.
- [172] Dragulescu A, Grosse-Wortmann L, Redington A, Friedberg MK, Mertens L. Differential effect of right ventricular dilatation on myocardial deformation in patients with atrial septal defects and patients after tetralogy of Fallot repair. *Int J Cardiol*. 2012.
- [173] Morcos M, Sheehan FH. Regional right ventricular wall motion in tetralogy of fallot: a three dimensional analysis. *Int J Cardiovasc Imaging*. 2013;29:1051-8.
- [174] Gan C, Lankhaar JW, Marcus JT, Westerhof N, Marques KM, Bronzwaer JG, Boonstra A, Postmus PE, Vonk-Noordegraaf A. Impaired left ventricular filling due to right-to-left ventricular interaction in patients with pulmonary arterial hypertension. *Am J Physiol Heart Circ Physiol*. 2006;290:H1528-33.
- [175] Hardegree EL, Sachdev A, Fenstad ER, Villarraga HR, Frantz RP, McGoon MD, Oh JK, Ammash NM, Connolly HM, Eidem BW, Pellikka PA, Kane GC. Impaired left ventricular mechanics in pulmonary arterial hypertension: identification of a cohort at high risk. *Circ Heart Fail*. 2013;6:748-55.
- [176] Marcus JT, Gan CT, Zwanenburg JJ, Boonstra A, Allaart CP, Gotte MJ, Vonk-Noordegraaf A. Interventricular mechanical asynchrony in

pulmonary arterial hypertension: left-to-right delay in peak shortening is related to right ventricular overload and left ventricular underfilling. *J Am Coll Cardiol*. 2008;51:750-7.

[177] Puwanant S, Park M, Popovic ZB, Tang WH, Farha S, George D, Sharp J, Puntawangkoon J, Loyd JE, Erzurum SC, Thomas JD. Ventricular geometry, strain, and rotational mechanics in pulmonary hypertension. *Circulation*. 2010;121:259-66.

[178] Lurz P, Puranik R, Nordmeyer J, Muthurangu V, Hansen MS, Schievano S, Marek J, Bonhoeffer P, Taylor AM. Improvement in left ventricular filling properties after relief of right ventricle to pulmonary artery conduit obstruction: contribution of septal motion and interventricular mechanical delay. *Eur Heart J*. 2009;30:2266-74.

[179] Foll D, Jung B, Staehle F, Schilli E, Bode C, Hennig J, Markl M. Visualization of multidirectional regional left ventricular dynamics by high-temporal-resolution tissue phase mapping. *J Magn Reson Imaging*. 2009;29:1043-52.

[180] Jung B, Foll D, Bottler P, Petersen S, Hennig J, Markl M. Detailed analysis of myocardial motion in volunteers and patients using high-temporal-resolution MR tissue phase mapping. *J Magn Reson Imaging*. 2006;24:1033-9.

[181] Simpson R, Keegan J, Firmin D. Efficient and reproducible high resolution spiral myocardial phase velocity mapping of the entire cardiac cycle. *J Cardiovasc Magn Reson*. 2013;15:34.

[182] Steeden JA, Knight DS, Bali S, Atkinson D, Taylor AM, Muthurangu V. Self-navigated tissue phase mapping using a golden-angle spiral acquisition-proof of concept in patients with pulmonary hypertension. *Magn Reson Med*. 2013.

[183] Zerhouni EA, Parish DM, Rogers WJ, Yang A, Shapiro EP. Human heart: tagging with MR imaging--a method for noninvasive assessment of myocardial motion. *Radiology*. 1988;169:59-63.

[184] Garot J, Bluemke DA, Osman NF, Rochitte CE, McVeigh ER, Zerhouni EA, Prince JL, Lima JA. Fast determination of regional

myocardial strain fields from tagged cardiac images using harmonic phase MRI. *Circulation*. 2000;101:981-8.

[185] Rosen BD, Lima JA, Nasir K, Edvardsen T, Folsom AR, Lai S, Bluemke DA, Jerosch-Herold M. Lower myocardial perfusion reserve is associated with decreased regional left ventricular function in asymptomatic participants of the multi-ethnic study of atherosclerosis. *Circulation*. 2006;114:289-97.

[186] Pai VM, Axel L. Advances in MRI tagging techniques for determining regional myocardial strain. *Curr Cardiol Rep*. 2006;8:53-8.

[187] Edvardsen T, Detrano R, Rosen BD, Carr JJ, Liu K, Lai S, Shea S, Pan L, Bluemke DA, Lima JA. Coronary artery atherosclerosis is related to reduced regional left ventricular function in individuals without history of clinical cardiovascular disease: the Multiethnic Study of Atherosclerosis. *Arterioscler Thromb Vasc Biol*. 2006;26:206-11.

[188] Kraitichman DL, Sampath S, Castillo E, Derbyshire JA, Boston RC, Bluemke DA, Gerber BL, Prince JL, Osman NF. Quantitative ischemia detection during cardiac magnetic resonance stress testing by use of FastHARP. *Circulation*. 2003;107:2025-30.

[189] Kramer CM, Lima JA, Reichek N, Ferrari VA, Llaneras MR, Palmon LC, Yeh IT, Tallant B, Axel L. Regional differences in function within noninfarcted myocardium during left ventricular remodeling. *Circulation*. 1993;88:1279-88.

[190] Marcus JT, Gotte MJ, Van Rossum AC, Kuijjer JP, Heethaar RM, Axel L, Visser CA. Myocardial function in infarcted and remote regions early after infarction in man: assessment by magnetic resonance tagging and strain analysis. *Magn Reson Med*. 1997;38:803-10.

[191] Nagel E, Stuber M, Lakatos M, Scheidegger MB, Boesiger P, Hess OM. Cardiac rotation and relaxation after anterolateral myocardial infarction. *Coron Artery Dis*. 2000;11:261-7.

[192] Edvardsen T, Rosen BD, Pan L, Jerosch-Herold M, Lai S, Hundley WG, Sinha S, Kronmal RA, Bluemke DA, Lima JA. Regional diastolic dysfunction in individuals with left ventricular hypertrophy measured by

tagged magnetic resonance imaging--the Multi-Ethnic Study of Atherosclerosis (MESA). *Am Heart J.* 2006;151:109-14.

[193] Bilchick KC, Dimaano V, Wu KC, Helm RH, Weiss RG, Lima JA, Berger RD, Tomaselli GF, Bluemke DA, Halperin HR, Abraham T, Kass DA, Lardo AC. Cardiac magnetic resonance assessment of dyssynchrony and myocardial scar predicts function class improvement following cardiac resynchronization therapy. *JACC Cardiovasc Imaging.* 2008;1:561-8.

[194] Nelson GS, Curry CW, Wyman BT, Kramer A, Declerck J, Talbot M, Douglas MR, Berger RD, McVeigh ER, Kass DA. Predictors of systolic augmentation from left ventricular preexcitation in patients with dilated cardiomyopathy and intraventricular conduction delay. *Circulation.* 2000;101:2703-9.

[195] Kanzaki H, Nakatani S, Yamada N, Urayama S, Miyatake K, Kitakaze M. Impaired systolic torsion in dilated cardiomyopathy: reversal of apical rotation at mid-systole characterized with magnetic resonance tagging method. *Basic Res Cardiol.* 2006;101:465-70.

[196] Young AA, Dokos S, Powell KA, Sturm B, McCulloch AD, Starling RC, McCarthy PM, White RD. Regional heterogeneity of function in nonischemic dilated cardiomyopathy. *Cardiovasc Res.* 2001;49:308-18.

[197] Ennis DB, Epstein FH, Kellman P, Fananapazir L, McVeigh ER, Arai AE. Assessment of regional systolic and diastolic dysfunction in familial hypertrophic cardiomyopathy using MR tagging. *Magn Reson Med.* 2003;50:638-42.

[198] Russel IK, Brouwer WP, Germans T, Knaapen P, Marcus JT, van der Velden J, Gotte MJ, van Rossum AC. Increased left ventricular torsion in hypertrophic cardiomyopathy mutation carriers with normal wall thickness. *J Cardiovasc Magn Reson.* 2011;13:3.

[199] Young AA, Kramer CM, Ferrari VA, Axel L, Reichek N. Three-dimensional left ventricular deformation in hypertrophic cardiomyopathy. *Circulation.* 1994;90:854-67.

[200] Rosen BD, Saad MF, Shea S, Nasir K, Edvardsen T, Burke G, Jerosch-Herold M, Arnett DK, Lai S, Bluemke DA, Lima JA. Hypertension

and smoking are associated with reduced regional left ventricular function in asymptomatic individuals the Multi-Ethnic Study of Atherosclerosis. *J Am Coll Cardiol*. 2006;47:1150-8.

[201] Ryf S, Spiegel MA, Gerber M, Boesiger P. Myocardial tagging with 3D-CSPAMM. *J Magn Reson Imaging*. 2002;16:320-5.

[202] Aletras AH, Ding S, Balaban RS, Wen H. DENSE: displacement encoding with stimulated echoes in cardiac functional MRI. *J Magn Reson*. 1999;137:247-52.

[203] Epstein FH, Gilson WD. Displacement-encoded cardiac MRI using cosine and sine modulation to eliminate (CANSEL) artifact-generating echoes. *Magn Reson Med*. 2004;52:774-81.

[204] Aletras AH, Ingkanisorn WP, Mancini C, Arai AE. DENSE with SENSE. *J Magn Reson*. 2005;176:99-106.

[205] Feng L, Donnino R, Babb J, Axel L, Kim D. Numerical and in vivo validation of fast cine displacement-encoded with stimulated echoes (DENSE) MRI for quantification of regional cardiac function. *Magn Reson Med*. 2009;62:682-90.

[206] Spottiswoode B, Russell JB, Moosa S, Meintjes EM, Epstein FH, Mayosi BM. Abnormal diastolic and systolic septal motion following pericardiectomy demonstrated by cine DENSE MRI. *Cardiovasc J Afr*. 2008;19:208-9.

[207] Spottiswoode BS, Zhong X, Hess AT, Kramer CM, Meintjes EM, Mayosi BM, Epstein FH. Tracking myocardial motion from cine DENSE images using spatiotemporal phase unwrapping and temporal fitting. *IEEE Trans Med Imaging*. 2007;26:15-30.

[208] Wen H, Marsolo KA, Bennett EE, Kutten KS, Lewis RP, Lipps DB, Epstein ND, Plehn JF, Croisille P. Adaptive postprocessing techniques for myocardial tissue tracking with displacement-encoded MR imaging. *Radiology*. 2008;246:229-40.

[209] Liu Y, Wen H, Gorman RC, Pilla JJ, Gorman JH, 3rd, Buckberg G, Teague SD, Kassab GS. Reconstruction of myocardial tissue motion and strain fields from displacement-encoded MR imaging. *Am J Physiol Heart Circ Physiol*. 2009;297:H1151-62.

- [210] Zhong X, Spottiswoode BS, Meyer CH, Kramer CM, Epstein FH. Imaging three-dimensional myocardial mechanics using navigator-gated volumetric spiral cine DENSE MRI. *Magn Reson Med*. 2010;64:1089-97.
- [211] Kim D, Kellman P. Improved cine displacement-encoded MRI using balanced steady-state free precession and time-adaptive sensitivity encoding parallel imaging at 3 T. *NMR Biomed*. 2007;20:591-601.
- [212] Osman NF, Sampath S, Atalar E, Prince JL. Imaging longitudinal cardiac strain on short-axis images using strain-encoded MRI. *Magn Reson Med*. 2001;46:324-34.
- [213] Neizel M, Korosoglou G, Lossnitzer D, Kuhl H, Hoffmann R, Ocklenburg C, Giannitsis E, Osman NF, Katus HA, Steen H. Impact of systolic and diastolic deformation indexes assessed by strain-encoded imaging to predict persistent severe myocardial dysfunction in patients after acute myocardial infarction at follow-up. *J Am Coll Cardiol*. 2010;56:1056-62.
- [214] Oyama-Manabe N, Ishimori N, Sugimori H, Van Cauteren M, Kudo K, Manabe O, Okuaki T, Kamishima T, Ito YM, Tsutsui H, Tha KK, Terae S, Shirato H. Identification and further differentiation of subendocardial and transmural myocardial infarction by fast strain-encoded (SENC) magnetic resonance imaging at 3.0 Tesla. *Eur Radiol*. 2011;21:2362-8.
- [215] Korosoglou G, Gitsioudis G, Voss A, Lehrke S, Riedle N, Buss SJ, Zugck C, Giannitsis E, Osman NF, Katus HA. Strain-encoded cardiac magnetic resonance during high-dose dobutamine stress testing for the estimation of cardiac outcomes: comparison to clinical parameters and conventional wall motion readings. *J Am Coll Cardiol*. 2011;58:1140-9.
- [216] Korosoglou G, Lehrke S, Wochele A, Hoerig B, Lossnitzer D, Steen H, Giannitsis E, Osman NF, Katus HA. Strain-encoded CMR for the detection of inducible ischemia during intermediate stress. *JACC Cardiovasc Imaging*. 2010;3:361-71.
- [217] Korosoglou G, Lossnitzer D, Schellberg D, Lewien A, Wochele A, Schaeufele T, Neizel M, Steen H, Giannitsis E, Katus HA, Osman NF. Strain-encoded cardiac MRI as an adjunct for dobutamine stress testing:

incremental value to conventional wall motion analysis. *Circ Cardiovasc Imaging*. 2009;2:132-40.

[218] Korosoglou G, Youssef AA, Bilchick KC, Ibrahim el S, Lardo AC, Lai S, Osman NF. Real-time fast strain-encoded magnetic resonance imaging to evaluate regional myocardial function at 3.0 Tesla: comparison to conventional tagging. *J Magn Reson Imaging*. 2008;27:1012-8.

[219] Hamdan A, Thouet T, Kelle S, Paetsch I, Gebker R, Wellnhofer E, Schnackenburg B, Fahmy AS, Osman NF, Fleck E. Regional right ventricular function and timing of contraction in healthy volunteers evaluated by strain-encoded MRI. *J Magn Reson Imaging*. 2008;28:1379-85.

[220] Shehata ML, Basha TA, Tantawy WH, Lima JA, Vogel-Claussen J, Bluemke DA, Hassoun PM, Osman NF. Real-time single-heartbeat fast strain-encoded imaging of right ventricular regional function: normal versus chronic pulmonary hypertension. *Magn Reson Med*. 2010;64:98-106.

[221] Gatehouse PD, Keegan J, Crowe LA, Masood S, Mohiaddin RH, Kreitner KF, Firmin DN. Applications of phase-contrast flow and velocity imaging in cardiovascular MRI. *Eur Radiol*. 2005;15:2172-84.

[222] van Dijk P. Direct cardiac NMR imaging of heart wall and blood flow velocity. *J Comput Assist Tomogr*. 1984;8:429-36.

[223] Zhu Y, Drangova M, Pelc NJ. Estimation of deformation gradient and strain from cine-PC velocity data. *IEEE Trans Med Imaging*. 1997;16:840-51.

[224] Wedeen VJ. Magnetic resonance imaging of myocardial kinematics. Technique to detect, localize, and quantify the strain rates of the active human myocardium. *Magn Reson Med*. 1992;27:52-67.

[225] Buckberg GD, Mahajan A, Jung B, Markl M, Hennig J, Ballester-Rodes M. MRI myocardial motion and fiber tracking: a confirmation of knowledge from different imaging modalities. *Eur J Cardiothorac Surg*. 2006;29 Suppl 1:S165-77.

[226] Codreanu I, Robson MD, Golding SJ, Jung BA, Clarke K, Holloway CJ. Longitudinally and circumferentially directed movements of the left

ventricle studied by cardiovascular magnetic resonance phase contrast velocity mapping. *J Cardiovasc Magn Reson*. 2010;12:48.

[227] Jung B, Markl M, Foll D, Hennig J. Investigating myocardial motion by MRI using tissue phase mapping. *Eur J Cardiothorac Surg*. 2006;29 Suppl 1:S150-7.

[228] Arai AE, Gaither CC, 3rd, Epstein FH, Balaban RS, Wolff SD. Myocardial velocity gradient imaging by phase contrast MRI with application to regional function in myocardial ischemia. *Magn Reson Med*. 1999;42:98-109.

[229] Markl M, Schneider B, Hennig J, Peschl S, Winterer J, Krause T, Laubenberger J. Cardiac phase contrast gradient echo MRI: measurement of myocardial wall motion in healthy volunteers and patients. *Int J Card Imaging*. 1999;15:441-52.

[230] Karwatowski SP, Mohiaddin RH, Yang GZ, Firmin DN, St John Sutton M, Underwood SR. Regional myocardial velocity imaged by magnetic resonance in patients with ischaemic heart disease. *Br Heart J*. 1994;72:332-8.

[231] Schneider B, Markl M, Geiges C, Winterer JT, Thuerl C, Laubenberger J, Hennig J, Langer M. Cardiac phase contrast gradient echo MRI: characterization of abnormal left ventricular wall motion in patients with ischemic heart disease. *J Comput Assist Tomogr*. 2001;25:550-7.

[232] Delfino JG, Johnson KR, Eisner RL, Eder S, Leon AR, Oshinski JN. Three-directional myocardial phase-contrast tissue velocity MR imaging with navigator-echo gating: in vivo and in vitro study. *Radiology*. 2008;246:917-25.

[233] Beache GM, Wedeen VJ, Weisskoff RM, O'Gara PT, Poncelet BP, Chesler DA, Brady TJ, Rosen BR, Dinsmore RE. Intramural mechanics in hypertrophic cardiomyopathy: functional mapping with strain-rate MR imaging. *Radiology*. 1995;197:117-24.

[234] Hennig J, Schneider B, Peschl S, Markl M, Krause T, Laubenberger J. Analysis of myocardial motion based on velocity measurements with a black blood prepared segmented gradient-echo sequence: methodology

and applications to normal volunteers and patients. *J Magn Reson Imaging*. 1998;8:868-77.

[235] Tonelli AR, Plana JC, Heresi GA, Dweik RA. Prevalence and prognostic value of left ventricular diastolic dysfunction in idiopathic and heritable pulmonary arterial hypertension. *Chest*. 2012;141:1457-65.

[236] Baker AE, Dani R, Smith ER, Tyberg JV, Belenkie I. Quantitative assessment of independent contributions of pericardium and septum to direct ventricular interaction. *Am J Physiol*. 1998;275:H476-83.

[237] Calvin JE. Optimal right ventricular filling pressures and the role of pericardial constraint in right ventricular infarction in dogs. *Circulation*. 1991;84:852-61.

[238] Glantz SA, Misbach GA, Moores WY, Mathey DG, Lekven J, Stowe DF, Parmley WW, Tyberg JV. The pericardium substantially affects the left ventricular diastolic pressure-volume relationship in the dog. *Circ Res*. 1978;42:433-41.

[239] Hinchcliff M, Desai CS, Varga J, Shah SJ. Prevalence, prognosis, and factors associated with left ventricular diastolic dysfunction in systemic sclerosis. *Clin Exp Rheumatol*. 2012;30:S30-7.

[240] Bradlow WM, Assomull R, Kilner PJ, Gibbs JS, Sheppard MN, Mohiaddin RH. Understanding late gadolinium enhancement in pulmonary hypertension. *Circ Cardiovasc Imaging*. 2010;3:501-3.

[241] Ntusi NA, Piechnik SK, Francis JM, Ferreira VM, Rai AB, Matthews PM, Robson MD, Moon J, Wordsworth PB, Neubauer S, Karamitsos TD. Subclinical myocardial inflammation and diffuse fibrosis are common in systemic sclerosis--a clinical study using myocardial T1-mapping and extracellular volume quantification. *J Cardiovasc Magn Reson*. 2014;16:21.

[242] Sachdev A, Villarraga HR, Frantz RP, McGoon MD, Hsiao JF, Maalouf JF, Ammash NM, McCully RB, Miller FA, Pellikka PA, Oh JK, Kane GC. Right ventricular strain for prediction of survival in patients with pulmonary arterial hypertension. *Chest*. 2011;139:1299-309.

[243] Di Cesare E, Battisti S, Di Sibio A, Cipriani P, Giacomelli R, Liakouli V, Ruscitti P, Masciocchi C. Early assessment of sub-clinical cardiac

involvement in systemic sclerosis (SSc) using delayed enhancement cardiac magnetic resonance (CE-MRI). *Eur J Radiol.* 2013;82:e268-73.

[244] Coon PD, Pollard H, Furlong K, Lang RM, Mor-Avi V. Quantification of left ventricular size and function using contrast-enhanced real-time 3D imaging with power modulation: comparison with cardiac MRI. *Ultrasound Med Biol.* 2012;38:1853-8.

[245] Jenkins C, Moir S, Chan J, Rakhit D, Haluska B, Marwick TH. Left ventricular volume measurement with echocardiography: a comparison of left ventricular opacification, three-dimensional echocardiography, or both with magnetic resonance imaging. *Eur Heart J.* 2009;30:98-106.

[246] Nucifora G, Marsan NA, Holman ER, Siebelink HM, van Werkhoven JM, Scholte AJ, van der Wall EE, Schalij MJ, Bax JJ. Real-time 3-dimensional echocardiography early after acute myocardial infarction: incremental value of echo-contrast for assessment of left ventricular function. *Am Heart J.* 2009;157:882 e1-8.

[247] Tan HC, Fung KC, Kritharides L. Agitated colloid is superior to saline and equivalent to levovist in enhancing tricuspid regurgitation Doppler envelope and in the opacification of right heart chambers: a quantitative, qualitative, and cost-effectiveness study. *J Am Soc Echocardiogr.* 2002;15:309-15.

[248] van den Bosch AE, Meijboom FJ, McGhie JS, Roos-Hesselink JW, Ten Cate FJ, Roelandt JR. Enhanced visualisation of the right ventricle by contrast echocardiography in congenital heart disease. *Eur J Echocardiogr.* 2004;5:104-10.

[249] Ota T, Fleishman CE, Strub M, Stetten G, Ohazama CJ, von Ramm OT, Kisslo J. Real-time, three-dimensional echocardiography: feasibility of dynamic right ventricular volume measurement with saline contrast. *Am Heart J.* 1999;137:958-66.

[250] van der Zwaan HB, Gommans F, Geleijnse ML, McGhie JS, Meijboom FJ, Van Dijk AP, Roos-Hesselink JW. P5504: Right ventricular visualization and quantification using contrast in real-time three-dimensional echocardiography. *Eur Heart J.* 2011;32 Suppl 1:1020-21.

- [251] Medvedofsky D, Addetia K, Patel AR, Sedlmeier A, Baumann R, Mor-Avi V, Lang RM. Novel Approach to Three-Dimensional Echocardiographic Quantification of Right Ventricular Volumes and Function from Focused Views. *J Am Soc Echocardiogr*. 2015.
- [252] Addetia K, Maffessanti F, Yamat M, Weinert L, Narang A, Freed BH, Mor-Avi V, Lang RM. Three-dimensional echocardiography-based analysis of right ventricular shape in pulmonary arterial hypertension. *Eur Heart J Cardiovasc Imaging*. 2015.
- [253] Schwaiger JP, Knight DS, Gallimore A, Schreiber BE, Handler C, Coghlan JG. P188: Knowledge-based 3D echocardiography reconstruction of the right ventricle documents improvement of right ventricular volumes in response to intervention. *Eur Heart J Cardiovasc Imaging*. 2014;15 Suppl 2:ii27.
- [254] Butrous G, Ghofrani HA, Grimminger F. Pulmonary vascular disease in the developing world. *Circulation*. 2008;118:1758-66.
- [255] Simpson R, Keegan J, Gatehouse P, Hansen M, Firmin D. Spiral tissue phase velocity mapping in a breath-hold with non-cartesian SENSE. *Magn Reson Med*. 2014;72:659-68.
- [256] Kvitting JP, Ebbes T, Engvall J, Sutherland GR, Wranne B, Wigstrom L. Three-directional myocardial motion assessed using 3D phase contrast MRI. *J Cardiovasc Magn Reson*. 2004;6:627-36.
- [257] Selskog P, Heiberg E, Ebbes T, Wigstrom L, Karlsson M. Kinematics of the heart: strain-rate imaging from time-resolved three-dimensional phase contrast MRI. *IEEE Trans Med Imaging*. 2002;21:1105-9.

APPENDIX 1

D. Knight, A. Grasso, M. Quail, V. Muthurangu, A. Taylor, C. Toumpanakis, M. Caplin, J. Coghlan and J. Davar

Accuracy and reproducibility of right ventricular quantification in patients with pressure and volume overload using single-beat three-dimensional echocardiography.

Journal of the American Society of Echocardiography, 2015, **28**(3), 363-74.

Accuracy and Reproducibility of Right Ventricular Quantification in Patients with Pressure and Volume Overload Using Single-Beat Three-Dimensional Echocardiography

Daniel S. Knight, BSc (Hons), MBBS, MRCP, Agata E. Grasso, MD,
Michael A. Quail, MB ChB (Hons), MRCPCH, Vivek Muthurangu, MD, MRCPCH,
Andrew M. Taylor, MD, FRCP, FRCP, Christos Toumpanakis, MD, PhD, Martyn E. Caplin, BSc, MD, FRCP,
J. Gerry Coghlan, MD, FRCP, and Joseph Davar, FRCP, MD, PhD, *London, United Kingdom*

Background: The right ventricle is a complex structure that is challenging to quantify by two-dimensional (2D) echocardiography. Unlike disk summation three-dimensional (3D) echocardiography (3DE), single-beat 3DE can acquire large volumes at high volume rates in one cardiac cycle, avoiding stitching artifacts or long breath-holds. The aim of this study was to assess the accuracy and test-retest reproducibility of single-beat 3DE for quantifying right ventricular (RV) volumes in adult populations of acquired RV pressure or volume overload, namely, pulmonary hypertension (PH) and carcinoid heart disease, respectively. Three-dimensional and 2D echocardiographic indices were also compared for identifying RV dysfunction in PH.

Methods: A prospective cross-sectional study was performed in 100 individuals who underwent 2D echocardiography, 3DE, and cardiac magnetic resonance imaging: 49 patients with PH, 20 with carcinoid heart disease, 11 with metastatic carcinoid tumors without cardiac involvement, and 20 healthy volunteers. Two operators performed test-retest acquisition and postprocessing for inter- and intraobserver reproducibility in 20 subjects.

Results: RV single-beat 3DE was attainable in 96% of cases, with mean volume rates of 32 to 45 volumes/sec. Bland-Altman analysis of all subjects (presented as mean bias \pm 95% limits of agreement) revealed good agreement for end-diastolic volume (-2.3 ± 27.4 mL) and end-systolic volume (5.2 ± 19.0 mL) measured by 3DE and cardiac magnetic resonance imaging, with a tendency to underestimate stroke volume (-7.5 ± 23.6 mL) and ejection fraction ($-4.6 \pm 13.8\%$) by 3DE. Subgroup analysis demonstrated a greater bias for volumetric underestimation, particularly in healthy volunteers (end-diastolic volume, -11.9 ± 18.0 mL; stroke volume, -11.2 ± 20.2 mL). Receiver operating characteristic curve analysis showed that 3DE-derived ejection fraction was significantly superior to 2D echocardiographic parameters for identifying RV dysfunction in PH (sensitivity, 94%; specificity, 88%; area under the curve, 0.95; $P = .031$). There was significant interobserver test-retest bias for RV volume underestimation (end-diastolic volume, -12.5 ± 28.1 mL; stroke volume, -10.6 ± 23.2 mL).

Conclusions: Single-beat 3DE is feasible and clinically applicable for volumetric quantification in acquired RV pressure or volume overload. It has improved limits of agreement compared with previous disk summation 3D echocardiographic studies and has incremental value over standard 2D echocardiographic measures for identifying RV dysfunction. Despite the ability to obtain and postprocess a full-volume 3D echocardiographic RV data set, the quality of the raw data did influence the accuracy of the data obtained. The technique performs better with dilated rather than nondilated RV cavities, with a learning curve that might affect the test-retest reproducibility for serial RV studies. (*J Am Soc Echocardiogr* 2015;28:363-74.)

Keywords: Three-dimensional echocardiography, Magnetic resonance imaging, Right ventricular function, Pulmonary hypertension, Carcinoid heart disease

From University College London Medical School, Royal Free Campus, London, United Kingdom (D.S.K.); the Department of Cardiology, Royal Free London NHS Foundation Trust, London, United Kingdom (D.S.K., A.E.G., J.G.C., J.D.); the UCL Centre for Cardiovascular Imaging, University College London, London, United Kingdom (D.S.K., M.A.Q., V.M., A.M.T.); and the Neuroendocrine Tumour Unit, Royal Free London NHS Foundation Trust, London, United Kingdom (C.T., M.E.C.). Drs Knight, Quail, and Muthurangu are funded by the British Heart Foundation. Dr Taylor is funded by the National Institute for Health Research. This work was carried out with support of the GOSH/ICH NIHR Biomedical Research Centre.

Reprint requests: Daniel S. Knight, BSc (Hons), MBBS, MRCP, University College London, Royal Free Campus, Division of Medicine, Rowland Hill Street, London, NW3 2PF, United Kingdom (E-mail: danielknight@doctors.org.uk).

0894-7317/\$36.00

Copyright 2015 by the American Society of Echocardiography. Published by Elsevier Inc. This is an open access article under the CC BY license (<http://creativecommons.org/licenses/by/3.0/>).

<http://dx.doi.org/10.1016/j.echo.2014.10.012>

Abbreviations

CMRI = Cardiac magnetic resonance imaging
COV = Coefficient of variation
EDV = End-diastolic volume
EF = Ejection fraction
ESV = End-systolic volume
ICC = Intraclass correlation coefficient
PH = Pulmonary hypertension
ROC = Receiver operating characteristic
RV = Right ventricular
RVOT = Right ventricular outflow tract
SV = Stroke volume
TAPSE = Tricuspid annular plane systolic excursion
3D = Three-dimensional
3DE = Three-dimensional echocardiography
2D = Two-dimensional
2DE = Two-dimensional echocardiography

Quantification of right ventricular (RV) size and function is prognostic in congenital and acquired heart disease.¹⁻⁴ The most convenient imaging modality for assessing the right ventricle is two-dimensional (2D) echocardiography (2DE). However, this is limited by the crescentic RV chamber shape and complex geometry, with inflow and outflow portions in different planes.^{5,6} Thus, cardiac magnetic resonance imaging (CMRI) has become the gold-standard imaging modality for RV quantification.⁷ Unfortunately, CMRI is expensive, time consuming, and of limited availability compared with echocardiography.

One possibility to overcome the limitations of 2DE is three-dimensional (3D) echocardiography (3DE), compared against CMRI in a range of congenital and acquired diseases for RV volumetric quantification.⁸ Three-dimensional echocardiography traditionally uses the disk summation method to reconstruct the right ventricle after sequential slice acquisition over consecutive electrocardiographically gated heartbeats.⁹

This technique, however, is limited by breath holding throughout successive cardiac cycles, stitching artifacts during acquisition, and difficulties identifying inlet and outflow regions in the basal slices during postprocessing.¹⁰

More recently, ultrasound transducer technology allows the real-time acquisition of a 90° × 90° data set in a single cardiac cycle.¹¹ We therefore compared RV volumetric quantification by single-beat full-volume 3DE against CMRI in homogenous patient populations of acquired RV pressure and volume overload, namely, pulmonary hypertension (PH) and carcinoid heart disease, respectively. We also sought to determine the potential incremental value of 3DE versus 2DE in PH and to evaluate the test-retest reproducibility of 3DE for both the acquisition and postprocessing components.

METHODS

Study Population

We performed a prospective cross-sectional study that enrolled 100 participants in sinus rhythm with no contraindications to magnetic resonance imaging, all of whom underwent comprehensive 2DE, single-beat 3DE of the right ventricle, and CMRI within 2 hours of one another. The participants were divided into four subgroups:

- A group of 49 consecutive patients with PH (diagnosed by right heart catheterization as a mean pulmonary artery pressure >25 mm Hg and a pulmonary capillary wedge pressure <15 mm Hg¹²) who presented for diagnosis and/or follow-up of PH by clinical evaluation and/or right heart catheteriza-

tion as a disease model of RV pressure overload. The etiologies of PH included idiopathic (*n* = 9), connective tissue disease associated (*n* = 32), and chronic thromboembolic disease (*n* = 8). Exclusion criteria comprised clinically significant restrictive or obstructive lung disease identified by pulmonary function tests, arrhythmia, and known independent left-sided cardiac disease unrelated to PH.

- A group of 20 consecutive patients undergoing 2DE for diagnosis and/or follow-up of carcinoid heart disease¹³ were studied as a disease model of RV volume overload.
- A control group of 20 healthy volunteers affiliated with our institution who were age and sex matched to the PH group.
- A control group of 11 age- and sex-matched patients with metastatic neuroendocrine tumor who were screened as negative for carcinoid valvular heart disease.

All control participants were eligible for study inclusion if they had no cardiac symptomatology, had no medical histories of cardiac disease including hypertension, and were not taking any cardiac medications. Normal 2D transthoracic echocardiographic findings were also required to exclude any occult structural cardiac disease before study inclusion.

The institutional research ethics committee approved the study, and informed written consent was obtained from all patients and control subjects.

2DE

All patients underwent comprehensive 2D and Doppler transthoracic echocardiography in the left lateral decubitus position using the Acuson Siemens SC2000 cardiac ultrasound system (Siemens Healthcare, Erlangen, Germany), with a 4V1c transducer (frequency bandwidth, 1.25–4.5 MHz). A standard study protocol was followed in conjunction with American Society of Echocardiography guidelines for chamber quantification^{14,15} and the British Society of Echocardiography guidelines for PH assessment¹⁶ as appropriate. RV function was assessed using M-mode tricuspid annular plane systolic excursion (TAPSE); RV fractional area change, calculated as [(end-diastolic area) – (end-systolic area)]/end-diastolic area × 100; and mean RV free wall peak systolic strain using syngo Vector Velocity Imaging (Siemens Medical Solutions USA, Inc, Mountain View, CA). A three-beat 2D echocardiographic digital clip of an apical four-chamber view optimized for RV visualization was acquired and exported to Velocity Vector Imaging, and 10 to 15 endocardial points were plotted in end-systole from the lateral to the medial tricuspid annulus.¹⁷ The adequacy of speckle-tracking was visually checked and manually adjusted as required.

3DE

Image Acquisition. Single-beat full-volume 3D echocardiographic RV data sets were acquired using the 4Z1c matrix-array transducer (frequency bandwidth, 1.5–3.5 MHz; maximum depth, 30 cm; maximum field of view, 90° × 90°). Probe position started from the apical four-chamber view with the patient in the left lateral decubitus position. Both the patient and transducer positions were subsequently modified for optimal simultaneous visualization of the tricuspid valve, cardiac apex, infundibulum, and RV outflow tract (RVOT) as assessed by the real-time 2D four-chamber, basal sagittal, and coronal views, and by inclusion of the RV chamber in the pyramidal data set. In our experience, a more lateral apical window with posterior tilt of the probe tail was beneficial to visualize the infundibulum and RVOT in the coronal window. Image depth and sector width were adjusted for maximal visualization of the right ventricle at the

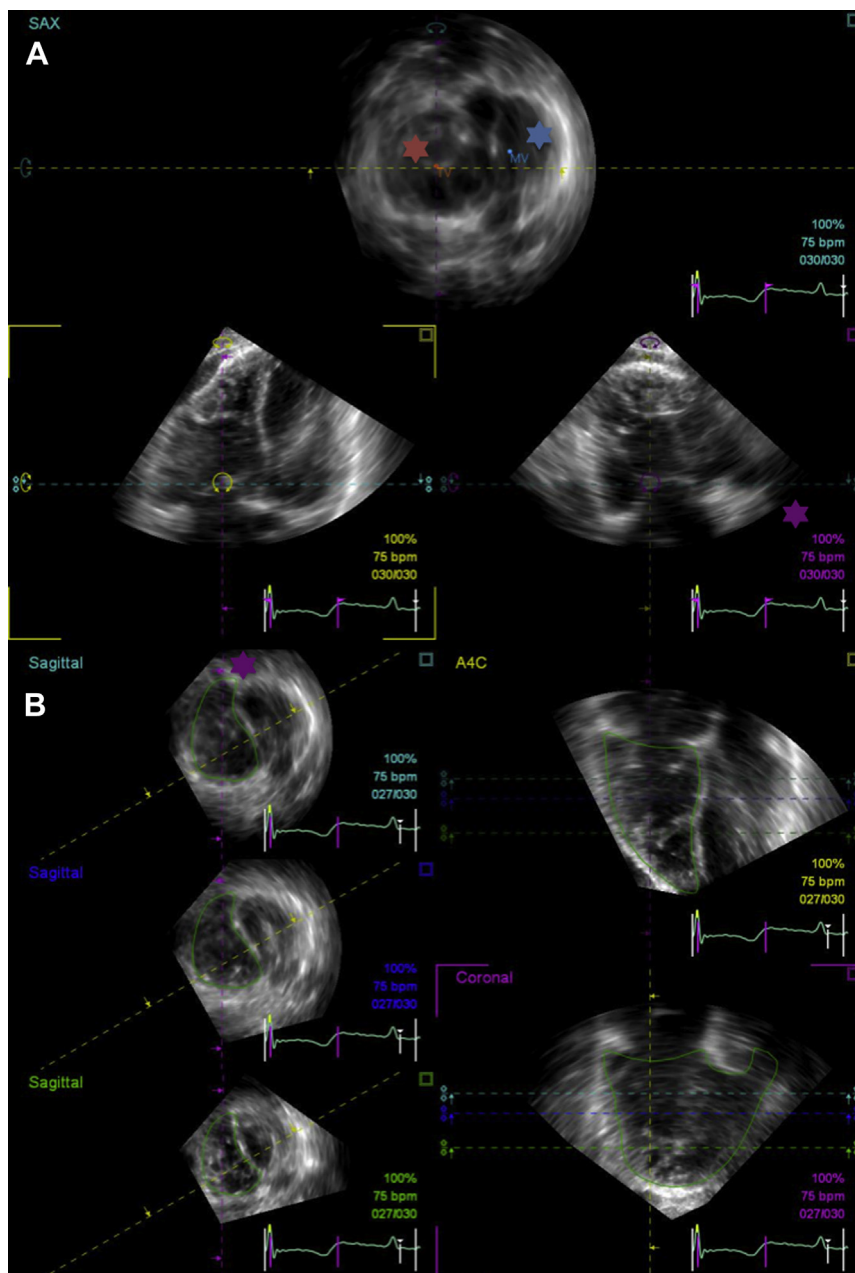


Figure 1 Example of the stepwise process of RV reconstruction by 3DE. **(A)** The cavity area is optimized in the three orthogonal views, and landmarks are identified (mitral valve indicated by the *blue asterisk*, tricuspid valve indicated by the *red asterisk*). Note the RVOT seen in the coronal view (indicated by the *purple asterisk*). **(B)** Having traced endocardial borders in three orthogonal views, the semi-automated border tracking results are displayed for inspection. Note how the purple guideline (indicated by the *purple asterisk*) bisects the tricuspid valve and RVOT in the short-axis views. This corresponds to the coronal RV reconstruction (*highlighted*), with clearly delineated RV inflow and outflow portions. A4C, Apical four-chamber.

highest volume rate. At least three 3D echocardiographic RV data sets were acquired during a breath-hold to ensure optimal image quality, which was subjectively graded on a five-point scale ranging from zero (very poor) to four (perfect).¹⁸ A score of two or less was attributed if ultrasound dropout was evident in greater than half of the RVOT border.

Postprocessing. Full-volume 3D echocardiographic RV data sets were imported into the on-cart RV Analysis application. Manual adjustment of the RV data set was initially required to ensure the

correct orientation of four-chamber, sagittal, and coronal slices; maximize the RV cavity area and identify the most apical RV view on visual assessment of the four-chamber window; and allow the identification of cardiac landmarks. This process was performed in a stepwise approach by rotation and angulation of the four-chamber window, with manipulation of this plane causing the simultaneous adjustment of the other two (sagittal and coronal) orthogonal planes (Figure 1A). Both atrioventricular valves followed by the left ventricular apex were identified as anatomic landmarks. When the apex of a dilated right ventricle overrode that of the left ventricle, the most apical cardiac

point was identified with the left ventricular apex marker. End-diastolic and end-systolic frames were assigned by visual identification of the largest and smallest RV four-chamber areas, respectively.

Endocardial RV borders were traced at end-diastole and end-systole in four-chamber, basal sagittal, and coronal views. The software algorithm obliges the operator to intersect the endocardial border tracing in sequential views with crosshair reference markers that are positioned in response to endocardial border traces from a preceding view. Therefore, correction of a previous slice tracing was undertaken when a crosshair position suggested a prior tracing error. Trabeculae were included in the blood pool volume. To assist with RVOT delineation in the basal sagittal view, the insertion point of the RV myocardium at the interventricular septum was routinely included in the endocardial tracing.

At the final stage, the algorithm presents the results of semiautomated contour tracking for the four-chamber, coronal and basal, middle and apical short-axis views. Misalignment of endocardial contours prompted identification of the region of suboptimal tracking followed by manual correction of the original tracing. Automated volumetric reconstruction was accepted only once the semiautomated endocardial border tracking was visually satisfactory and represented meaningful RV shapes in all views (Figure 1B), as optimization of this final reconstruction stage significantly affects the results generated.¹⁹ The algorithm from which the final RV volume is generated has been previously described.^{20,21}

Test-Retest Reproducibility of 3DE. Reproducibility was studied in 20 randomly selected subjects (14 with PH, one with carcinoid heart disease, and five healthy volunteers) for both the 3D echocardiographic acquisition and postprocessing stages by two independent sonographers (D.S.K. and A.E.G.), as described previously.²² The two sonographers had equal experience with 2DE but differing levels of experience with 3D echocardiographic RV full-volume acquisition (10 and 3 months, respectively). Sonographer 1 (D.S.K.) obtained a 3D echocardiographic RV data set, after which sonographer 2 (A.E.G.) independently obtained a 3D echocardiographic RV data set. Then, sonographer 1 acquired a second separate 3D echocardiographic RV data set. The sonographers, who were blinded to each other's results, performed postprocessing of their own 3D echocardiographic RV data sets. Data sets for intraobserver test-retest reproducibility were postprocessed separately at time intervals of >2 weeks.

Cardiac MRI

Image Acquisition. All cardiac magnetic resonance images were acquired using a 1.5-T magnetic resonance scanner (Avanto; Siemens Healthcare) using a 12-element phased-array coil for signal reception and the body coil for signal transmission. A vector electrocardiographic system was used for cardiac gating. Ventricular volumes and great vessel flow were measured in all patients. Volumetric RV data were obtained using either retrospectively gated balanced steady-state free precession ($n = 19$) cine imaging of contiguous short-axis slices²³ or real-time radial k - t sensitivity encoding imaging ($n = 81$) of contiguous transaxial slices²⁴ depending on the pathology under investigation and the patient's ability to hold his or her breath. Real-time radial k - t sensitivity imaging allows the collection of high spatiotemporal resolution real-time images during free breathing and is part of the standard clinical CMRI work flow at our institution in the pediatric PH population.²⁵ Transaxial RV slices were preferred for the PH cohort and their respective control population because of

the relative preservation of longitudinal versus radial RV function that is manifest in this condition.²⁶ Blood flow data were acquired in the ascending aorta, in the right and left branch pulmonary arteries, and at the level of the atrioventricular valves using a velocity-encoded prospectively triggered spiral phase-contrast magnetic resonance flow sequence.²⁷ This provided an internal check for the RV volumetric data.

Postprocessing. All image postprocessing was performed using "in-house" plug-ins for the open-source OsiriX Digital Imaging and Communications in Medicine software.^{24,28,29} Endocardial RV borders were traced manually at end-diastole and end-systole, the time points of which were identified by the largest and smallest RV cavity areas, respectively. The inclusion of RV trabeculae was the same as that performed by 3D echocardiographic postprocessing. Ventricular stroke volume (SV) was the difference between end-diastolic volume (EDV) and end-systolic volume (ESV), and ejection fraction (EF) was calculated as $(SV/EDV) \times 100$. Phase-contrast magnetic resonance flow data were segmented using a semiautomatic vessel edge detection algorithm with manual operator correction.²⁸ The CMRI data sets for the patients who underwent 3D echocardiographic test-retest reproducibility scans were also tested for interobserver (D.S.K. and M.A.Q.) and intraobserver postprocessing reproducibility.

Statistical Analysis

Statistical analysis was performed using SPSS version 21.0 (IBM Corporation, Armonk, NY) and Prism 6.0b for Mac (GraphPad Software, Inc, La Jolla, CA). Normally distributed continuous data were expressed as mean \pm SD. Systematic differences between measurements were evaluated with Student paired t tests (two tailed), with Pearson correlation coefficients used to assess the relationship between 3DE- and CMRI-derived RV volumes and EF. Differences between the four participant subgroups were analyzed using one-way analysis of variance, with the Tukey post hoc tests identifying which specific means differed. P values $< .05$ were considered statistically significant. Image scoring data were nonparametrically distributed, represented by medians with 25th and 75th percentiles. Rank sum tests were used for comparisons of image scoring data, with the Mann-Whitney U test and the Kruskal-Wallis test used for comparisons of two and three independent groups, respectively.

Intermodality, interobserver, and intraobserver agreement was studied using the Bland-Altman method,³⁰ whereby the mean difference was presented as the bias and 95% limits of agreement around the bias expressed as the mean difference \pm 1.96 SDs. Differences between test-retest measurements were analyzed by one-way repeated measures analysis of variance, with the Bonferroni post hoc test identifying which specific means differed. The Greenhouse-Geisser correction was used if the assumption of sphericity had been violated. Test-retest variability was expressed using intraclass correlation coefficients (ICC), relative differences, and coefficients of variation (COVs). The ICC was quantified by the two-way random-effects model with absolute agreement. An ICC > 0.85 was considered excellent. Relative differences were calculated by taking the absolute difference between two observations divided by the mean of the repeated observations and expressed as a percentage. COVs were calculated as the standard deviation of the difference between two acquisitions divided by their mean value and expressed as a percentage.³¹ A COV $\leq 10\%$ was considered excellent.

Table 1 Clinical characteristics of study populations

Variable	PH (n = 46)	Carcinoid heart disease (n = 19)	Healthy volunteers (n = 20)	Carcinoid (no valvulopathy) (n = 11)	P*
Age (y)	56 ± 13	63 ± 8	50 ± 12	59 ± 10	
Women	35 (76%)	7 (37%)	15 (75%)	7 (64%)	
Height (cm)	164 ± 9	171 ± 10	169 ± 8	168 ± 10	.035
Weight (kg)	69 ± 17	72 ± 18	72 ± 12	77 ± 20	.54
Body surface area (m ²)	1.8 ± 0.2	1.8 ± 0.3	1.8 ± 0.2	1.9 ± 0.3	.37
Heart rate (beats/min)	74 ± 14	67 ± 13	68 ± 9	69 ± 12	.19
Mean PASP on RHC (mm Hg)	44 ± 16				
Pulmonary vasodilators					
Endothelin antagonist	21 (46%)				
PDE-5 antagonist	31 (67%)				
Prostanoid infusion	2 (4%)				
Oral prostanoid	1 (2%)				
Prostaglandin receptor agonist	1 (2%)				
Carcinoid heart disease: affected valves	TV = 19 (100%), PV = 13 (68%), MV = 3 (16%), AV = 3 (16%)				
EDV (mL/m ²)	87 ± 26	100 ± 35	64 ± 14	52 ± 8	<.0001
ESV (mL/m ²)	52 ± 25	33 ± 15	22 ± 7	16 ± 5	<.0001
EF (%)	43 ± 14	68 ± 7	65 ± 7	71 ± 7	<.0001
3D echocardiographic temporal resolution (volumes/sec)	34 ± 5	32 ± 7	40 ± 5	45 ± 6	<.0001

AV, Aortic valve; ESV, end-systolic volume; MV, mitral valve; PASP, pulmonary artery systolic pressure; PDE-5, phosphodiesterase-5; PV, pulmonary valve; RHC, right heart catheterization; TV, tricuspid valve.

Data are expressed as mean ± SD or as number (percentage).

*One-way analysis between groups.

Receiver operating characteristic (ROC) curves were derived for 2D and 3D echocardiographic parameters to identify CMRI-derived RV EFs of <50% in patients with PH and healthy volunteers.³² Patients with carcinoid disease were excluded from this analysis to avoid the confounding effects of severe valvular regurgitation on ventricular function. The area under the ROC curve for an echocardiographic parameter is presented together with the optimal cutoff threshold for detecting CMRI-derived RV EF < 50%, defined as the value of the parameter that corresponded to the highest sum of sensitivity and specificity. The Delong method was used to compare the areas under the curve between ROC curves³³ (Analyse-it Software, Ltd, Leeds, United Kingdom).

RESULTS

Population Characteristics and 3DE Technical Data

Of 100 individuals who were recruited, four had unobtainable RV echocardiographic windows. The clinical characteristics and 3D echocardiographic technical data of the final cohort of 96 subjects are presented in Table 1. Patients with PH had significantly larger and impaired right ventricles than controls, whereas the right ventricles of patients with carcinoid heart disease were also significantly dilated but with preserved EFs. The dilated right ventricles of the patient groups resulted in a significantly lower mean volume rate compared

with controls because of the greater 3D sector angles ($P < .001$), but the median image quality score was significantly higher among patients (3.00; interquartile range, 2.00–3.00) than controls (2.00 interquartile range, 1.00–3.00) ($P < .001$). The image quality among three successive, equally populated subgroups of patients significantly improved with increasing experience with 3DE (Figure 2; $P = .031$). There was a trend, albeit not statistically significant, for greater differences in SV between modalities with worse subjective image scores (Figure 3; $P < .13$ for percentage intermodality difference in SV for image score groups 1 and 2 combined vs groups 3 and 4 combined).

Volumetric Analysis by 3DE versus CMRI

Correlation coefficients showed good to excellent correlations between modalities for RV metrics in patient groups and moderate to good correlations for control subjects (Table 2). RV volumes and EFs by 3DE showed differences with CMRI in both patient groups, with a bias for underestimating SV and EF but with overall acceptable limits of agreement (Figure 4). By contrast, 3DE underestimated EDV for control subjects (Table 3), with a consequent negative bias for quantifying SV in this group (Figure 5).

RV Quantification by 3DE and 2DE versus CMRI

Three-dimensional echocardiographic EF was the most superior echocardiographic parameter for identifying CMRI-derived RV EF

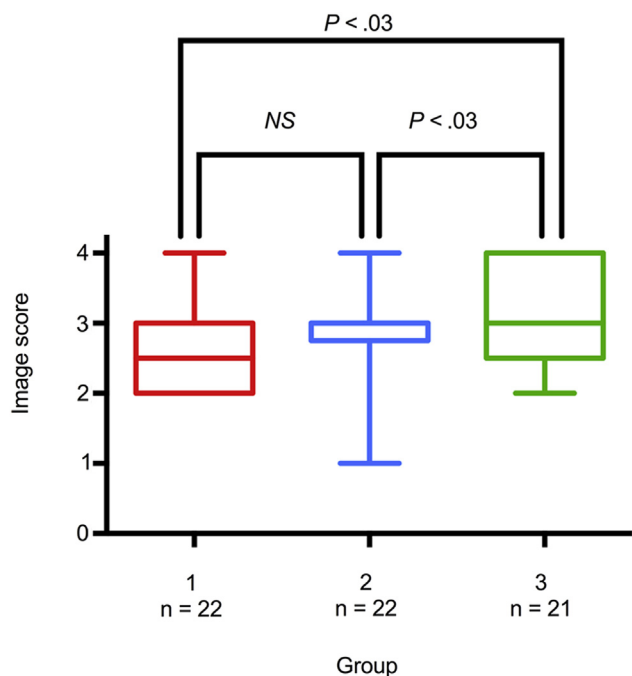


Figure 2 Box-and-whisker plots of subjective image quality scores among three successive subgroups of patients (group 1 acquired in the earliest phase of the study, group 3 in the latest phase of the study). Image quality significantly improved with increasing experience with 3DE ($P = .031$).

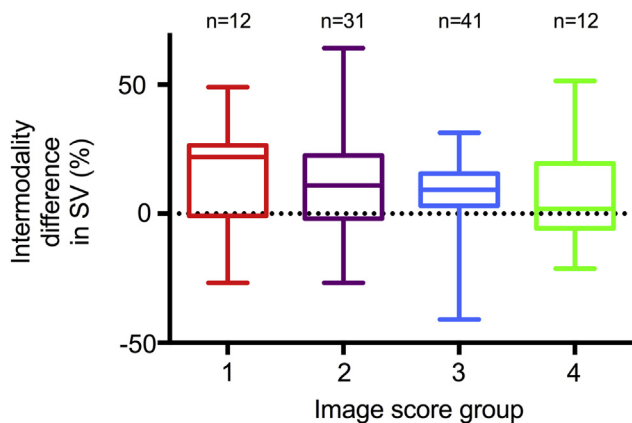


Figure 3 Box-and-whisker plots of differences in stroke volume between modalities (expressed as a percentage of the CMRI reference value) for image scoring groups 1 to 4. There was a trend, albeit not statistically significant, for the intermodality difference to increase with reductions in subjective image score. Median percentage intermodality differences in stroke volume by image score group were as follows: group 1, 22% (interquartile range [IQR], -1% to 26%); group 2, 11% (IQR, -2% to 23%); group 3, 9% (IQR, 3% to 16%); group 4, 2% (IQR, -6% to 19%).

$< 50\%$ (Figure 6; $P = .031$), with sensitivity of 94%. A fractional area change of 39% (sensitivity, 85%) was the best conventional 2D echocardiographic measure, superior to both peak systolic strain and TAPSE ($P = .0443$). TAPSE was the weakest marker to predict CMRI-derived RV EF $< 50\%$, with sensitivity of 56% at a cutoff threshold of 19 mm.

Table 2 RV volumes and EFs by single-beat full-volume 3DE versus CMRI

Group	Measurement	3DE	CMRI	P*
PH	EDV (mL)	158 ± 53	154 ± 52	.043
	ESV (mL)	100 ± 44	92 ± 47	<.0001
	SV (mL)	58 ± 18	63 ± 17	.011
	EF (%)	39 ± 11	43 ± 14	.00029
Carcinoid heart disease	EDV (mL)	182 ± 69	185 ± 71	.21
	ESV (mL)	67 ± 28	62 ± 3	.01
	SV (mL)	115 ± 42	124 ± 45	.014
	EF (%)	64 ± 5	68 ± 7	.001
Healthy volunteers	EDV (mL)	105 ± 26	117 ± 27	<.0001
	ESV (mL)	41 ± 12	41 ± 14	.80
	SV (mL)	65 ± 16	76 ± 18	<.0001
	EF (%)	61 ± 5	65 ± 7	.014
Carcinoid (no valvulopathy)	EDV (mL)	88 ± 21	98 ± 27	.05
	ESV (mL)	32 ± 13	30 ± 14	.24
	SV (mL)	56 ± 10	68 ± 14	.009
	EF (%)	64 ± 7	71 ± 7	.004

ESV, End-systolic volume.
Data are expressed as mean ± SD.
*Paired Student t tests.

Test-Retest Intraobserver and Interobserver Reproducibility

Limits of agreement were acceptable for intra- and interobserver 3D echocardiographic studies, with good to excellent ICCs (Table 4). However, there was a significant interobserver bias for underestimating RV EDV ($P = .001$; Table 5) that resulted in underestimation of SV ($P = .002$) and EF ($P = .033$), with accompanying large interobserver COVs and relative differences. Moreover, despite no significant differences between intraobserver EDV and ESV, the differences translated into statistically significant test-retest differences for SV ($P = .032$) and EF ($P = .005$). The interobserver and intraobserver reproducibility for RV volumes and EF by CMRI showed no significant bias and superior limits of agreement compared with 3DE.

DISCUSSION

This study demonstrates the feasibility of single-beat full-volume 3DE for RV quantification in, to our knowledge, the largest homogenous acquired RV pressure- and volume-overloaded patient populations. Single-beat 3DE is an agreeable technique compared with CMRI, albeit with significant differences especially in subjects with nondilated right ventricles. Furthermore, 3D echocardiographic parameters are of incremental benefit for RV functional quantification compared with traditional 2DE measures.

Accurate quantitation of RV size and function is important in many congenital and acquired cardiac diseases and is of particular relevance in our study populations. RV size and function are of greater prognostic significance in PH than the afterload to which the right heart is exposed,^{34,35} with RV EF being the key determinant of outcome regardless of changes in pulmonary vascular resistance afforded by pulmonary vasodilator therapy.³⁶ Similarly, right heart dilatation is independently associated with poor outcomes in patients with advanced carcinoid heart disease.³⁷ However, the right ventricle responds differently to pressure- and volume-overload conditions, with dilatation occurring in both but with relative preservation of

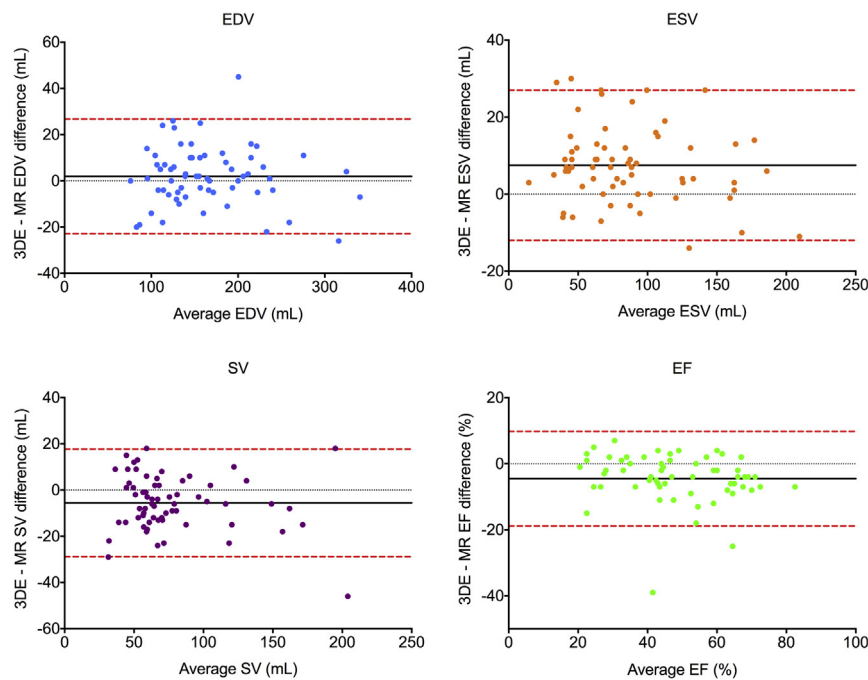


Figure 4 Bland-Altman analysis of bias (*black solid line*) and 95% limits of agreement (*red dashed line*) for 3DE versus CMRI quantification of RV EDV, ESV, SV, and EF in patients with PH and carcinoid heart disease.

Table 3 Bias, limits of agreement, and correlation between single-beat full-volume 3DE and CMRI for RV volumes and EFs					
Group	Measurements	Bias ± SD	Limits of agreement	r	P*
All subjects	EDV (mL)	−2.3 ± 13.7	−29.1 to 24.5	0.97	<.0001
	ESV (mL)	5.2 ± 9.5	−13.4 to 23.9	0.98	<.0001
	SV (mL)	−7.5 ± 11.8	−30.6 to 15.7	0.94	<.0001
	EF (%)	−4.6 ± 6.9	−18.2 to 9.0	0.91	<.0001
PH	EDV (mL)	4.0 ± 13.1	−21.6 to 29.7	0.97	<.0001
	ESV (mL)	8.4 ± 10.6	−12.3 to 29.1	0.98	<.0001
	SV (mL)	−4.3 ± 10.8	−25.5 to 17.0	0.82	<.0001
	EF (%)	−4.8 ± 8.3	−21.1 to 11.5	0.81	<.0001
Carcinoid heart disease	EDV (mL)	−3.1 ± 10.1	−22.9 to 16.8	0.99	<.0001
	ESV (mL)	5.4 ± 8.2	−10.6 to 21.4	0.96	<.0001
	SV (mL)	−8.6 ± 13.9	−35.9 to 18.6	0.95	<.0001
	EF (%)	−3.8 ± 4.1	−11.9 to 4.2	0.82	<.0001
Healthy volunteers	EDV (mL)	−11.9 ± 9.0	−29.5 to 5.8	0.94	<.0001
	ESV (mL)	−0.4 ± 6.7	−13.6 to 12.9	0.88	<.0001
	SV (mL)	−11.2 ± 10.1	−31.0 to 8.7	0.84	<.0001
	EF (%)	−3.9 ± 6.5	−16.6 to 8.8	0.51	.021
Carcinoid (no valvulopathy)	EDV (mL)	−10.1 ± 15.0	−39.6 to 19.4	0.84	.001
	ESV (mL)	2.1 ± 5.5	−8.7 to 12.9	0.92	<.0001
	SV (mL)	−12.2 ± 12.3	−36.3 to 11.9	0.53	.096
	EF (%)	−6.2 ± 5.6	−17.1 to 4.7	0.69	.019

ESV, End-systolic volume.
*Pearson correlation coefficient.

function in elevated preload rather than afterload. What remains unclear is to what extent this preserved EF represents normality of function in the presence of severe tricuspid regurgitation, a valvular lesion common to all patients in our carcinoid heart disease cohort.

The incremental benefit of 3DE over 2DE has previously been shown in congenital heart disease,³⁸ and single-beat 3DE showed similar added value over 2DE metrics in acquired RV pressure over-

load. Although this is due in part to equivalent parameters being assessed by 3DE and CMRI, it is, importantly, also a reflection of the limitations of conventional 2D echocardiographic measures. TAPSE had the poorest sensitivity for detecting low RV EF in PH, with a cutoff of 19 mm having the highest combined sensitivity and specificity. This is higher than the recommended threshold of 16 mm for detecting RV dysfunction,¹⁴ suggesting that TAPSE would have performed worse

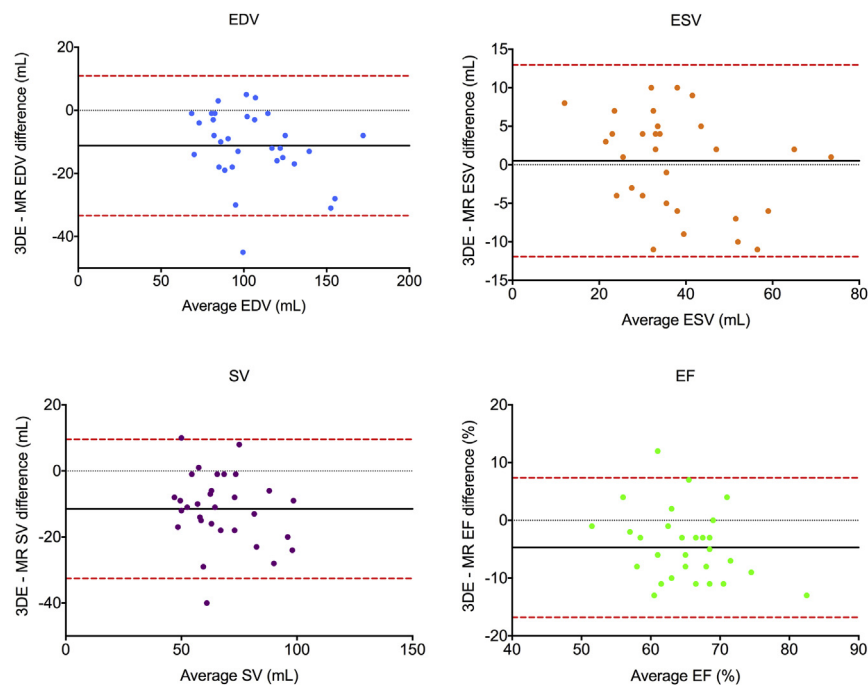


Figure 5 Bland-Altman analysis of bias (black solid line) and 95% limits of agreement (red dashed line) for 3DE versus CMRI quantification of RV EDV, ESV, SV, and EF for subjects in the control populations.

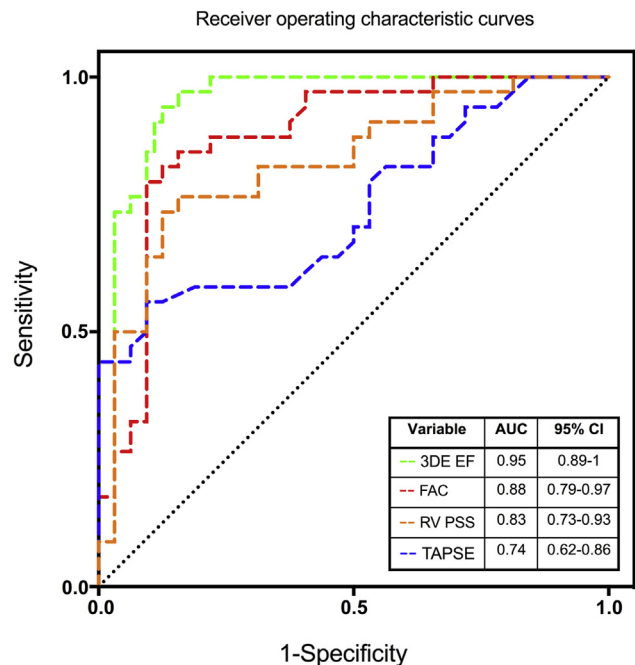


Figure 6 ROC curves for 3DE, fractional area change (FAC), RV free wall peak systolic strain by speckle-tracking echocardiography, and TAPSE to identify RV dysfunction (defined as RV EF < 50% on CMRI).

by current guidelines in our cohort. The rocking motion of the right ventricle in pressure overload can give rise to apparently normal TAPSE values,³⁹ and TAPSE also does not account for the radial component of RV function that contributes significantly to RV EF.²⁶ By contrast, fractional area change was the most superior 2D echocar-

diographic marker for identifying RV dysfunction in PH, most likely a reflection of being the only 2D echocardiographic marker that accounts for radial function. These findings are consistent with previous studies comparing 2D echocardiographic markers of RV function in PH⁴⁰ and suggest that 3DE may have an important additive role in assessing RV function.

RV quantification by echocardiography is advantageous through being more readily available and less expensive than CMRI. Since the first use of 3DE for RV volumetric quantification,¹⁸ improvements in matrix-array transducer technology permit the simultaneous visualization of orthogonal 2D RV planes at the time of acquisition. The technique used in this study allows a pyramidal data set of up to 90° × 90° to be acquired at higher temporal resolutions than previously reported for 3DE.⁴¹ Acquisition of a full volume in a single heartbeat avoids stitching artifacts associated with acquiring slices over serial heartbeats and also confers the advantage of shorter breath-hold durations. These reasons might explain the narrower limits of agreement for RV volumetric parameters between single-beat 3DE and CMRI compared with previous data from adult PH groups using the disk summation method.^{41,42}

The disadvantages of echocardiography include constraints that afford inadequate transthoracic windows, including body habitus, hyperinflated lungs, and chest deformities. Acquisition and postprocessing was feasible in 96% of subjects, consistent with previously reported studies using the technique.^{43,44} However, patients with significant lung disease were excluded to ensure that PH was the predominant disease process in the RV pressure-overload group, and this may in turn have biased the echogenicity of the study population. Although all postprocessed 3D echocardiographic data sets had a reconstructed RV polygon that tracked throughout the cardiac cycle, 45% of studies were judged by subjective image scoring to have some endocardial dropout of the outflow portion of the right ventricle. This was reflected by a trend toward increasing differences

Table 4 Interobserver and intraobserver reproducibility for RV volumes and EF by 3DE and CMRI

Variable	EDV (mL)	ESV (mL)	SV (mL)	EF (%)
3DE intraobserver				
ICC	0.992	0.974	0.96	0.906
COV (%)	3.0	6.6	8.0	6.9
RD (%)	4.3	9.4	11.3	9.8
Bias	−0.2	4.6	−4.7	−3.6
LOA	−16.2 to 15.8	−12.8 to 22.0	−19.0 to 9.7	−12.2 to 5.0
SD	8.2	8.9	7.3	4.4
CMRI intraobserver				
Bias	−2.6	−2.4	−0.1	0.7
LOA	−15.4 to 10.2	−11.3 to 6.5	−11.8 to 11.6	−5.9 to 7.2
SD	6.5	4.6	6.0	3.4
3DE interobserver				
ICC	0.955	0.965	0.867	0.827
COV (%)	7.7	8.0	16.6	9.4
RD (%)	10.3	11.4	23.5	13.3
Bias	−12.5	−2.0	−10.6	−4.0
LOA	−40.0 to 15.1	−24.0 to 20.1	−33.2 to 12.1	−16.2 to 8.3
SD	14.1	11.3	11.6	6.3
CMRI interobserver				
Bias	−1.9	−2.80	1.1	0.9
LOA	−18.2 to 14.4	−13.1 to 7.5	−9.3 to 11.5	−4.1 to 5.8
SD	8.3	5.2	5.3	2.5

ESV, End-systolic volume; LOA, limits of agreement; RD, relative difference.

Table 5 Interobserver and intraobserver test-retest RV metrics by 3DE

Variable	Sonographer 1			Sonographer 2		
	First (S1.1)	Second (S1.2)	<i>P</i> * S1.1 vs S1.2	Acquisition	<i>P</i> * vs S1.1	<i>P</i> * vs S1.2
EDV (mL)	145 ± 63	145 ± 62	NS	133 ± 59	.003	.003
ESV (mL)	78 ± 44	83 ± 42	NS	76 ± 39	NS	NS
SV (mL)	67 ± 31	63 ± 29	.032	57 ± 27	.002	.046
EF (%)	48 ± 13	44 ± 12	.005	44 ± 11	.033	NS

ESV, End-systolic volume.

Data are expressed as mean ± SD.

*One-way repeated-measures analysis of variance with Bonferroni post hoc test.

in SVs between modalities with decreasing image quality, with a median difference of $\geq 11\%$ when the RVOT was incompletely visualized. This is a consistent problem with 3DE that has been well documented previously and is due to the anterior position of the right ventricle in the thorax. Postprocessing software extrapolates the endocardial borders during semiautomated border tracking,⁴⁵ and hence although it is possible to analyze data sets with incomplete RVOT visualization, the accuracy of reconstructions will most likely deteriorate with progressive dropout in the outflow tract.

When comparing studies of RV quantification by 3DE, the homogeneity of the study population must be taken into account. Our populations of acquired RV disease were favorable for the 3D echocardiographic postprocessing software algorithm, because it is

set up for an adult-shaped right ventricle rather than a congenital heart.⁴⁶ This may be a reason why our limits of agreement were narrower than reported in congenital heart disease.⁴⁵ No substantial bias was observed in either the PH or carcinoid heart disease group, but subgroup analysis showed that EDVs, and consequently SVs, were underestimated in controls. This is despite the higher temporal resolution of images in this group and is likely a result of low spatial resolution with single-beat 3DE. Lower spatial resolution confers less ability to resolve myocardium and trabeculae, thus directing the operator to trace the endocardium further inside the RV cavity and hence underestimate volumes. This is supported by previous data showing greater variability and negative bias for 3DE to quantify RV volumes in nondilated right hearts.⁴⁷ Conversely, RV endocardial delineation is

known to be easier in the setting of RV hypertrophy or dilatation for both magnetic resonance imaging and 3DE^{41,47} and is reflected by the higher image quality scores observed with our disease cohorts.

The progressive increase in 3D echocardiographic image quality over the study duration reflects a significant learning curve with the technique, as also described in previous studies.³⁸ This is important clinically, as follow-up studies will vary depending on operator experience for both acquisition and postprocessing. Few studies so far have addressed 3D echocardiographic test-retest reproducibility for both the acquisition and postprocessing stages.^{22,41} Our interobserver test-retest study demonstrated a second operator bias for EDV underestimation, conferring lower SV and EF measurements. This was a systematic error likely reflecting relative operator inexperience with the technique. The susceptibility of 3DE to underestimate RV volumes has been well documented,⁸ and our data suggest that operator experience is related to this underestimation.

Furthermore, nonsignificant differences in intraobserver EDV and ESV nevertheless resulted in significant differences in SV and EF when the errors in the raw volumes were combined. Given that small changes in endocardial border delineation are known to confer significant changes in 3DE-derived volumetric parameters in the left ventricle,⁴⁸ this is also likely to be a problem with 3DE reconstruction of the right ventricle too. This is clinically important because a change of as little as 10 mL in SV by CMRI is clinically significant in PH,⁴⁹ but a change of this magnitude may be masked by 3DE's reproducibility error and/or the degradation of accuracy found with poorer quality 3D echocardiographic data sets. For example, the interobserver measurement of RV SV by 3DE showed a significant bias with a standard deviation more than double that of CMRI. Our CMRI reproducibility data show narrow limits of agreement, with no major bias between observers, consistent with previous reproducibility studies of RV quantification by transaxial slices^{50,51} and sensitive enough to detect small changes in RV indices on serial studies.

Limitations

This study was a single-center study based on acquisitions made by one sonographer with experience using single-beat 3DE for RV volumetric quantification. As demonstrated by our test-retest reproducibility, results cannot be applied across operators with variable experience in 3D echocardiographic RV analysis. Patients with arrhythmias were excluded because of the extra variability introduced by irregular cardiac cycles when comparing modalities. Single-beat acquisition is advantageous over traditional disk summation techniques that are limited by stitching artifacts due to irregular R-R intervals, and this patient group requires further investigation with the technique.

We found a bias to underestimate cavity size, particularly in control subjects, but the study was not designed to compare the accuracy of the technique in patients with large versus small cavity sizes. This question should be addressed in a separate prospectively designed analysis of large versus small right ventricles. The sensitivity and specificity values for 3DE and 2DE to identify CMRI-derived RVEF < 50% were calculated by applying the ROC cutoff values to the same patients used to derive them as described previously,³⁸ hence representing a "best case" scenario. A more appropriate method would be to identify cut-off values using ROC analysis in a derivation group, then prospectively evaluate the cutoff values in a separate test group in whom outcomes could be verified independently. Thus the

diagnostic performance of the cutoff values found in this study needs to be confirmed independently.

Finally, the study was not designed to provide CMRI test-retest reproducibility similar to the 3D echocardiographic study design for acquisition and postprocessing. However, CMRI does not have the same acquisition window restrictions inherent to transthoracic echocardiography, as contiguous transaxial RV slices of fixed thickness are acquired from the base of the right heart to the main pulmonary artery with the patient in the supine position. However, this difference in technique methodology is a potential source of discrepancy, with the reference standard of CMRI building volumes from multiple slices compared with the full-volume data sets of 3DE.¹⁰

CONCLUSIONS

Single-beat full-volume 3DE is a feasible technique for quantifying RV size and function in acquired right heart pressure and volume overload. The limits of agreement of 3DE are acceptable compared with CMRI but may not be sensitive enough to detect small yet clinically significant responses to treatment demonstrated by this modality.⁴⁹ The test-retest reproducibility of 3DE suggests a significant learning curve that needs to be considered, and thus results cannot necessarily be extrapolated to less experienced operators. Nevertheless, 3DE showed incremental benefit over conventional 2D echocardiographic measures, suggesting an important role in assessing acquired RV pathology. Future work should focus on improving spatial resolution to optimize RV endocardial delineation, in particular for adequate visualization of the RVOT in nondilated right ventricles.

REFERENCES

1. de Groote P, Millaire A, Foucher-Hossein C, Nague O, Marchandise X, Ducloux G, et al. Right ventricular ejection fraction is an independent predictor of survival in patients with moderate heart failure. *J Am Coll Cardiol* 1998;32:948-54.
2. Ghio S, Gavazzi A, Campana C, Inerra C, Klersy C, Sebastiani R, et al. Independent and additive prognostic value of right ventricular systolic function and pulmonary artery pressure in patients with chronic heart failure. *J Am Coll Cardiol* 2001;37:183-8.
3. Knauth AL, Gauvreau K, Powell AJ, Landzberg MJ, Walsh EP, Lock JE, et al. Ventricular size and function assessed by cardiac MRI predict major adverse clinical outcomes late after tetralogy of Fallot repair. *Heart* 2008;94:211-6.
4. Sun JP, James KB, Yang XS, Solankhi N, Shah MS, Arheart KL, et al. Comparison of mortality rates and progression of left ventricular dysfunction in patients with idiopathic dilated cardiomyopathy and dilated versus nondilated right ventricular cavities. *Am J Cardiol* 1997;80:1583-7.
5. Ho SY, Nihoyannopoulos P. Anatomy, echocardiography, and normal right ventricular dimensions. *Heart* 2006;92(Suppl 1):i2-13.
6. Mertens LL, Friedberg MK. Imaging the right ventricle—current state of the art. *Nat Rev Cardiol* 2010;7:551-63.
7. Vonk-Noordegraaf A, Souza R. Cardiac magnetic resonance imaging: what can it add to our knowledge of the right ventricle in pulmonary arterial hypertension? *Am J Cardiol* 2012;110:25S-31.
8. Shimada YJ, Shiota M, Siegel RJ, Shiota T. Accuracy of right ventricular volumes and function determined by three-dimensional echocardiography in comparison with magnetic resonance imaging: a meta-analysis study. *J Am Soc Echocardiogr* 2010;23:943-53.

9. Lang RM, Badano LP, Tsang W, Adams DH, Agricola E, Buck T, et al. EAE/ASE recommendations for image acquisition and display using three-dimensional echocardiography. *J Am Soc Echocardiogr* 2012;25:3-46.
10. Sugeng L, Mor-Avi V, Weinert L, Niel J, Ebner C, Steringer-Mascherbauer R, et al. Multimodality comparison of quantitative volumetric analysis of the right ventricle. *JACC Cardiovasc Imaging* 2010;3:10-8.
11. Bhan A, Kapetanakis S, Monaghan MJ. Three-dimensional echocardiography. *Heart* 2010;96:153-63.
12. Galie N, Hooper MM, Humbert M, Torbicki A, Vachiery JL, Barbera JA, et al. Guidelines for the diagnosis and treatment of pulmonary hypertension: the Task Force for the Diagnosis and Treatment of Pulmonary Hypertension of the European Society of Cardiology (ESC) and the European Respiratory Society (ERS), endorsed by the International Society of Heart and Lung Transplantation (ISHLT). *Eur Heart J* 2009;30:2493-537.
13. Plockinger U, Gustafsson B, Ivan D, Szpak W, Davar J. ENETS consensus guidelines for the standards of care in neuroendocrine tumors: echocardiography. *Neuroendocrinology* 2009;90:190-3.
14. Rudski LG, Lai WW, Afilalo J, Hua L, Handschumacher MD, Chandrasekaran K, et al. Guidelines for the echocardiographic assessment of the right heart in adults: a report from the American Society of Echocardiography endorsed by the European Association of Echocardiography, a registered branch of the European Society of Cardiology, and the Canadian Society of Echocardiography. *J Am Soc Echocardiogr* 2010;23:685-713. quiz 86-8.
15. Lang RM, Bierig M, Devereux RB, Flachskampf FA, Foster E, Pellikka PA, et al. Recommendations for chamber quantification: a report from the American Society of Echocardiography's Guidelines and Standards Committee and the Chamber Quantification Writing Group, developed in conjunction with the European Association of Echocardiography, a branch of the European Society of Cardiology. *J Am Soc Echocardiogr* 2005;18:1440-63.
16. Howard LS, Grapsa J, Dawson D, Bellamy M, Chambers JB, Masani ND, et al. Echocardiographic assessment of pulmonary hypertension: standard operating procedure. *Eur Respir Rev* 2012;21:239-48.
17. Hardegger EL, Sachdev A, Villarraga HR, Frantz RP, McGoon MD, Kushwaha SS, et al. Role of serial quantitative assessment of right ventricular function by strain in pulmonary arterial hypertension. *Am J Cardiol* 2013;111:143-8.
18. Kjaergaard J, Petersen CL, Kjaer A, Schaadt BK, Oh JK, Hassager C. Evaluation of right ventricular volume and function by 2D and 3D echocardiography compared to MRI. *Eur J Echocardiogr* 2006;7:430-8.
19. Ostendorf E, Carlsson M, Shahgaldi K, Roijer A, Holm J. Manual correction of semi-automatic three-dimensional echocardiography is needed for right ventricular assessment in adults; validation with cardiac magnetic resonance. *Cardiovasc Ultrasound* 2012;10:1.
20. Iriart X, Montaudon M, Lafitte S, Chabaneix J, Reant P, Balbach T, et al. Right ventricle three-dimensional echography in corrected tetralogy of Fallot: accuracy and variability. *Eur J Echocardiogr* 2009;10:784-92.
21. Niemann PS, Pinho L, Balbach T, Galuschky C, Blankenhagen M, Silberbach M, et al. Anatomically oriented right ventricular volume measurements with dynamic three-dimensional echocardiography validated by 3-tesla magnetic resonance imaging. *J Am Coll Cardiol* 2007;50:1668-76.
22. van der Zwaan HB, Geleijnse ML, Soliman OI, McGhie JS, Wieggers-Groeneweg EJ, Helbing WA, et al. Test-retest variability of volumetric right ventricular measurements using real-time three-dimensional echocardiography. *J Am Soc Echocardiogr* 2011;24:671-9.
23. Puranik R, Tsang VT, Broadley A, Nordmeyer J, Lurz P, Muthialu N, et al. Functional outcomes after the Ross (pulmonary autograft) procedure assessed with magnetic resonance imaging and cardiopulmonary exercise testing. *Heart* 2010;96:304-8.
24. Muthurangu V, Lurz P, Critchely JD, Deanfield JE, Taylor AM, Hansen MS. Real-time assessment of right and left ventricular volumes and function in patients with congenital heart disease by using high spatiotemporal resolution radial k-t SENSE. *Radiology* 2008;248:782-91.
25. Moledina S, Pandya B, Bartsota M, Mortensen KH, McMillan M, Quayam S, et al. Prognostic significance of cardiac magnetic resonance imaging in children with pulmonary hypertension. *Circ Cardiovasc Imaging* 2013.
26. Kind T, Mauritz GJ, Marcus JT, van de Veerdonk M, Westerhof N, Vonk-Noordegraaf A. Right ventricular ejection fraction is better reflected by transverse rather than longitudinal wall motion in pulmonary hypertension. *J Cardiovasc Magn Reson* 2010;12:35.
27. Steeden JA, Atkinson D, Hansen MS, Taylor AM, Muthurangu V. Rapid flow assessment of congenital heart disease with high-spatiotemporal-resolution gated spiral phase-contrast MR imaging. *Radiology* 2011;260:79-87.
28. Odille F, Steeden JA, Muthurangu V, Atkinson D. Automatic segmentation propagation of the aorta in real-time phase contrast MRI using nonrigid registration. *J Magn Reson Imaging* 2011;33:232-8.
29. Rosset A, Spadola L, Ratib O. OsiriX: an open-source software for navigating in multidimensional DICOM images. *J Digit Imaging* 2004;17:205-16.
30. Bland JM, Altman DG. Statistical methods for assessing agreement between two methods of clinical measurement. *Lancet* 1986;1:307-10.
31. Tamborini G, Marsan NA, Gripari P, Maffessanti F, Brusoni D, Muratori M, et al. Reference values for right ventricular volumes and ejection fraction with real-time three-dimensional echocardiography: evaluation in a large series of normal subjects. *J Am Soc Echocardiogr* 2010;23:109-15.
32. Pavlicek M, Wahl A, Rutz T, de Marchi SF, Hille R, Wustmann K, et al. Right ventricular systolic function assessment: rank of echocardiographic methods vs. cardiac magnetic resonance imaging. *Eur J Echocardiogr* 2011;12:871-80.
33. DeLong ER, DeLong DM, Clarke-Pearson DL. Comparing the areas under two or more correlated receiver operating characteristic curves: a nonparametric approach. *Biometrics* 1988;44:837-45.
34. van Wolferen SA, Marcus JT, Boonstra A, Marques KM, Bronzwaer JG, Spreeuwenberg MD, et al. Prognostic value of right ventricular mass, volume, and function in idiopathic pulmonary arterial hypertension. *Eur Heart J* 2007;28:1250-7.
35. Chin KM, Kim NH, Rubin LJ. The right ventricle in pulmonary hypertension. *Coron Artery Dis* 2005;16:13-8.
36. van de Veerdonk MC, Kind T, Marcus JT, Mauritz GJ, Heymans MW, Bogaard HJ, et al. Progressive right ventricular dysfunction in patients with pulmonary arterial hypertension responding to therapy. *J Am Coll Cardiol* 2011;58:2511-9.
37. Moller JE, Pellikka PA, Bernheim AM, Schaff HV, Rubin J, Connolly HM. Prognosis of carcinoid heart disease: analysis of 200 cases over two decades. *Circulation* 2005;112:3320-7.
38. van der Zwaan HB, Geleijnse ML, McGhie JS, Boersma E, Helbing WA, Meijboom FJ, et al. Right ventricular quantification in clinical practice: two-dimensional vs. three-dimensional echocardiography compared with cardiac magnetic resonance imaging. *Eur J Echocardiogr* 2011;12:656-64.
39. Tamborini G, Muratori M, Brusoni D, Celeste F, Maffessanti F, Caiani EG, et al. Is right ventricular systolic function reduced after cardiac surgery? A two- and three-dimensional echocardiographic study. *Eur J Echocardiogr* 2009;10:630-4.
40. Shiran H, Zamanian RT, McConnell MV, Liang DH, Dash R, Heidary S, et al. Relationship between echocardiographic and magnetic resonance derived measures of right ventricular size and function in patients with pulmonary hypertension. *J Am Soc Echocardiogr* 2014;27:405-12.
41. Grapsa J, O'Regan DP, Pavlopoulos H, Durighel G, Dawson D, Nihoyannopoulos P. Right ventricular remodelling in pulmonary arterial hypertension with three-dimensional echocardiography: comparison with cardiac magnetic resonance imaging. *Eur J Echocardiogr* 2010;11:64-73.
42. Morikawa T, Murata M, Okuda S, Tsuruta H, Iwanaga S, Murata M, et al. Quantitative analysis of right ventricular function in patients with pulmonary hypertension using three-dimensional echocardiography and a two-dimensional summation method compared to magnetic resonance imaging. *Am J Cardiol* 2011;107:484-9.

43. Tamborini G, Brusoni D, Torres Molina JE, Galli CA, Maltagliati A, Muratori M, et al. Feasibility of a new generation three-dimensional echocardiography for right ventricular volumetric and functional measurements. *Am J Cardiol* 2008;102:499-505.
44. Zhang QB, Sun JP, Gao RF, Lee AP, Feng YL, Liu XR, et al. Feasibility of single-beat full-volume capture real-time three-dimensional echocardiography for quantification of right ventricular volume: validation by cardiac magnetic resonance imaging. *Int J Cardiol* 2013;168:3991-5.
45. van der Zwaan HB, Helbing WA, McGhie JS, Geleijnse ML, Luijnenburg SE, Roos-Hesselink JW, et al. Clinical value of real-time three-dimensional echocardiography for right ventricular quantification in congenital heart disease: validation with cardiac magnetic resonance imaging. *J Am Soc Echocardiogr* 2010;23:134-40.
46. Schattke S, Wagner M, Hattasch R, Schroeckh S, Durmus T, Schimke I, et al. Single beat 3D echocardiography for the assessment of right ventricular dimension and function after endurance exercise: intraindividual comparison with magnetic resonance imaging. *Cardiovasc Ultrasound* 2012;10:6.
47. Fang F, Chan A, Lee AP, Sanderson JE, Kwong JS, Luo XX, et al. Variation in right ventricular volumes assessment by real-time three-dimensional echocardiography between dilated and normal right ventricle: comparison with cardiac magnetic resonance imaging. *Int J Cardiol* 2013;168:4391-3.
48. Mor-Avi V, Jenkins C, Kuhl HP, Nesser HJ, Marwick T, Franke A, et al. Real-time 3-dimensional echocardiographic quantification of left ventricular volumes: multicenter study for validation with magnetic resonance imaging and investigation of sources of error. *JACC Cardiovasc Imaging* 2008;1:413-23.
49. van Wolferen SA, van de Veerdonk MC, Mauritz GJ, Jacobs W, Marcus JT, Marques KM, et al. Clinically significant change in stroke volume in pulmonary hypertension. *Chest* 2011;139:1003-9.
50. Alfakih K, Plein S, Bloomer T, Jones T, Ridgway J, Sivananthan M. Comparison of right ventricular volume measurements between axial and short axis orientation using steady-state free precession magnetic resonance imaging. *J Magn Reson Imaging* 2003;18:25-32.
51. Fratz S, Schuhbaeck A, Buchner C, Busch R, Meierhofer C, Martinoff S, et al. Comparison of accuracy of axial slices versus short-axis slices for measuring ventricular volumes by cardiac magnetic resonance in patients with corrected tetralogy of fallot. *Am J Cardiol* 2009;103:1764-9.

Did you know?

You can link from references cited in
JASE to abstracts and articles in
other participating journals.

Visit www.onlinejase.com today!

APPENDIX 2

D. Knight, J. Schwaiger, S. Krupickova, J. Davar, V. Muthurangu and J. Coghlan

Accuracy and test-retest reproducibility of two-dimensional knowledge-based volumetric reconstruction of the right ventricle in pulmonary hypertension.

Journal of the American Society of Echocardiography, 2015, **28**(8), 989-98.

Accuracy and Test-Retest Reproducibility of Two-Dimensional Knowledge-Based Volumetric Reconstruction of the Right Ventricle in Pulmonary Hypertension

Daniel S. Knight, BSc (Hons), MBBS, MRCP, Johannes P. Schwaiger, MD, Sylvia Krupickova, MD, PhD, Joseph Davar, FRCP, MD, PhD, Vivek Muthurangu, MD, MRCPCH, and J. Gerry Coghlan, MD, FRCP, *London, United Kingdom*

Background: Right heart function is the key determinant of symptoms and prognosis in pulmonary hypertension (PH), but the right ventricle has a complex geometry that is challenging to quantify by two-dimensional (2D) echocardiography. A novel 2D echocardiographic technique for right ventricular (RV) quantitation involves knowledge-based reconstruction (KBR), a hybrid of 2D echocardiography-acquired coordinates localized in three-dimensional space and connected by reference to a disease-specific RV shape library. The aim of this study was to determine the accuracy of 2D KBR against cardiac magnetic resonance imaging in PH and the test-retest reproducibility of both conventional 2D echocardiographic RV fractional area change (FAC) and 2D KBR.

Methods: Twenty-eight patients with PH underwent same-day echocardiography and cardiac magnetic resonance imaging. Two operators performed serial RV FAC and 2D KBR acquisition and postprocessing to assess inter- and intraobserver test-retest reproducibility.

Results: Bland-Altman analysis (mean bias \pm 95% limits of agreement) showed good agreement for end-diastolic volume (3.5 ± 25.0 mL), end-systolic volume (0.9 ± 19.9 mL), stroke volume (2.6 ± 23.1 mL), and ejection fraction ($0.4 \pm 10.2\%$) measured by 2D KBR and cardiac magnetic resonance imaging. There were no significant interobserver or intraobserver test-retest differences for 2D KBR RV metrics, with acceptable limits of agreement (interobserver end-diastolic volume, -0.9 ± 21.8 mL; end-systolic volume, -1.3 ± 25.8 mL; stroke volume, -0.2 ± 24.2 mL; ejection fraction, $0.7 \pm 14.4\%$). Significant test-retest variability was observed for 2D echocardiographic RV areas and FAC.

Conclusions: Two-dimensional KBR is an accurate, novel technique for RV volumetric quantification in PH, with superior test-retest reproducibility compared with conventional 2D echocardiographic RV FAC. (*J Am Soc Echocardiogr* 2015;28:989-98.)

Keywords: Transthoracic echocardiography, Right ventricular function, Pulmonary hypertension, Reproducibility of results, Magnetic resonance imaging

From the University College London Medical School, London, United Kingdom (D.S.K.); the Department of Cardiology, Royal Free London NHS Foundation Trust, London, United Kingdom (D.S.K., J.P.S., J.D., J.G.C.); and the UCL Centre for Cardiovascular Imaging, University College London, London, United Kingdom (D.S.K., S.K., V.M.).

Drs Knight and Muthurangu are funded by the British Heart Foundation (BHF CRTF FS/11/72/28955). This work was carried out with support of the GOSH/ ICH NIHR Biomedical Research Centre.

Reprint requests: Daniel S. Knight, BSc (Hons), MBBS, MRCP, Division of Medicine, University College London, Royal Free Campus, Rowland Hill Street, London, NW3 2PF, United Kingdom (E-mail: danielknight@doctors.org.uk).

0894-7317/\$36.00

Copyright 2015 by the American Society of Echocardiography. Published by Elsevier Inc. This is an open access article under the CC BY license (<http://creativecommons.org/licenses/by/4.0/>).

<http://dx.doi.org/10.1016/j.echo.2015.02.020>

Right ventricular (RV) function is the key symptomatic and prognostic determinant in pulmonary hypertension (PH).¹ Cardiac magnetic resonance imaging (CMRI) is the gold standard for volumetric quantification of the right ventricle,² but cardiac ultrasound is a comparatively cheaper and more widely available modality. However, the anatomy and complex geometry of the right ventricle confer significant limitations to two-dimensional (2D) echocardiography (2DE).^{3,4} Fractional area change (FAC), for example, is a simple measure of RV size and function that visualizes only one 2D plane of this complex chamber.⁵ Three-dimensional echocardiography (3DE) has shown promise for RV volumetric analysis in PH⁶⁻⁸ but requires operator experience for acquisition and postprocessing beyond that of 2DE, with lower spatial and temporal resolution, typically leading to underestimation of RV volumes.⁹

Abbreviations**CMRI** = Cardiac magnetic resonance imaging**FAC** = Fractional area change**KBR** = Knowledge-based reconstruction**PH** = Pulmonary hypertension**RV** = Right ventricular**3DE** = Three-dimensional echocardiography**2D** = Two-dimensional**2DE** = Two-dimensional echocardiography

A novel 2D echocardiographic technique for volumetric RV quantitation involves knowledge-based reconstruction (KBR). This hybrid approach uses the benefits of conventional 2DE in conjunction with a reference library of RV shapes to reconstruct a 3D RV polygon. The feasibility and accuracy of 2D KBR has been demonstrated in a small PH population,¹⁰ but the ability to accurately identify changes in RV function in response to treatment is also of clinical and prognostic significance.^{2,11} This will depend on the acquisition and postprocessing elements of 2D

KBR that both contribute to its variability. We therefore sought to provide further validation data for 2D KBR RV quantification in PH and to investigate the test-retest reproducibility of this novel technique compared with FAC.

METHODS**Study Population**

We performed a prospective cross-sectional study that enrolled 28 patients in sinus rhythm with no contraindications to magnetic resonance imaging who presented for diagnosis and/or follow-up of PH (diagnosed by right heart catheterization as a mean pulmonary artery pressure > 25 mm Hg and a pulmonary capillary wedge pressure < 15 mm Hg¹²). All participants underwent comprehensive 2D transthoracic echocardiography and CMRI on the same day (median scan interval, 116 min; interquartile range, 104–150 min). The etiologies of PH were idiopathic ($n = 5$), connective tissue disease associated ($n = 14$), chronic thromboembolic disease ($n = 8$) and portopulmonary ($n = 1$). Exclusion criteria were arrhythmia and known independent left-sided cardiac disease unrelated to PH.

The study complied with the Declaration of Helsinki. The institutional research ethics committee approved the study, and informed written consent was obtained from all participants.

Two-Dimensional Echocardiography and KBR

Image Acquisition. All patients underwent comprehensive 2D and Doppler transthoracic echocardiography in the left lateral decubitus position using the Philips iE33 echocardiographic system (Philips Medical Systems, Andover, MA) with an S5-1 transducer (frequency bandwidth, 1–5 MHz). A standard clinical protocol for all examinations was followed in conjunction with American Society of Echocardiography guidelines for chamber quantification.^{5,13}

A magnetic localizer was attached to the S5-1 transducer by a molded plastic sheath. The magnetic localizer was connected to a dedicated console, from which a mechanical arm with an attached magnetic field generator hung over the patient (Figure 1; VentrPoint Diagnostics Ltd, Seattle, WA). The localizer mounted on the ultrasound transducer detects orthogonal magnetic fields from the generator hanging over the patient, and in this manner the ultrasound probe position is localized in 3D space at the point of any 2D acquisition. A cushioned wedge was placed on the echocardiography

couch to ensure that the metallic couch apparatus did not interfere with the magnetic field, and patients were instructed to remain entirely stationary in the left lateral decubitus position for the duration of a study acquisition. The ultrasound depth required to visualize all relevant structures was determined before commencing the study and remained fixed throughout.

Seven 2D transthoracic echocardiographic views were obtained in all subjects: parasternal long axis, parasternal short axis at the papillary muscle and apical levels, parasternal RV inflow, parasternal RV outflow including pulmonary valve hinge points and infundibulum, apical four chamber, and an off-axis RV apical view. The 2D KBR acquisition from each view consists of a 2-sec period (usually containing two or three heartbeats) acquired during end-expiratory breath-holds. The electrocardiograph was connected to the echocardiographic system via the dedicated 2D KBR console, and the console images were reproduced from the echocardiographic system's video output and digitized at 30 frames/sec. Image quality was subjectively graded on a 5-point scale from 0 (very poor) to 4 (perfect).¹⁴

Postprocessing: RV FAC. End-diastolic and end-systolic frames were assigned by visual identification of the largest and smallest RV four-chamber cavity areas, respectively, on the 2D KBR console. These frames were exported to the open-source OsiriX Digital Imaging and Communications in Medicine software for the measurement of RV FAC by tracing the RV endocardium in both frames and using the formula $[(\text{end-diastolic area} - \text{end-systolic area}) / \text{end-diastolic area}] \times 100$.

Postprocessing: 2D KBR. The largest and smallest RV four-chamber cavity areas were visually identified as end-diastole and end-systole, respectively, on the 2D KBR console, with the software subsequently assigning the same time interval between these frames to all other views. On the 2D KBR console, a series of anatomic RV landmarks were identified on the 2D echocardiography images (Figures 2A–2G) in the end-diastolic frames and subsequently in the end-systolic frames. A minimum of 26 points was plotted for each of the end-diastolic and end-systolic data sets. RV endocardial points were placed at the junction between trabeculations and myocardium. The plotted anatomic landmarks with their respective 3D spatial coordinates were then submitted via the Internet to a secure remote server for remote processing by a proprietary 2D KBR algorithm. The algorithm interpolates between the plotted points by referencing against a catalogue of RV shapes generated by CMRI from patients with known diagnoses of PH.

End-diastolic and end-systolic 3D models of the right ventricle were reviewed in a systematic fashion. Intersections between the borders of the 3D model and the original 2D scan plane were inspected to ensure concordance between 2D images and 3D reconstructions (Figures 2A–2G), and marked points were checked for alignment with the surface of the 3D model. Where significant deviations between the reconstructed model and either the plotted points and/or 2D echocardiographic endocardial borders existed, points were re-plotted and the algorithm was rerun. Where significant border versus 2D image misalignment suggested a shift in patient position or an inadequate breath-hold, all points from that 2D view were removed, and the erroneous 2D echocardiographic view was excluded from the 2D KBR reconstruction. A maximum of one view of the seven required in the data acquisition protocol could be excluded for any given study because of a change in patient position or an inadequate breath-hold. If this problem was encountered in more than one of the seven required views, the entire study was excluded from the final analysis.

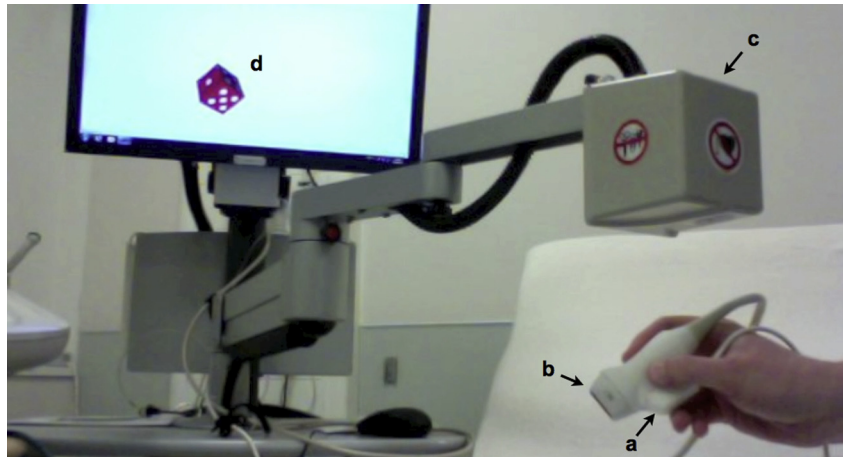


Figure 1 Two-dimensional KBR apparatus: a localizing transducer (A) attached by a molded plastic sheath to a conventional 2D echocardiographic probe (B) detects orthogonal magnetic fields emitted by the generator (C) attached to the mechanical arm that hangs over the patient. Here in the 2D KBR calibration module, the die on the screen (D) represents the 2D echocardiographic probe, which moves synchronously with any movement of the 2D echocardiographic probe. Note the cushioned wedge in the background that is placed on the echocardiography couch to ensure that the metallic apparatus underneath couch does not interfere with detection of the magnetic fields.

The final check entailed inspection of the nested view of end-diastolic and end-systolic models to verify alignment of the tricuspid and pulmonary annular planes (Figure 2H). The final 2D KBR polygon was assessed for precision by subjectively scoring on a 5-point scale depending on the proximity of intersections of the plotted landmarks with the reconstructed polygon: 4 (all points intersect), 3 (three or fewer points significantly deviate from polygon), 2 (five or fewer points significantly deviate from polygon), 1 (seven or fewer points significantly deviate from polygon), and 0 (poor agreement).

FAC and 2D KBR Test-Retest Reproducibility. All subjects underwent serial 2D echocardiographic acquisition and postprocessing by two independent sonographers (D.S.K. and J.P.S.), as described previously.¹⁵ The two sonographers had similar experience in 2D transthoracic echocardiography (>4 years each) and received the same vendor training for the 2D KBR system. Sonographer 1 (D.S.K.) obtained a 2D KBR data set, after which sonographer 2 (J.P.S.) independently obtained a 2D KBR data set. Sonographer 1 then acquired a second 2D KBR data set. The sonographers, who were blinded to each other's results and the results from CMRI, performed postprocessing of their own data sets for FAC and 2D KBR. Data sets analyzed for intraobserver test-retest reproducibility were postprocessed separately at time intervals of >2 weeks.

CMRI

Image Acquisition. All CMRI images were acquired using a 1.5-T magnetic resonance scanner (Avanto; Siemens Healthcare, Erlangen, Germany) using a 12-element phased-array coil for signal reception and the body coil for signal transmission. A vector electrocardiographic system was used for cardiac gating. In all patients, ventricular volumes and great vessel flow were measured as previously described.⁷ Volumetric RV data were obtained using real-time radial *k-t* sensitivity-encoded imaging of contiguous transaxial slices.¹⁶ Real-time radial *k-t* sensitivity-encoded imaging allows the collection of high-spatiotemporal resolution, real-time images during free breathing and is part of the standard clinical CMRI work flow at our institution in the pediatric PH population.¹⁷

Postprocessing. All image postprocessing was performed using “in-house” plugins for the open-source OsiriX Digital Imaging and Communications in Medicine software.^{16,18,19} Endocardial RV borders were traced manually at end-diastole and end-systole, the time points of which were identified by the largest and smallest RV cavity areas, respectively. The inclusion of RV trabeculations was the same as that performed in echocardiographic postprocessing. Ventricular stroke volume was the difference between the end-diastolic volume and end-systolic volume, and ejection fraction was calculated as (stroke volume/end-diastolic volume) \times 100.

Statistical Analysis

Statistical analysis was performed using SPSS version 22.0 (IBM Corporation, Armonk, NY) and Prism version 6.0b for Mac (GraphPad Software, Inc, La Jolla, CA). All continuous data were normally distributed and expressed as mean \pm SD. Systematic differences between measurements were evaluated with Student's paired *t* test (two tailed). *P* values < .05 were considered to indicate statistical significance. Intermodality agreement was studied using the Bland-Altman method, whereby the mean difference was presented as the bias and 95% limits of agreement around the bias expressed as the mean difference \pm 1.96 SDs.²⁰

Differences between test-retest measurements were analyzed using one-way repeated-measures analysis of variance, with the Bonferroni post hoc test identifying which specific means differed. The Greenhouse-Geisser correction was used if the assumption of sphericity had been violated. Test-retest variability was expressed using intraclass correlation coefficients, relative differences and coefficients of variation. The intraclass correlation coefficient was quantified by the two-way random-effects model with absolute agreement. An intraclass correlation coefficient > 0.85 was considered excellent. Relative differences were calculated by taking the absolute difference between two observations divided by the mean of the repeated observations and expressed as a percentage. Coefficients of variation were calculated as the SD of the difference between two acquisitions divided by their mean value and expressed as a percentage.²¹ A coefficient of variation \leq 10% was considered excellent.

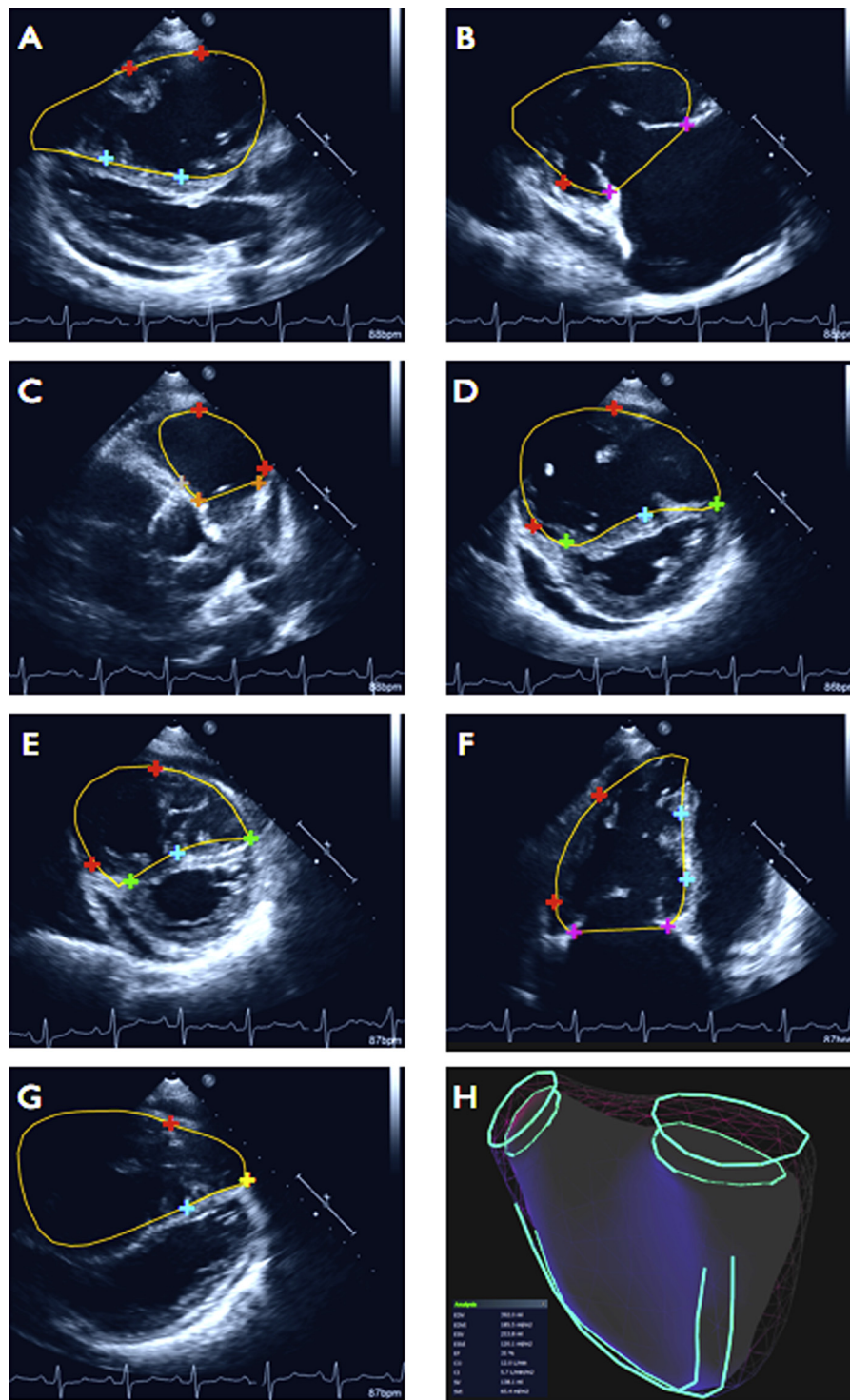


Figure 2 Postprocessed 2D KBR data from a participant with pulmonary hypertension. All of the required 2D echocardiographic scan planes in end-diastole are displayed: **(A)** parasternal long-axis (PLAX), **(B)** PLAX RV inflow, **(C)** PLAX RV outflow including infundibulum and pulmonary valve hinge points, **(D)** parasternal short-axis (PSAX) at midcavity (papillary muscle) level, **(E)** PSAX apical level, **(F)** four-chamber RV, **(G)** off-axis RV apical view (note how the RV apex rides over the left ventricular apex). The *differently colored cross-hairs* represent user-defined plots for different RV structures; for example, *red crosses* are plotted along the RV endocardium, *turquoise crosses* along the RV side of the interventricular septum, a *yellow cross* at the RV apex, *orange crosses* at the pulmonary valve annulus, and *purple crosses* at the tricuspid valve annulus. The *yellow border tracings* are superimposed projections of the 2D KBR RV reconstruction onto the original 2D echocardiographic scan data, also showing how the polygon extends beyond the original 2D echocardiographic image sector. Landmarks can be checked and repositioned by the user if required, and the 2D KBR algorithm subsequently rerun. A final check is the nested view **(H)** of end-diastolic and end-systolic polygons to ensure alignment of the tricuspid and pulmonary valve orifices.

Table 1 Clinical characteristics of study population ($n = 28$)

Variable	Value
Age (y)	54 \pm 13
Women	20 (71%)
Height (cm)	165 \pm 11
Weight (kg)	71 \pm 18
Body surface area (m ²)	1.8 \pm 0.3
Heart rate (beats/min)	79 \pm 13
Mean PASP on RHC (mm Hg)	47 \pm 12
Pulmonary vasodilators	
Endothelin antagonists	11 (39%)
PDE ₅ antagonists	18 (64%)
Oral prostanoid	1 (4%)
Inhaled prostanoid	1 (4%)
RV EDV (mL/m ²)	98 \pm 26
RV ESV (mL/m ²)	59 \pm 23
RV EF (%)	41 \pm 11

EDV, End-diastolic volume; EF, ejection fraction; ESV, end-systolic volume; PASP, pulmonary artery systolic pressure; PDE₅, phosphodiesterase 5; RHC, right heart catheterization.

Data are expressed as mean \pm SD or as number (percentage). RV volumes are derived from cardiac magnetic resonance imaging.

RESULTS

Population Characteristics and 2D KBR Technical Data

The clinical characteristics of the 28 participants are presented in Table 1, all of whom had adequate 2D echocardiographic windows for the specified protocol. Participants' heart rates recorded on the 2D echocardiographic loop acquired first were similar to those recorded on the 2D echocardiographic loop acquired last ($P = .90$). Image acquisition for one data set took on the order of approximately 5 min per patient, with 2D KBR postprocessing and analysis taking no longer than about 15 min. Good mean subjective scores were observed for 2D echocardiographic image acquisition (2.9 ± 0.9) and 2D KBR reconstruction (3.2 ± 0.7), with moderate correlation between the two scores ($r = 0.54$, $P = .003$).

RV Quantification by 2D KBR versus CMRI

RV volumes and ejection fractions for all participants measured by 2D KBR showed no significant differences with CMRI (Table 2), with no significant bias and clinically acceptable limits of agreement (Figure 3).

Test-Retest Intraobserver and Interobserver Reproducibility

One patient moved in the first data set acquisition, one patient moved in the third data set acquisition, and two patients moved in both the second and third data set acquisitions. The 2D KBR data sets for these four individuals were therefore excluded from the final test-retest reproducibility analysis because of significant movement artifact.

Good reproducibility metrics and acceptable limits of agreement were observed for the 24 intra- and interobserver 2D KBR test-retest studies (Table 3, Figure 4). There were no significant differences for RV volumes or ejection fraction between serial 2D KBR studies, but significant intra- and interobserver test-retest variability was demonstrated for serial RV areas and FAC (Table 4).

Table 2 RV volumes and EF by 2D KBR versus CMRI

Measurement	2D KBR	CMRI	P^*
RV EDV (mL)	179 \pm 66	176 \pm 61	.16
RV ESV (mL)	107 \pm 47	106 \pm 47	.63
RV SV (mL)	73 \pm 27	70 \pm 26	.26
RV EF (%)	42 \pm 10	41 \pm 11	.66

EDV, End-diastolic volume; EF, ejection fraction; ESV, end-systolic volume; SV, stroke volume.

Data are expressed as mean \pm SD; $n = 27$ (one patient excluded because of movement artifact during 2D KBR study).

*Paired Student's t test.

DISCUSSION

This study demonstrates the feasibility and accuracy of 2D KBR for RV quantification in PH and provides the first test-retest reproducibility data for this technique. These results suggest a role for 2D KBR in serial follow-up studies of this patient population. The sources of variability at the acquisition and postprocessing stages of 2D KBR have been tested in an approach more akin to clinical practice, with no significant differences demonstrated between serial interobserver and intraobserver test-retest studies. By comparison with conventional RV FAC, 2D KBR has incremental benefit in quantifying RV function through superior test-retest reproducibility.

Two-dimensional KBR is an emerging technique that has been validated in congenital heart disease populations²²⁻²⁴ and more recently in a small population of patients with PH.¹⁰ The utility of applying a hybrid knowledge-based approach to 2DE of the right ventricle is reflected by the known differences in RV shapes that are encountered not only in congenital and acquired disease but also among different subtypes of PH.²⁵ Moreover, algorithms for RV reconstruction by conventional 3DE are typically based on generic healthy adult RV shapes rather than taking into account differences in congenital populations or subtle changes in volume- and pressure-overload states.²⁶ The reconstruction of a 3D model from 2D landmark coordinates makes the use of the piecewise smooth subdivision surface technique, with gaps between the user-defined points filled by a catalogue registration method that is well validated in vitro.^{27,28} The piecewise smooth subdivision surface technique itself also has greater accuracy over the conventional Beutell method for RV volume reconstruction in vivo by 3DE.²²

Our limits of agreement are clinically acceptable compared with the gold standard of CMRI, slightly more favorable than those obtained previously in idiopathic PH,¹⁰ and similar to previous work in children following surgical repair of tetralogy of Fallot.²² A potential explanation for these differences might be our quantification of RV volumes by CMRI using a transaxial stack of RV slices rather than the short-axis stack approach. This has the advantage of avoiding partial voluming of the basal RV slices that is of particular relevance in PH because of the relative preservation of longitudinal over radial function.²⁹ A transaxial slice orientation facilitates the identification of the inflow and outflow components of the right ventricle and ultimately confers better reproducibility for RV volumetric quantification by CMRI.³⁰⁻³² The 2D KBR hardware used in our study also differs from that in previous studies in terms of the position of the magnetic field generator either above or underneath the patient bed. Our equipment used a magnetic field generator suspended

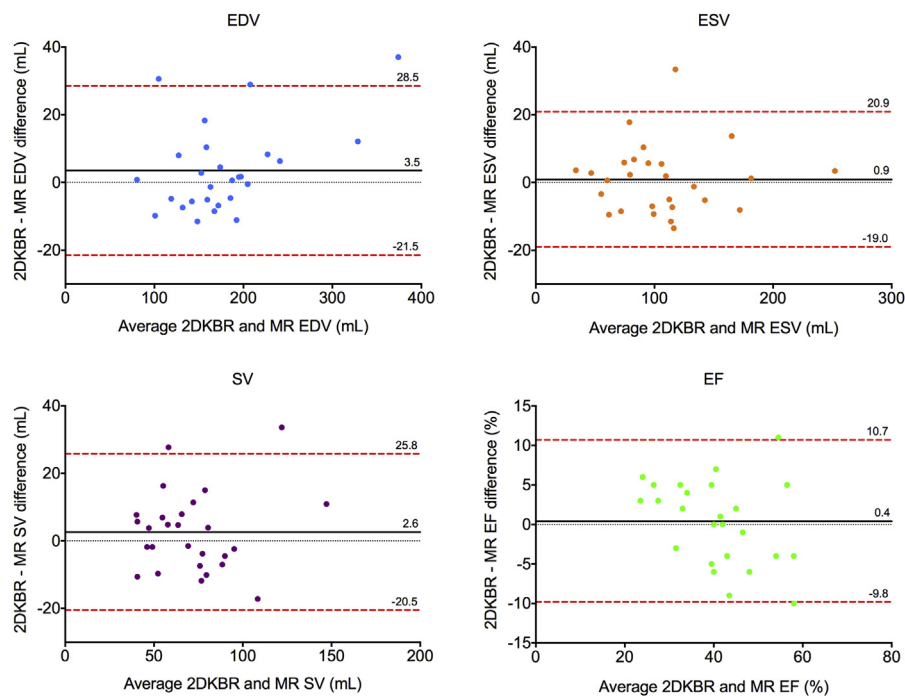


Figure 3 Bland-Altman analysis of bias (black solid line) and 95% limits of agreement (red dashed line) for 2D KBR versus CMRI quantification of right ventricular end-diastolic volume (EDV), end-systolic volume (ESV), stroke volume (SV), and ejection fraction (EF); $n = 27$ (one patient excluded because of movement artifact during 2D KBR study).

Table 3 Test-retest reproducibility results for 2D KBR and 2D echocardiographic RV metrics

Variable	Intraobserver			Interobserver		
	ICC	COV (%)	RD (%)	ICC	COV (%)	RD (%)
2D KBR						
RV EDV	0.985	3.0	4.2	0.986	3.9	5.5
RV ESV	0.987	4.3	6.1	0.960	7.7	10.9
RV SV	0.953	8.3	11.7	0.856	11.7	16.5
RV EF	0.919	6.4	9.0	0.758	10.5	14.8
2DE						
RV EDA	0.885	9.0	12.7	0.394	25.0	35.4
RV ESA	0.931	9.3	13.2	0.440	31.0	43.9
RV FAC	0.784	18.1	25.6	0.619	20.8	29.4

COV, Coefficient of variation; EDA, end-diastolic area; EDV, end-diastolic volume; EF, ejection fraction; ESA, end-systolic area; ESV, end-systolic volume; ICC, intraclass correlation coefficient; RD, relative difference; SV, stroke volume.

directly above the patient’s chest. However, the magnetic field generator location above or below the echocardiography couch should not theoretically affect the spatial detection of the 2D echocardiographic probe localizer.

To our knowledge, this is the first study designed to assess the test-retest reproducibility of 2D KBR. Importantly, the 2D KBR technique showed no significant differences for interobserver or intraobserver test-retest reproducibility, whereas FAC had significant test-retest variability. The only previous study of test-retest reproduc-

ibility of 2D echocardiographic RV area metrics, to our knowledge, had a comparable intraobserver test-retest coefficient of variation for RV FAC of 16.5%.³³ The reproducibility of FAC postprocessing alone (not including variability in image acquisition) has also been shown to have significant interobserver bias and wide limits of agreement in children after surgical repair of tetralogy of Fallot compared with 2D KBR.²² The test-retest reproducibility of 2D KBR RV volumetric quantification is also improved compared with that previously demonstrated by 3DE in either congenital heart disease¹⁵ or acquired PH.⁷

The superior reproducibility of 2D KBR compared with conventional 2DE and that previously reported for 3DE may be accounted for by several reasons. First, FAC and 3DE require good endocardial delineation to trace the RV border, whereas 2D KBR requires the user to define single points along the endocardium rather than the border in its entirety. Second, in contrast to 2D FAC, the 3D spatial localization of the 2D echocardiographic probe compensates for the acquisition variability in transthoracic windows among operators.³⁴ Postprocessing reproducibility is also likely to be enhanced by the KBR process, with our protocol mandating review of the reconstructed models relative to the original 2D echocardiographic pictures. Landmarks are adjusted to ensure acceptable agreement between the raw 2D echocardiographic images and the KBR polygons, thus conferring an element of reproducibility through the KBR algorithm itself. KBR also differs from 3DE by using a shape-specific reconstruction algorithm rather than a generic adult-based algorithm,²⁶ hence taking account of the impact of the underlying disease process conferred upon RV morphology.

Compared with 3DE, the use of 2D echocardiographic technology for data acquisition also has methodologic advantages. Fundamentally, spatial and temporal resolutions of 2DE are higher than those of 3DE. Underestimation of RV volumes is a known

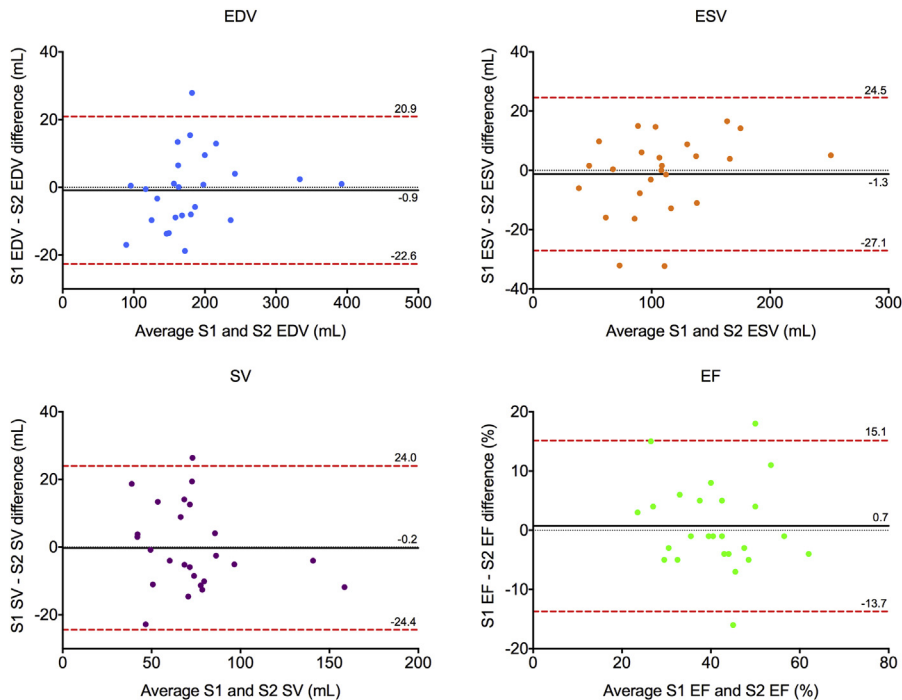


Figure 4 Bland-Altman analysis of bias (black solid line) and 95% limits of agreement (red dashed line) for interobserver 2D KBR test-retest reproducibility of right ventricular end-diastolic volume (EDV), end-systolic volume (ESV), stroke volume (SV), and ejection fraction (EF); *n* = 25 (three patients excluded because of movement artifact during 2D KBR study). S1, Sonographer 1; S2, sonographer 2.

Table 4 Interobserver and intraobserver test-retest reproducibility of RV volumes and EF by 2D KBR and RV areas and FAC by 2DE

Variable	Sonographer 1.1	Sonographer 2	Sonographer 1.2	P*
2D KBR				
RV EDV (mL)	184 ± 68	185 ± 65	180 ± 66	.17
RV ESV (mL)	110 ± 49	111 ± 45	111 ± 48	.80
RV SV (mL)	74 ± 27	74 ± 30	69 ± 27	.15
RV EF (%)	41 ± 10	41 ± 11	40 ± 10	.39
2DE				
RV EDA (cm ²)	23 ± 6	32 ± 7	23 ± 7	<.001
RV ESA (cm ²)	15 ± 6	22 ± 6	16 ± 6	<.001
RV FAC (%)	36 ± 15	31 ± 10	34 ± 14	.05

EDA, end-diastolic area; EDV, end-diastolic volume; EF, ejection fraction; ESA, end-systolic area; ESV, end-systolic volume. Data are expressed as mean ± SD; *n* = 24 for 2D KBR (four patients excluded because of movement artifact), *n* = 27 for FAC (one patient had an unanalyzable four-chamber image that precluded FAC but not 2D KBR).
*One-way repeated measures analysis of variance.

limitation of 3DE due to the inferior spatial resolution, conferring blurred endocardial borders and thus a visually smaller RV cavity.⁹ In particular, the contribution from the RV outflow tract is known to be an important determinant of the overall accuracy of RV volumes.³⁵ However, accurate visualization of this region can be technically difficult by 3DE.^{7,36} The 2D KBR acquisition protocol includes

dedicated imaging of the RV outflow tract by 2DE, affording higher spatial resolution when imaging this region that may contribute to more accurate volumetric quantification (Figure 5). Furthermore, given that echocardiography of the right ventricle has inherent acquisition difficulties due to its anterior position in the chest wall, complex geometry, thin walls, and heavy trabeculations,^{3,4} our subjective image scoring suggests that the requirement for the identification of landmarks rather than the entirety of a cardiac border still permits adequate reconstruction despite cases of poor-quality transthoracic 2D echocardiographic windows.

However, subtle changes in RV function may nevertheless be masked by the margins of error demonstrated in the study. CMRI data demonstrates that a change in RV stroke volume in PH of as little as 10 mL can be regarded as clinically significant,¹¹ and therefore 2D KBR may not be able to differentiate minor variations in RV volumes from the variance in reproducibility. CMRI does not have the same acquisition window restrictions and variability inherent to transthoracic echocardiography, with data sets consisting of contiguous fixed-thickness RV slices acquired from the base of the right heart to the main pulmonary artery with the patient in the supine position. A further consideration with respect to the use of 2D KBR in the serial evaluation of patients is that a change in RV volume might confer a change in cavity shape, which could also have implications for the application of the KBR algorithm to follow-up studies.

A disadvantage of 2D KBR is the requirement for several 2D planes to be acquired over separate cardiac cycles. Image acquisition over several cardiac cycles with potential beat-to-beat variability is also a limitation shared by traditional disk summation 3DE and by CMRI, but not with single-beat full-volume 3DE. However, no significant differences were found in heart rates between the start and end of our studies. Acquiring several 2D echocardiographic planes also requires reproducible breath-holding and a stable patient position throughout

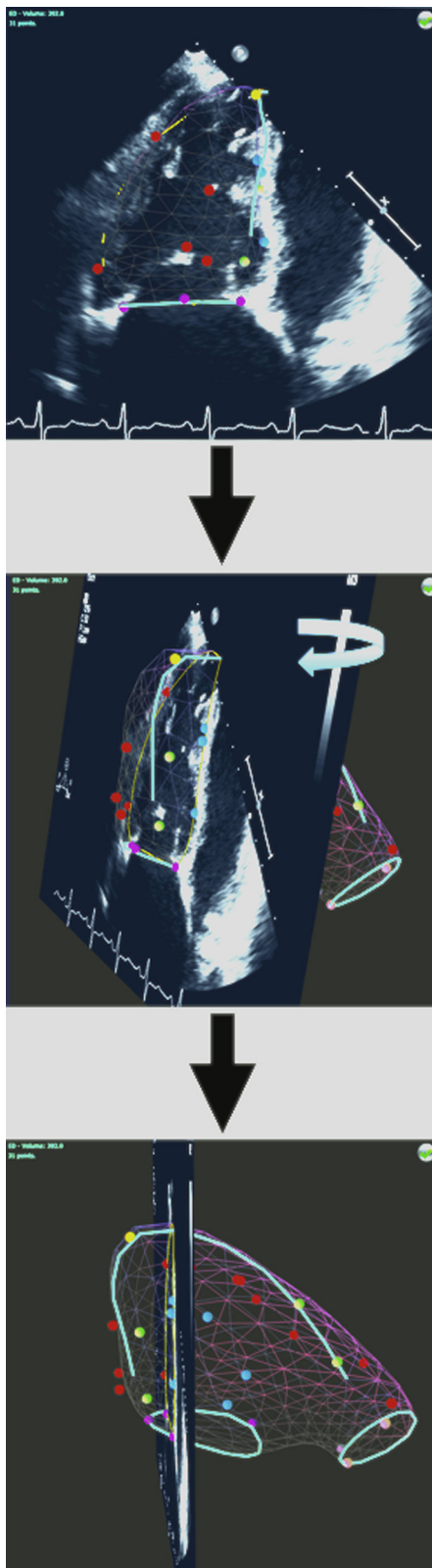


Figure 5 Demonstration of the interaction between the reconstructed 2D knowledge-based reconstruction polygon with a four-chamber view 2D echocardiographic scan plane. The reconstructed polygon can be rotated in any direction (here through 90° from top to bottom, indicated by the curved arrow). Any original 2D echocardiographic acquisition can be dis-

played (here, the four-chamber view) and viewed in relation to the polygon by clicking on one of the dots. In this way, the reconstructed polygon can be inspected to ensure accurate alignment with the original 2D echocardiographic data. From this view, it is also readily appreciable how much of the right ventricle, predominantly the outflow portion, is neglected in a standard four-chamber view used to derive fractional area change.

the study. Repeated breath-holding is also conventionally associated with CMRI, but we used a real-time, high-spatiotemporal resolution sequence as per our institution protocol for PH imaging that allows free breathing and the rapid acquisition of ventricular volumes.¹⁶ Once image acquisition for a 2D KBR study has commenced, the operator is unable to maneuver the patient to optimize transthoracic echocardiographic windows. Therefore, an optimal patient position for parasternal and apical views must be decided upon before commencing 2D KBR data acquisition. These optimal breath-hold and positional constraints may confer difficulty when applied to acutely unwell individuals, and hence 2D KBR is more likely to be practically applicable in the stable outpatient setting. It should also be remembered that although global volumetric indices of RV function are highly prognostic, they do not account for the heterogeneity in RV regional function in different disease states, as shown by 2D and 3D echocardiographic deformation imaging.^{37,38} Finally, 2D KBR includes the RV trabeculations together with the blood volume, which may in turn affect the accuracy of volumetric indices. However, this is also a limitation shared with 3D echocardiographic techniques and has been shown by CMRI to improve reproducibility metrics compared with excluding trabeculations from the RV cavity volume.³⁹

Limitations

Our study represents a single-center experience with a small participant sample size. However, we have supported the validation data for 2D KBR obtained by previous single-center studies using similar sample sizes,^{10,22,23} and a total of 84 2D echocardiographic studies were performed in our study for test-retest reproducibility purposes. The increase in excluded studies with successive repeated scans was due more to the serial 2D echocardiographic scan acquisition protocol for test-retest reproducibility rather than the 2D KBR technique itself. Only one of 28 patients moved in the first 2D echocardiographic data set image acquisition. Therefore, this limitation is unlikely to be so prevalent for individual clinical scans, and the study analysis times would allow the reacquisition of a second data set within a scheduled clinical echocardiographic examination.

Patients with arrhythmia were specifically excluded from this study, but patients with atrial fibrillation, for example, would require a different approach to 2D KBR post-processing. In atrial fibrillation, the end-diastolic frame for each view would have to be manually selected by visually determining the largest RV cavity size. This could theoretically affect the border alignment of the reconstructed polygon, as different cardiac cycles in separate views will inherently have different end-diastolic volumes because of the variability of irregular R-R intervals. Several reconstructions could be performed on the same data set by selecting different cardiac cycles for each reconstruction, with the resulting 2D KBR RV metrics averaged over the number of cardiac cycles analyzed. However, the accuracy and

played (here, the four-chamber view) and viewed in relation to the polygon by clicking on one of the dots. In this way, the reconstructed polygon can be inspected to ensure accurate alignment with the original 2D echocardiographic data. From this view, it is also readily appreciable how much of the right ventricle, predominantly the outflow portion, is neglected in a standard four-chamber view used to derive fractional area change.

reproducibility of this approach using 2D KBR in atrial fibrillation requires further investigation.

Finally, CMRI reproducibility data were not acquired in a test-retest format that allowed comparison of the acquisition and postprocessing variability of this technique. However, as detailed above, the acquisition stage of CMRI consists of a set acquisition of cross-sectional, fixed-thickness, contiguous craniocaudal slices that include the entirety of the heart with the patient supine. Therefore CMRI fundamentally has less potential for acquisition variability compared with 2DE, which has imaging windows obtained from different rib spaces acquired in nonuniform patient positions.

CONCLUSIONS

Novel 2DKBR is a feasible and clinically reproducible technique for RV volumetric quantification in PH, with superior test-retest reproducibility compared with 2D echocardiographic FAC for quantifying RV function. It offers the benefits of using operator experience with conventional 2DE for image acquisition and uses algorithmic reconstruction that takes into account the heterogeneity in shape of the RV cavity in different disease states. The applicability of 2D KBR to serial follow-up studies for assessing the response to treatment should be the focus for further work in advancing this novel echocardiography technique.

ACKNOWLEDGMENT

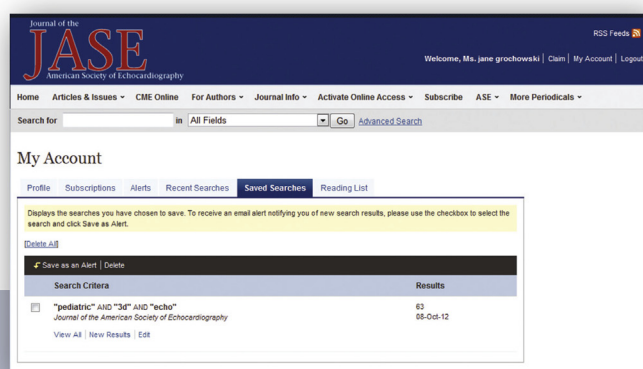
We are grateful to Dr James Willis for providing reproducibility data for RV FAC.

REFERENCES

- Chin KM, Kim NH, Rubin LJ. The right ventricle in pulmonary hypertension. *Coron Artery Dis* 2005;16:13-8.
- van Wolferen SA, Marcus JT, Boonstra A, Marques KM, Bronzwaer JG, Spreeuwenberg MD, et al. Prognostic value of right ventricular mass, volume, and function in idiopathic pulmonary arterial hypertension. *Eur Heart J* 2007;28:1250-7.
- Ho SY, Nihoyannopoulos P. Anatomy, echocardiography, and normal right ventricular dimensions. *Heart* 2006;92(Suppl 1):i2-13.
- Mertens LL, Friedberg MK. Imaging the right ventricle—current state of the art. *Nat Rev Cardiol* 2010;7:551-63.
- Rudski LG, Lai WW, Afilalo J, Hua L, Handschumacher MD, Chandrasekaran K, et al. Guidelines for the echocardiographic assessment of the right heart in adults: a report from the American Society of Echocardiography endorsed by the European Association of Echocardiography, a registered branch of the European Society of Cardiology, and the Canadian Society of Echocardiography. *J Am Soc Echocardiogr* 2010;23:685-713. quiz 86-8.
- Grapsa J, O'Regan DP, Pavlopoulos H, Durighel G, Dawson D, Nihoyannopoulos P. Right ventricular remodelling in pulmonary arterial hypertension with three-dimensional echocardiography: comparison with cardiac magnetic resonance imaging. *Eur J Echocardiogr* 2010;11:64-73.
- Knight DS, Grasso AE, Quail MA, Muthurangu V, Taylor AM, Toumpanakis C, et al. Accuracy and reproducibility of right ventricular quantification in patients with pressure and volume overload using single-beat three-dimensional echocardiography. *J Am Soc Echocardiogr* 2015;28:363-74.
- Morikawa T, Murata M, Okuda S, Tsuruta H, Iwanaga S, Murata M, et al. Quantitative analysis of right ventricular function in patients with pulmonary hypertension using three-dimensional echocardiography and a two-dimensional summation method compared to magnetic resonance imaging. *Am J Cardiol* 2011;107:484-9.
- Shimada YJ, Shiota M, Siegel RJ, Shiota T. Accuracy of right ventricular volumes and function determined by three-dimensional echocardiography in comparison with magnetic resonance imaging: a meta-analysis study. *J Am Soc Echocardiogr* 2010;23:943-53.
- Bhave NM, Patel AR, Weinert L, Yamat M, Freed BH, Mor-Avi V, et al. Three-dimensional modeling of the right ventricle from two-dimensional transthoracic echocardiographic images: utility of knowledge-based reconstruction in pulmonary arterial hypertension. *J Am Soc Echocardiogr* 2013;26:860-7.
- van Wolferen SA, van de Veerdonk MC, Mauritz GJ, Jacobs W, Marcus JT, Marques KM, et al. Clinically significant change in stroke volume in pulmonary hypertension. *Chest* 2011;139:1003-9.
- Galie N, Hoeper MM, Humbert M, Torbicki A, Vachiery JL, Barbera JA, et al. Guidelines for the diagnosis and treatment of pulmonary hypertension: the Task Force for the Diagnosis and Treatment of Pulmonary Hypertension of the European Society of Cardiology (ESC) and the European Respiratory Society (ERS), endorsed by the International Society of Heart and Lung Transplantation (ISHLT). *Eur Heart J* 2009;30:2493-537.
- Lang RM, Bierig M, Devereux RB, Flachskampf FA, Foster E, Pellikka PA, et al. Recommendations for chamber quantification: a report from the American Society of Echocardiography's Guidelines and Standards Committee and the Chamber Quantification Writing Group, developed in conjunction with the European Association of Echocardiography, a branch of the European Society of Cardiology. *J Am Soc Echocardiogr* 2005;18:1440-63.
- Kjaergaard J, Petersen CL, Kjaer A, Schaadt BK, Oh JK, Hassager C. Evaluation of right ventricular volume and function by 2D and 3D echocardiography compared to MRI. *Eur J Echocardiogr* 2006;7:430-8.
- van der Zwaan HB, Geleijnse ML, Soliman OI, McGhie JS, Wiegers-Groeneweg EJ, Helbing WA, et al. Test-retest variability of volumetric right ventricular measurements using real-time three-dimensional echocardiography. *J Am Soc Echocardiogr* 2011;24:671-9.
- Muthurangu V, Lurz P, Critchely JD, Deanfield JE, Taylor AM, Hansen MS. Real-time assessment of right and left ventricular volumes and function in patients with congenital heart disease by using high spatiotemporal resolution radial k-t SENSE. *Radiology* 2008;248:782-91.
- Moledina S, Pandya B, Bartsota M, Mortensen KH, McMillan M, Quayam S, et al. Prognostic significance of cardiac magnetic resonance imaging in children with pulmonary hypertension. *Circ Cardiovasc Imaging* 2013;6:407-14.
- Odille F, Steeden JA, Muthurangu V, Atkinson D. Automatic segmentation propagation of the aorta in real-time phase contrast MRI using nonrigid registration. *J Magn Reson Imaging* 2011;33:232-8.
- Rosset A, Spadola L, Ratib O. OsiriX: an open-source software for navigating in multidimensional DICOM images. *J Digit Imaging* 2004;17:205-16.
- Bland JM, Altman DG. Statistical methods for assessing agreement between two methods of clinical measurement. *Lancet* 1986;1:307-10.
- Tamborini G, Marsan NA, Gripari P, Maffessanti F, Brusoni D, Muratori M, et al. Reference values for right ventricular volumes and ejection fraction with real-time three-dimensional echocardiography: evaluation in a large series of normal subjects. *J Am Soc Echocardiogr* 2010;23:109-15.
- Dragulescu A, Grosse-Wortmann L, Fackoury C, Mertens L. Echocardiographic assessment of right ventricular volumes: a comparison of different techniques in children after surgical repair of tetralogy of Fallot. *Eur Heart J Cardiovasc Imaging* 2012;13:596-604.
- Dragulescu A, Grosse-Wortmann L, Fackoury C, Riffle S, Waiss M, Jaeggi E, et al. Echocardiographic assessment of right ventricular volumes after surgical repair of tetralogy of Fallot: clinical validation of a new echocardiographic method. *J Am Soc Echocardiogr* 2011;24:1191-8.
- Kutty S, Li L, Polak A, Gribben P, Danford DA. Echocardiographic knowledge-based reconstruction for quantification of the systemic right ventricle in young adults with repaired D-transposition of great arteries. *Am J Cardiol* 2012;109:881-8.
- Leary PJ, Kurtz CE, Hough CL, Waiss MP, Ralph DD, Sheehan FH. Three-dimensional analysis of right ventricular shape and function in pulmonary hypertension. *Pulm Circ* 2012;2:34-40.

26. Schattke S, Wagner M, Hattasch R, Schroeckh S, Durmus T, Schimke J, et al. Single beat 3D echocardiography for the assessment of right ventricular dimension and function after endurance exercise: intraindividual comparison with magnetic resonance imaging. *Cardiovasc Ultrasound* 2012;10:6.
27. Hubka M, Bolson EL, McDonald JA, Martin RW, Munt B, Sheehan FH. Three-dimensional echocardiographic measurement of left and right ventricular mass and volume: in vitro validation. *Int J Cardiovasc Imaging* 2002;18:111-8.
28. Wong SP, Johnson RK, Sheehan FH. Rapid and accurate left ventricular surface generation from three-dimensional echocardiography by a catalog based method. Rapid LV surface generation by three-dimensional echo. *Int J Cardiovasc Imaging* 2003;19:9-17.
29. Kind T, Mauritz GJ, Marcus JT, van de Veerdonk M, Westerhof N, Vonk-Noordegraaf A. Right ventricular ejection fraction is better reflected by transverse rather than longitudinal wall motion in pulmonary hypertension. *J Cardiovasc Magn Reson* 2010;12:35.
30. Alfakih K, Plein S, Bloomer T, Jones T, Ridgway J, Sivananthan M. Comparison of right ventricular volume measurements between axial and short axis orientation using steady-state free precession magnetic resonance imaging. *J Magn Reson Imaging* 2003;18:25-32.
31. Fratz S, Schuhbaeck A, Buchner C, Busch R, Meierhofer C, Martinoff S, et al. Comparison of accuracy of axial slices versus short-axis slices for measuring ventricular volumes by cardiac magnetic resonance in patients with corrected tetralogy of Fallot. *Am J Cardiol* 2009;103:1764-9.
32. Atalay MK, Chang KJ, Grand DJ, Haji-Momenian S, Machan JT, Sheehan FH. The transaxial orientation is superior to both the short axis and horizontal long axis orientations for determining right ventricular volume and ejection fraction using Simpson's method with cardiac magnetic resonance. *ISRN Cardiol* 2013;2013:268697.
33. Willis J, Augustine D, Shah R, Stevens C, Easaw J. Right ventricular normal measurements: time to index? *J Am Soc Echocardiogr* 2012;25:1259-67.
34. Legget ME, Leotta DF, Bolson EL, McDonald JA, Martin RW, Li XN, et al. System for quantitative three-dimensional echocardiography of the left ventricle based on a magnetic-field position and orientation sensing system. *IEEE Trans Biomed Eng* 1998;45:494-504.
35. Horton KD, Meece RW, Hill JC. Assessment of the right ventricle by echocardiography: a primer for cardiac sonographers. *J Am Soc Echocardiogr* 2009;22:776-92. quiz 861-2.
36. van der Zwaan HB, Helbing WA, McGhie JS, Geleijnse ML, Luijnenburg SE, Roos-Hesselink JW, et al. Clinical value of real-time three-dimensional echocardiography for right ventricular quantification in congenital heart disease: validation with cardiac magnetic resonance imaging. *J Am Soc Echocardiogr* 2010;23:134-40.
37. Dragulescu A, Grosse-Wortmann L, Redington A, Friedberg MK, Mertens L. Differential effect of right ventricular dilatation on myocardial deformation in patients with atrial septal defects and patients after tetralogy of Fallot repair. *Int J Cardiol* 2013;168:803-10.
38. Morcos M, Sheehan FH. Regional right ventricular wall motion in tetralogy of Fallot: a three dimensional analysis. *Int J Cardiovasc Imaging* 2013;29:1051-8.
39. Winter MM, Bernink FJ, Groenink M, Bouma BJ, van Dijk AP, Helbing WA, et al. Evaluating the systemic right ventricle by CMR: the importance of consistent and reproducible delineation of the cavity. *J Cardiovasc Magn Reson* 2008;10:40.

Did you know?



You can save your online searches and get the results by email.

Visit **www.onlinejase.com** today!

APPENDIX 3

J. Steeden, D. Knight, S. Bali, D. Atkinson, A. Taylor and V. Muthurangu

Self-navigated tissue phase mapping using a golden-angle spiral acquisition – proof of concept in patients with pulmonary hypertension.

Magnetic Resonance in Medicine, 2014, **71**(1), 145-55.

APPENDIX 4

D. Knight, J. Steeden, S. Moledina, A. Jones, G. Coghlan and V. Muthurangu

Left ventricular diastolic dysfunction in pulmonary hypertension predicts functional capacity and clinical worsening: a tissue phase mapping study.

Submitted with revisions.

APPENDIX 5

M. Quail, J. Steeden, D. Knight, P. Segers, A. Taylor and V. Muthurangu

Development and validation of a novel method to derive central aortic systolic pressure from the MR aortic distension curve.

Journal of Magnetic Resonance Imaging, 2014, **40**(5), 1064-70.

APPENDIX 6

M. Quail, D. Knight, J. Steeden, L. Taelman, S. Moledina, A. Taylor, P. Segers, G. Coghlan and V. Muthurangu

Noninvasive pulmonary artery wave intensity analysis in pulmonary hypertension.

American Journal of Physiology – Heart and Circulatory Physiology,
2015, **308**(12), H1603-11.

APPENDIX 7

G. Kowalik, D. Knight, J. Steeden, O. Tann, F. Odille, D. Atkinson, A. Taylor and V. Muthurangu

Assessment of cardiac time intervals using high temporal resolution real-time spiral phase contrast with UNFOLDed-SENSE.

Magnetic Resonance in Medicine, 2015, **73**(2), 749-56.